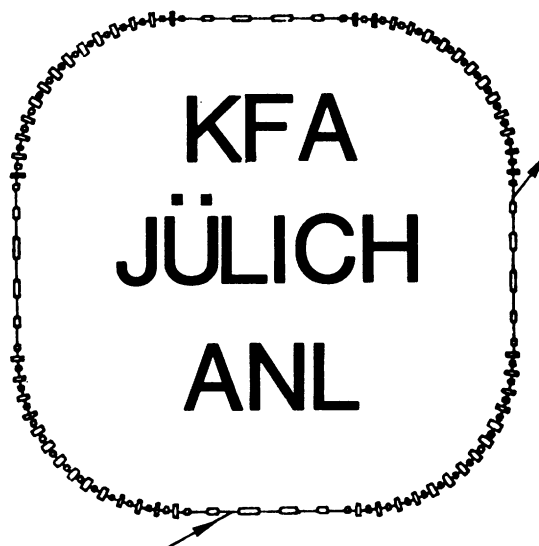


**ARGONNE RECORD COPY
DO NOT DESTROY**

**CONCEPTUAL DESIGN OF A
RAPID CYCLING SYNCHROTRON
FOR THE KFA – JÜLICH
SPALLATION NEUTRON SOURCE**



ARGONNE NATIONAL LABORATORY, ARGONNE, ILLINOIS

**Operated for the U. S. DEPARTMENT OF ENERGY
under Contract W-31-109-Eng-38**

ANL-83-13

ARGONNE NATIONAL LABORATORY
9700 South Cass Avenue
Argonne, Illinois 60439

CONCEPTUAL DESIGN OF A
RAPID CYCLING SYNCHROTRON
FOR THE KFA-JÜLICH
SPALLATION NEUTRON SOURCE

ANL-KFA Study Group

January 1983

Work supported by KFA-Jülich
under Proposal No. P-826-C

FOREWORD

A group was established by request of KFA-Julich to carry out a conceptual design study and cost estimate for a rapid-cycling synchrotron as a possible first stage program on neutron sources at KFA-Julich. Members of the ANL-KFA study group are:

Y. Cho	P. Meads**
E. Crosbie	J. Norem
M. Foss*	W. Praeg
T. Khoe	K. Thompson
R. Kustom	W. Wustefeld***
R. Martin	

This report is primarily compiled from a series of individual notes on the entire range of topics covered by study group members. The group met weekly to discuss the issues so that the contents had input from several members of the group. A draft report was submitted to communicate the essential results of the study at as early a date as possible. The draft report was not reviewed by most members of the study group so that this final report differs from the draft report in some respects. Thanks are due to Rosemary McHenry, Judith McGhee, Beverly Marzec, Adelle Pearson, and Bill Mehler for their patience and persistence in producing the initial individual accelerator notes, and in compiling, correcting, and assembling them into this report.

R. L. Martin

ANL, January 1983

*Now at Los Alamos National Laboratory.
**Consultant supported by KFA, Julich.
***Assigned to ANL from KFA, Julich.

ABSTRACT

This report contains the results of a study undertaken in collaboration with and supported by KFA-Julich to carry out a conceptual design study and cost estimate of a rapid-cycling synchrotron as a possible first stage program on neutron sources at KFA-Julich. An injector of 200 MeV is assumed producing up to 50 mA of H^- ions for 500 μ sec at a rate of 50 Hz. Charge exchange injection into the synchrotron will give a circulating beam of 6.25×10^{13} protons/pulse. The magnetic field of the synchrotron will be constant for 1.5 msec during injection and capture, after which it will be ramped with a halfwave sinusoidal pulse at a $33\frac{1}{3}$ Hz rate for acceleration, and reset at a 143 Hz rate to allow 50 pulses/sec. The beam will be accelerated to 1100 MeV by an rf system consisting of 20 cavities generating a maximum accelerating voltage of 10 kV each. The cavities are driven by a very low impedance cathode-follower driver system. Beam length manipulation at the end of the acceleration cycle can produce a total pulse duration of 200 nsec and extraction is provided for beam occupying the full transverse aperture of the synchrotron. The credibility of the design for achieving the goals of high beam current, low beam loss, and beam stability is given priority over cost and had led to a design somewhat more expensive than might otherwise be the case. It does not necessarily present an optimized design but should provide a starting point for comparison of other alternative techniques or components. The conversion of the synchrotron to serve as a full energy (1100 MeV) accumulator/compressor ring for 3×10^{14} protons/pulse in a possible future upgrade of the KFA-Julich neutron source program appears feasible.

TABLE OF CONTENTS

	<u>Page No.</u>
I. OVERVIEW	
1. Introduction.....	1
2. Preliminary Survey of Options.....	4
3. Summary of Report.....	6
II. SYNCHROTRON PARAMETERS AND BEAM DYNAMICS	
1. Lattice, Beam Dynamics, Magnet Requirements.....	31
2. Magnet Tolerances.....	33
3. Working Point.....	37
4. Instabilities and Their Compensation.....	42
5. RF Capture and Acceleration Requirements.....	65
6. Injection.....	73
7. RF System Options.....	82
8. Extraction.....	87
9. Vacuum Considerations.....	90
10. Beam Loss.....	96
III. SYNCHROTRON COMPONENTS	
1. Ring Magnets.....	131
2. Ring Magnet Power Supplies.....	135
3. Other Magnets and Power Supplies (Correction, Injection, Extraction).....	146
4. RF System Design.....	148
5. Vacuum System, Control System, Diagnostics.....	156

IV. CONVERSION TO FULL ENERGY ACCUMULATION RING.....175

V. RECOMMENDATIONS FOR FURTHER STUDY AND R & D.....187

Appendices

A.1. LATTICE PROPERTIES.....191

A.2. RING MAGNETS.....215

A.3. COST ESTIMATE.....223

Note.: References and Figures are at the end of each major section.

**CONCEPTUAL DESIGN OF A RAPID-CYCLING SYNCHROTRON FOR
KFA-JULICH SPALLATION NEUTRON SOURCE**

SECTION I

OVERVIEW

I.1. INTRODUCTION

This report is the result of a study undertaken at the request of and in collaboration with KFA-Julich, Germany, to carry out a conceptual design of a rapid-cycling synchrotron as a possible first stage of a spallation neutron source (SNQ). The goals of the study were to do a preliminary design and cost estimate of a proton synchrotron system with the following characteristics:

1.1 GeV protons

0.5 mA average current (6.25×10^{13} /pulse at 50 Hz)

50-100 Hz

Individual pulse duration \leq 200 nsec

Pulse separation up to 10 μ sec with maximum pulse train duration of 30 μ sec

Synchrotron should be able to be converted to a full-energy compression ring.

The major issues in meeting these criteria include: (1) beam loss, (2) credibility, (3) reliability, and (4) cost. The study is a preliminary effort to produce a credible system design, and reasonable, though non-engineering, cost estimate to allow comparison of the rapid-cycling synchrotron option with other possible alternatives, i.e., a partial energy linac with or without a compressor ring. Nevertheless, the trade-offs between credibility and cost are often a judgemental choice and, at least for this base design, the credibility factor (as viewed by the designers) is given priority. Later optimization studies might reduce the cost while maintaining adequate credibility.

This study benefitted considerably from the design and ongoing construction of the SNS synchrotron at the Rutherford-Appleton Laboratory, England. The latter was somewhat constrained to be compatible with an existing linac, ring magnet power supply, and building layout. The full energy is to be 800 MeV with a repetition rate of 50 Hz and a design current of 200 μ A average. The parameters are sufficiently similar to the requirements of this study that it was felt that demonstrated solutions to the vacuum chamber design (with ceramic vacuum chambers containing rf shields) and rf systems for acceleration would be applicable to the rapid-cycling synchrotron involved in this study. Therefore, design of these two component systems were not initially intended as a part of this study, and costs for these systems were to be estimated by appropriate scaling of the Rutherford costs.

The higher average current (by a factor of 2.5) desired of the Julich synchrotron, however, caused some concern about the credibility of utilizing a scaled up approach for the synchrotron design. The higher current would make many factors, such as allowable beam loss, instability thresholds, resonances and space charge forces in general, more critical. Consequently, it was decided to initially examine several options before focusing the effort on a single machine design.

In addition to a preliminary examination of a single ring operating at 50 Hz with the desired beam current, four other options studied were: (1) two rings, each at 50 Hz with one-half the desired beam current, possibly in push-pull for an effective 100 Hz operation, (2) an independent prebuncher ring to allow injection, capture and bunching in a dc magnetic field with higher credibility for minimum beam loss before transferring the beam to the synchrotron, (3) the use of four stacked rings (similar to the CERN booster)

operating at 50 Hz with each having one-fourth the desired beam current, and (4) a fixed-field alternating gradient (FFAG) synchrotron. The latter is a promising concept being pursued independently by Argonne as part of its advanced neutron source study.

By agreement with KFA-Julich, the first two months were devoted to a preliminary study of these five options. This first phase of the study was completed with a review of the results at Argonne on August 26-27, 1982, and a decision was made at that time to focus the effort on the single ring approach to the rapid-cycling synchrotron with the full desired beam current.

I.2. PRELIMINARY SURVEY OF OPTIONS

The meeting at Argonne on August 26-27, 1982, to review the preliminary survey of options was attended by H. Stiller, G. Bauer, C. Zettler, and S. Martin of KFA-Julich, in addition to the Argonne group. J. Griffin, FNAL, attended a portion of the meeting to discuss rf systems, and F. Cole and S. Snowden, FNAL, attended the presentations on the FFAG.

The presentations of the five options with their estimated costs were summarized in a report by P. Meads.¹ Since it seemed from the initial study that achievement of the study goals could be met with one ring, that the brief studies of instabilities could not quantify a clear level of risk between the options, and that the two-ring, four-ring, and prebuncher-ring options were more expensive, the decision was made to concentrate effort on the single-ring rapid-cycling synchrotron design. In addition, the studies of the single ring would be applicable to the two-ring and prebuncher-ring options. The FFAG synchrotron is a quite different concept and, while viewed as very interesting and cost competitive, was nevertheless considered to require further study and a mature design before it could be compared to a conventional synchrotron and therefore not suitable for continued study under this program. However, Argonne will continue the study of the FFAG synchrotron system as part of its ongoing program.

Other decisions at the August meeting were to settle on 200 MeV injection and to include at least a conceptual design of a workable rf system. The latter had been recognized as a rather critical issue since a simple scale-up of the SNS rf system design from 6 to 10 cavities does not appear necessarily adequate for the higher beam current (in addition to the frequency difference since the SNS synchrotron will operate on the second harmonic and we propose

to utilize the first harmonic for the Julich synchrotron). The choice of 200 MeV injection appears somewhat conservative from the space charge limit point of view. However, since this synchrotron will have higher circulating current than any existing machine, this conservatism seems justified. In addition, two operating proton linacs at 200 MeV exist (at BNL and FNAL).

The rapid-cycling synchrotron designed in this study is often referred to as the SNQ-SRA synchrotron. The letters SRA are an acronym for Storage Ring Accelerator, used to distinguish the lattice from several others initially considered.

I.3. SUMMARY OF REPORT

General Issues

The projected beam intensity of the SNQ-SRA is higher than that of any synchrotron in operation or under construction. This requirement leads to an examination of several major issues including space charge forces, beam stability, and minimum beam loss. The examination of solutions to these questions has led to a number of choices which form the basis of the design proposed. In this study the credibility of the solution, or the degree of confidence that it will meet the goal, is given priority over cost factors, at least for the initial design. Later optimization studies might be able to reduce the cost while maintaining an adequate confidence level. Some of these choices are summarized below.

The compensation for transverse space charge forces is enhanced by having a relatively high tune in the machine. For the same magnet apertures the space charge limit is directly proportional to the machine time. A high tune also means a high transition energy ($\gamma_T \sim v_x$), a consequence which adds to both the longitudinal and transverse stability of the beam. A high tune necessarily means a large number of unit cells, hence large numbers of both bending and quadrupole magnets.

For reasons of longitudinal stability and to preserve the relatively long bunch length through the critical period of maximum space charge forces during acceleration (thus minimizing the ratio of peak to average circulating current at the critical time) it is proposed to inject a large momentum spread, $\Delta p/p$. The beam size in the straight sections, which is a product of this factor and a dispersion function, would then be excessive unless the dispersion function in the straight sections was small. Besides requiring

larger aperture magnets, a large beam size in the straight section places more severe requirements on the critical extraction system, making loss free extraction more difficult. The lower momentum dispersion in the straight sections also simplifies the injection matching process.

For all of the reasons discussed above, the lattice having a tune of about 11 and a large number of magnets was retained for this study, in spite of the fact that the initial motivation, that of providing dispersion-free straight sections to avoid the head-tail effect observed in some electron synchrotrons, is questionable. We believe that the advantages of this lattice outweigh the possible added cost of many small magnets and power supplies.

The vertical and horizontal tunes are made different by about one unit in order to avoid possible problems with horizontal-vertical coupling. Again this is a stability consideration, but here, fortunately, not one that has a noticeable cost impact.

The large circulating current, a factor of 2.5 over that of the SNS, also raises questions about the adequacy of an rf system similar to that under construction for the SNS. When the power delivered to the beam becomes comparable to that absorbed in the cavity, the longitudinal phase space area available for acceleration decreases. This effect is called the "Robinson Instability" and could present a problem if not adequately compensated. The problem is alleviated to some extent by having a magnetic field that rises at a slower rate ($33\frac{1}{3}$ Hz), thereby requiring significantly less rf voltage/turn, and is reset at a higher rate in order to maintain 50 pulses/sec. Nevertheless, some uncertainty still remains and we chose to design a very low impedance cavity/driver system that makes use of a cathode-follower as a final power amplifier. The system might be somewhat more

expensive than more conventional systems but it is a higher power system and less likely to have the beam loading problems mentioned above.

Techniques for minimizing beam loss were made by comparison with the ANL Rapid-Cycling Synchrotron (RCS), currently the most intense proton synchrotron in operation. The allowable beam loss in the SNQ-SRA in order to avoid serious problems with induced radioactivity is much lower than for the ANL-RCS because of the higher average currents and beam energies involved (500 μ A at 200-1100 MeV compared to 10 μ A at 50-500 MeV for the ANL-RCS). Therefore, many features which should serve to reduce the beam loss in the SNQ-SRA ring, compared to that in the ANL-RCS, are incorporated into the design. One of the major ones is the provision for a constant magnetic field for 1.5 msec at the beginning of the cycle. Injection would require 0.5 msec leaving 1 msec for capture and preacceleration bunch shaping. Injection and capture efficiencies should therefore be significantly enhanced, justifying the added power supply costs. Other techniques by which beam loss will be minimized include a fast chopper preceding the linac to eliminate beam that might otherwise be lost, beam scrapers in the linac transport line to eliminate halo, adequate rf voltage to insure that beam is not lost during acceleration, and the conservative design of the extraction system to handle a beam occupying the full aperture of the ring at full energy (the accelerated beam should damp to less than full aperture). Beam that is inevitably lost will be absorbed by beam scrapers and collectors in localized positions so that there will not be a high level of general activity around the ring.

Overall Description of the Synchrotron Operation

A rapid-cycling synchrotron is designed and costed which would operate at a repetition frequency of 50 pulses per second with an average proton beam

current of 0.5 mA at 1100 MeV. The final pulse duration would be no greater than 200 nsec.

The ring will be ~ 240 m in circumference, will have horizontal and vertical tunes of 10.3 and 11.3, respectively, acceptances of $500 \times 300 \pi$ mm-mrad in horizontal and vertical planes, and near zero momentum dispersion in the straight sections. It will have a constant magnetic field for 1.5 msec during injection, capture and bunching, a rising field to a maximum of 1.05T at a $33\frac{1}{3}$ Hz rate, and the field would be reset at a 143 Hz rate. The total cycle will require 20 msec, allowing 50 Hz operation.

The layout of the 4 sector machine designed is shown schematically in Fig. I.3-1. There are 12 straight sections of 3.1 m each and 8 straight sections of 2.59 m each, in addition to many smaller spaces between magnets. Ten of the longer straight sections will be used for rf cavities and one each for injection and extraction.

A 200 MeV linac with an H^- current of 50 mA is assumed (21 mA required) with a normalized emittance of 10π mm-mr in both transverse planes (98% of the beam) and a momentum spread, $(\Delta p/p)$, of 2.7×10^{-3} , equivalent to a longitudinal emittance $(\Delta E \cdot \Delta t)$ of 0.7 eV-sec. This beam will be injected into the ring using charge exchange injection during 360 turns (500 μ sec) to fill both the horizontal and vertical acceptance of the machine, and the momentum spread will be adjusted (by a debuncher or ramping of the linac) to fill the nonaccelerating bucket of the rf system.

The rf will be supplied by 20 cavities operating on the first harmonic providing a total accelerating voltage of 200 kV/turn. The rf voltage will be turned on adiabatically (for one mode of rf capture) during 1 msec after beam injection, and the voltage subsequently ramped to accelerate the beam with a near constant bucket acceptance of 3 eV-sec (requiring lower voltage as \dot{B}

decreases in the last half of the cycle). Near the end of the accelerating cycle, the rf voltage will again be increased to compress the beam longitudinally to a duration of 200 nsec, followed by extraction and transport to the target.

Some of the parameters of the machine are given in Table I.3-1.

Lattice, Beam Dynamics, Magnet Requirements

Initially, six lattices were examined as documented in Mead's report.¹ The one chosen had zero dispersion in the straight sections. Later modifications to separate the horizontal and vertical tunes by one unit reintroduced a small dispersion, but not a significant one. To achieve this and provide adequate straight section space resulted in a large number of cells/sector (11). This choice results in a large number of relatively small magnets, a consequence which has advantages and disadvantages as discussed above.

Choosing a 4 sector machine and a phase advance of about 90° per cell leads to betatron tunes of ~ 11 . Such high tunes lead to smaller aperture magnets for the same space charge limit than would otherwise be the case. Lattices for two cases are given in Section II.1: horizontal and vertical tunes of 11.30 and 11.25, respectively, and one with horizontal and vertical tunes of 10.38 and 11.25, respectively. The latter is chosen for the proposed synchrotron in order to avoid any possibility of x-y coupling, although operation is possible with the former tunes. A choice of acceptances of $500 \pi \text{ mm-mr}$ and $300 \pi \text{ mm-mr}$ in horizontal and vertical planes was made, and further calculations (aperture requirements, injection energy, etc.) were based on these values. This choice was somewhat arbitrary, and more detailed

studies of cost trade-offs with other acceptance choices might be considered when time for optimization is available.

The beta functions and beam amplitudes calculated for a momentum spread, $\Delta p/p$, of $\pm 1.5\%$ are also given in Section II.1. From these results, one can summarize the magnet requirements as follows:

<u>Magnets-Number</u>	<u>Length (m)</u>	<u>B or B' (T,T/m)</u>	<u>Max x,y Beam Env. Half Width (cm)</u>
Bending Magnets			
M - 24	0.90	1.05	7.3 x 4.0
M1 - 32	0.45	1.05	6.2 x 3.8
Quadrupoles			
QF - 28	0.50	6.03	8.9 x 2.3
QD - 24	0.50	6.63	4.4 x 5.1
Q1 - 8	0.50	6.37	3.4 x 5.1
Q2 - 8	0.50	11.51	7.2 x 2.7
Q3 - 8	0.50	9.70	5.6 x 3.5
Q4 - 8	0.85	9.67	7.2 x 2.8
Q5 - 16	0.50	9.05	5.5 x 3.5

These apertures do not include allowances for vacuum chamber or orbit errors. Allowances for these, as well as some modifications to reduce the number of different magnet laminations, will be made in Section III.1 on magnet design. In addition, aperture modifications are required on the Q2 and Q3 quadrupole apertures to accommodate injection and extraction.

Magnet Tolerances

The distortions of the closed orbit due to four sources is calculated in Section II.2. These calculations were used as the basis for the machine design proposed because differences due to later modifications of the design are very small. The error sources include a tilt in the bending magnet, a field deviation in the bending magnet, a position error (δx or δy) in the quadrupole, and the influence of stray fields in the straight sections. The

results, to 98.5% probability, are $x_M = 1.41$ cm and $y_M = 1.74$ cm with random errors of 10^{-4} radians in bending magnet tilt, $\Delta B/B = 5 \times 10^{-4}$ in the bending magnet field, and 10^{-4} m position error in the quadrupoles in both x and y directions (stray fields in the straight sections could be reduced to zero if necessary).

These orbit errors would be quite significant if the magnet tolerances were of the magnitude assumed and the errors not corrected. However, we believe that orbit corrections can easily be effected to less than 0.5 cm (particularly necessary in the vertical plane) by a series of simple dipole correction magnets. We assume that four correction magnets in each betatron period per transverse plane (for a total of 80-88 correction magnets), will be included, but since these present a very small cost factor they are not considered in detail.

Working Point

The choice of working point of the SNQ-SRA, $\nu_x = 10.3$ and $\nu_y = 11.3$, is discussed in Section II.3. The horizontal and vertical tunes were displaced from each other by one unit in order to avoid the possibility of horizontal-vertical coupling of the beam. Even with both tunes in the same quadrant, one might avoid this coupling during the short time of the acceleration cycle (15 msec), but it would require higher tolerance on the magnets. With the high intensity anticipated for this machine, it seems prudent to eliminate the coupling possibility.

The relatively high tune is a necessary result of a design to make dispersion-free straight sections. While this choice leads to a large number of magnets, it also leads to larger intensity limits for the same magnet apertures, or equivalently, smaller magnet apertures for a prescribed beam intensity. With the assumed circulating intensity (6.25×10^{13} protons) the

tune shifts reach a maximum after 1.5 msec of acceleration. These tune shifts are $\Delta\nu_x = 0.14$ and $\Delta\nu_y = 0.19$ for beam emittances assumed to decrease adiabatically from injection values of 500π mm-mr and 300π mm-mr, respectively.

The most serious resonance is the third order resonance $\nu_x + 2\nu_y = 33$. This resonance will be compensated by sextupole correction magnets. Correction magnet strengths for this purpose depend upon the harmonic content of the magnetic fields of the bending magnets (sextupole fields) and require detailed field calculations in order to evaluate the harmonic content. However, estimates of the maximum sextupole field allowed in the bending magnet is larger than would be anticipated, particularly if care is taken in the magnet design and construction. There are a number of fourth order resonances of which the most serious is apt to be $\nu_x + 3\nu_y = 44$, because the lattice contains 44 cells. These are all imperfection resonances, however, and can be adequately compensated by accurate orbit control.

Compensation of these resonances is required to utilize the design working point. Otherwise, the working point would be $\nu_x = 10.2$, $\nu_y = 11.2$ with somewhat less margin of safety to accommodate the designed beam current.

Instabilities

We examine in Section II.4 possible longitudinal and transverse instabilities and their compensation in terms of sufficiently large momentum spread, sextupole magnets to control the chromaticity, and octupole magnets to control the amplitude-dependent tune spread.

The chromaticity will be controlled by a set of 16 sextupoles to have a negative value of 0.1-0.3. Similarly a set of 16 octupoles appears adequate to introduce sufficient Landau damping to control the transverse

instabilities. Required strengths of both sets of magnets are, at this stage, only an estimate. The requirements must be examined in more detail when the harmonic content of the dipole and quadrupole magnets that form the main lattice are known.

The longitudinal stability is primarily effected by the coupling impedance of the beam to the surrounding walls and by the momentum spread of the beam. A third important factor is how far away the operation energy is from the transition energy. The high tune (and thus high transition energy of the SNQ-SRA design) make the latter factor advantageous. The coupling of the beam to the vacuum chamber, even one made of stainless steel, would only require a $\Delta p/p$ of 0.4% in order that the beam be stable. We plan to inject a ramped energy beam with an effective momentum spread larger than this and the momentum spread will increase during the acceleration cycle. Inasmuch as the stability criterion is proportional to the square of the momentum spread longitudinal stability seems assured for the machine designed. Care must be taken, however, in the design and impedance coupling of the extraction kickers and the rf cavities. For the SNQ-SRA design the latter have quite low shunt impedance so that the longitudinal coupling of high modes to these elements should not be large.

Transverse stability is achieved when the betatron tune spread of the beam exceeds the tune spread introduced by beam coupling to the wall of the chamber, equipment within the ring, or to ions or electrons from ionization of the residual gas. These frequency spreads can be translated into units of impedance which can then be compared to the transverse coupling impedance. Some tune spread in the beam is introduced by tune variation with respect to momentum spread, and this spread can be controlled by the sextupoles. However, control of tune spreads by sextupoles is not as effective because of the synchrotron motion. Therefore, the transverse instabilities are mainly

controlled by the octupoles. Our calculations indicate that a tune spread, introduced by octupoles, of 0.15-0.20 is adequate for transverse stability. Again, however, transverse coupling impedances from the kicker magnets and rf cavities must be considered. The stability is enhanced to some extent by the design of this lattice, which makes the local β function small through the rf cavity and extraction kicker area.

The transverse resistive-wall instability of the bunched beam, in which wake fields created by the head of the bunch affect the tail of the bunch, can be adequately controlled by the negative chromaticity planned with the sextupoles. Calculations of the interactions of the beam with either the ions or the electrons created by ionization of the residual gas indicate that these do not cause instability problems with a vacuum pressure of 10^{-7} Torr.

RF Capture and Acceleration Requirements

We chose to operate the rf system on the first harmonic, $h = 1$. Having only one beam bunch in the ring places much less demand on the kicker system for extraction and allows a large local momentum spread. The latter may become essential to avoid the longitudinal microwave instability.

Acceleration will take place over 15 msec with the field rising at a 33-1/3 Hz rate. The required energy gain is about 100 keV/turn so that a total rf voltage of 200 keV allows a synchronous phase angle of 30° .

The constant magnetic field during 0.5 msec injection, and for an additional 1 msec, is to facilitate efficient injection, capture, and pre-acceleration bunch manipulation. The injected beam energy is ramped to inject a longitudinal emittance, $\Delta E \cdot \Delta t$, of 1.3 eV-sec. The rf voltage is raised to 25 keV to capture adiabatically with a bucket acceptance of 2.0 eV-sec. The rf voltage is then programmed as acceleration begins, to maintain a bucket acceptance nearly constant at 3.0 eV-sec. This gives a maximum $\Delta p/p$ of about

$\pm 1.5\%$. The longitudinal beam emittance, might grow to be 2.4 eV-sec. If it did not then several alternatives are possible to keep the bunch length relatively long during the early part of the acceleration cycle. The bunch length decreases during acceleration such that the bunch length is about 70% of the circumference at 1.5 msec, where the space charge limit is encountered. The bunch length continues to decrease to about 50% of the circumference at high energy with the rf voltage dropping to maintain the same bucket area. The revolution period is 890 nsec at high energy so the bunch length is about 445 nsec at this time. Near the end of the accelerating cycle increasing the rf voltage to 200 kV would cause the bunch length to reduce to ~ 300 nsec. This transition would be made adiabatically. The major part (perhaps 90%) of the beam would still be within the 200 nsec time duration specified. In order to compress the bunch length so that all beam is within the 200 nsec duration it would be necessary to reduce the rf voltage near the end of the acceleration cycle to about 40 kV to increase the bunch length to > 500 nsec, followed by a very rapid increase of the rf voltage to 216 kV. The beam distribution in longitudinal phase space will then rotate within the rf bucket such that after $1/4$ synchrotron oscillation period (or 110 μ sec) the entire bunch length will be 200 nsec. Extraction must occur at this time because the bunch length within the bucket would be oscillating and would subsequently increase.

A second alternative to achieving 200 nsec bunch length would be to use the 2nd harmonic rf frequency. This option has not been studied in detail for this report.

Injection

Both injection and extraction from the SRA lattice are possible in either transverse plane, and preliminary designs of horizontal injection and

extraction were presented during the August review. However, we selected vertical injection and extraction because of the smaller vertical apertures and beam sizes. Vertical injection is described in Section II.6.

We assume a linac beam emittance in both transverse planes of $10 \pi \text{ mm-mr}$. This would include 98% of the beam for the required 21 mA of H^- and should be easy to achieve since 50 mA sources are possible. The higher current would allow a beam chopper before the linac and scrapers between linac and ring to eliminate halo. A smaller beam emittance from the linac is not necessarily useful because of the necessity of filling the transverse acceptances of the synchrotron. The energy spread of the linac beam is assumed to be $\pm 1 \text{ MeV}$ at 200 MeV, based on existing experience, and this results in a momentum spread, $\Delta p/p$, of $\pm 2.7 \times 10^{-3}$.

Injection will be accomplished by 4 fast orbit bump magnets in the vertical plane, a septum magnet, and a stripping foil to accomplish charge exchange injection. Modification of the vertical orbit bump during injection will serve to fill the vertical phase acceptance. Horizontal phase space can be simultaneously filled by either a fast horizontal orbit bump oscillating several times during the injection period, or use of an oscillating steering magnet in the H^- injection line. Either of these methods appears quite feasible. Neither has been studied in detail.

At an injected beam current of 21 mA and nearly 100% efficiency, injection would occur over 360 turns requiring 500 μsec . In theory, this would fill the phase space area with a somewhat bumpy density since a dilution of a factor of 4 is required to fill the acceptance uniformly. In practice, however, space charge forces would smear the fluctuations, and there is ample flexibility for other injection alternatives such as producing hollow beams or otherwise shaping the phase space density.

The anticipated energy spread of the linac beam must be increased at injection into the ring in order to fill the rf bucket acceptance in an efficient way with little beam loss. The central energy of the injected beam should be modulated (either by a separate debuncher cavity or by ramping the linac itself) to match the desired momentum spread. Filling the rf bucket appropriately can either be done by adiabatic capture of a dc-injected beam (the additional 1 msec of constant field after injection appears adequate for this purpose), or by chopping the beam at the rf frequency (prior to the linac) in order to inject synchronously into the stable phase area of an operating rf system. The latter method requires 30 mA of injected current but should be no problem. Therefore, compared to presently operating machines, very efficient injection appears feasible.

The magnets of the injection system have not been designed in detail because we do not consider this a critical issue nor a major cost item, and solutions appear straightforward.

RF System Options

It was not initially intended to include the rf system in this study, but rather, to adopt the rf design and cost developed for the SNS machine. This appeared a logical choice since Rutherford has developed cavities and amplifiers of 13.5 kV/gap with 12 gaps (six cavities) around the ring for a total of 162 kV. While our voltage requirement is higher because of the higher energy (1100 MeV compared to 800 MeV) and larger circumference (237 m compared to 163 m), we will operate with a magnet field rising at a rate of $33\frac{1}{3}$ Hz instead of 50 Hz. In addition, we have space in the SNQ-SRA lattice for 10 cavities of the Rutherford type capable of 270 kV/turn, more than required on this machine. However, we chose to operate on the first harmonic rather than the second in order to reduce the requirement on the extraction

kickers and allow larger momentum spread. Also, the current in this machine will be more than double that of the SNS. Therefore, concern about the "Robinson Instability", which becomes important when the power delivered to the beam approaches the power dissipated in the cavity, has caused us to examine the rf system requirements in more detail.

Three solutions have been proposed to accommodate cavity beam loading at high beam currents. These are: (1) good active feedback systems to correct average voltage and phase, (2) active, instantaneous compensation of the image currents induced in the cavity by means of feed-forward systems, and (3) the use of a cathode-follower, or a low impedance cavity/driver system to provide instantaneous passive compensation of beam loading. The first is necessary and used on almost all accelerator rf systems irrespective of beam loading. In addition, the Rutherford SNS will use the feed-forward system which requires an additional independent rf amplifier and driver chain for each cavity.

The rf problem on this machine is more difficult than on the SNS because the current is a factor of 2.5 higher, thus requiring more beam power. Consequently, we have chosen to outline a cathode-follower system even though it may be more expensive. This system would be able to respond very rapidly to applied voltage changes, a characteristic that may be necessary for bunch length minimization at the end of the cycle. With this system, the average rf power is quite high so that the ratio of beam power to cavity power is relatively low. Such a choice might be examined more critically in later optimization studies and perhaps the costs could be reduced. The rf issues are discussed in Section II.7 and a typical cavity design given in Section III.4. The latter would have an average rf power of 3.8 MW while the power delivered to the beam is 500 kW.

Extraction

The extraction system is designed to accommodate a full aperture beam in order to be suitable as an accumulator ring at full energy. This choice is conservative because, even in the latter case, the full machine aperture is not required to reach the design current. However, conservatism at this point is important in order to make the extraction system as lossless as possible. Under these conditions, nearly loss-free extraction appears feasible.

For the same reasons as for injection, we chose to extract in the vertical plane. A description of the beam dynamics and extraction magnet requirements is given in Section II.8. It requires one fast kicker magnet, which can be separated into 2 or 3 sections, and a septum magnet, which can also be made of 2 or 3 separate elements. Since this system is so critical to the reliable operation of the machine, the design of these magnets and power supplies is very important. Nevertheless, the operating parameters for the existing kicker and septum magnets in use on the rapid-cycling synchrotron (RCS) of Argonne's IPNS system are more than adequate. Thus, the feasibility of this system is assured and no detailed design is undertaken at this time.

Vacuum Considerations

The vacuum requirements are examined in Section II.9. While the design of the vacuum system was not a part of the goals of this study, it seemed necessary to assure ourselves that adequately high vacuum was attainable so that beam loss due to residual gas scattering was tolerable and no instabilities due to beam-gas interaction arise. Some aspects of the latter require knowledge of conductances and pumping speeds of the system.

Simple calculations indicate that an average pressure of $< 10^{-7}$ Torr can be easily achieved with pumping speeds attainable and pump locations within the proposed SNQ-SRA lattice.

The potential from the beam to the wall could be 500 volts, or perhaps somewhat more at injection, and decreases during acceleration, substantially lower than the 2-3 kV experienced in the CERN ISR. Thus, there does not seem to be any concern about the pressure bump phenomena of gas desorption, produced by ions driven into the surface, causing pressure runaway. Stated another way, a desorption coefficient η (ratio of desorbed ions to incident ions) of 4 or 5 could be tolerated. Well-prepared stainless steel can have $\eta < 0.05$ for ion energies of < 1 keV, although we do not know the desorption coefficient for ceramic vacuum chambers similar to the SNS type that we are considering.

Beam Loss

The degree of beam loss, at least that loss which is uncontrolled and deposited in other than intended and localized areas, is one of the major issues in the design of the synchrotron. Even 1% uncontrolled loss at an average beam current of 500 μ A is equivalent to the total output of most conventional synchrotrons and would induce an uncomfortably high level of activity around the ring. This issue is discussed in Section II.10. An analysis of the losses of Argonne's 30 Hz RCS, accelerating protons from 50 - 500 MeV with an average current of 10 μ A, is given. With a transmission efficiency of 90% between the linac and neutron target, the RCS is probably the most efficient synchrotron in operation. The analysis is used as a starting point to define techniques and systems which might significantly reduce the beam loss projected in the present design. These differences from standard RCS operation include beam choppers after the preaccelerator and before linac acceleration, halo absorbers between the linac and the synchrotron, a phase ramped debuncher-like system after the linac to match the beam in longitudinal phase space, injection into a constant magnetic field

with adiabatic capture (or chopped beam injection synchronously into non-accelerating buckets), manipulation of the bunch length before the field begins to rise and acceleration begins, adequate rf voltage to prevent beam spilling out of the accelerating bucket, and a conservative extraction system from the point of view of extracted beam size. Provision should be made to remove from the linac beam that part which has been stripped to H^+ or partially stripped to H^0 by the residual gas of the linac. Those protons not stripped or partially stripped in the stripping foil within the ring have well-defined trajectories and can be absorbed locally. These features should eliminate many of the significant sources of loss in the ANL-RCS.

Finally, beam scrapers and collectors will be provided to localize the most likely unavoidable losses. The latter will mostly be the result of protons which escape from the accelerating rf bucket and are thus at lower energy than the protons being accelerated. These low momentum particles will have a maximum amplitude excursion in both horizontal and vertical planes at the center of a superperiod. Thus, four properly designed beam scrapers for each plane will serve to absorb those protons which lose synchronism with the rf voltage. If necessary, provision for additional absorbers at 90° and 180° in phase space from these points might serve to absorb those protons undergoing edge scattering in the beam scrapers.

It is difficult to be quantitative about such projections, and it was certainly beyond the scope of this study to make any kind of serious quantitative effort. In addition, the degree of success in reducing losses is a learning process depending on optimization of all of the various operations. As a rough goal, one might limit the residual activity in the ring to be comparable to that of the RCS, which operates with about a 90% reliability factor (ratio of actual beam time to scheduled beam time and not to be confused with the 90% beam efficiency defined earlier) with nearly $10 \mu A$

of average proton current at 500 MeV. A large fraction of the losses occur near the injection energy, 50 MeV for the RCS compared to 200 MeV for this machine. Approximating this effect as a simple factor of 4 in activity per proton, and taking into account the six times larger circumference of the SNQ-SRA, the unlocalized beam loss goal for this synchrotron would be

$$10\% \times (30/50 \text{ Hz}) \times (2 \times 10^{12}/6.2 \times 10^{13} \text{ppp}) \times (50/200 \text{ MeV}) \times 6 \cong 0.3\%$$

The above goal only represents unlocalized loss and not the total loss from the linac to the neutron target. We propose that most of the beam loss will occur in well defined locations in the linac line and the ring, and that equipment and shielding at these locations will be treated specially. In the ring such specific locations include the stripping mechanism and absorbers of unstripped or partially stripped beam, the beam scrapers and absorbers, and the extraction septa. Radiation problems around the latter are particularly serious since protons lost here will have the full beam energy so that induced activity/proton is greater. For such equipment one should plan for localized shielding, quick disconnect design, and shielded conveyance to transport the radioactive equipment.

Synchrotron Components

The design of synchrotron components is discussed in Section III. Of these the lattice magnets and power supplies and the rf system form the major part of the cost of the machine.

As described in the earlier sections the high tune of the machine is important for reasons of space charge and stability in such a high current synchrotron. This choice has led to the large number of relatively short magnets (56 bending magnets and 100 quadrupoles), although their aperture is

less than that of the SNS design. An additional constraint on these magnets is the requirement to operate with the full current in a dc mode in order to be compatible with conversion to a full energy accumulator/ compressor ring in a later stage of the program.

The power supply consists of many independent supplies and is required to provide a constant excitation current of 1.5 msec, after which the current increases at a 33-1/3 Hz rate, and then is reset to its initial value at a higher rate in order to allow 50 pulses/second. This degree of flexibility demanded of the system is certainly a cost factor. However, the constant field for injection, capture, and bunch manipulation should make it possible to carry out these operations with nearly 100% efficiency. In addition the slower rate of rise of the magnetic field during acceleration significantly reduces the burden on the rf system (a factor of 1.5 compared to a more conventional 50 Hz synchrotron) so that this feature of the power supply design is very important to the success of the SNQ-SRA design.

A detailed design of the rf system is not carried out. However, a conceptual design of a low impedance cathode-follower system is discussed in enough detail to appear credible and allow an initial cost estimate for such a system.

Other machine components including injection, extraction, and correction magnets and their power supplies, and vacuum, control, and diagnostic systems do not present questions of feasibility nor do they represent large cost items. Therefore, design of these components is not discussed. One possible exception to the statement above is the ferrite kicker magnet for extraction. Here a direct comparison with similar magnets in operation on the ANL-RCS leads to the conclusion that the ANL magnets fulfill the requirements so that the feasibility of these critical components is assured.

Conversion to Full Energy Accumulator Ring

It would be attractive as a neutron source upgrade with a full energy linac to convert the SNQ-SRA into a dc isochronous ring similar to the IKOR design. The advantages of such a system are quite significant and have been studied by another group in some detail. One of the primary advantages is the lack of the requirement of an rf system to maintain the bunch length (with a gap around the circumference to allow excitation of the extraction kickers without beam loss). It is presumed here that the SNQ-SRA could be readily converted into an isochronous machine which operates at its transition energy by reducing the machine tune (decreasing the quadrupole current) from 11 to about 4. The beam dynamics for this case, however, have not been studied for reasons discussed below.

The requirement in this study to produce an extracted beam with a maximum duration of 200 nsec was not considered in the IKOR study (where the bunch length was 680 nsec and the current 66 A). A pulse duration of 200 nsec (and corresponding current of 250 A, assuming 100 Hz and 5 mA average current) is a very severe requirement, and would represent a circulating beam significantly beyond the space charge limit (by $\sim 3 \times$) of the IKOR design, or of the SNQ-SRA with tune reduced to make it isochronous. The only possibility to achieve the goal in this case would be to have three bunches of 200 nsec each circulating in the ring, and an extraction system which could extract one bunch without affecting the other two. Since there would be ~ 100 nsec (in the circumference of the SNQ-SRA) between bunches this presents very severe requirements on the extraction system, and the probability of low loss extraction would be much reduced.

The total required charge (3.1×10^{14} protons at 100 Hz) could possibly be accumulated in one 200 nsec bunch in the SNQ-SRA within the space charge limit if the tune were not decreased to make the ring isochronous. It would be

near the space charge limit utilizing the full aperture of the ring, however, would require 100 kV of rf to maintain the bunch length against the longitudinal space charge forces, and the probability of low loss accumulation and extraction is again significantly reduced. In addition the linac requirements to produce this charge with the beam chopped into bunches of 200 nsec every 890 nsec would also be much greater. We, therefore, do not favor this mode of operation for the proposed conversion.

There remains two alternative approaches to achieve the study goals and these are discussed in Section IV. They are: 1) To accumulate full energy beam with a circulating bunch duration of ~ 600 nsec, and utilizing the rf system with fast bunch compression to reduce the bunch length to 200 nsec for extraction, and 2) To accumulate two bunches of 200 nsec each and arrange that the bunches can be extracted independently. This latter approach has not been investigated in this study.

For the first approach beam accumulation would not require the full aperture of the ring so that high efficiency extraction appears feasible. The rf system of the synchrotron is adequate to contain the beam and to compress the bunch length at the end of accumulation. Longitudinal and transverse instabilities are not a problem. There would appear to be little or no cost impact involved in this conversion, other than that we would here propose to inject H^0 , derived from an H^- beam by magnetic stripping, rather than injecting the H^- ions directly, as is done for the synchrotron.

Cost Estimate

The estimate of the cost of the accelerator components designed is \$46.9M in FY 1983 dollars. This does not include the cost of the injector linac and linac building, and the transport lines from the linac to the synchrotron and from the synchrotron to the experimental targets. Adding the estimate for

buildings and utilities, EDIA engineering, design, inspection, administration and contingency nearly doubles the total estimate to \$95.8M.

The major items in the accelerator cost are the ring magnets, the ring magnet power supplies, and the rf system. Each of these three component systems contain features which add to the credibility of achieving the goals of high current, low beam loss, and beam stability. As a result, they are more expensive than would be the case for a lower current synchrotron design. Optimization of the design of these components, research and development, and incorporating the results from additional experience with high current machines (for instance, the ANL-RCS, and the SNS, when the latter becomes operational) might serve to reduce the cost estimate.

The 200 MeV injector linac will also be a major cost item for this accelerator system although its design was not a part of this study. Its cost basis must be related to a more detailed design study on linacs being carried out at Julich, with due consideration to the factor of 10 different average current level between this injector linac and a full SNQ current linac proposed as an alternative first stage to the neutron source program.

References for Section I

1. P. F. Meads, Jr., "Notes on the Meeting of 26-27 August, 1982, on the Spallation Neutron Source", (October 1982).

Table I.3-1.

SNQ-SRA Parameters

Kinetic Energy	200 MeV - 1.1 GeV
Repetition Rate	50 Hz
Flat Bottom	1.5 ms
Acceleration Time	15 ms (33-1/3 Hz)
Circumference	237.14 m
Revolution Time	1.396 μ sec - .890 μ sec
Revolution Frequency	.716 MHz - 1.24 MHz
Average Radius	37.742 m
Cell Length	5.388 m
Magnet Lengths	(24) .9 m (32) .45 m
Bend Radius	5.7296 m
Field Strength	.375 T - 1.053 T
No. of Superperiods	4
Betatron Tunes	$Q_x \sim 10.38$; $Q_y \sim 11.25$
Transition Gamma	7.006

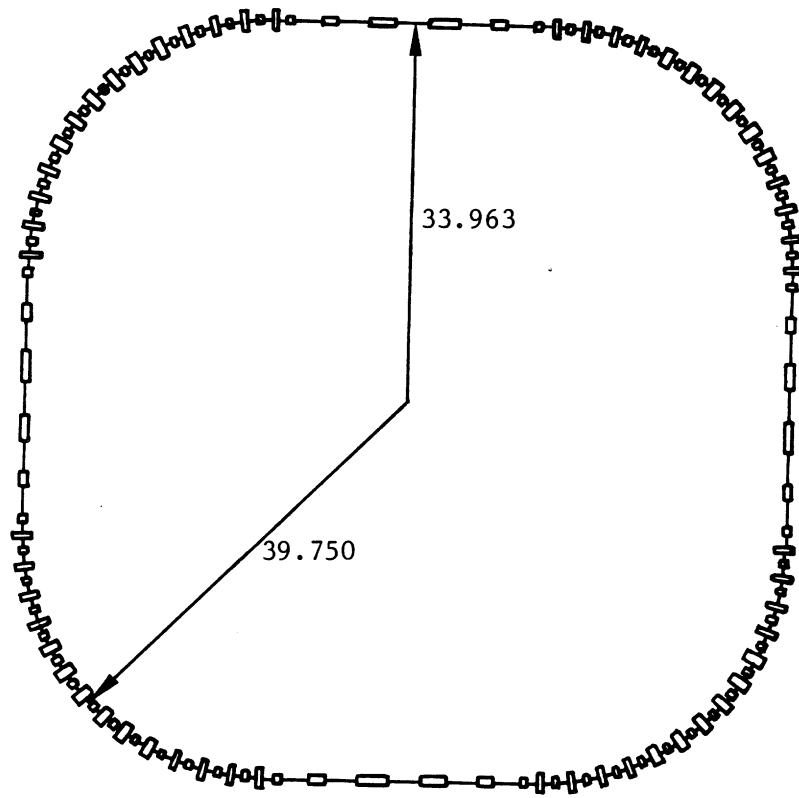


Fig. I.3-1 Layout of Synchrotron

CONCEPTUAL DESIGN OF A RAPID-CYCLING SYNCHROTRON FOR
KFA-JULICH SPALLATION NEUTRON SOURCE

SECTION II

SYNCHROTRON PARAMETERS AND BEAM DYNAMICS

II.1 LATTICE, BEAM DYNAMICS, MAGNET REQUIREMENTS

Introduction

This section describes the lattice¹ chosen for the conceptual design and two sets of tunes: one with $\nu_x = 11.30$, $\nu_y = 11.25$ and the other with $\nu_x = 10.38$, $\nu_y = 11.25$. This lattice is most suitable for vertical extraction and is quite similar to a lattice design for horizontal extraction. Some minor adjustments of the quadrupole strengths and the short straight section lengths is performed for the vertical extraction lattice compared to the one for horizontal extraction. The main feature of the lattice is that it consists of four sectors with each sector consisting of three normal cells, two dispersion suppressor cells at each end of the normal cells, and two matching and straight section cells at each end of the sector. Thus the total number of cells per sector is 11.

Lattice with $\nu_x = 11.30$ and $\nu_y = 11.25$

By making the phase advance per cell equal to approximately 90° in the 11 cell sector, the tunes of the machine are $\nu_x = 11.30$ and $\nu_y = 11.25$. Figure II.1-1 shows the β and η functions of one complete sector of the machine beginning and ending in the center of the middle normal cells. The dispersion free region of this lattice is quite long and the entire matching and straight section cells have the η function equal to zero. More detail, including expanded β and η functions of the normal cells, of the dispersion eliminator and matching and straight section cells, as well as the properties of these cells, are given in Appendix A.1.

Lattice with $\nu_x = 10.38$ and $\nu_y = 11.25$

This tune set is obtained by adjusting the phase advances of the normal cells and dispersion suppressor cells. The horizontal phase advances were reduced to approximately $83^\circ/\text{cell}$ and the vertical phase advances remained about 90° . The elimination of the dispersion function through the straight-section area is best achieved for $90^\circ/\text{cell}$ phase advances so that compared to the $\nu_x = 11.3^\circ$ lattice, this lattice does not have a long dispersion free region. This is evident in Figure II.1-2, which shows the β and η functions of one complete sector of this lattice. Nevertheless, the dispersion function is still very small throughout the long straight section region. Again more detail on this lattice is included in Appendix A.1.

For this lattice, which is the one chosen to have the x and y tunes separated by approximately an integer, the x and y amplitudes are shown in Figure II.1-3. These calculations assume horizontal and vertical emittances of 500 and $300 \pi \text{ mm-mr}$, respectively, and include the effects of a momentum spread, $\Delta p/p$, of $\pm 1.5\%$. They are used to determine the required apertures of the magnets. The results, taken from the Table A.1-7 of lattice properties in Appendix A.1, are listed in Section I.3.

To determine the required magnet apertures, allowances for vacuum chamber with rf shields and orbit errors must be added to beam envelope requirements. In addition magnet apertures in the Q2 and Q3 quadrupoles must be larger to accommodate injection and extraction. These allowances are included in the required apertures for the magnets whose design and cost are discussed in Section III.1.

II.2 MAGNET TOLERANCES

Introduction

Magnet apertures must include an allowance based on distortions of the closed orbit which are calculated from three error sources. Each of these errors can be expressed as an equivalent beam kick $\Delta y'_i$ ($\Delta x'_i$) at the position of the error source. The values of $\Delta y'_i$ ($\Delta x'_i$) are given as follows:

Vertical kick due to a tilt ψ in the bending magnet

$$\Delta y'_i = \frac{BL_o}{B\rho} \cdot \psi, \quad \psi = 0.1 \cdot 10^{-3} \text{ rad}$$

L_o = length of bending magnet

Radial kick due to a field deviation in the bending magnet

$$\Delta x'_i = \frac{BL_o}{B\rho} \cdot \frac{\Delta B}{B}, \quad \frac{\Delta B}{B} = 5 \cdot 10^{-4}$$

Transverse kick due to a position error δy (or δx) of a quadrupole

$$\Delta y'_i = \Delta x'_i = \frac{B'}{B} \frac{L_Q}{\rho} \delta y, \quad \delta y = \delta x = 10^{-4} \text{ m}$$

L_Q = length of quadrupole

The errors caused a closed orbit deviation Δy_{ki} at point k as:

$$\Delta y_{ki} = \sqrt{\beta_k \beta_i} A \Delta y'_i / \frac{BL_o}{B\rho}, \quad (\text{similar for } \Delta x_{ki})$$

$$\text{with } A = \frac{1}{2 \sin \pi Q} \frac{BL_o}{B\rho}$$

The tune Q is always chosen as $Q = \text{integer} + 0.25$. For a more realistic calculation, the changing of Q should be taken into account. If $L_s =$ total length of bending magnets per superperiod ($L_s = \sum_i L_{o_i}$), the value of A is

$$A = \frac{1}{2 \sin \pi Q} \frac{BL_s}{B\rho} \cdot \frac{L_o}{L_s} = \frac{\pi \sqrt{2}}{N} \cdot \frac{L_o}{L_s} \quad N = \text{number of superperiods.}$$

The β functions are chosen as

$\beta_i =$ maximum value of β function inside each element,

$\beta_k =$ maximum value of all β_i values to get the maximal displacement.

Assuming no correlations between the errors, the Δy_{ki} values can be summed as an rms expression at point k

$$\langle y_k^2 \rangle = \sum_i \Delta y_{ki}^2$$

Due to a probability distribution of the errors, we assume for y_k the relation (also for x_k)

$$y_k \leq y_M = 3.5 \sqrt{\langle y_k^2 \rangle}$$

with a 98.5% probability. The factor 3.5 is a result of Monte Carlo computations of typical error sources, which could occur. The deviation y_k is related to the half width of the beam.

The influence of stray fields outside of the magnets and quadrupoles are added, by using the relation

$$\Delta y_{ik} = \sqrt{\beta_i \beta_k} \cdot \frac{1}{2 \sin \pi Q} \frac{\Delta B \ell_i}{B\rho} ,$$

where ℓ_i is the length of the straight section, and $\Delta B = 10^{-4}$ T is the value of the stray field. The $B\rho$ is smallest at injection, 1.772 Tm at 140 MeV, 2.060 Tm at 185 MeV, and 2.148 Tm at 200 MeV

Several lattice types were calculated by this procedure. Table II.2-1 lists the single error displacements for a typical lattice of the type used for this conceptual design.

Table II.2-1

Element Name	Length (m)	Field B, B' (T),(T/m)	No. of Elements n	β-Functions (m)		Single Error Displacement (mm)	
				$\langle \beta_{ix} \rangle$	$\langle \beta_{iy} \rangle$	Δx_{ki}	Δy_{ki}
M	0.90	1.054	6	6.0	6.0	0.419	0.090
M1	0.45	1.054	8	5.0	5.0	0.191	0.041
QF	0.50	6.44	6	9.5	2.0	0.358	0.177
QD	0.50	6.71	7	2.0	9.0	0.171	0.391
Q1	0.50	6.38	2	9.0	2.0	0.345	0.175
Q2	0.50	11.90	2	3.0	10.0	0.372	0.731
Q3	0.50	10.00	6	4.0	6.0	0.361	0.476
Q4	0.85	10.00	2	2.5	11.0	0.485	1.09
D1	0.647	10^{-4} *	16	4.0	4.0	0.159	0.171
D2	1.55	"	6	3.5	3.0	0.357	0.355
D3	0.15	"	6	3.0	7.0	0.032	0.053
D4	0.30	"	2	2.0	9.0	0.052	0.119
DM	0.90	"	2	4.0	4.0	0.221	0.238
DX	0.872	"	16	4.4	3.9	0.225	0.228

* Stray field at injection energy (140 MeV)

$$\beta_{xk} = 9.5 \text{ m} \quad \beta_{yk} = 11 \text{ m}.$$

The maximum tolerances imposed on the design require $x_M = 1.41$ cm and $y_M = 1.74$ cm without stray fields and $x_M = 1.74$ cm and $y_M = 2.03$ cm with stray fields. However, with careful closed orbit error measurements and using four dipole orbit correction elements per betatron period, these errors can be further reduced to less than 0.5 cm. This calculation serves as a guide to the degree of accuracy needed in the alignment and imposes the requirements on the orbit correction elements. This is not a critical issue and is not carried out in further detail.

II.3 WORKING POINT

Introduction

The proposed lattice has a four-sector symmetry, and each sector has 11 cells consisting of three normal cells, four dispersion suppressor cells, two matching cells and two straight section cells. The phase advance could be made to be approximately $90^\circ/\text{cell}$ so that the machine tune in both the horizontal and vertical planes can be made to be approximately 11. The expected space charge tune depression is the order of $\Delta\nu \approx 0.15$ at injection, and we plan to install a set of octupoles to facilitate Landau damping by introducing an amplitude dependent tune spread $\sim \Delta\nu_{\text{inc}} - \Delta\nu_{\text{coh}}$, where $\Delta\nu_{\text{inc}}$ and $\Delta\nu_{\text{coh}}$ are the Laslett incoherent and coherent tune shifts, respectively. It is important to avoid the $\nu_x - \nu_y = 0$ coupling resonance and especially its coincident fourth order $2\nu_x - 2\nu_y = 0$ resonance. Therefore, we decided to make $\nu_y \approx \nu_x + 1$. This choice also takes into account that the vertical space charge tune shift is larger than that of the horizontal, and that vertical extraction may be preferable to horizontal extraction. Although it is implicit, a further choice is that the tune should be a number between an integer and the next highest half integer. This choice insures against the resistive wall effect of a single bunch machine. The preferred ranges of the tune then become:

$$10 < \nu_x < 10.5$$

$$11 < \nu_y < 11.5$$

Space Charge Effects

This effect for the SNQ-SRA is discussed in some detail elsewhere.² It is customary to invoke various assumptions and approximations in the

transverse space charge limit calculation of an accelerator. For an accelerator which is to achieve a very high intensity such as the SNQ, it is prudent to use conservative yet reasonable assumptions and judgement factors in the estimate of the transverse space charge effect. The factors used in the calculations are beam size and linear charge density along the circumference. Here we use the average beam size within the machine and the peak estimated linear charge density. Although space charge detuning is highest at the smallest beam size, the degradation of beam comes from the multiple traverses of the resonances, thus the use of the peak density and average beam size is a reasonable approach.

In a rapid-cycling synchrotron such as the SNQ-SRA, the maximum transverse space charge effect does not occur at injection but a few msec into the acceleration process. This phenomenon is a result of rapidly increasing charge density due to shrinkage of the beam bunch length. For the SNQ-SRA with an effective acceleration rate of $33\frac{1}{3}$ Hz, this occurs about 1.5 msec into acceleration. At this time the proton kinetic energy is about 220 MeV.

For a given aperture and circumference of the ring, the space charge limit of the ring is proportional to its betatron tune. Therefore, it is desirable to have a higher tune. This is one reason why the tune of this machine is much higher than that of other accelerators of comparable energy. A high tune also leads to a higher transition energy, which plays a very important role in high intensity beam stability. On the other hand, this would be far from the isochronous condition which was planned for the IKOR scheme. However, conversion from a synchrotron to an accumulator ring can be done with this lattice and will be discussed elsewhere.

Returning to the discussion of the transverse space charge effect, we expect to have tune shifts of $\Delta\nu_x = 0.14$ and $\Delta\nu_y = 0.19$, with the

approximations noted above, emittances at injection of $\epsilon_H = 500 \pi$ mm-mr, $\epsilon_V = 300 \pi$ mm-mr, (decreasing adiabatically during acceleration) and 6.25×10^{13} protons per pulse. As stated above, due to the varying bunch lengths and the linear charge density distribution, the tune shift is expected to be maximum at 223 MeV kinetic energy.

Working Point and Tune Diagram

Figure II.3-1 shows the tune diagram near $\nu_x = 10$ and $\nu_y = 11$. Also shown in Fig. II.3-1 are the third and fourth order resonances. Taking into account the space charge tune shifts of $\Delta\nu_x = 0.14$ and $\Delta\nu_y = 0.19$, the bare machine (i.e., zero current) tune points can be placed near $\nu_x = 10.2$ and $\nu_y = 11.2$ at first glance. Doing so would avoid all of the resonance lines. However, further study of these resonance lines shows that the bare machine working point can be placed somewhat higher than 10.2 and 11.2. Doing so would increase the space charge limit of the machine.

Nonlinear Resonances

Transverse oscillation amplitudes can be in a resonant state due to perturbations of the azimuthal distribution of the guide field or the focusing power. These perturbations can come from either alignment and construction tolerances of the ring elements or from the intrinsic nature of the magnetic field which must obey Maxwell's equations. Both the intrinsic and imperfection perturbations would manifest themselves to the beam in the form of high order multipole magnetic fields such as sextupole, octupole, etc. The sextupole and octupole fields can drive third and fourth order resonances, respectively. These resonances are characterized by the relation $m\nu_x + n\nu_y = p$, where m , n and p are integers, and $|m| + |n|$ is the order of the

resonance. If the integer p is a multiple of any periodicity of the ring the resonance can become serious. There is a superperiodicity of four and there are 11 cells in a superperiod in the SNQ-SRA. The 11 periods in a sector is a weak constraint because there are many variations of cells within a sector.

The following table shows the nonlinear resonance lines near the proposed working point.

Table II.3-1.

m	n	p	Resonance
<u>3rd Order</u>			
3	0	31	$3v_x = 31$
0	3	34	$3v_y = 34$
1	2	33	$v_x + 2v_y = (33)$
2	1	32	$2v_x + v_y = 32$
<u>4th Order</u>			
4	0	41	$4v_x = 41$
0	4	45	$4v_y = 45$
1	3	44	$v_x + 3v_y = (44)$
2	2	43	$2v_x + 2v_y = 43$
3	1	42	$3v_x + v_y = 42$

The third order resonance, $v_x + 2v_y = 33$, whose driving force can come from the 33rd harmonic of sextupole components from the ring magnet elements, especially the fringing fields of the dipoles, needs further consideration.

Detailed calculations of the resonance strength have to wait until field properties of the ring magnets are known. However, we can estimate the tolerable strength of the 33rd harmonic component of the sextupole field. We find this 33rd harmonic integrated over the entire ring to be:

$$\int_0^{2\pi R} \frac{1}{\beta\rho} \frac{\partial^2 B}{\partial x^2} \cos\left(33 \frac{s}{R}\right) ds < 6 \text{ m}^{-2}$$

In general, we would not expect to have the strength of the 33rd harmonic in a bending magnet as large as this, and some care should be taken in the magnetic field design to minimize it. When the driving term of this resonance is eliminated or minimized, the proposed working point can be moved up to this resonance provided that we take care of the fourth order resonances.

These are due to imperfections in the ring magnets and alignment errors. Compensation or elimination of such imperfection resonances have become a standard technique, and when we need to cross this resonance the correction can be made by a method similar to that used in the ISR.^{3,4} Once these fourth order resonances are corrected, the working point can be moved upward to $\nu_x = 10.3$ and $\nu_y = 11.3$.

II.4 INSTABILITIES AND THEIR COMPENSATION

1. Chromaticity and Amplitude Dependent Tune Controls

Introduction

In order to control the transverse stability while accelerating a very high number of protons, it is necessary to have a negative chromaticity for an accelerator such as the SNQ-SRA operating below its transition energy. We define the chromaticity, ξ , to be $(\frac{\Delta v}{v})/(\frac{\Delta p}{p})$. The natural chromaticity of a strong focusing machine, i.e., the chromaticity of a machine made of perfect magnets, is -1.4 in both horizontal and vertical planes. This natural chromaticity has the right sign, but the magnitude is too large for the SNQ-SRA. We propose to utilize a large momentum spread, as large as $\pm 1.5\%$ at the base line, and a natural chromaticity of -1.4 implies that protons of 1.2% off-momentum would have a tune difference of 0.17 compared to that of the on-momentum particles. This tune variation caused by momentum spread in the beam is too high. Therefore, the chromaticity must be reduced from the natural value by means of judiciously placed sextupole magnets around the lattice. As discussed elsewhere,⁵ the planned operating chromaticity would be around -0.3. In a real machine there are several other sources of sextupole components such as the fringing fields of dipoles, eddy currents due to ramping of ring magnets, etc. In this discussion these other sources of sextupole fields are ignored for the time being until the magnetic field design is done. The purpose of this study is to estimate an order of magnitude of the sextupole strength, and the location and numbers of such correction magnets required to control the chromaticity.

A properly placed set of octupoles would control the betatron amplitude-dependent tune, which is a necessary part of initiating Landau damping of the

transverse oscillations. Here again, as done for the sextupoles, the octupole components coming from the quadrupoles and other origins are ignored in this discussion. (When detailed magnetic field calculations are available or actual machine components are built and measured, the sextupole and octupole strengths described here will have to be adjusted accordingly). This study is limited to an estimate of the order of magnitude of the octupole strength, and geometrical layout required to introduce the amplitude-dependent tune spreads in both horizontal and vertical planes of the transverse motion.

Locations and Numbers of Sextupoles and Octupoles

The multipole magnets (sextupoles and octupoles) located at a place where the horizontal β function is large compared to that of the vertical should have a larger effect on the horizontal tune spread than that of the vertical, and vice versa. Thus it is possible to facilitate almost orthogonal control of tune spread in the two planes of the transverse motion. Figure II.4-1 shows the lattice layout of one half of a sector and its β -functions together with the proposed locations of the F-correction and D-correction magnets. These magnets are to be located in the medium length straight sections of the dispersion suppression cells. This figure implies that there would be a set of eight sextupoles controlling the horizontal chromaticity, a set of eight sextupoles controlling the vertical, and two similar sets of octupoles for Landau damping. A multiple function magnet system comprised of single magnets having windings with all desired higher pole fields is one possibility to be studied.

Sextupoles

Under the given geometrical layout noted above and the assumption that there are no other contributing sextupole fields except those for the

chromaticity controls, we carry out an analysis of the required sextupole strength to make the chromaticities in both planes -0.1 . The off-momentum dependent beam dynamics parameters, and the harmonic analyses of these sextupoles have been calculated by using a computer code,⁶ "PATRICIA." The results showed that eight F-type sextupoles of an integrated strength in each of $s = 10.5 \text{ m}^{-2}$, and eight D-type sextupoles of an integrated strength in each of $s = -11.5 \text{ m}^{-2}$ can reduce the chromaticities in both planes to desired values. No harmonics of these sextupoles other than the fundamental have been found. Here s is defined to be $s = (B''L)/B\rho$ and L is the length of the sextupole. The tune variation as a function of the momentum spread was found to be:

$$\cos(2\pi\nu_x) = \cos(2\pi\nu_{x0}) - \frac{\sin 2\pi\nu_{x0}}{\nu_{x0}} \left[-\frac{1.57}{4} \left(\frac{\Delta p}{p}\right)^2 + 0 \cdot \left(\frac{\Delta p}{p}\right)^3 \right]$$

$$\nu_{x0} = \left[10.37^2 - 0.22 \frac{\Delta p}{p} + 1228 \left(\frac{\Delta p}{p}\right)^2 - 2500 \left(\frac{\Delta p}{p}\right)^3 \right]^{1/2}$$

$$\cos(2\pi\nu_y) = \cos(2\pi\nu_{y0}) - \frac{\sin 2\pi\nu_{y0}}{\nu_{y0}} \left[-\frac{0.095}{4} \left(\frac{\Delta p}{p}\right)^2 + 0 \cdot \left(\frac{\Delta p}{p}\right)^3 \right]$$

$$\nu_{y0} = \left[11.25^2 - 5 \frac{\Delta p}{p} - 485 \left(\frac{\Delta p}{p}\right)^2 + 734 \left(\frac{\Delta p}{p}\right)^3 \right]^{1/2}$$

where $\pm \Delta p/p$ is the momentum spread expressed in terms of the base line.

The off-momentum β functions and η function normalized to those of the on-momentum particles at the midpoint of the superperiod is shown in Fig. II.4-2. The variation of the β function with the momentum spread can be used for a design of the beam scrapers.

Octupoles

Because the purpose of the octupoles is to control the amplitude dependent tune spread, a somewhat simpler analysis has been performed without taking into account the momentum spread contribution directly. As done in the case of sextupoles, a similar assumption that there are no other octupole components except those under consideration is used for the analysis. Here again a new analysis must be done after knowing all higher-pole components.

The theoretical amplitude dependent tune spread for Landau damping is the difference between the Laslett tune spreads of incoherent and coherent terms. For the SNQ-SRA this spread is on the order of 0.1 at the largest amplitude. In this analysis we introduce this amount of tune spread in one transverse plane with the other plane unchanged, i.e., orthogonal adjustments of the tune spreads. The following table illustrates this. The β functions of the F-type and D-type octupoles are $\beta_x = 8.4$ m, $\beta_y = 1.9$ m, and $\beta_x = 2.2$ m, $\beta_y = 8.2$ m, respectively.

Table II.4-1

Tune Spread at $A_x = 6.8$ cm, $A_y = 5.0$ cm		Octupole Strength (*)	
Δv_x	Δv_y	OF (m^{-3})	OD (m^{-3})
0	0	0	0
+ 0.1	0	4.3	2.0
0	+ 0.1	1.4	9.0

(*) Strength is defined here to be $(B'''L)/B\rho$ where L is the octupole length.

The expression of strength used is chosen to be independent of the acceleration energy. This expression can be translated to the pole tip field strength at the peak energy assuming the octupole length is 0.2 m and the bore radius is 0.1 m. In this geometry the strength of 9.0 m^{-3} can be translated to a pole tip field of 0.27 T, which is a very reasonable value.

2. Longitudinal Stability For The SNQ-SRA

Introduction

During the course of this study several papers have been written about the stability of the beam in the SNQ-SRA. Here we attempt to summarize these studies and to relate the results to the planned hardware. The most important parameter under consideration for the longitudinal stability is the momentum spread of the beam coming from the linac and during acceleration. The linac parameters and the rf parameters described later satisfy the stability requirements.

Longitudinal Instability - Threshold

Starting very early in the lattice design, ideas of accelerating a very large momentum spread and of having the transition energy of the accelerator very high have been put forth to alleviate longitudinal instability problems. The goal was to stay below the threshold of instability. To do this, the dispersion function of the lattice is quite small, and the tune of the machine is very high. At this juncture the large $\Delta p/p$ has no direct effect on the high rf voltage needed (200 kV per turn).

Three papers written by G. Wüstefeld⁷ discuss this problem. Using the beam and the smooth vacuum chamber geometry derived from the lattice calculation, the longitudinal coupling impedance of the vacuum chamber system

can be estimated using the following equations with an assumption that a circular centric beam occupies a circular smooth vacuum chamber:

$$Z_{\parallel}/n = R_{\parallel}/n + X_{\parallel}/n$$

$$R_{\parallel}/n = \frac{1}{b} \sqrt{\frac{RZ_0 \beta}{2\sigma n}} \quad (\text{resistive part})$$

$$X_{\parallel}/n = i \frac{Z_0}{\beta\gamma^2} \left[\frac{1}{2} + \ln \left(\frac{b}{a} \right) \right] \quad (\text{reactive part})$$

where

$Z_0 = 377 \Omega$ free space coupling impedance

$R = 37.7 \text{ m}$ average radius of the machine

$\sigma = 7.7 \times 10^5 / \Omega\text{m}$ stainless steel conductivity

$a =$ the radius of circular beam [m]

$b =$ the radius of circular chamber [m]

$n =$ unstable oscillation mode number, and could be many thousand in the microwave region, and the cutoff, n , is $2\gamma R/b$.

The following table shows some of the typical values of the impedance.

Table II.4-2.

T[MeV]*	$X_{\parallel}/n[\Omega]$	$R_{\parallel}/n[\Omega]$
200	321	$1.37/\sqrt{n}$
1100	112	$1.71/\sqrt{n}$

* Beam and chamber half-sizes used are 4.3 cm and 5.3 cm, respectively, at 200 MeV. At 1100 MeV, the beam size is assumed to be damped by $\sqrt{3}$.

The reactive part plays a role in determining the threshold of instability, and the resistive part in the risetime. Since the mode number, n , is expected to be in thousands, $R_{||}/n$ in the above table is negligible compared to additional parts which can come from the rf cavities and the extraction kickers. For these, some special care must be taken to make the longitudinal impedance/mode number small.

To investigate whether or not a beam under consideration is stable, the Keil-Schnell criterion is applied to the beam parameters. The criterion is:

$$\left| \frac{Z_{||}}{n} \right| < F \frac{m_0 \beta^2 \gamma |\eta|}{I} \left(\frac{\Delta p}{p} \right)_{FWHM}^2$$

where

$|Z_{||}|/n$ = the longitudinal coupling impedance

m_0 = proton rest mass in eV

I = beam current in amperes (local peak current for the bunched beam).

β, γ = relativistic velocity and mass variables

$\eta = 1/\gamma_t^2 - 1/\gamma^2$ where γ_t is the transition energy

F = form factor assumed to be 1

$(\Delta p/p)_{FWHM}$ = FWHM momentum spread which is approximately equal to the half-width at the baseline of distribution. This approximation enables use of the bucket height directly.

There are two distinctive beam conditions that must be considered separately. One case is for the injection process while the stack is being formed, and the other is for the acceleration process. The reason for this separation is that during injection, the accumulated beam size and beam current change continuously. Thus, the coupling impedance, which depends on the beam size, changes. The consequence of the 200 MHz micro-bunch structure

of the linac turns out to be inconsequential. We calculate the minimum $\Delta p/p$ for the assumed current and beam size to stay below the instability threshold.

To accumulate 6.25×10^{13} protons in a 500 μsec linac pulse requires about 360 turns of injection with 20 mA of linac current. The linac beam parameters used for this consideration are described in Section II.6 of this report. Figure II.4-3 shows the stable-unstable region as a function of the stack momentum spread and number of turns being accumulated. This shows that if the stack momentum spread, $(\Delta p/p)_{\text{FWHM}}$, is larger than 4×10^{-3} , the stack would be stable. While the linac momentum spread is expected to be below this value, the energy will be ramped during injection so that the beam current would always be below the longitudinal instability threshold.

For the application of the criterion to the acceleration process, a method similar to that for injection can be used to derive the threshold momentum spread to stay within the stable region. The varying bunch length, the β and γ of the beam during acceleration, and adiabatic damping of the transverse beam size as the momentum increases is taken into account. Figure II.4-4 shows the threshold momentum spread $(\Delta p/p)_{\text{FWHM}}$ along with the rf bucket momentum spread which is derived from the longitudinal phase space, $\epsilon = \Delta E \cdot \Delta t = 2.4 \text{ eV}\cdot\text{sec}$. The bucket half-height is always larger than the threshold (note that the threshold current is proportional to the square of $[\Delta p/p]$).

Longitudinal Instability - Risetime

Although the designed beam would stay below the threshold of instability, it may be instructive to investigate the risetime of the instability. In doing so, we assume that $\Delta p/p$ of the beam is zero so the beam current is much above threshold.

In the limit of $\Delta p/p = 0$, the risetime, τ , can be written as

$$\frac{1}{\tau} = \frac{n\omega}{2} \cdot \frac{R||/n}{X||/n} \cdot \sqrt{\frac{\hat{I}|\eta|}{2\pi\beta^2\gamma m_0}}$$

where ω is the angular revolution frequency and the cut-off value, $n = \frac{2\gamma R}{b}$, can be used for n . In order to stay below the instability threshold, $\eta = 1/\gamma_t^2 - 1/\gamma^2$ is made very large, and as a result, the risetime would become shorter by $|\eta|^{-1/2}$.

To calculate and study the risetime, again the injection process and the acceleration process have been considered separately, using the methods described earlier. Figure II.4-5 shows the risetime as a function of the number of turns being accumulated in the stack. Figure II.4-6 shows the growth rate for the acceleration process together with the synchrotron frequencies during the acceleration.

The conclusion is that even in the limit of $\Delta p/p = 0$, the risetime of the instability is of the order of 10^{-3} sec (or 1 kHz). This time is longer than the synchrotron oscillation period of $0.2-0.4 \times 10^{-3}$ sec, so that even in this worst case example the effect is reduced.

3. Transverse Stability for the SNQ-SRA

Introduction

This section discusses in detail three transverse instabilities considered during the study. These transverse effects are:

1. Coasting beam, single stream instabilities,
2. Bunched beam, single stream instabilities,
3. Two-stream instabilities (ion-proton and electron-proton coupling instabilities).

Although there is no plan to operate the SNQ-SRA in the coasting mode, the coasting beam instability is discussed here because, with appropriate modifications, most of the stability criteria are applicable to the bunched beam. Special attention is given to the head-tail instability of the bunched beam and to the Landau damping system which is planned for the machine. It is anticipated that there would not be major problems with the transverse instability.

Transverse Stability Criterion and Introduction of Tune Spreads

The statement of stability is that: Beam equipment interactions, beam-wall interactions and ion-proton oscillations are stabilized if the betatron frequency spread (ΔS) of the beam exceeds the frequency shift ($\Delta\omega$) introduced by these interactions via the transverse coupling impedance, or $\Delta S > |\Delta\omega|$. There are two common sources of betatron frequency spread. The tune variation with respect to momentum spread is one source, which can be controlled by sextupoles, and the other is the betatron amplitude-dependent tune variations, which can be controlled by octupoles. We define ΔS_p and ΔS_a to be the momentum-dependent and the amplitude-dependent frequency spread, respectively.

$$\Delta S_p = [(n-\nu)\eta - \xi\nu] \omega_{\text{rev}} \frac{\Delta p}{p}$$

$$\Delta S_a = \omega_{\text{rev}} \frac{\partial \nu}{\partial a^2} a^2 ,$$

where

n = an integer greater than ν and is the mode number,

$$\eta = \frac{1}{\gamma^2} - \frac{1}{\gamma_t^2}$$

ω_{rev} = angular revolution frequency

ξ = $(\frac{\Delta v}{v})/(\frac{\Delta p}{p})$ is the chromaticity

$\frac{\partial v}{\partial a^2} a^2$ = amplitude-dependent tune spread across beam due to non-linearity such as octupoles.

The contributions of ΔS_p and ΔS_a to ΔS do not add linearly. In the bunched beam case, ΔS_p may not contribute much to the ΔS , because Δp is oscillatory due to the synchrotron motion. Furthermore, introduction of too large a frequency spread by either sextupole or octupole magnets should be avoided in order not to overlap with the resonance lines on the tune diagram (Fig. II.3-1).

Coasting Beam Instabilities and Tune Spread for Landau Damping

G. Wustefeld's paper⁸ touches on this matter. Although the coasting beam criterion is used for the investigation, the beam current and size are chosen to represent the bunched beam case and the tune spread dependence on the chromaticity is left as a variable. The problem has been to derive the tune spread needed to have transverse damping. This calculated tune spread can be supplied by the octupoles, while the sextupoles and the chromaticity are considered elsewhere.⁵

The frequency spread described earlier can be translated into units of impedance which then can be compared to the coupling impedance. The transverse coupling impedance of the vacuum chamber Z_{\perp} , and the stability criterion can be written:

$$|Z_{\perp}| = \frac{R Z_0}{\beta^2 \gamma^2} \left(\frac{1}{a^2} - \frac{1}{b^2} \right) \quad [\Omega/m]$$

$$|Z_{\perp}| < 2 \pi \frac{E_0}{e} \frac{v\beta\gamma}{RI} \left[\frac{\Delta p}{p} |\eta(n-v) - v\xi| + \Delta v^{\text{oct}} \right] \quad [\Omega/\text{m}]$$

where

- R = radius of machine [m],
- a = beam half-size [m],
- b = chamber half-size [m],
- E_0 = proton rest mass [eV],
- β, γ = relativistic variables,
- n = any integer greater than v ,

$$\eta = \frac{1}{\gamma_t^2} - \frac{1}{\gamma^2}$$

- I = beam current

$$\xi = \text{chromaticity } \left(\frac{\Delta v}{v} \right) / \left(\frac{\Delta p}{p} \right)$$

$$\Delta v^{\text{oct}} = \text{tune spread which can come from octupoles.}$$

For an accelerator operating below its transition energy, i.e., $\gamma < \gamma_t$, η is always negative. In order to have a positive contribution from the chromaticity of the machine in the transverse stability, the chromaticity must be negative for the machine below transition.

Some numerical values of the transverse coupling impedance of the machine as calculated from the equation above are:

$$Z_{\perp} = 5.6 \text{ M}\Omega/\text{m at 200 MeV}$$

$$Z_{\perp} = 4.6 \text{ M}\Omega/\text{m at 1.1 GeV}$$

It is instructive to calculate three contributing terms in the stability inequality separately, and doing so would provide the ranges of adjustments each term can supply to the stability. The following result is for 200 MeV, $I = 7A$, $n = 12$, $\nu = 11.3$, and ξ and $\Delta\nu^{\text{oct}}$ variable.

$$\eta \text{ term: } 2 \pi \frac{E_0}{e} \frac{\nu\beta\gamma}{RI} \left[\frac{\Delta p}{p} |\eta| (n - \nu) \right] = 1.2 \times 10^6 \Omega/\text{m}$$

$$\xi \text{ term: } 2 \pi \frac{E_0}{e} \frac{\nu\beta\gamma}{RI} \left[\frac{\Delta p}{p} |\nu\xi| \right] = 2.88 \times 10^7 \xi \Omega/\text{m}$$

$$\Delta\nu^{\text{oct}} \text{ term: } 2 \pi \frac{E_0}{e} \frac{\nu\beta\gamma}{RI} [\Delta\nu^{\text{oct}}] = 1.7 \times 10^8 \Delta\nu^{\text{oct}} \Omega/\text{m}$$

Now we can compare the Z_{\perp} calculated at 200 MeV of $5.6 \text{ M}\Omega/\text{m}$ and the above three terms. The idea of independent adjustment is that either the ξ term or the octupole term should be able to compensate separately the difference between $Z_{\perp} = 5.6 \times 10^6 \Omega/\text{m}$ and the η term of $1.2 \times 10^6 \Omega/\text{m}$. Simple numerical manipulations show the following:

$\Delta\nu^{\text{oct}}$ should be greater than 0.026 if $\xi = 0$, and

$|\xi|$ should be greater than 0.15 if $\Delta\nu^{\text{oct}} = 0$.

As discussed in the next section, the expected operating range of ξ is -0.1 to -0.3 in order to prevent the onset of the head-tail instability, and the octupole tune spread is planned for a range of $\sim 0.2 - 0.15$. These would be sufficient to take care of the transverse instabilities originating from the transverse coupling impedance. For higher energy, although the peak current of the accelerating beam increases due to the changing velocity of the particles and the shrinkage of the bunch length, the $\beta\gamma$ term in the stability inequality compensates for this increase to maintain the stability.

Local Contributions to Impedance

Additional contributions to the transverse coupling impedance coming from the kicker magnets and especially from the rf cavities whose total length is expected to be some 20 m, must be considered. To do this, two important points must be made. The stability criterion is actually a comparison of local impedance expressed in terms of $[\Omega/m]$ against the local tune spread expressed in the same unit. Therefore, the additional contributions to the impedance by the cavities can be treated locally. Furthermore, the stability inequality has the term $\frac{\nu}{R}$, which is the inverse of the average value of the betatron β function. To treat locally, we can substitute $\frac{\nu}{R}$ by the local $(1/\beta)$ function.

The second point to be made is that while designing the lattice, special care has been given to make the β functions through the rf cavity area small. In the design of the SNQ-SRA, the β functions in the long straight sections are smaller by a factor of 1.7 compared to the average. Therefore, the local contribution of the rf cavities can be larger by the same factor. In other words, the cavity can have a few $M\Omega/m$ of transverse coupling impedance and still satisfy the stability criterion.

Transverse Resistive-Wall Instability of Bunched Beam (Head-Tail Effect)⁹

Several accelerators, PSB, CPS, KEK-Booster, and ANL-RCS have observed troublesome head-tail effects. Usually the cure comes from adjustment of the machine chromaticity to shift the mode number of the unstable oscillation to a higher value to take advantage of a longer risetime of the higher order mode. The instability is driven by the surrounding environment, which extracts energy from the circulating bunch in the form of wake fields and converts it into a growing transverse oscillation. That is to say, a short-

range wake field created by the head of the bunch is affecting the tail of the bunch. The instability manifests itself on a fast beam position signal in the form of a standing wave oscillation between the head and tail of the bunch.

The important quantity in this consideration is the betatron phase of a particle at each position along the bunch as compared to the phase of the synchronous particles. The total phase-shift, χ , between the head and tail has contributions from the tune variation, the rotation frequency variation and the finite transit time. However, the last two terms cancel, and

$$\chi = \frac{\xi}{\eta} v \omega_{\text{rev}} \tau_L \text{ (radians)}$$

where the chromaticity ξ , η , and ω_{rev} have been defined previously, and τ_L is the bunch length in seconds. It is worthwhile to note that when χ is negative all modes of oscillation are unstable, and therefore χ must be made positive. To do this in our case the chromaticity must be negative because η is negative. The meaning of χ is that if $\chi = 3 \times 2 \pi$ radians, then three oscillations (mode = 2) along the bunch are possible. However, doing so would shift the bunch spectrum functions of the mode number 2 to the stable region where the real part of the transverse coupling impedance is positive.

The calculations done elsewhere⁵ show the results of this shifting of χ to suppress up to $m = 2$ oscillations. The chromaticity required to do so is found to be about -0.2 , and this agrees well with that found in the coasting beam consideration discussed above of -0.15 . In Ref. 5, we have also calculated the risetime of this instability in the absence of the tune spread which is an unreasonable assumption. Nevertheless, the calculation shows a risetime of less than one millisecond during the acceleration. However, the

machine would have enough tune spread coming from sextupoles to shift to higher order modes and enough octupoles to damp the transverse instability.

Two-Stream Instabilities (Ion-Proton and
Electron-Proton Coupling Instabilities)

With an assumption that the vacuum pressure of the SNQ-SRA is to be better than 10^{-7} Torr, the effects of ions and electrons created from the residual gas by the circulating beam are considered in two separate notes.^{10,11} In principle the ions created by this interaction could cause a coherent tune shift of the beam in the same way as image currents in the chamber wall. For the conditions assumed, however, the tune shift introduced by this effect is quite small compared to the tune spread in the beam. The beam is thus stable against the ion-proton effect during both accumulation and acceleration so that the ion effect on the circulating beam will not be considered further.

It is also shown that there will be no net accumulation of electrons produced from the residual gas and hence no instability due to e-P coupling. Here, however, the threshold value of the allowed neutralization of the circulating proton beam is surprisingly low, and the risetime of the instability, if it occurs, so rapid, that we will reproduce these calculations here.

For both this discussion and that of the pressure bump phenomena in Section II.9 we need the ion production rate and the potential between the beam and the wall.

a. Ion Production Rate

The number of ions (electrons) produced per revolution by 6.25×10^{13} protons can be written:

$$\text{No. of Ions/rev} = 6.25 \times 10^{13} \times n \times \sigma \times 2\pi R$$

where n is number of residual gas atoms/cc, σ is the atomic ionization cross-section of the residual gas, and R is the mean radius of the machine. The residual gas is mainly nitrogen so that $n = 7 \times 10^9$ atoms/cc at 10^{-7} Torr. The circumference is 240 m.

Various authors use a value for the atomic cross-section ranging from 0.8×10^{-18} cm² to 1.2×10^{-18} cm² for the minimum ionizing projectiles. The value of 1.2×10^{-18} cm²/atom will be used. This value corresponds to an average energy transfer to the electron of some 33 eV per collision. The cross-section to be used for this calculation has to be scaled from the minimum ionizing value, because the protons under consideration have a kinetic energy between 200 MeV to 1100 MeV. In order to simplify the calculation an average kinetic energy of 600 MeV is used. The standard scaling of the ionization is done by a factor $1/\beta^2$, which is 1.6 for 600 MeV. The ionization cross-section then becomes 1.9×10^{-18} cm²/atom and the number of ions produced is 2×10^{10} per revolution or 2×10^{16} per second. For an average energy gain/turn of 50 keV, the number of ions produced per acceleration cycle is 4×10^{14} . This number of ions will be accelerated by the space charge potential toward the chamber wall, and an equal number of electrons will be attracted toward the beam if the proton beam is in a dc mode, as for instance at injection. There is a self-clearing mechanism of the electrons if the beam is bunched. This is discussed later.

b. Space Charge Potential

Two geometries are considered: 1) circular beam in the transverse dimension with a diameter of $2a$ and circular chamber in the transverse direction with a diameter of $2A$, and 2) circular beam in the transverse direction with diameter of $2a$ and an infinitely flat chamber on the top and bottom separated by $2A$. The potential U is

$$U(s) = \frac{e\lambda(s)g}{4\pi\epsilon_0\gamma^2},$$

where

$$g = 1 + 2\ln \frac{A}{a} \quad \text{for circular chamber,}$$

$$g = 1 + 2\ln \frac{4A}{\pi a} \quad \text{for flat chamber,}$$

and where s is the length variable in the azimuthal direction along the beam path, ϵ_0 is the dielectric constant of free space, and $\lambda(s)$ is the linear charge density along s . For $a = 4$ cm and $A = 4.5$ cm, then $g = 1.24$ and 1.72 for the circular and parallel plate geometries, respectively. In the SNQ-SRA, the chamber would be neither circular nor parallel plate geometry, thus the worst case of the parallel plate geometry is chosen.

During injection, the accumulated $\lambda(s) = 6.25 \times 10^{13}/240 = 2.6 \times 10^{11}$ protons/m. During acceleration, the peak value of $\lambda(s)$ can become several times higher depending on how the beam is bunched. Then average potential $\langle U \rangle$ becomes

$$\langle U \rangle = 640 \frac{1}{\gamma^2} = 435 \text{ V at } 200 \text{ MeV}$$

$$= 150 \text{ V at } 1 \text{ GeV}$$

The space charge potential can exceed 500 V shortly after injection and initial bunching and decreases as the particles increase in energy. Furthermore this decrease would compensate the increase of local current due to bunch length compression of the beam at extraction. The average potential of 500 V is substantially lower than that of 2-3 kV of the ISR. Lower potential implies that the residual gas ions would have lower kinetic energy when they are driven toward the chamber wall.

c. Neutralization of Beam and e-p Instability

In the case of coasting beam, electrons produced by the ionization of residual gas will be trapped by the proton potential, and will neutralize the electrostatic charge of the protons. The charge neutralization, $\eta(t)$, is defined as the ratio of the number of electrons/number of protons. The trapped electrons can change the betatron tune of the circulating protons, and can initiate an instability known as the e-p instability when η reaches a threshold value. This section considers the threshold of the instability for the coasting beam, the risetime of the instability if initiated, and the self-clearing mechanism built into the bunched beam operation. The details of this consideration can be found in Schönauer and Zotter's work.¹²

The trapped electrons oscillate transversely and couple electromagnetically to the protons. Unstable coherent oscillations of both beams may result. In order to estimate the proper frequencies of the electrons with respect to the protons in the potential well of the other species, the beam dimensions along the circumference are needed. This calculation also determines the spread in electron frequencies due to the size variation. The characteristic frequencies of electrons and protons in each other's potential well can be expressed in terms of multiples of the revolution frequency of protons for a given beam size:

$$Q_e = \sqrt{\frac{2Nr_e R}{\pi\bar{\beta}^2 b(a+b)}} \quad \text{for electrons} \quad ,$$

$$Q_p = Q_e \sqrt{\frac{m_e}{m_p} \frac{\eta}{\gamma}} \quad \text{for protons} \quad ,$$

where r_e is the classical radius of electron, η is the neutralization parameter, R is the radius of the machine, $\bar{\beta}$ is the average proton velocity, and N is the number of protons. It should be noted that Q_p is different from the tune of the machine ν (often called Q). The spread of Q_e and Q_p can be obtained by considering the beam size variation along the circumference. The minimum and maximum values of these are derived from:

$$(a + b) \cdot b|_{\max} = 45.4 \text{ cm}^2 \quad ,$$

$$(a + b) \cdot b|_{\min} = 20.5 \text{ cm}^2 \quad .$$

Then

$$Q_{e \max} = 80.2 \quad ,$$

$$Q_{e \min} = 53.8 \quad ,$$

$$\pm \frac{\Delta Q_e}{Q_e} \equiv \frac{Q_{e \max} - Q_{e \min}}{Q_{e \max} + Q_{e \min}} = 0.20 \quad ,$$

and

$$Q_{p \text{ max}} = 1.70 \sqrt{\eta} \quad ,$$

$$Q_{p \text{ min}} = 1.14 \sqrt{\eta} \quad .$$

The theoretical threshold value of Q_p is given by

$$Q_p^{\text{th}} = \frac{8Q}{3\pi} \sqrt{\frac{\Delta Q}{Q} \cdot \frac{\Delta Q_e}{Q_e}} \quad .$$

From this together with $Q = 10.3$ and $\Delta Q = 0.2$, we obtain

$$1.70 \sqrt{\eta} < \frac{8Q}{3\pi} \sqrt{\frac{\Delta Q}{Q} \cdot \frac{\Delta Q_e}{Q_e}} = 0.54$$

or

$$\eta < 0.1.$$

This states that for the coasting beam condition (i.e injection period) the neutralization must be less than 0.1. In case this condition is not met, then the e-p instability risetime is given as

$$\tau = \frac{2}{Q_p \Omega_o} \sqrt{\frac{Q}{Q_e}} \approx 0.1 \times 10^{-6} \text{ sec},$$

for $\eta = 0.1$. Because of this extremely fast risetime, the neutralization must be kept below threshold. The production rate of these electrons is quite high as shown in a.) above, however, there is a built-in self clearing mechanism due to the bunching of protons. Even the injected beam could be bunched by using the chopper prior to the linac.

The low energy electron cloud in the vacuum chamber would be affected by focusing and defocusing forces when proton bunches pass through. The focusing force is due to the attractive space charge potential of the protons when the proton bunch is passing, and these electrons would experience their own repulsive force during the time between the passage of the proton bunch. Thus, stationary electron clouds (low energy) would see a time varying focusing-defocusing force, and this is equivalent to the AG principle. Therefore, we can calculate the transfer matrix and the phase advance of such a F-D structure:

$$\begin{aligned} \cos\mu = & \cosh \left[2\pi Q_e \left(\frac{1}{\sqrt{B}} - \sqrt{B} \right) \sqrt{\eta} \right] \cos \left[2\pi Q_e \sqrt{1-\eta B} \right] \\ & - \frac{1-2\eta B}{2\sqrt{\eta B(1-\eta B)}} \cdot \sinh \left[2\pi Q_e \left(\frac{1}{\sqrt{B}} - \sqrt{B} \right) \sqrt{\eta} \right] \\ & \cdot \sin \left[2\pi Q_e \sqrt{1-\eta B} \right] \end{aligned}$$

where B is the bunching factor.

In order to determine stability of electrons in this situation, the regions of stability where $|\cos\mu| < 1$ as a function of Q_e and η for given value of B must be located. It turns out that the η - Q_e plane has many bands of stability which become very narrow as η increases or B decreases. In order to consider these bands, the center of the stable band ($\cos\mu = 0$), and the width (from $\cos\mu = \pm 1$) can be determined from the following expressions:

$$\text{center of stable band } Q_e = \frac{k}{2\sqrt{1-\eta B}}, \text{ where } k \text{ is an integer}$$

$$\text{slope } \frac{d\eta}{dQ_e} = \frac{2}{Q_e} \frac{1-\eta B}{B}$$

$$\text{width } \delta Q_e = \frac{1}{\pi\sqrt{1-\eta B}} \sin^{-1} \left[1 + \frac{\sinh^2 2\pi Q (\sqrt{B} + \sqrt{1-B}) \sqrt{\eta}}{4\eta B(1-\eta B)} \right]^{-\frac{1}{2}}$$

$$\text{spacing } \Delta Q_e = \frac{1}{2\sqrt{1-\eta B}}$$

We note here in the expression of width, when B decreases the width becomes narrower. Now we turn to consider the effective neutralization rate, $\dot{\eta}_{\text{eff}}$. From part a.) above, $\dot{\eta} = (\text{no. of electrons produced/sec})/\text{no. of protons} = 320/\text{sec}$. However, not all of the electrons produced would be in the stable band discussed above. We can argue that the fraction of electrons which contributes to the e-p instability is the ratio of the width of stable band, δQ_e , and the spacing of the band, ΔQ_e , i.e.,

$$\dot{\eta}_{\text{eff}} = \dot{\eta} \frac{\delta Q_e}{\Delta Q_e}$$

In order to estimate the $\dot{\eta}_{\text{eff}}$, the following values are used for the SNQ-SRA: $Q_e \approx 65$, $B = 0.7$, $\eta = 0.1$, and $\dot{\eta} = 320/\text{sec}$. The calculated value of $\dot{\eta}_{\text{eff}}$ is 6×10^{-20} . The value of $\dot{\eta}_{\text{eff}} \approx 0$, so there will be no net accumulation of neutralizing electrons.

II.5 RF CAPTURE AND ACCELERATION REQUIREMENTS

Introduction

In this section we describe rf parameter requirements for a synchrotron operating with a flat-bottom guide field of 1.5 msec duration for injection, capture and bunch manipulation, a rising magnetic field equivalent to a sinusoidal field of $33\frac{1}{3}$ Hz for acceleration, and a falling field at a higher rate to make the overall repetition rate 50 pulses per second. The lower \dot{B} compared to biased sinusoidal 50 Hz operation has the advantage of requiring much less peak rf voltage. The introduction of a constant guide field for injection facilitates manipulating the capture process and bunch length after capture and before the start of acceleration. This technique should provide greater flexibility and higher efficiency in the injection and capture process. At the end of the acceleration cycle, the bunch length has to be reduced to about 200 nsec for extraction.

For an injection energy of 200 MeV, the minimum field of the ring would be 3.753 kG, and at 1100 MeV, the maximum field would be 10.538 kG. The dB/dt during acceleration is a half sine wave with a $33\frac{1}{3}$ Hz rate with a maximum dB/dt of 70.7 T/sec halfway through the acceleration cycle. The origin of the accelerator clock is defined as the time at which acceleration starts. Thus the flat-bottom field is defined to be on the negative side of $T = 0$, and the $33\frac{1}{3}$ Hz rate implies that the acceleration period is 15 msec.

We chose to operate the rf system on the fundamental frequency, or $h = 1$. This choice has two advantages: 1) having a single circulating bunch allows a slower risetime of the kicker system with no requirements on the decay of the kicker field, and 2) the rf can accommodate a larger momentum spread. The latter may be essential for controlling instabilities.

Bucket Area vs. rf Voltage Programming

The maximum $dB/dt = 70.7$ T/sec implies that the maximum energy gain/turn is 96.3 keV/turn, and if we assume a synchronous phase angle of the beam with respect to the rf wave of 30° , then the peak rf voltage becomes 192.6 kV. Here, we take 200 kV as the nominal peak voltage. At injection where the dB/dt is zero, an rf voltage of 11 kV would contain a $\Delta p/p$ of $\pm 5.4 \times 10^{-3}$. As shown in Section II.4, this momentum spread is just above that required for longitudinal stability.

In this section we will use what we define as a longitudinal emittance, $\epsilon = \Delta E \cdot \Delta t$, where ΔE is the maximum energy variation from the synchronous value, and Δt is 1/2 the total bunch duration, $T_r (\psi_2 - \psi_1)/2\pi$, with T_r the revolution period. The same units will be used for rf bucket acceptance, where the factors are the maximum values allowed at any given rf voltage.

This definition is useful although the product $\Delta E \cdot \Delta t$ is not directly related to the longitudinal phase space area unless the distribution in phase space is elliptical (bucket area much larger than beam area).

An ideal adiabatic trapping of a linac beam with $\pm \Delta E_L$ requires a minimum bucket (half) height $\Delta E = (\pi/2)\Delta E_L$. Thus for adiabatic capture, if we inject with a longitudinal emittance of 1.3 eV-sec, the bucket acceptance should be about 2.0 eV-sec or greater, and the beam emittance will grow to fill this acceptance during the capture process (although the injected phase space area will not have changed).

We have calculated the required rf voltage, bunch length, and synchronous phase angles for 2.4, 3.0, and 4.0 eV-sec. In all of these calculations, the longitudinal space charge effect is ignored because it could give no more than about a 10% effect at injection, and it is a minor problem at this juncture. Figure II.5-1 shows the rf voltage function, bunching factor, and the

synchronous phase angles with the bucket acceptance constrained to be 3.0 eV-sec. If the beam bunch is formed initially with an emittance of 2.0 eV-sec, it will not fill the entire bucket acceptance of 3 eV-sec. Some emittance growth might occur during acceleration, possibly increasing the longitudinal emittance to 2.4 eV-sec. Thus the rf proposed is quite adequate to accelerate the beam, likely without beam loss.

As discussed previously, the transverse space charge effect becomes maximum at some time during acceleration. This is due to the fact that although the $\beta^2 \gamma^3$ term in the space charge equation increases as the beam is being accelerated, the bunch length decreases as the synchronous phase angle increases, while the beam transverse emittance damps with $\beta\gamma$. Therefore, the net space charge effect is proportional to $B_f \cdot \beta\gamma^2$ during acceleration, where B_f is the ratio of bunch length to circumference. Figure II.5-2 shows time variations of $B_f \cdot \beta\gamma^2$ for $\epsilon = 2.4$ eV-sec and $\epsilon = 3.0$ eV-sec. There is a minimum value of this term at about $T = 1.5$ msec. Also shown in the figure is the variation of the factor B_f as a function of the longitudinal emittance at $T = 1.5$ msec. It is clear from this figure that if the longitudinal emittance is constrained to 2 eV-sec, the maximum allowed bunching factor is about 50%, while the bunching factor can be about 70% if the accelerator can operate with an ϵ of 3 eV-sec.

For the reasons stated above it is important to preserve a long bunch length through this region of maximum tune depression by space charge forces. This requirement implies having an appropriate longitudinal emittance, here taken to be 2.4 eV-sec, while we anticipate a beam emittance of 2.0 eV-sec after capture. This growth can be stimulated by a somewhat larger rf voltage than required for adiabatic capture (in which case a distortion occurs after a few synchrotron oscillation periods because of the

varying synchrotron oscillation frequencies within the beam) or by normal growth during acceleration (as experienced on the ANL-RCS) due to rf control errors, etc. Alternatively, the longitudinal emittance could be increased by injecting a larger energy spread, or by employing some second harmonic rf. The latter redistributes the beam in longitudinal phase space by decreasing the energy spread and increasing the bunch length without changing the phase space area (or longitudinal emittance) of the beam. Such bunch lengthening with application of a second harmonic rf voltage has been demonstrated on the ANL-RCS.

Basic Ideas of Bunch Length Adjustment

The length of a bunch in a rf bucket can be changed by adjustment of the bucket height which is a function of the rf voltage. This process can be described by the use of the Hamiltonian of the motion of particles within the bucket. The Hamiltonian can be expressed

$$H(\phi, W) = \frac{h\eta\omega_s}{2p_s R} W^2 + \frac{eV_o}{2\pi} [\cos\phi - \cos\phi_s + (\phi - \phi_s) \sin\phi_s] = \frac{h\eta\omega_s}{2p_s R} \hat{W}^2$$

where $W = \Delta E / \omega_s$ is the energy variable which is canonically conjugate to the position variable ϕ , \hat{W} is the peak value, h is the rf harmonic number, $\eta = 1/\gamma_t^2 - 1/\gamma^2$, ω_s is the angular rotation frequency of the synchronous particle, p_s is the momentum of the synchronous particle, R is the average radius of the machine, and V_o is the rf voltage. The parameters η , ω_s , p_s , W and V_o can vary with time and the Hamiltonian is therefore, in general, time-dependent. However, in most cases, the variation is slow enough that it can be neglected for the discussion of synchrotron motion over a few periods of oscillation. For this, we mean $\frac{dH}{dt} = \frac{\partial H}{\partial t} = 0$, and as we shall

see later, the synchrotron period of the machine is several kHz, therefore, changes of parameters over a few milliseconds satisfy this assumption.

From the Hamiltonian described above, the allowed range of ϕ can be derived by setting $W = 0$ and solving the transcendental equation. Under the given condition, the effect of an adiabatic variation of the rf voltage on the bunch length (the range of allowed ϕ) can be calculated using the same Hamiltonian and a different voltage.

Bunch Length Adjustment After Capture and Before Acceleration

The introduction of the injection field flat-bottom of 1.5 msec is to facilitate low-loss capture and preacceleration bunch manipulation. We assume that the injection period is about 0.5 msec and the remaining 1 msec of the flat-bottom, which is about 3 or 4 synchrotron periods, is sufficient to tailor the bunch in an optimum way. For the purposes of this discussion, we assume that the longitudinal emittance of the injected beam as defined earlier is 1.3 eV-sec, and that of the trapped beam is 2.0 eV-sec. The 2 eV-sec beam can be contained by a stationary bucket with an rf voltage of 25 kV. The angular range covered by this bucket is $\pm 180^\circ$, and the bunch fills the bucket.

An increase of the voltage would decrease the bunch length according to the Hamiltonian formalism described. The beam then would not fill the available rf bucket. An additional 7 kV would make the bunch length 83% of the bucket length. This is illustrated in Figure II.5-3 where the bucket acceptance is limited to 2.4 eV-sec for the first half of the cycle, and is allowed to grow in the last half in order to reduce the bunch length in preparation for extraction.

Bunch Length Adjustment for Extraction

The required bunch length for the utilization of the accelerator is some 200 nsec or less, and the revolution period of the particles in the synchrotron at full energy is 890 nsec. Under normal operating conditions the bunch length would be about 50% of the circumference at the end of the operating cycle. Therefore, rf manipulations will be required to reduce the beam bunch length to satisfy the goals of this program.

There are two methods to accomplish this bunch length adjustment: The rf voltage can be increased adiabatically, in which case the bunch length is in equilibrium with the rf voltage, or beam can be manipulated in longitudinal phase space in much the same manner as focusing beams in transverse phase space, commonly called beam optics. The latter requires extending the bunch length to a longer pulse duration followed by a very fast rf voltage increase and extraction at the time ($1/4$ synchrotron oscillation period) when the bunch length is a minimum.

Adiabatic Method

Slow increase of the rf voltage over several synchrotron periods would make the bucket area large, while the bunch obeys the Hamiltonian with $\epsilon = \Delta E \cdot \Delta t$ constant, so that it does not fill the bucket. Figure II.5-4A shows an example with $\epsilon = 2.4$ eV-sec and an rf voltage of 910 kV. In this case, the equilibrium bunch length is 200 nsec. If the final rf voltage were 200 kV, the equilibrium bunch length would be 300 nsec as shown in Figure II.5-4B. The very high voltage required at the end of the cycle to compress the beam to 200 nsec duration (at the baseline) is a direct result of the large longitudinal emittance used. As stated above a large emittance is necessary to avoid longitudinal instabilities and to maintain a long bunch

length during the early part of the acceleration cycle to alleviate the transverse space charge limit.

An rf voltage of 185 kV can contain the $\epsilon = 2.4$ eV-sec beam as shown in Fig. II.5-3. If we maintain 185 kV through the later part of the acceleration cycle rather than reducing it to maintain the same bucket area as \dot{B} decreases, the bunch length decreases as shown in the figure. The $\Delta p/p$ and the synchrotron frequency for this rf programming are shown in Fig. II.5-5. The minimum bunch length is about 300 nsec. This time duration, however, is the full extent of the beam. Even in this case, it would be likely that 90% of the beam would be contained within 200 nsec, a situation which might be adequate for some scientific experiments.

For a final rf voltage limited to 185 kV, Fig. II.5-6A shows the minimum bunch length achievable with adiabatic compression as a function of longitudinal emittance, ϵ . A 200 nsec bunch length can be achieved with 185 kV rf in a single bunch machine if ϵ were ~ 1 eV-sec. Although we have not studied the two-bunch machine, it is obvious that the problem of final bunch length would be much simpler with a second harmonic rf system. The longitudinal emittance per bunch would be one-half that of an $h = 1$ machine. The rf voltage needed to achieve a final bunch length of 200 nsec with various ϵ 's is shown in Fig. II.5-6B.

Fast Bunch Rotation

During the later part of the acceleration cycle the bunch length can be increased by adiabatically decreasing the rf voltage. This implies that the energy spread is reduced in the process. A sudden increase in the rf voltage, in a time short compared to a quarter of a synchrotron oscillation period, will cause the bunch to rotate in longitudinal phase space (with the bunch

length and energy spread no longer in equilibrium but the phase space area constant). After a quarter of a synchrotron period, the bunch would be upright as shown in Fig. II.5-7A. The energy spread is large at this time, the bunch length short, and these parameters will continue to oscillate as the beam rotates in phase space. Extraction should occur when the bunch length is a minimum. The minimum bunch length can be reduced by making the bunch longer initially (lower rf voltage) since $\Delta E \cdot \Delta t$ is a constant (for upright ellipses). Figure II.5-7B shows the initial rf voltage required as a function of longitudinal emittance such that a sudden increase of rf to 215 kV will result in a 200 nsec bunch length after a quarter of a synchrotron period ($\sim 110 \mu\text{sec}$). Thus it will be quite possible to achieve final beam duration times (base-to-base) of 200 nsec by this method with the equipment proposed.

II.6 INJECTION

Introduction

In this section we describe the methods and transport system by which the injected beam can be matched into the synchrotron in 6-dimensional phase space. We begin by summarizing the pertinent parameters of operating linacs. Assumptions used here are: H^- injection, 200 MeV linac energy, beam current pulse width of 500 μ sec, and an average pulse current of less than or equal to 50 mA. The latter two numbers, together with the revolution period at the injection field of 1.4×10^{-6} sec, determine the number of turns required to achieve 6.25×10^{13} protons per pulse.

Since the transverse acceptances of the synchrotron are $\epsilon_H = 500 \pi$ mm-mr and $\epsilon_V = 300 \pi$ mm-mr and, as shown later, the linac transverse emittances are $\epsilon_H = \epsilon_V = 5-10 \pi$ mm-mr. The ideal transverse stacking by charge exchange injection requires 1500 to 3000 turn injection. Injection would then result in a uniform charge distribution in transverse phase space. However, this would require a linac pulse length of 2-4 msec, and the requirement is unreasonable with regard to excitation of the synchrotron guide field and demand for linac power. Furthermore, uniform charge distribution can lead to beam instability and we prefer a hollow charge distribution in transverse phase space. The assumption that the linac pulse would be some 500 μ sec implies that the number of turns planned is about 350-400.

Survey of Operating Linacs

A few years ago, N. D. West¹³ surveyed operating proton linacs for the design consideration of the Rutherford-SNS. Here we summarize the work and

add new information.^{14,15} Since the new measurements are from the operating H^- linacs at Argonne and Fermilab, these are quite pertinent for the SNQ-SRA injector.

In his note, West points out that one has to interpret with caution the published results on linac emittance measurements. For example, all the LAMPF figures are for beams which have been collimated before injection into the linac, and for the Saclay data, there is some 20-30% discrepancy between the tabulated and graphical data presented by C. Curtis at the 1976 Proton Linear Accelerator Conference.¹⁶ He then discusses the ratio of emittances which contain 90% of the beam vs. those which contain 98% of the beam. After showing the ratio measurements at various energies and currents at different laboratories, he concluded that the ratio 2 is a reasonable assumption. Actual measurements vary from 1.5 to 2.7. This ratio is useful in two respects. If one is designing a beam scraper for the injection line transport system, then this is useful information. The other use of this ratio is in considering the ratio of the acceptance of the synchrotron to the linac emittance. By definition, the acceptance includes 100% of the beam, thus the emittance containing 98% of the beam is relevant.

Figures II.6-1 and -2 are from West's note plus new data. The definition of emittance used is $\epsilon = A/\pi$, and the normalized emittance means $\beta\gamma\epsilon$. It should be noted here that all data points except point (a), point (g) and new data points (x), (y) and (z) are for H^+ ions. The new measurements by Curtis et. al.,¹⁵ should replace the old data points (a) and (g) for H^- ions.

Parameters of the SNQ-SRA Injector System

Our recent measurements of the 50 MeV H^- beam showed $\beta\gamma\epsilon_H = 1.7 \pi \text{ mm-mr}$ and $\beta\gamma\epsilon_V = 2.4 \pi \text{ mm-mr}$ with a beam current of 6 mA. The Fermilab measurements

show that the 200 MeV, 35 mA H^- beam has $\beta\gamma\epsilon_H = 4.2 \pi \text{ mm-mr}$ and $\beta\gamma\epsilon_V = 4.1 \pi \text{ mm-mr}$. These points are superimposed on the West's Figures II.6-1 and 2. It should be noted again that these emittances are for 90% of the beam under consideration. Since the proposed injector of the SNQ-SRA is a 200 MeV linac with a pulse current of the order of 50 mA, it seems reasonable to assume that the injector would have beam properties similar to those of the Fermilab injector. Therefore, we assume the injected beam to have emittances in both transverse planes of $10 \pi \text{ mm-mr}$. If this emittance area were to contain 98% of the linac beam, the remaining 2% would be removed by halo scrapers in the transport line between the linac and ring. Even this transverse emittance is smaller than could be tolerated for 360-turn injection so that one could tailor the injected transverse charge distribution, and in particular, produce a hollow distribution in phase space.

A literature search shows that most proton injector linacs have an un-debunched beam energy spread, $\Delta T/T$, of about 0.5%.¹⁷ The debunched beam energy spread of the CERN 50 MeV Linac¹⁸ and the ANL 50 MeV Linac^{14,19} was found to be $\pm 150 \text{ KeV}$. If one assumes 0.5% energy spread of the SNQ-SRA injector, then $\Delta E = \Delta T = 1 \text{ MeV}$, or $\Delta p/p = 2.7 \times 10^{-3}$. The energy spread can probably be reduced about a factor of two by means of a debuncher. Thus one can expect to be able to reduce the injected beam momentum spread to $\Delta p/p = 1.35 \times 10^{-3}$ with a debuncher system. However, if we take the longitudinal acceptance, $\epsilon = \Delta E \cdot \Delta t$, of 1.3 eV-sec as discussed in Section II.5, we want to inject with $\Delta p/p$ of about 5×10^{-3} . Thus debunching should not be needed for reducing the momentum spread, but the debuncher may instead be useful to ramp the injected beam energy.

Vertical Injection Into the SNQ-SRA

The beam can be injected into the vertical plane by using a localized vertical bumped orbit in the upstream portion of one of the four long straight sections. The first of four vertical bumper magnets, B_1 , is located just downstream of the last bending magnet before the long straight section. As shown in Fig. II.6-3, the second bumper magnet, B_2 , and the H^- injection magnet are located between Q1 and the Q2, Q3 quadrupole doublet. The stripping foil (S in Fig. II.6-3) is 0.3 m downstream of Q3. Bumper magnets B_3 and B_4 restore the orbit before the next quadrupole.

The injection point is 32 cm above the midplane at the downstream end of Q1. The injection angle is 7.4° . The H^- ion beam is first bent upward by 154 mr (8.8°) in the injection magnet before merging with the maximum bumped orbit at the downstream end of the Q2, Q3 doublet. The opposite bends for H^- ions and protons in this doublet produce ~ 3 cm separation between the H^- injected beam and the maximum displaced circulating protons at the end of the septum injection magnet. The largest aperture requirement is in Q2 where the upper edge of the H^- beam is about 9 cm above the midplane. The separation between the maximum amplitude envelope of the circulating beam and the bottom of the stripper is 1 cm.

The squared amplitude of the vertical oscillations produced at the stripping foil is

$$A^2 = [\beta(Y'_O - Y'_B)^2 + \alpha(Y_O - Y_B)]^2 + [Y_O - Y_B]^2$$

where Y_O, Y'_O are the position and angle of the H^- ions, Y_B, Y'_B are the position and angle of the bumped orbit, and (β, α) are the lattice Twiss parameters, all at the azimuthal position of the stripper. If the two conditions

$$(1) \quad \beta Y'_0 + \alpha Y_0 = 0, \text{ and}$$

$$(2) \quad \beta Y'_B + \alpha Y_B = 0$$

are satisfied, the protons produced at the stripper are at the maximum of their betatron oscillations and unnecessary penetration of the foil by the circulating beam on subsequent revolutions is eliminated. The ratio of Y'_B to Y_B remains constant for all Y_B if the bumper ratios, $B1/B2/B3/B4 = 0.705/0.329/0.811/1.000$ shown in Fig. II.6-3, are maintained as Y_B is changed during injection. The stripper is located 0.3 m downstream from Q3 where $\beta = 3.784$, $\alpha = 0.3765$, $Y_0 = 4.98$ cm, and $Y'_0 = -4.96$ mr.

For the purpose of filling the vertical phase space, injection starts with the bumped orbit near the position shown in Fig. II.6-3 for the smallest desired vertical amplitude of the circulating protons. As the injection continues, the bumper magnet fields are reduced, pulling the smaller oscillations away from the foil, and at the same time injecting protons with larger vertical oscillation amplitudes. This process continues until the bumped orbit at the stripper location is 1 cm above the midplane. At this time, the maximum vertical oscillation amplitudes are being produced. The injection is stopped and the bumper magnets are turned off, pulling the whole beam away from the foil. The maximum deflections required in the four bumper magnets are shown in the figure. B4 has the largest values and requires a maximum field of 1.1 kG to produce the required 26 mr of bend.

Filling the entire 500×300 (mm-mr)² phase space with the desired density distribution is achievable in principal but requires more detailed study. We plan to inject for 500 μ sec (360 turns) using a constant magnetic field. For 6.25×10^{13} total protons, the injected H^- should be limited to about 20 mA. If the injected beam quality in both transverse planes is about 10π mm-mr, the total acceptance phase space will be about 25% occupied by

beam. This leaves considerable flexibility to tailor the injected charge distribution in phase space with the optimum distribution determined experimentally.

The previous paragraphs describe how the beam is injected from the vertical plane, missing the upstream quadrupoles and filling the vertical phase space area. If the stripper is moved radially outward by about 4 cm, additional horizontal bumper magnets can be used to fill the horizontal phase space. Since the vertical filling moves in one direction only (to minimize stripper heating by the circulating beam), the horizontal bumps should move the orbit so that the entire horizontal space is filled for each amplitude of vertical phase space. Therefore, the horizontal bumpers must oscillate as the vertical bumper magnet fields are slowly reduced.

In another method, the width of the stripping foil could be increased to about 4 cm and the beam moved horizontally across the stripper by means of an oscillating steering magnet placed 90° upstream (about 2.9 m upstream of Q2) in the H^- injection line. About 23 mr are required to move the beam by 4 cm at the stripper. Another alternative is to use a combination of steering magnets and horizontal orbit bumper magnets along with proper mismatching of the injected beam.

Matching in Longitudinal Phase Space

For trapping of injected beam by the rf system of the synchrotron, two options are available which are not mutually exclusive, and both can be installed at the beginning. One option is to capture adiabatically and to shape the bunch by using the flat-bottom feature of the ring magnet guide field, and the other is to use a chopper at the input to the linac and to tailor the bunches to be captured synchronously in a standing rf bucket of the

ring. A process similar to the latter one has been tried experimentally at the IPNS-RCS very recently and is described in Section II.10.

As noted in the first part of this section, based on the Fermilab 200 MeV linac experience, the expected linac momentum spread is too small by a factor of two, and we must devise a system by which overall momentum spread of the beam being injected can be increased and made adjustable so that any value desired is possible. One way to achieve this is to use a cavity which can modulate the energy and energy spread. An example of this is the debuncher system employed at the ANL-ZGS. Injecting a debunched beam of small energy spread with its central energy modulated during the injection period to match the bucket area of the ring has more flexibility than any other system.

In the adiabatic capture scheme, the procedure would be the following: Debunched linac beam starts to arrive in the ring at $t = -1.5$ msec which is defined as the time in the ring magnet excitation at which a 1.5 msec flat-bottom starts. The injection beam pulse is to be 500 μ sec long and has a pulse current of 20 mA. The accumulated current in the ring is then 7.1 A. During the injection period, a debuncher or some other energy modulating cavity should vary the central value of the beam energy being injected to make an overall energy spread of the accumulated beam to match the final rf bucket. While the injected beam is arriving in the ring, the ring rf cavity system should have very little or no voltage. At this time however, one must pay attention to and compensate for a transient beam loading phenomenon on the cavities. This low voltage condition should continue about 100 μ sec or so after the end of the injection pulse. The voltage should be increased gradually to about 25 kV in several hundred μ sec to complete the capture. At this time the synchrotron has a phase oscillation frequency of about 5 kHz. The injection field flat-bottom has another 500-800 μ sec left for performing a

bunch length adjustment by the voltage programming before the start of acceleration. With respect to the longitudinal phase space, the stacked beam before capture would have $\epsilon = \Delta E \cdot \Delta t = 1.3 \text{ eV-sec}$, and during the capture it would become about 2 eV-sec , for acceleration.

In the chopped beam synchronous transfer scheme, trapping of the beam can be achieved by the following method: The H^- beam injected into the linac can be chopped at the rf frequency (properly phased with the master oscillator of the rf system). As for the previous scheme, the injected beam energy would be ramped to match the desired momentum spread, and the time duration of the chopped pulses of the injected beam would vary depending on its energy to match a standing, non-accelerating bucket in the ring. It is estimated that on the average, the beam would be on about 70% of the time so that a linac current of 29 mA would be required to give the same circulating charge, 6.25×10^{13} protons in 500 μsec , as for 20 mA with adiabatic capture. This technique, while more complicated, could result in more efficient beam capture, and the probability of longitudinal phase space dilution in this case is less likely than the case of adiabatic capture. The initial rf voltage might be somewhat greater than 11 kV as proposed in Section II.5, and it would be properly programmed during the remainder of the flat-bottom field and into acceleration to optimally adjust the momentum spread and bunch length.

Comments and Implication for Other Hardware

A. Bunch Length Feedback System

In order to keep the bunch length as long as possible within limiting boundaries, it seems desirable to have a bunch-length feedback system which operates on the rf voltage. This is particularly important during

the early part of acceleration. A feedback system of this type was developed during the early 70's at the CPS, the AGS, and the ZGS.

B. Low Energy Chopper

Regardless of which method of capture one uses, the low energy chopper is a very useful device to have. It can be used for adjusting the synchrotron intensity without changing ion source or linac parameters. An adjustment of the source parameter usually introduces beam parameter changes.

C. Injection Transport Line

Energy modulation of the injected beam can either be achieved by modulation of the rf level in the linac tank or by an external cavity system, such as a debuncher. In order to transport the increased energy spread of the beam, the injection transport line should have provisions to accommodate $\Delta p/p = \pm 5 \times 10^{-3}$. If the energy modulation is accomplished by a debuncher-like cavity, then the transport elements downstream of this cavity must be achromatic, and if the modulation is done by the linac tank itself, then the whole transport system must be achromatic.

In addition, the injection transport line should contain elements to make scraping of the beam halo possible. It would also prove most desirable if the system designed to accomplish this were adjustable to limit the injected beam emittance to any desired value, including very small emittances for ring diagnostics and initial ring tuneup. With H^- beams, such a system can be relatively simple because of the possibility of stripping and then separating unwanted beam, avoiding the normal slit-scattering problem.

II.7. RF SYSTEM OPTIONS

Introduction

The rf requirements for the proposed accelerator were set forth in section II.5. The acceleration period will correspond to an effective magnet excitation rate of $33\frac{1}{3}$ Hz, leading to a peak rf voltage required of 200 kV/turn, and acceleration for 15 msec of the total cycle period of 20 msec. The average circulating current at injection, (200 MeV), will be 7.1 A. The peak current will increase after capture and bunching due to the decreased length of the bunch (to 70% of the circumference at 220 MeV, which occurs 1.5 msec into the acceleration cycle and is the time of maximum space charge detuning, and to 50% of the circumference at a later time), to the higher velocity during acceleration, and to the beam density distribution within the stable rf bucket. The peak beam current might then be about 20 A. In addition, the rf system must be capable of very fast response (in voltage changes) near the end of the acceleration cycle in order to provide fast manipulation of the bunch length prior to extraction.

During the early part of this study, it was felt that the cavities and rf system developed at Rutherford, England, for the SNS machine, properly modified for the frequency differences, would be quite adequate for the SNQ-SRA application. The SNS will have 6 cavities of 2 gaps each capable of developing 13.5 kV/gap for a total of 162 kV. On the SNQ-SRA there is room for 10 such cavities or 20 gaps capable of generating 270 kV, more than adequate for the design requirements. In addition, the SNS rf system will include a separate and independent amplifier for each cavity, whose purpose is

to supply to the cavity a current equal and opposite to that induced in the cavity by the beam. This feed-forward system is intended to compensate for the beam loading on the cavity.

It may be that the SNS-type cavities would operate satisfactorily on the SNQ-SRA. Nevertheless, there is very little experience on acceleration of such high currents and no experience on feed-forward techniques for compensation of beam loading in the cavities. The circulating current in the SNQ-SRA will be more than a factor of two higher than in the SNS (and the average power a factor of 3.5 higher) so that there is concern about the "Robinson Instability." The latter refers to a decrease in available bucket area when the power delivered to the beam becomes comparable to the power dissipated in the cavity.²⁰ The higher current makes this a more serious question here than for the SNS.

In addition, adequate voltage must be available to contain any longitudinal emittance growth during the acceleration cycle. Some growth is measured during the acceleration cycle on the ANL-RCS by studying losses as a function of rf voltage. It is seen in Fig. II.7-1 that the phase space area occupied by 85% of the beam (and other curves of 80% and 75%) increases during the acceleration period. This growth may be due to a number of factors including resistive wall effects and rf control errors. Nevertheless, it is a concern until it is understood and compensated.

Beam Loading and Compensation

For reasons described above, we believe it is prudent to consider other options to the compensation of beam loading effects. Three solutions have been proposed for beam loading at high beam currents. These are: 1) good active feedback systems to correct average voltage and phase²¹, 2) active, instantaneous compensation of the image current through the cavity by means of

feed-forward²², and 3) the use of a cathode-follower or low impedance cavity/driver system to provide instantaneous passive compensation of beam loading. Active, average voltage and phase feedback is presently used on almost all accelerator systems, and considerable understanding of the operational characteristics of these methods have been achieved over the years. As larger and larger beam currents are considered, however, the difficulties of compensating the beam loading increase, and it seems desirable in this study to look at options which seem: a) inherently more stable at high beam currents, and b) have not been studied as extensively. These options include the feed-forward systems presently in operation in the ISR and under construction at the SNS²², and the cathode-follower system being considered at the PSR²³.

In the feed-forward system, the bunch intensity and profile are sensed upstream and amplified in the final amplifier, which can either produce or absorb the wall currents associated with the beam. In the SNS system, the cavities have been designed with high capacitance and low inductance so that the beam induced voltages will be minimized, and stored energy in the cavity will be maximized. In order to accurately compensate for beam loading the beam amplification systems must be wideband with large dynamic range and low noise. As there will inevitably be some noise in the beam pickup and amplifiers and mismatches in the system, control of the active compensation may be troublesome, and may in fact have control problems similar to the systems actively controlling average phase.

The system presently proposed would use instantaneous, passive compensation of beam loading by means of a low impedance cathode-follower as a final amplifier. These systems, although studied extensively^{24,25,26} have not thus far been used on large synchrotrons, although they have been used on

other accelerators. The primary cause of this reluctance to use cathode-followers seems to be: 1) concern over possible oscillation modes of the final amplifier, 2) larger power consumption of a cathode-follower system, and 3) uncertainties about how higher harmonic components of the beam current are handled by the cathode-follower. As the proposed beam currents are raised, however, the comparative simplicity of the cathode-follower operation seems to offer increased reliability that the system will perform as designed, which seems to justify some penalty in initial and operating costs. It should also be noted that any system capable of stably handling large beam currents would be inefficient if the power ratio $P = \text{beam power}/\text{rf power}$ was significantly less than one.

Calculations by T. Hardek²⁷ of LANL and M. Puglizi²⁵ of BNL have shown that the tendency of the cathode-follower to oscillate can be eliminated by proper damping components, principally additional anode grid capacitance and resistance in the grid circuit.

Second Harmonic Acceleration

An additional option that should be considered is the addition of a second harmonic component to the accelerating voltage. Since the maximum acceleration voltage is required at $\dot{B} \text{ max}$, roughly halfway through the acceleration cycle, and space charge losses primarily occur early in the cycle (before the energy increase has significantly damped the emittances ϵ_x, ϵ_y), it is possible to use some of the rf cavities at the second harmonic early in the cycle to stretch out the bunch length (lowering the local beam density and increasing the effective space charge limit). Calculations have been done for the ANL-RCS which have shown that increases of 20-30% in beam intensity over the space charge limit of the accelerator are possible if the harmonic voltage is about 1/2-3/4 of the fundamental for the first 4 msec of the acceleration

cycle. After ~ 4 msec, the harmonic cavities are reduced to zero voltage, tuned to the fundamental and turned back on. Tests performed on the IPNS-RCS using a second harmonic component to spread the beam longitudinally have shown that: 1) bunch lengthening during the first part of the cycle does occur, 2) the bunches are stable during the capture and acceleration period, and 3) the transition from harmonic to fundamental operation is smooth if the harmonic cavity is turned off in a reasonably long time (i.e., $0.5 \text{ ms} \approx$ two synchrotron periods).²⁸

Second harmonic cavities could also be used to help with the fast bunch rotation at the end of the cycle. Bunch shortening is being accomplished by lowering the rf voltage until the bucket area is only slightly larger than the bunch, then rotating this large Δt , small ΔE bunch into a small Δt , large ΔE bunch using $1/4$ of a synchrotron oscillation with 200 kV of rf voltage. The bunch can be further shortened by using second harmonic components of the rf voltage to stretch the bunch out in time and lower its energy spread before the final bunch rotation. Bunch length increase of about a 30-40% (achieved on the ANL-RCS) would be accompanied by 30-40% reduction in energy spread and would eventually result in roughly this order of improvement in bunch length. Filamentation of long bunches probably provides the ultimate limit to the gains that can be achieved by harmonic bunch manipulation, but significant bunch length improvements should be possible.

II.8 EXTRACTION

Introduction

In this section we describe the extraction trajectories and the aperture requirements for the SNQ-SRA lattice, which was designed to facilitate vertical extraction. The advantage of vertical extraction over horizontal is that the beam size in the two planes can differ by a factor of 1.3. This implies a smaller increase in the apertures of certain quadrupoles through which the displaced beam being extracted must pass in order to enter the extraction channel. It also implies lower requirements on the extraction kicker magnet which must supply a displacement equal to the sum of the septum thickness and the full beam size at the septum. We have built into the design the capability of extracting a beam occupying the full aperture of the ring.

Extraction will require a fast kicker magnet located in a long straight section and a septum magnet located in the following straight section. These magnets are separated by a quadrupole pair, Q_2 and Q_3 , through which the beam being extracted must pass. The placement of the kicker and septum magnets are shown in Fig. II.8-1.

The computer output in this section has the x and y polarities and the x and y emittances reversed. This is due to the limitation of the program being used, so that vertical extraction is represented in the horizontal plane.

Extraction Orbits

The kicker straight section is 3.10 m long and the length of the septum straight section is 2.585 m. The kicker length is 2.5 m (preferably in 2 sections), and the septum length is 2.1 m (chosen here to be in 3 sections). A 700 G kicker magnet bends the 1.1 GeV proton beam by 29 mr, and an 8 kG

septum magnet bends the beam by 278 mr. These bends provide a separation of 60 cm between the central orbit and the central line of the beam being extracted at the Q1 quadrupole magnet. This distance is large enough for the extracted beam to clear the quadrupole magnet.

Figure II.8-2 shows the trajectory of the beam kicked by the 700 G kicker with the septum magnet not energized, and in Figure II.8-3 we show the trajectory of the beam with a 700 G kicker and 8 kG septum magnets. The circulating beam envelope along the straight section region is shown in Figure II.8-1 along with the specification of the lattice elements, while Figure II.8-4 shows the superposition of the acceptance envelope and that of the beam being extracted. All considerations given here are for the full-aperture extraction. The jump distance as a function of the kicker strength is shown in Figure II.8-5. A kicker field strength of about 600 G would be sufficient for extraction.

Aperture Requirements of Kicker and Septum

An estimate of the apertures for the kicker and septum can be made from Figures II.8-1 and II.8-4. Remembering that extraction is planned for the vertical direction, the current sheets of both the kicker and septum have to be located above and below. These figures show that a kicker aperture of 9 cm \times 9 cm for the first half of the magnet, and an aperture of 9 cm (H) and 11 cm (V) for the second half should be sufficient for extraction.

For the septum magnet composed of three sections the aperture of the first third can be about 15 cm (H) and 6 cm (V), the middle third could have aperture of 10 cm (H) and 8 cm (V), and the last third could be 8 cm (H) \times 10 cm (V). The beam size at the first third of the septum is just right to use a Lambertson-type septum.

Aperture Requirements for Q₂ and Q₃

The apertures of Q₂ and Q₃ quadrupoles must be considered in order to provide clearance for the beam being extracted. These are 16 cm for Q₂ and 14 cm for Q₃. Figure II.8-4 provides the vertical requirements for Q₂ and Q₃. These are 16 cm for Q₂ and 18 cm for Q₃.

II.9 VACUUM CONSIDERATIONS

Introduction

The purpose of this section is to insure that adequate vacuum can be achieved with realizable pumps within the lattice structure proposed and to identify the pumping speeds as they pertain to the pressure bump phenomena. Therefore, a preliminary analysis of the engineering requirements of the vacuum pumping system is carried out.

For reasons of stability against ion-proton and electron-proton interactions as discussed in Section II.4, and minimizing the circulating proton beam loss by interaction with the residual gas, the operating pressure must be $< 10^{-7}$ Torr. The appropriate vacuum parameters are:

vacuum chamber diameter	=	16 cm,
length of the chamber	=	24,000 cm,
volume of the chamber	=	5000 ℓ,
surface area	=	$1.2 \times 10^6 \text{ cm}^2$.

Fore-Pumps

Since the machine has a four-sector geometry, a roughing pump can be installed in each long straight section. These four roughing pumps are to reach a pressure of 10^{-3} Torr within a reasonable pumping time.

With a pumping speed of 8 ℓ/sec in four equally spaced stations, the time constant of the system is 0.0064/sec, and 10^{-3} Torr can be reached within an hour.

High Vacuum

Each sector has eleven cells, and the average cell length is 545 cm. A pump is located in each cell. We have 44 pumps in a periodic arrangement. The pertinent parameters are:

pump separation	$2L = 540 \text{ cm}, L = 270 \text{ cm}$
pumping speed	$2S = 500 \text{ l/sec}, S = 250 \text{ l/sec}$
outgassing rate	Metals or ceramic materials have outgassing rates of $10^{-8} - 10^{-14} \text{ Torr l/cm}^2 \text{ sec}$ depending on how the materials are prepared, according to literature. A goal of $10^{-10} \text{ Torr l/cm}^2 \text{ sec}$ is assumed. Then $q \equiv$ outgassing rate/unit length of chamber = $5 \times 10^{-9} \text{ Torr l/cm sec}$.
conductance at 20°C of N_2	$C = 12.3 D^3/L = 185 \text{ l/sec}$ and $c = CL = 5 \times 10^4 \text{ lcm/sec}$ $= 5 \times 10^7 \text{ cm}^4/\text{sec}$.

The pumping speed assumed of $S = 250 \text{ l/sec}$ is a good match to the conductance of 185 l/sec . This system should provide an ultimate pressure at the midpoint between pumps of 9×10^{-9} or $\sim 10^{-8} \text{ Torr}$. A rough estimate of the pumping time needed to reach 10^{-7} Torr is approximately 8.5 hours.

Pressure Bump Phenomenon

This effect, first discovered at the ISR²⁹, is caused by residual gas ions being accelerated into the vacuum chamber wall by the space charge potential of the circulating beam. The energetic residual gas ions liberate adsorbed molecules and raises the chamber pressure, which in turn results in more ions being generated. At a critical current, I_{crit} , the effect exceeds a threshold and leads to an uncontrolled pressure bump which destroys the beam.

It is reasonable to approximate the beam occupation time of the SNQ-SRA with a dc beam because the duty factor is 75%; i.e., the beam is in the

accelerator for 15 msec out of a cycle period of 20 msec. Furthermore, at a very high vacuum, the effective pumping speed is very low and could be comparable to the desorption yield.

What follows is a theoretical treatment of this phenomenon commonly found in the literature²⁹. The differential equation for the pressure in a vacuum tube as a function of time and position along the tube is solved where the desorption and readsorption of the residual gas on the wall is included.

If $n(x,t)$ represents the gas density, then $n(x,t)$ satisfies the following differential equations:

$$A \frac{\partial n}{\partial t} = a + c \frac{\partial^2 n}{\partial x^2} - w \frac{\partial \theta}{\partial t},$$

$$\frac{\partial \theta}{\partial t} = \left(\frac{\bar{v}s}{4} - \frac{\sigma}{ew} \eta I \right) \cdot n - \frac{\theta}{\tau}$$

with a boundary condition $C \frac{\partial n}{\partial x} \pm Sn = 0$ at location $x = \pm L$ where pumps of speed $2S$ are located. The parameters in the above equations are:

A = cross sectional area of the tube,

w = its perimeter,

a = wall degassing rate ($\text{cm}^{-1} \text{sec}^{-1}$),

C = conductance per unit length ($\text{cm}^4 \text{sec}^{-1}$),

s = sticking coefficient (in our case $\rightarrow 0$),

\bar{v} = mean thermal velocity of gas molecule,

σ = residual gas ionization cross section, $1.9 \times 10^{-18} \text{cm}^2$,

τ = sojourn time of adsorbed molecules in the wall (in our case $\rightarrow \infty$)

I = circulating current in Amp, and

η = net desorption coefficient of the wall (\equiv no. of gas molecules released/ion -1).

Above equation simplifies for our case as:

$$A \frac{\partial n}{\partial t} = a + C \frac{\partial^2 n}{\partial x^2} + \frac{\sigma}{e} I n n$$

The solution to this equation is:

$$n(x,t) + \sum_{v=1}^{\infty} \cos \lambda_v \left[\frac{C_v}{k_v} + \left(B_v - \frac{C_v}{k_v} \right) e^{-\frac{k_v t}{A}} \right]$$

where

$$C_v = \frac{2a \sin \lambda_v L}{\lambda_v \left[L + \frac{1}{2\lambda_v} \sin 2\lambda_v L \right]}$$

$$k_v = C \lambda_v^2 - \frac{\sigma}{e} I \eta$$

$$B_v = \frac{\int_{-L}^L n(x,0) \cos \lambda_v dx}{L + \frac{1}{2\lambda_v} \sin 2\lambda_v L}$$

$n(x,0)$ = initial density without the beam, and λ_v is the solution to the transcendental equation

$$\lambda \tan \lambda L = S/c.$$

For the vacuum system described above, λ_v would have the following values

$$\lambda_v = 3.5 \times 10^{-3}, 1.3 \times 10^{-2}, 2.4 \times 10^{-2}.$$

These values of λ_v assure that the series expansion of $n(x,t)$ converges, and the convergence occurs within a few terms (we take the first term only).

The equilibrium gas density in the presence of beam is:

$$n(x, \infty)_{I \neq 0} = \sum_{v=1}^{\infty} \cos \lambda_v \left(\frac{C_v}{k_v} \right) \approx \cos \left(\lambda_1 \frac{C_1}{k_1} \right).$$

In the absence of beam, $n(x, \infty)_{I=0}$ is equal to $n_0(x, 0)$ by definition, and

$$n_0(x, 0)_{I=0} = \sum_{v=1}^{\infty} \cos \lambda_v \left(\frac{C_v}{C \lambda_v^2} \right) \approx \cos \left(\lambda_1 \frac{C_1}{C \lambda_1^2} \right).$$

The ratio of pressure between the case in which the equilibrium has been reached with the beam and the initial pressure without the beam is the ratio of the above two density functions. Thus

$$\frac{p}{p_o} = \frac{c_1^2}{k_1} \quad \text{or} \quad p = p_o / \left(\frac{c\lambda_1^2 - \frac{\sigma}{e} \eta I}{c\lambda_1^2} \right) ,$$

$$p = p_o / \left(1 - \frac{\sigma \eta I}{e c \lambda_1^2} \right) .$$

The equilibrium pressure becomes infinite for a critical current

$$I_{\text{crit}} = \frac{e c \lambda_1^2}{\sigma \eta} .$$

The value of λ , for the SNQ is $3.5 \times 10^{-3}(\text{cm}^{-1})$; therefore,

$$\eta I_{\text{crit}} = \frac{e c \lambda_1^2}{\sigma} ,$$

$$= 49 \text{ Amperes.}$$

Thus in order to prevent the pressure runaway, the effective stored current must be less than I_{crit} . The only unknown quantity in our discussion is the net desorption coefficient, η , for the chamber material, which also depends on the kinetic energy of the bombarding ions. The estimate of the kinetic energy is an average of ≤ 500 eV. The value of η for well-prepared stainless steel has been shown to be less than 0.05 with ion energy of 1 keV or less. Since the effective stored beam current in the SNQ-SRA is about 10 A, the above criterion shows that we can have values of η up to 4 or 5. The value of η is not well known for ceramic.

II.10 BEAM LOSS

Introduction

The proposed SNQ-SRA would operate with the highest current and highest number of protons/sec or per pulse of any proton synchrotron in this energy range. Since designed proton flux is 3.1×10^{15} protons/sec, a few percent loss is equivalent to the entire proton flux being accelerated by a conventional slow cycling proton synchrotron. Slow cycling synchrotrons can usually tolerate as much as 50% loss.³⁰ We believe that the most efficient proton synchrotron in operation is that of the ANL-RCS which operates at about 2×10^{12} protons per pulse with a 30 Hz repetition rate (6×10^{13} protons/sec). The ANL-RCS routinely operates with better than 90% efficiency (the efficiency is defined to be the ratio of the proton current hitting the neutron production target measured by a full energy Faraday Cup and the injection linac output current measured by a 50 MeV Faraday Cup). Although the number of protons per pulse in the RCS is a factor of 30 less than that of the proposed SNQ-SRA, the circulating current in the RCS is smaller by only a factor of five due to the sizes of the machines; therefore, it seems reasonable to compare and to extrapolate the performance of the RCS to that of the SNQ-SRA since any predictive calculation of performances of an accelerator by means of analytical or simulative method will only be as good as the assumptions used. The goal is to design, as well as possible, a no-loss accelerator with the provision to catch in a controlled manner those losses that might be encountered in a real machine.

ANL-RCS Beam Loss Discussions

Measurements have shown that the injected beam of the RCS has an instantaneous $\Delta p/p$ of $\pm 0.155\%$ in which is contained 90% of the beam,³¹ and also the linac has a natural energy ramp of ~ 100 keV/100 μ sec.³² The linac pulse is injected into the machine for about 50 μ sec, approximately 500 μ sec before the minimum field of the ring magnets. These three sources contribute to the energy spread of the injected beam. First, the natural spread in the linac of $\Delta p/p$ of $\pm 0.155\%$, or $\Delta E = \pm 152$ keV, contains 90% of the beam. The energy spread is 1.7 times larger for 98% of the beam. Another 50 keV is added to ΔE because of the energy ramp on the linac, and finally another 50 keV is added due to the \dot{B} of the ring magnet. The total energy spread is ± 358 keV. The rotation frequency at injection is 2.2 MHz. If we define the longitudinal emittance to be $\Delta E \cdot \Delta t$ where ΔE and Δt are half widths at the baseline, ϵ_L is 358 keV \cdot 227 nsec = 0.08 eV \cdot sec. The rf voltage during injection is about 1.9 kV. This voltage is on for about an extra 100 μ sec after injection is completed and is then raised very rapidly as shown in Fig. II.10-1.

A close inspection of Fig. II.10-1 near $t = 0$ shows that 1.9 kV rf voltage corresponds to a longitudinal emittance of 0.09 eV-sec which is in good agreement with the value of 0.08 eV-sec discussed earlier. Before acceleration starts, the voltage is raised to about 8 kV which corresponds to a bucket acceptance of 0.19 eV-sec at $t = 0$, roughly a factor of two enlargement in longitudinal phase space. The expected theoretical enlargement is $\pi/2$ if ideal adiabatic trapping process has taken place. The factor 2 instead of 1.7 is reasonable since an ideal capture is difficult due to the rapidly changing magnetic field, and the very short time to do any other beam manipulations.

The RCS has an available rf voltage limit of about 20 kV, and because of this fact, the bucket acceptance cannot be maintained to 0.19 eV-sec. Inspection of Fig. II.10-1 near $t = 0$ to 6 msec shows the bucket acceptance decrease from 0.19 eV-sec to 0.15 eV-sec. Actual beam loss occurs during this period with a loss pattern similar to the decrease in bucket area. If the voltage at $t = 0$ is lowered then the capture efficiency decreases, but the acceleration efficiency becomes constant throughout the period. Although the decrease in the bucket area is about 21%, the observed loss is only about 5-10%. This may be due to an uneven proton density distribution within phase space. In particular the density around the periphery of phase space might be below average. This non-uniformity of distribution has been shown in a Monte Carlo calculation.³³

The RCS would need a peak voltage of 25 kV to maintain a bucket acceptance of 0.19 eV-sec. An independent calculation using a Monte Carlo method also showed that the RCS would need 25 kV to capture and to accelerate 99% of the injected beam. The nature of these improvements and the related calculation can be used to guide the injection philosophy on the SNQ-SRA.

A simple accelerator experiment was performed with the RCS to study the proposed injection scheme of the SNQ-SRA even though many of the hardware provisions which the SNQ-SRA would have are lacking. Chopped beam synchronous injection was studied in a rising field (since the ANL-RCS does not have the flat-bottom provision). A 750 keV chopper controlled by the RCS rf master oscillator was used to chop the preinjector beam to facilitate synchronous injection. A standing rf bucket in the ring had a large bucket area to trap both incoming beam and the beam already in the bucket. The latter, of course, was constantly accelerated due to the ramping guide field. A beam chopped to 70% of its unchopped length was accelerated to full energy with as high an

intensity as achieved with un-chopped injection. This result shows that the 30% portion of the beam that was normally lost during capture and acceleration with these conditions was eliminated at 750 keV. A full simulation was limited by the hardware, but encouraging results have been achieved, even though injection was done on a rising field. Further study is planned.

Application to the SNQ-SRA

The goal of the proposed system is to achieve as low a beam loss as possible. A phase ramped rf cavity system in the injection line is proposed to control and match the longitudinal phase space of the linac to that of the ring rf system. A constant injection field would allow either adiabatic capture or chopped beam synchronous injection without introducing too large an energy spread, and at the same time enable manipulation of the bunch length before beginning acceleration. The injected beam would have a longitudinal emittance $\epsilon = \Delta E \cdot \Delta t$, of 1.3 eV-sec, and the proposed rf system should be able to handle $\epsilon = 3$ eV-sec.

There would be a beam scraper system to handle unexpected beam loss in a controlled manner. A description of this idea is the subject of the following section.

Beam Scrapers

Ideal locations for beam scrapers are the points along the lattice where the β and η functions are maximal so that the particles being lost have large displacement from the other particles. The η function plays a more dominant role in the case of acceleration because the particles being lost are most likely to be out of the rf bucket and at the same time the other particles which are synchronous to the acceleration have gained energy. Thus the particles being lost would have lower energy orbits with respect to the

synchronous orbit. This implies that the first order scraping could be done in the radial plane and inward direction.

An additional consideration that could be added to the above is the variation of the β function with momentum spread (Δp) at a given momentum (p_0). An ideal point in the lattice is a place where the η function is large, the β function is large, and $\beta(p_0 + \Delta p) > \beta(p_0)$. This condition assures that low energy particles being lost would have large displacement at this point, and that the point is suitable to place the beam scraper.

Inspection of the β and η functions of this SNQ-SRA lattice shown in Fig. II.1-2 indicate that the midpoint of the sector, which is the beginning point of the figure, has the largest η function and somewhat large β_x function. Figure II.1-3 shows the envelope function which makes use of both the β and η functions. This figure shows that the horizontal beam size is largest at the point indicated above. A lower momentum of -1.5% would contribute about 2 cm to the horizontal beam size at this point.

Figure II.4-2 shows the variation of the β and η functions at the designated scraper point with respect to off-momentum deviation, $\frac{\Delta p}{p}$. The variation of the horizontal β function and the η function with respect to $\Delta p/p$ is almost constant through $\Delta p/p$ of $\pm 2.0\%$. On the other hand the vertical β function at this point is about a factor of 1.5 times larger than that for the on-momentum particles when the momentum deviation is - 2.0%. The vertical size of a beam with 2% lower momentum will be 23% larger at this point compared to the vertical size for on-momentum particles.

This would indicate that the midpoint of each superperiod is a suitable location to install the scraper system to catch the beam loss in both vertical and horizontal planes. With four-fold symmetry of the machine, there would be four such systems.

The following summary can be made for the scrapers: After injection, provided there are no beam instabilities and the rf frequency is properly controlled, particles would be lost either because they were untrapped by the rf bucket or spilled out of the bucket. Thus, by the time these particles reach the chamber wall, their momenta would be substantially lower than that of the particles being accelerated. Therefore, these particles would hit the inside walls of the chamber. Linear beam dynamics implies that these particles can be caught at a place where the radial β and η functions are largest. However, since the particles being lost in this manner would necessarily have a larger $\Delta p/p$ compared to those being accelerated, it is prudent to consider the non-linear beam dynamics. In the radial direction there would be little or no effect, and in the vertical direction the particles being lost can be caught by a vertical scraper utilizing the variation of β_y with respect to $\Delta p/p$.

This study is by no means exhaustive, and as the machine parameters are decided, the search for the optimum scraper location should continue using the method proposed here together with a computer simulation such as TURTLE.

References for Section II

1. Y. Cho, "V-Lattices for SNQ-SRA," AAD-N-14 (September 1982).
2. Y. Cho, "Transverse Space Charge Limits in the SNQ-SRA," AAD-N-9 (August 1982).
3. J. P. Gouber, "Control of Betatron Frequencies and Resonance Excitation in the ISR," Proceedings of 4th All-Union National Conference on Particle Accelerators (Moscow, 1975).
4. G. Guignard, "A General Treatment of Resonances in Accelerators," CERN 78-11, (November 1978).
5. Y. Cho and G. Wustefeld, "Transverse Stabilization of Bunched Beam," AAD-N-28 (December 1982).
6. H. Wiedemann, "Users Guide for PATRICIA," PEP-TM 230 (February 1981).
7. G. Wüstefeld, "Longitudinal Coupling Impedance," AAD-N-6 (August 1982). G. Wüstefeld, "Keil-Schnell Criterion," AAD-N-18 (November 1982). G. Wüstefeld, "Risetime of Longitudinal Resistive Wall Instability," AAD-N-19 (November 1982).
8. G. Wustefeld, "Landau Damping to Get Transverse Stability," AAD-N-31 (December 1982).
9. F. J. Sacherer, "Transverse Bunched Beam Instabilities-Theory," Proceedings of the IXth International Conference on High Energy Accelerators, 347 (Stanford, 1974).
10. G. Wustefeld, "Coherent Instability due to Ions in the Residual Gas, : AAD-N-27 (November 1982).
11. Y. Cho and G. Wustefeld, "Some Aspects of Vacuum Considerations for the SNQ-SRA," AAD-N-32 (December 1982).
12. H. Schönauer and B. Notter, "Electron-Proton Instability in the SPS", Spring Study on Accelerator Theory (CERN, 1972).
13. N. D. West, "Injector Beam Emittance and Beam Collimation," SNS/INJ/N3/78 (June 1978).
14. Y. Cho et al, "Determination of Transverse Phase-Space and Momentum Error from Size Measurements Along the 50 MeV H⁻ RCS Injectin Line," IEEE Transaction on Nuclear Science NS28, 3046 (1981).
15. C. D. Curtis et al, "Linac H⁻-Beam Operatin and Use at Fermilab," IEEE, Transaction on Nuclear Science NS-26, 3760 (1979).

16. C. D. Curtis, "Ion Source and Injector Development" Proceedings of the 1976 Proton Linear Acceleration Conference, 179 (Chalk River).
17. See Catalogue of High Energy Accelerators in Proceedings of IXth International Conference on High Energy Accelerator (1974, Stanford).
18. E. Boltezar et al, "The New CERN 50-MeV Linac," Proceedings of the 1979 Linear Accelerator Conference, 66 (1979, Brookhaven).
19. E. F. Parker, "Recent Measurement of the ZGS Injector Beam Characteristics", Proceedings of the 1972 Linear Accelerator Conference, 63 (1972, Los Alamos).
20. J. Griffin, "Phys. of High Energy Particle Accelerators," R. A. Carrigan, F. Huson, M. Month (Ed.), Amer. Inst. Phys. Conf. Proc. No. 87 (1982) p. 564.
21. D. J. Bell, P. A. Cook, N. Munro, T. E. Swain, IEEE Trans. Nucl. Sci., NS-29 (1982) p. 1415.
22. D. Boardman (Ed.), "Spallation Neutron Source: Description of Accelerator and Target," Rutherford Appleton Laboratory Report RL 82-006 (1982).
23. T. Hardek, "2.8 MHz Buncher Proposal," PSR Technical Note 102 LANL (1982).
24. "IPNS - A National Facility for Condensed Matter Research," Argonne National Laboratory Report ANL-78-88 (1978).
25. A. Luccio and M. Puglisi, IEEE Trans. on Nucl. Sci., NS-28 (1981) p. 2893.
26. M. Puglisi and M. Cornacchia, IEEE Trans. on Nucl. Sci., NS-28 (1981) p. 2729.
27. T. Hardek, Los Alamos National Laboratory, private communication (1982).
28. J. Norem, F. Brandeberry, and A. Rauchas, submitted to the 1983 Particle Accelerator Conference, Sante Fe, NM.
29. See for example, R. Calden et al., "Vacuum Conditions for Proton Storage Rings", The IXth International Conference on H. E. Accelerators (Stanford, 1974); G. Spalek, "PSR Beam Induced Desorption", PSR Tech Note-19 (Los Alamos, 1979).
30. The following synchrotrons are known to operate with 50% or more losses: ZGS, AGS, and PSB. These are all H^+ injection machines.
31. Y. Cho, E. A. Crosbie and H. Takeda, "Determination of Transverse Phase-Space and Momentum Error from Size Measurements along the 50 MeV H^- RCS Injection Line," IEEE Transactions on Nuclear Science, NS-28, 3046 (1981).

32. Y. Cho, ZGS Experiment Notes (Feb. 1978).
33. Y. Cho, C. W. Potts, A. V. Raugas, S. A. Shin and H. Takeda, "Study of the RF Capture Process in the Argonne Rapid Cycling Synchrotron," IEEE Transactions on Nuclear Science, NS-28, 3040 (1981).

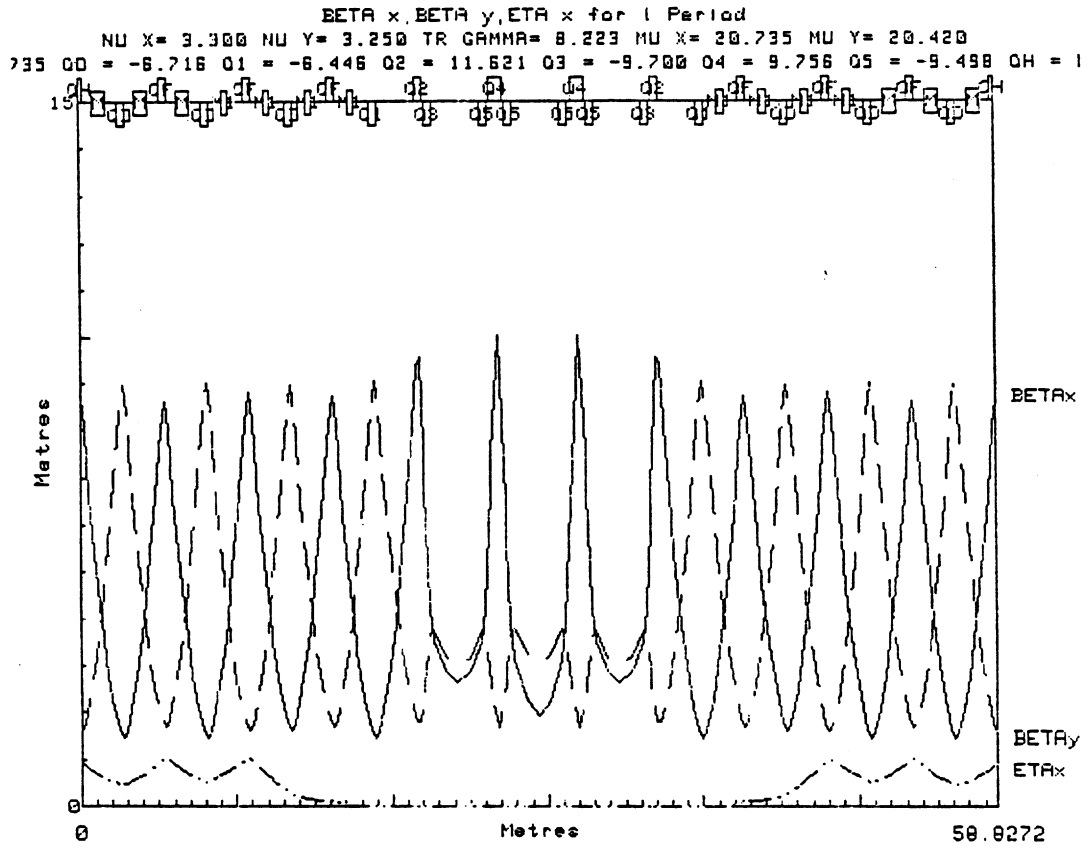


Fig. II.1-1

BEAM RIGIDITY=6.03200 X,Y EMITT=50.0000,30.0000 PI CM-MR,DPP=.01000													COMMANDS				
ELEMENTS: 17 ELEMENT DEFINITIONS													BEAM				
NAM	TYPE	VAR	LEN,ANG	B,B'	N,GAP	D4	DRFT	0.0	.39056	0.0000	0.000	0.000	ELEMENTS				
QF	QUAD	1.2	.50000	6.0268	0.000	DX	DRFT	0.0	.87200	0.0000	0.000	0.000	LATTICE				
D1	DRFT	0.0	.64700	0.0000	0.000	M1	BEND	0.0	.45000	1.0538	0.000	0.000	PERIODS				
E	EDGE	0.0	2.0000	1.0538	0.000	Q4	QUAD	0.0	.85000	9.6691	0.000	0.000	FIT				
M	BEND	0.0	.90000	1.0538	0.000	QH	QUAD	1.2	.25000	6.0268	0.000	0.000	TRANSPOR				
QD	QUAD	2.2	.50000	-6.628	0.000	Q5	QUAD	0.0	.50000	-9.049	0.000	0.000	INSERT				
DM	DRFT	0.0	.90000	0.0000	0.000								MATRIX				
Q1	QUAD	0.0	.50000	-6.370	0.000								GO				
Q2	QUAD	0.0	.50000	11.511	0.000								CYCLE				
Q3	QUAD	0.0	.50000	-9.700	0.000								GRAPH				
D2	DRFT	0.0	1.5500	0.0000	0.000								ITERATE				
D3	DRFT	0.0	.15000	0.0000	0.000								HELP				
LATTICE: 45 ELEMENTS: QH D1 M D1 QD D1 M D1 QF D1 M D1													SAVE				
QD	DX	M1	DX	QF	DX	M1	DX	QD	DX	M1	DX	QF	DX	M1	DX	Q1	RECALL
D1	DM	D1	D4	Q2	D3	Q3	D2	D2	Q5	D3	Q4	D3	Q5	D2	RFL		QUIT
PERIODS FIT: NU X =2.380,NU Y =3.300,													NEW CASE				
4													PRINT				

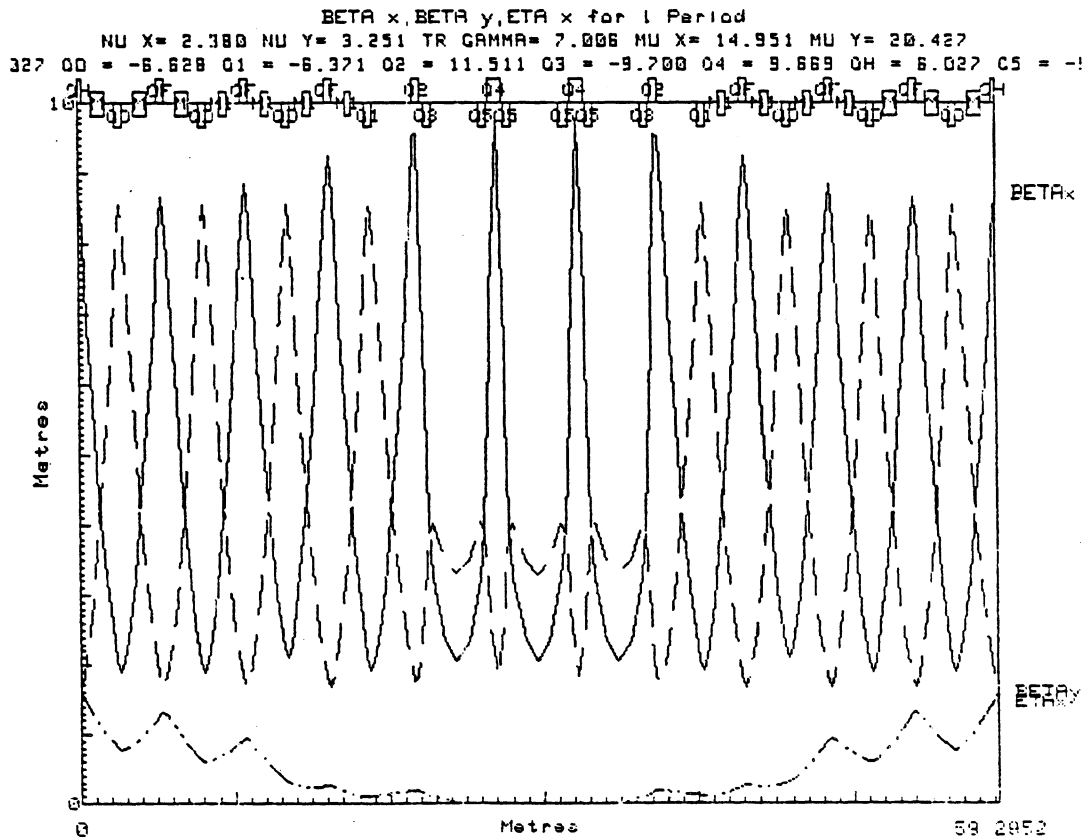


Fig. II.1-2

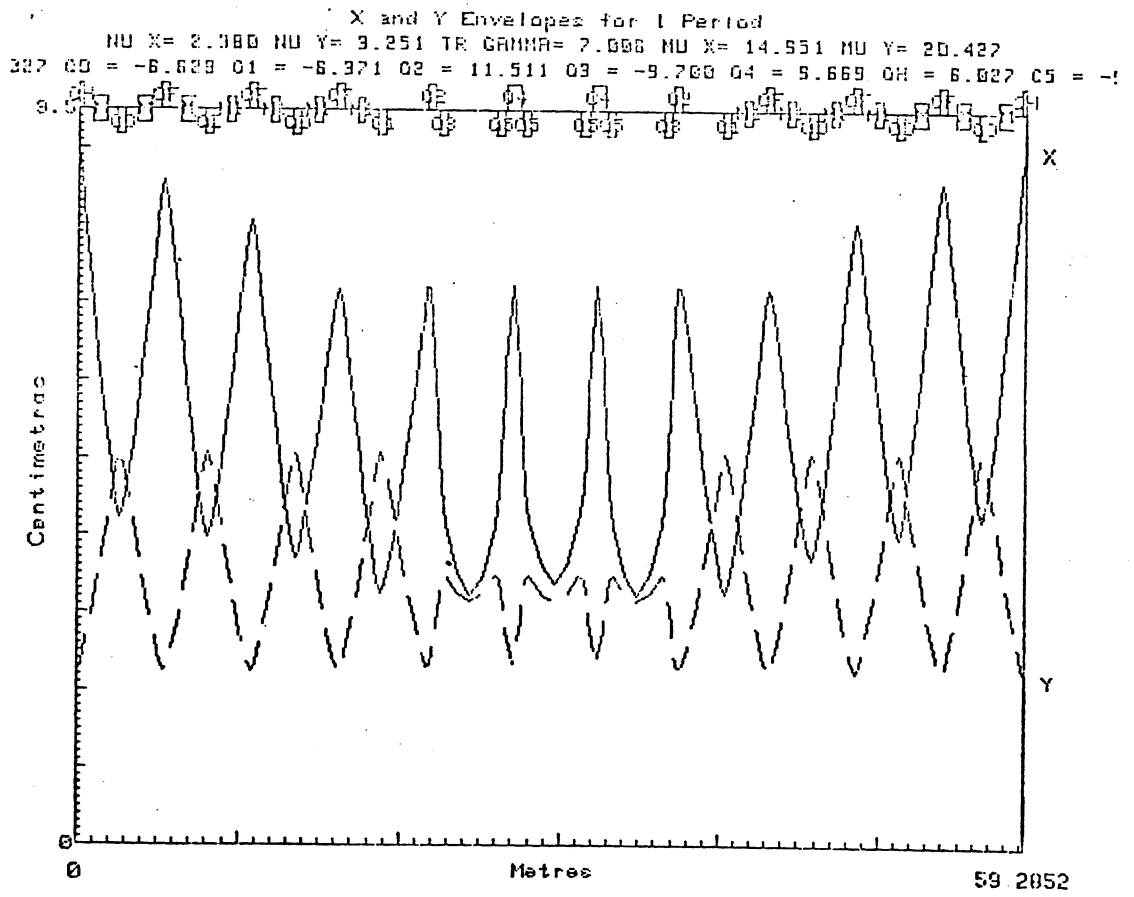


Fig. II.1-3

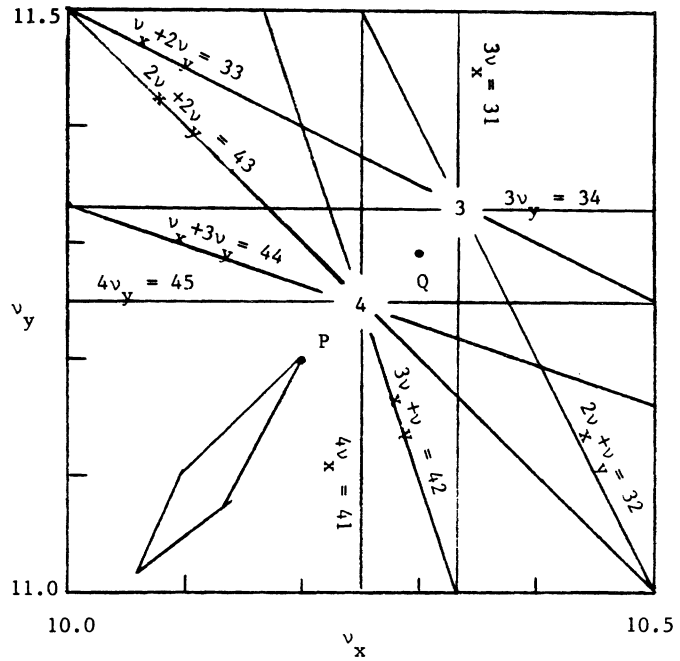


Fig. II.3-1 Betatron Tune Space

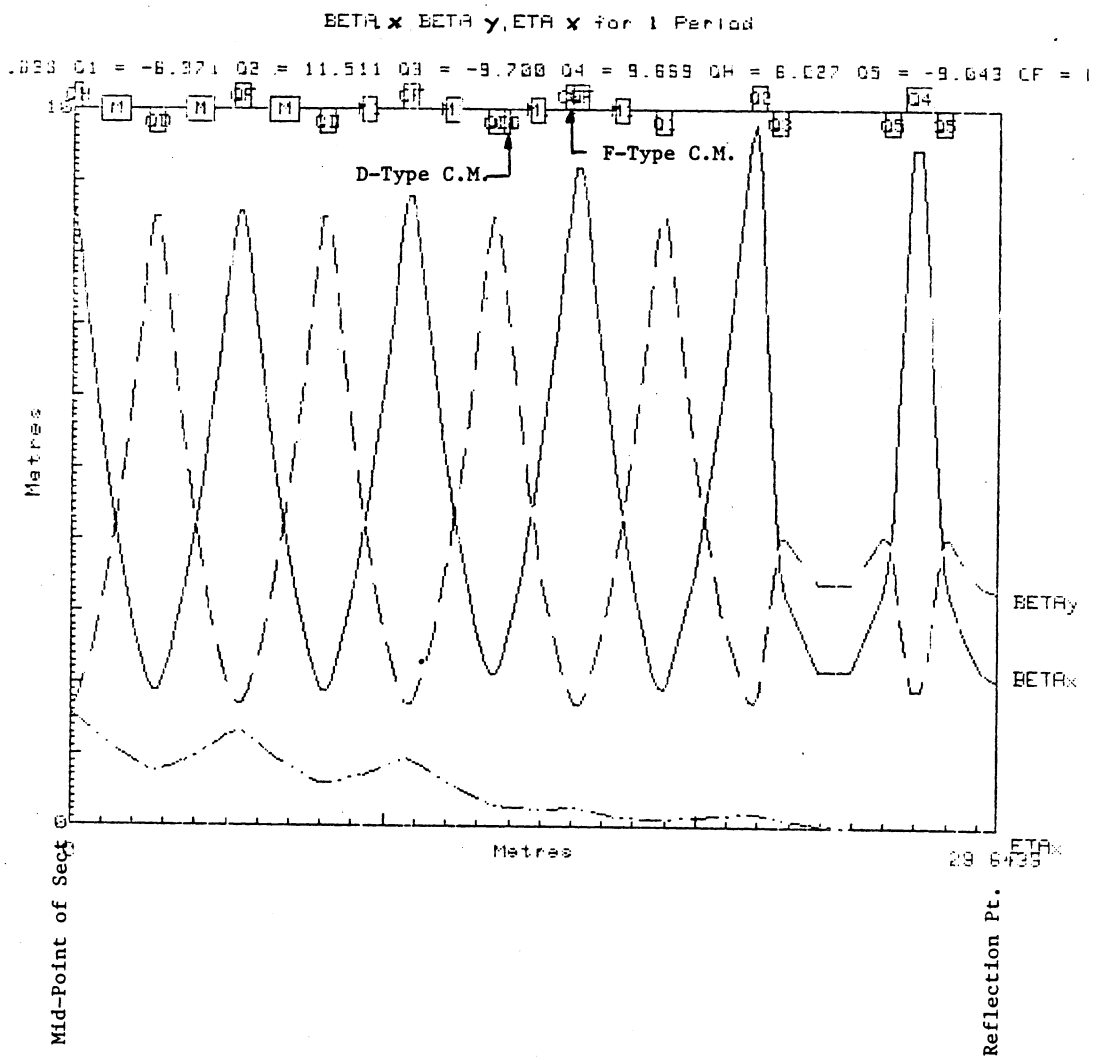


Fig. II.4-1

$\beta(\Delta p/p) / \beta(\Delta p/p=0)$ at Mid-point of sector

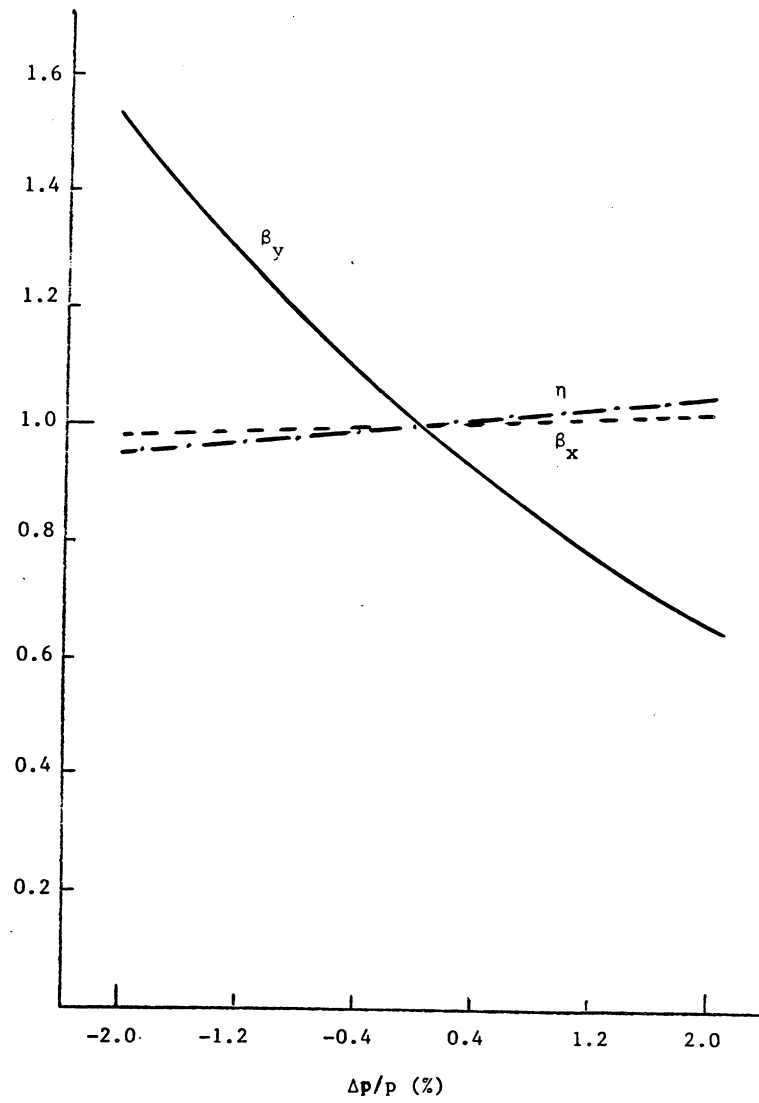


Fig. II.4-2

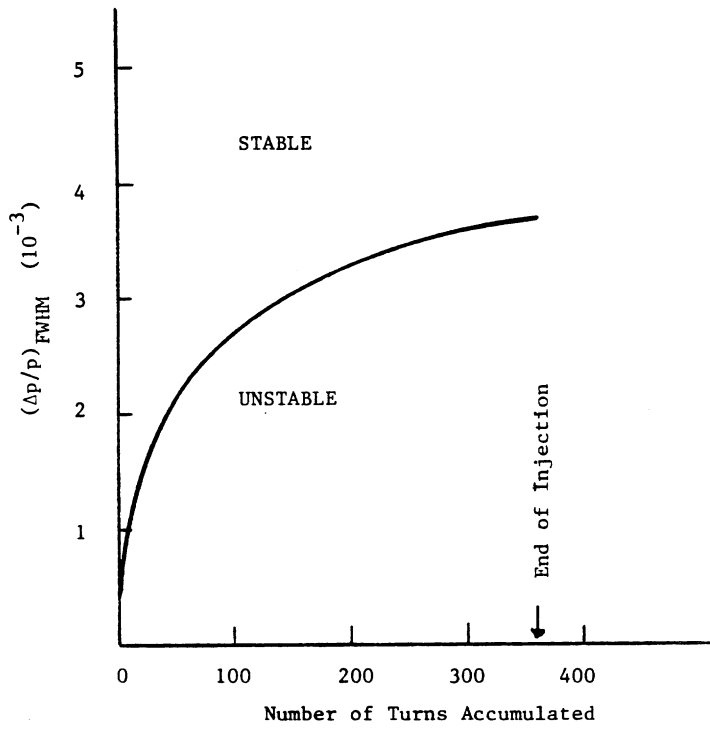


Fig. II.4-3 Threshold Momentum Spread for Instability During Injection

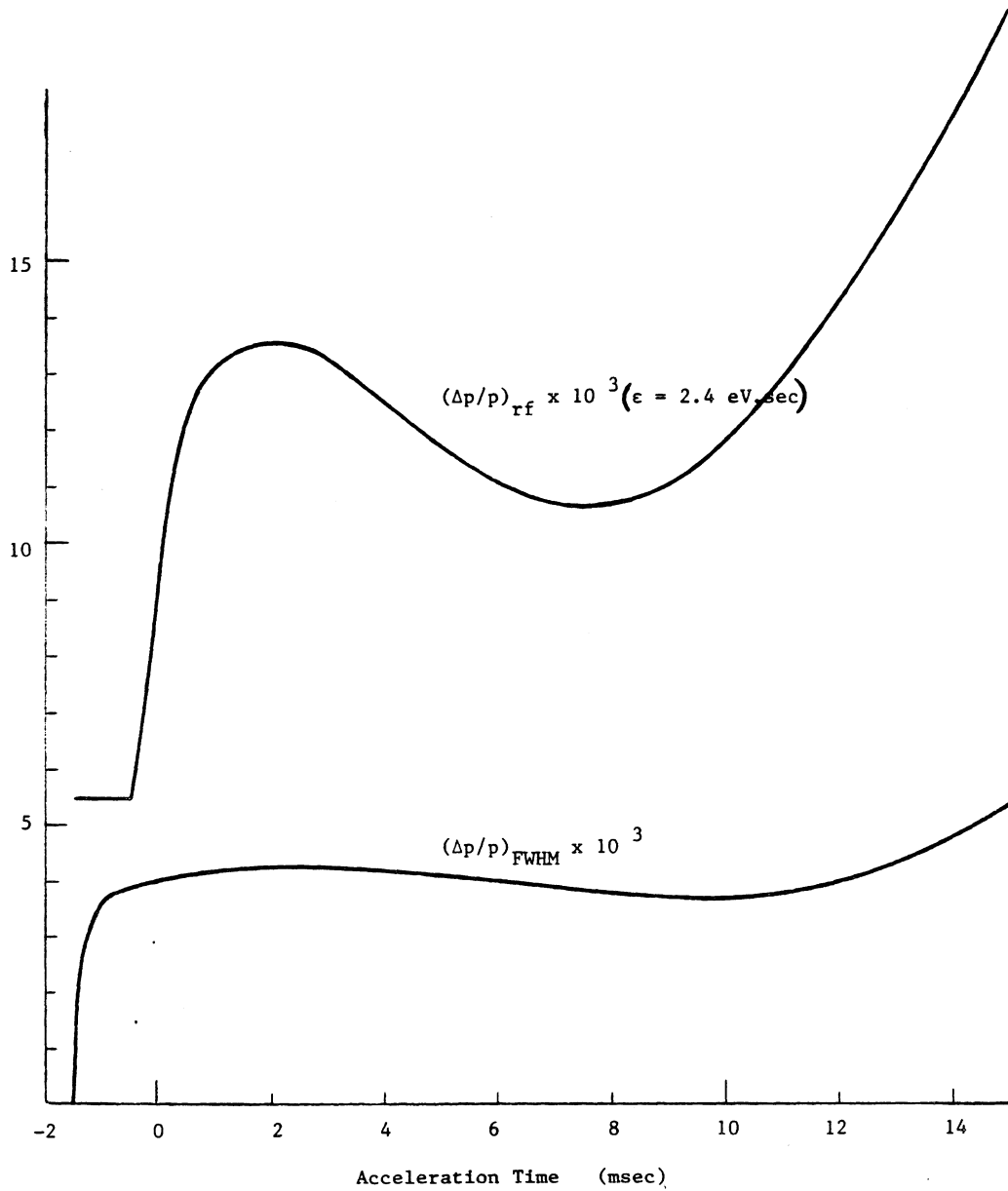


Fig. II.4-4 Threshold Momentum Spread for Instability and Beam Bunch Half-Height

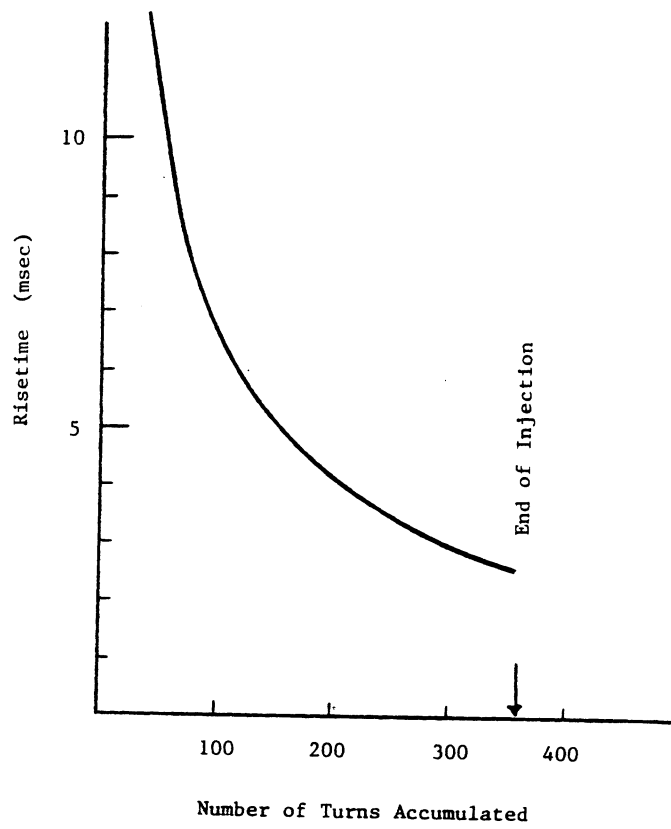


Fig. II.4-5 Risetime of Instability During Injection for $\Delta p/p=0$ Beam

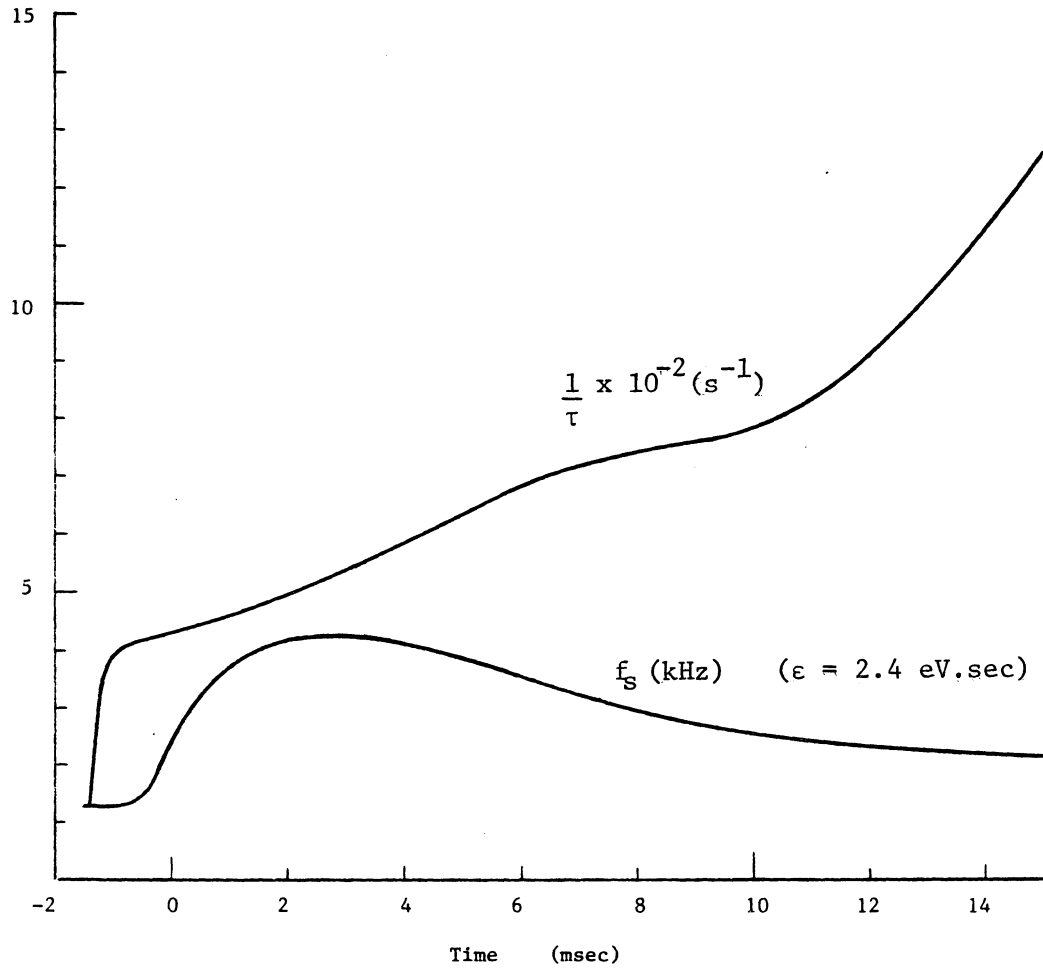


Fig. II.4-6 Growth Rate of Instability for $\Delta p/p = 0$ Beam and Synchrotron Frequency During Acceleration Period

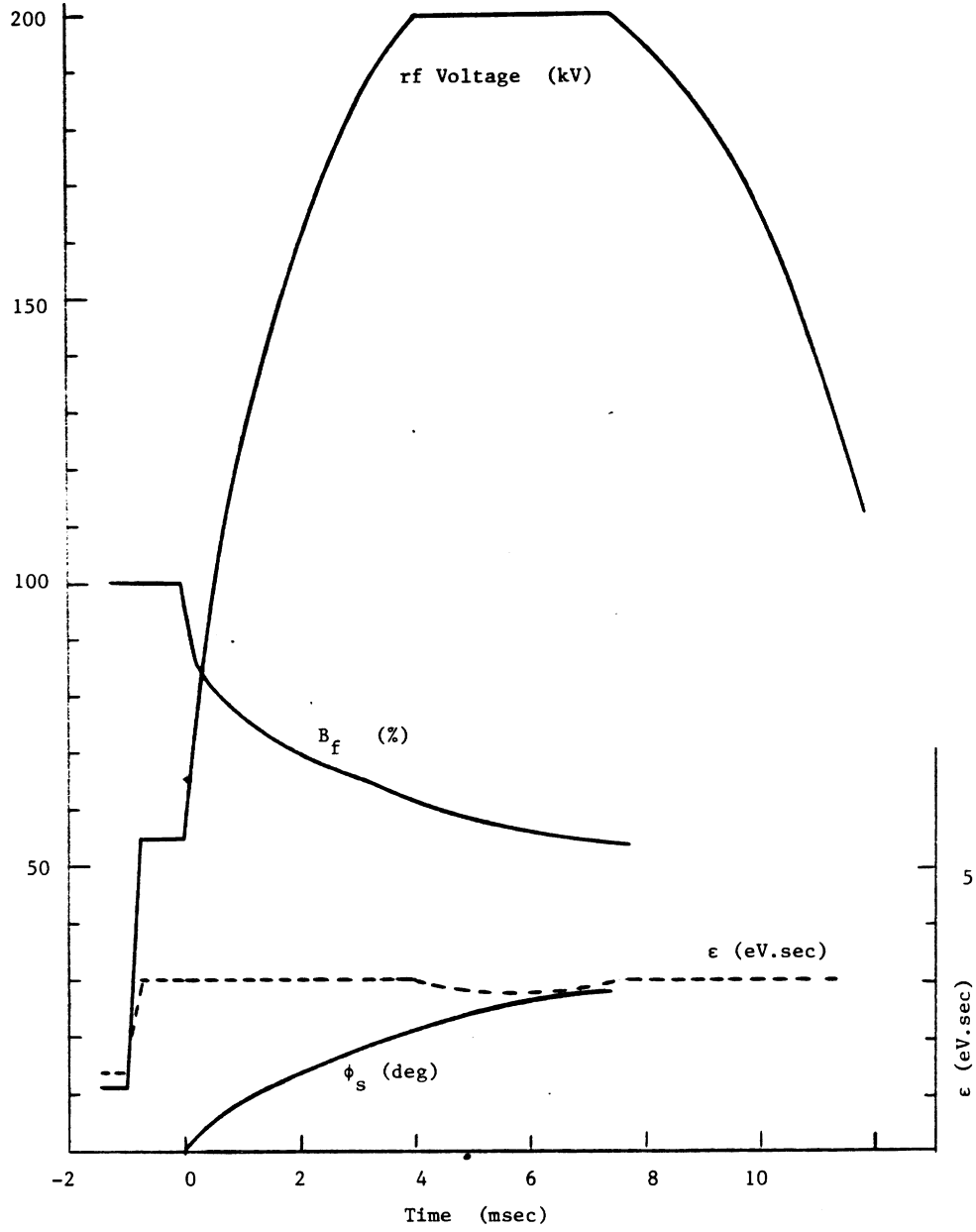


Fig. II.5-1 Acceleration Parameters

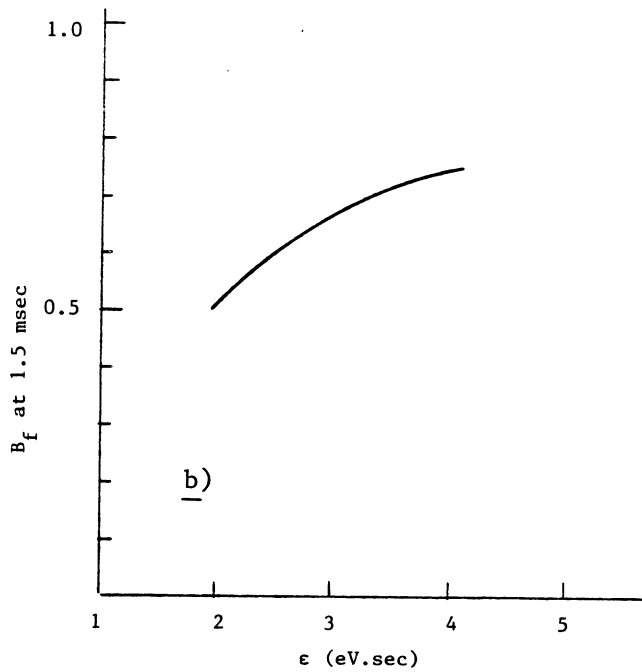
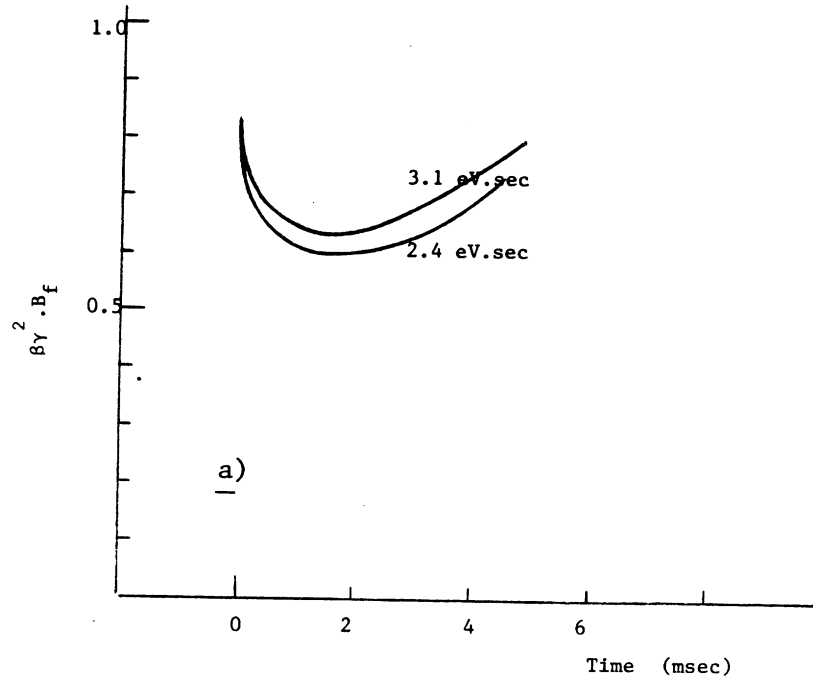


Fig. II.5-2 a) Space Charge, and b) Bunching Factor after Bunching

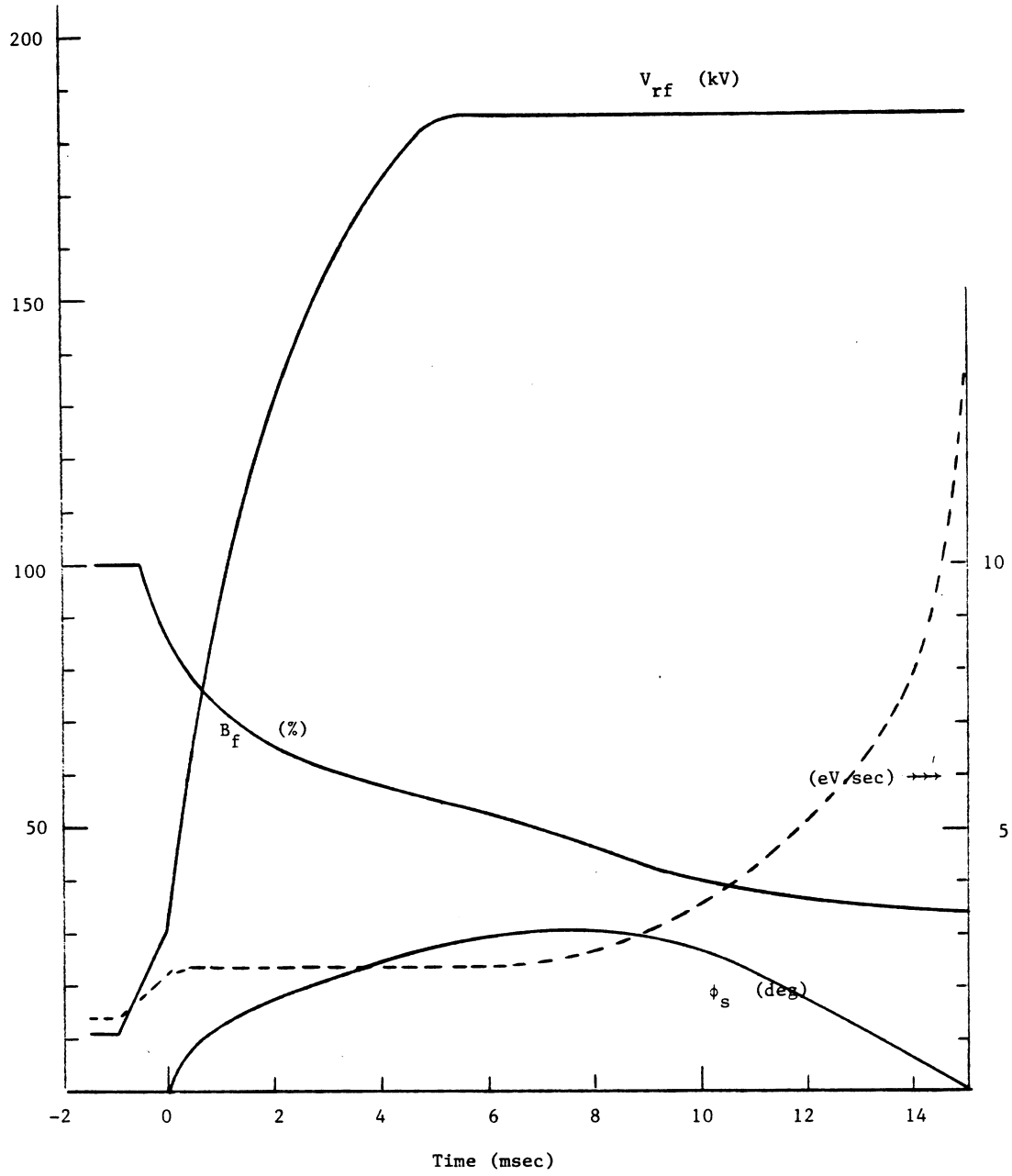


Fig. II.5-3 rf Voltage, Bunching Factor, ϕ_s , and Bucket Acceptance for $\epsilon = 2.4$ eV,sec

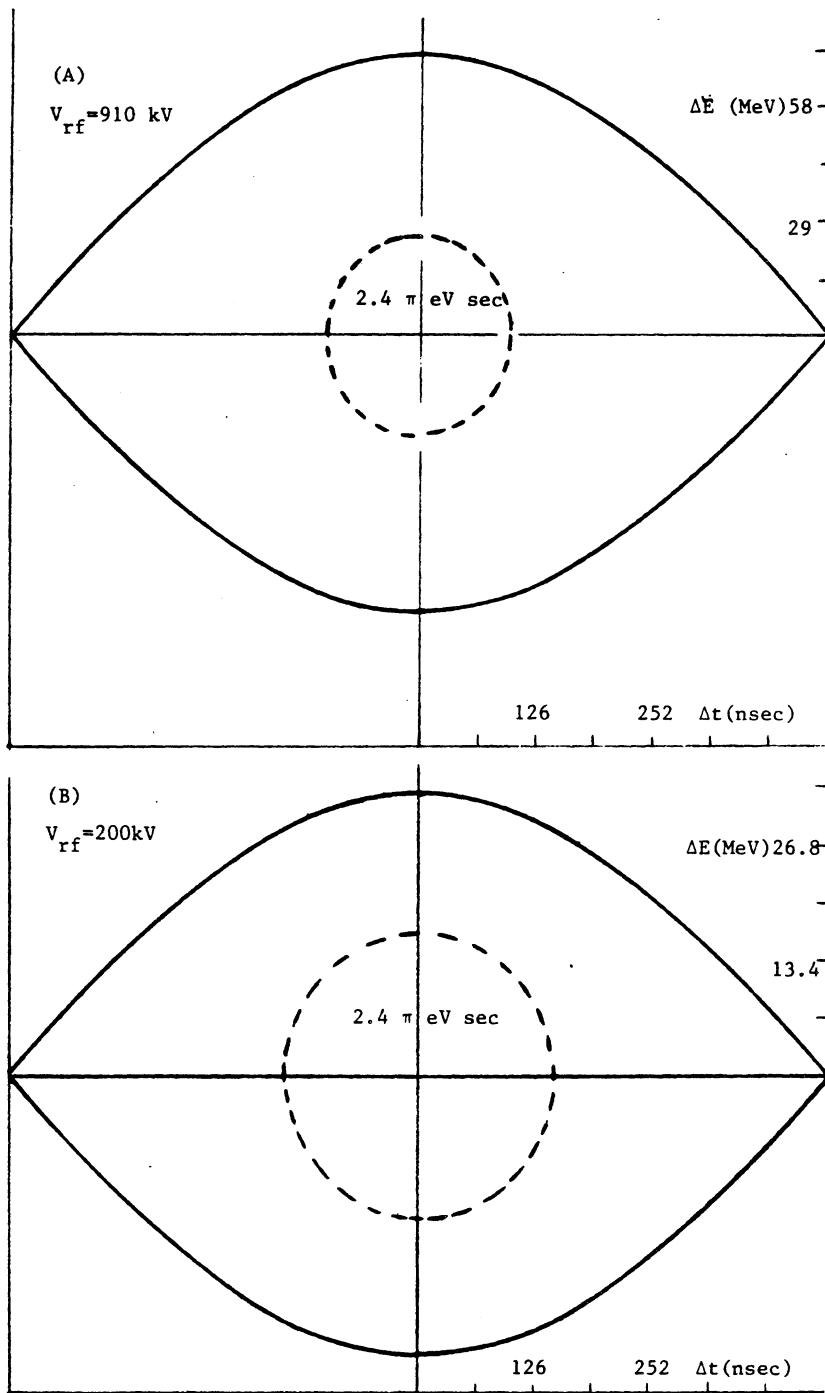


Fig. II.5-4 rf Bucket and Beam Bunch for $\epsilon = 2.4 \text{ eV sec}$ Beam at the Peak Field

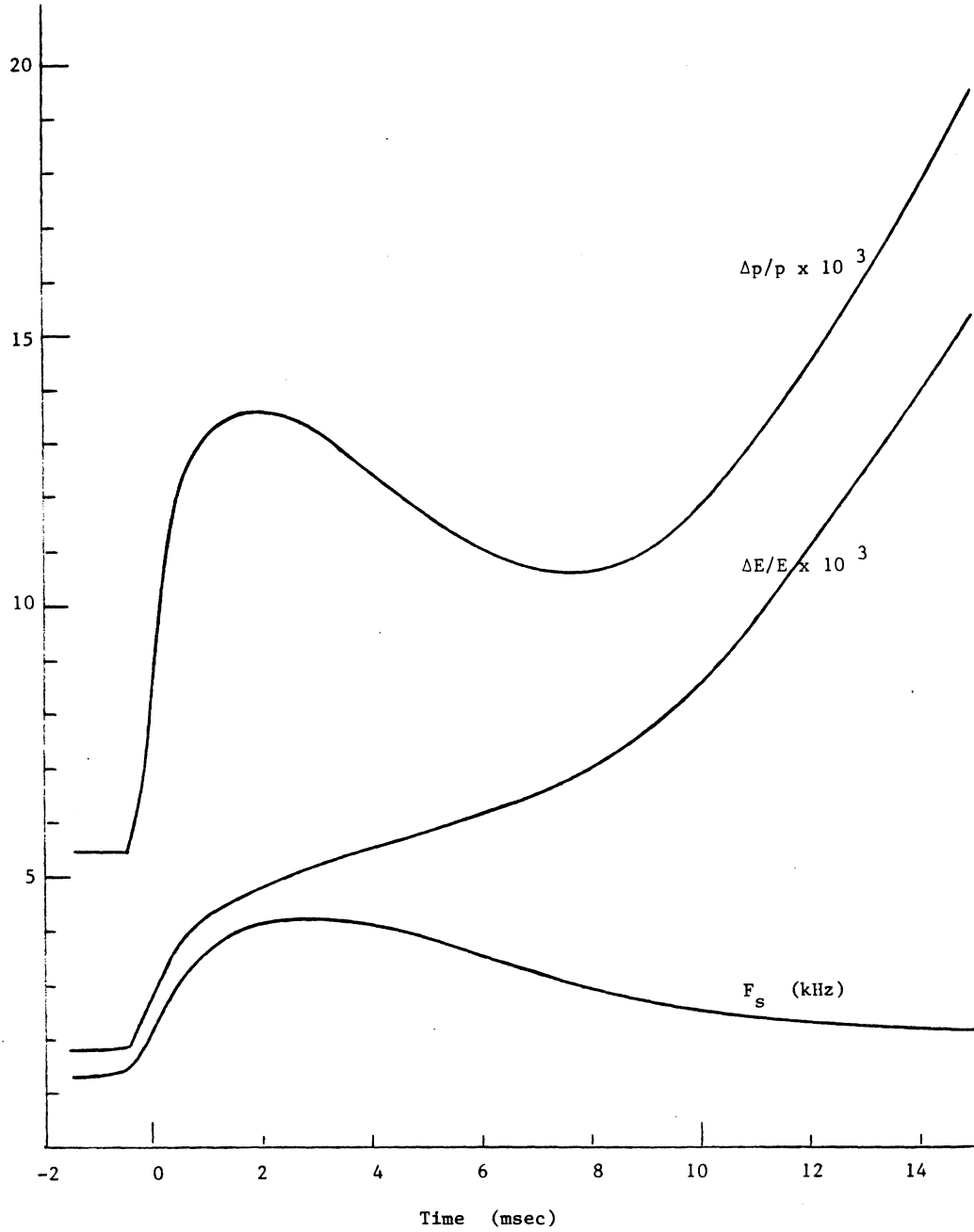
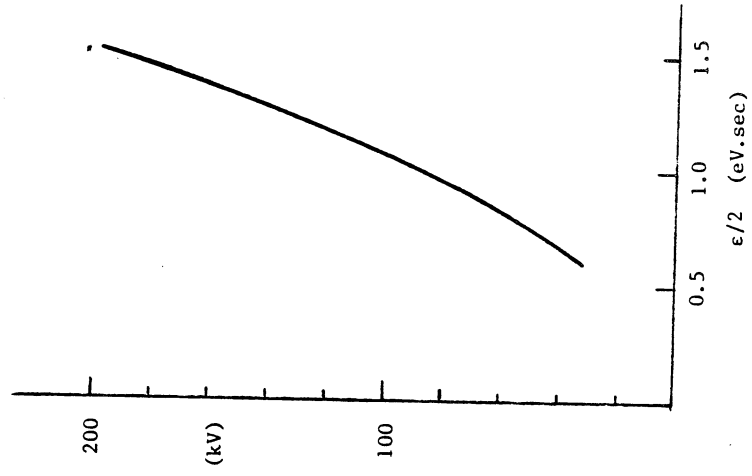


Fig. II.5-5 $\Delta p/p$, $\Delta E/E$ and Synchrotron Frequency (F_s) for $\epsilon = 2.4$ eV.sec Beam with rf Voltage Shown in Figure II.5-3.

(B) rf Voltage Needed to Have 200 nsec Bunch for $h=2$ and Adiabatic Compression as a Function of $\epsilon/2$



(A) Final Bunch Length as a Function of ϵ for $h=1$ Adiabatic Compression with Final rf Voltage of 185 kV

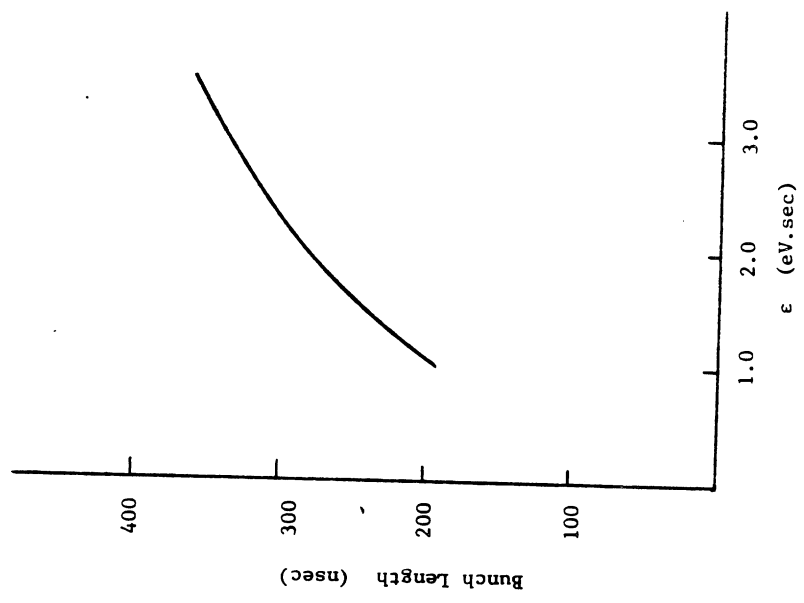


Fig. II.5-6

Initial rf Voltage to make 200 nsec
by Sudden Rotation of Bunch with
215 kV Final Voltage as a function of
 ϵ .

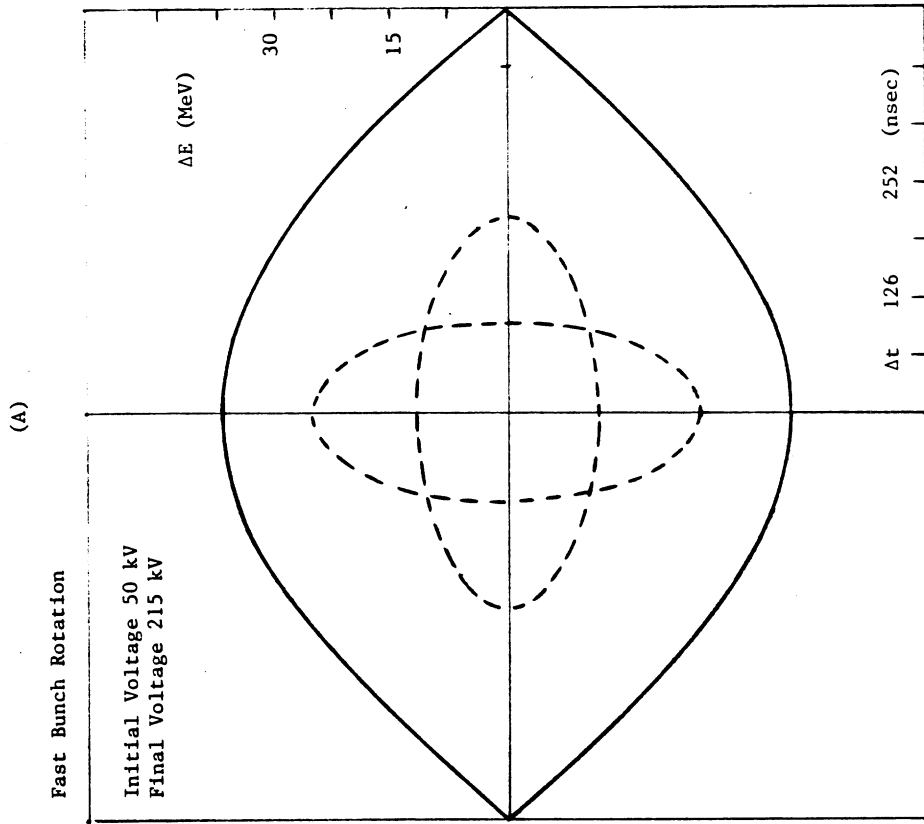
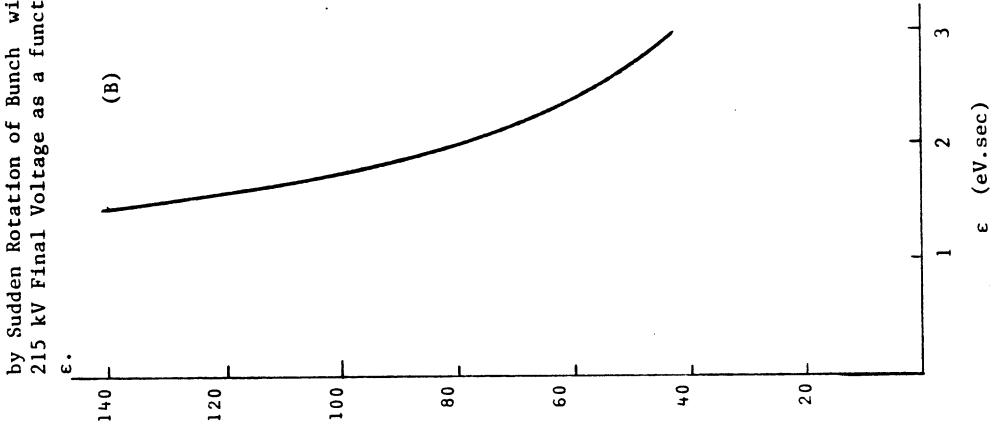


Fig. II.5-7

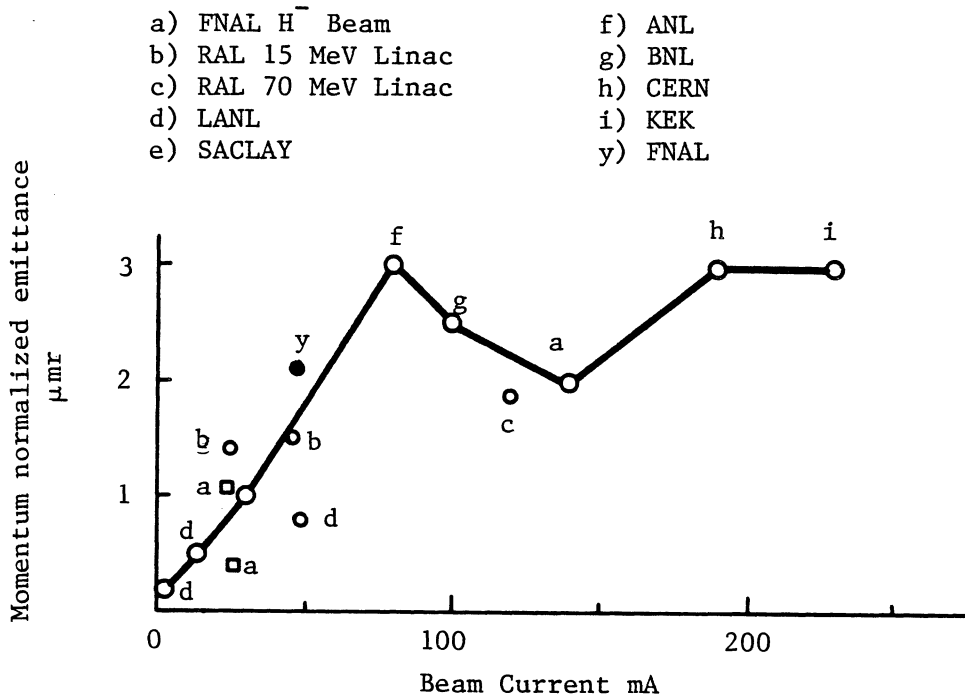


Fig. II.6-1 Measured values of normalized emittance at the input to a linac for 90% of the total beam current.

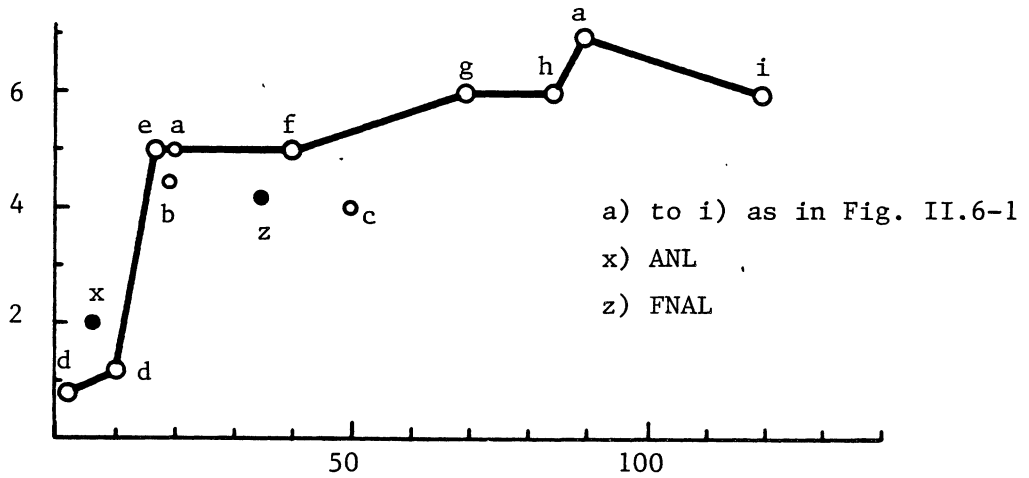


Fig II.6-2 Measured values of normalized emittance at the output of a linac for 90% of the total beam current.

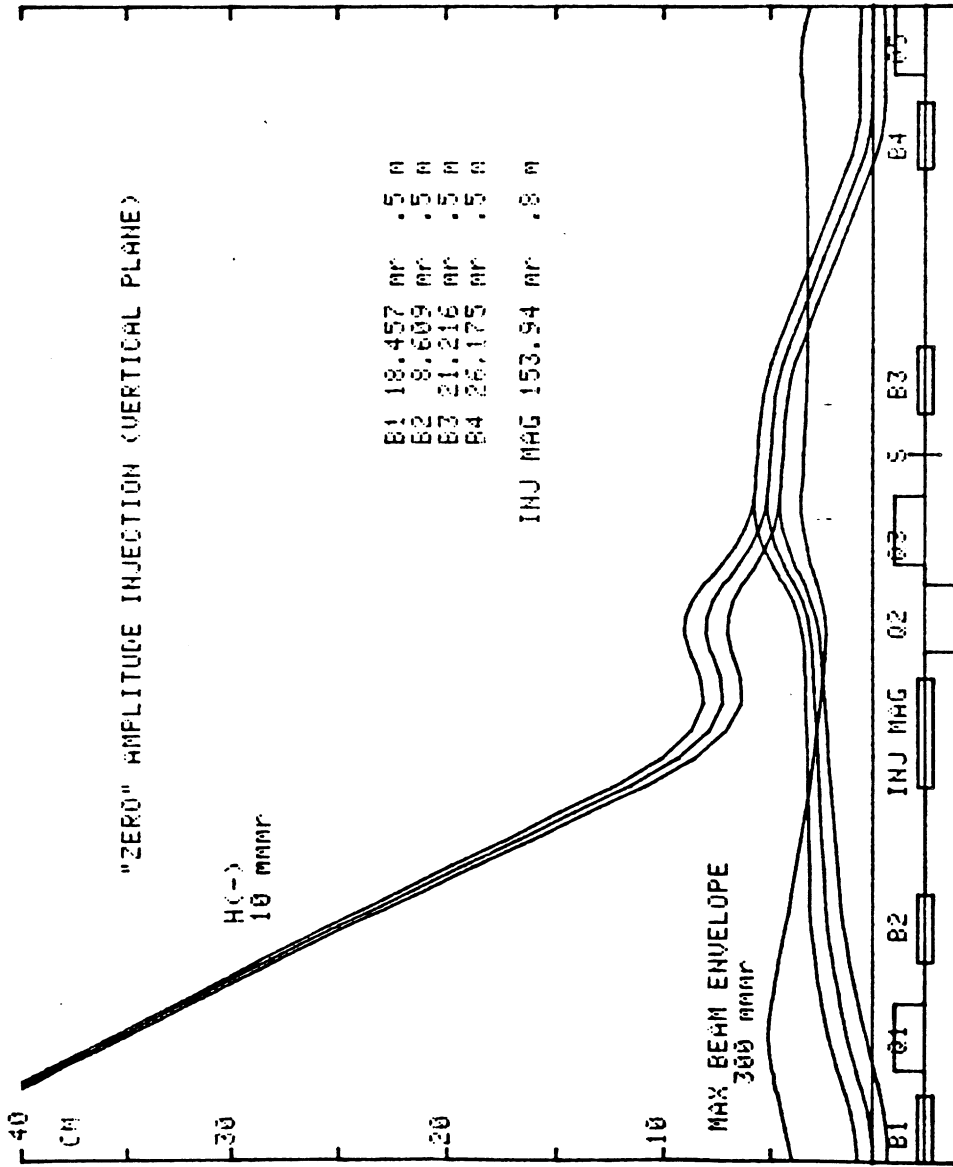


Fig. II.6-3

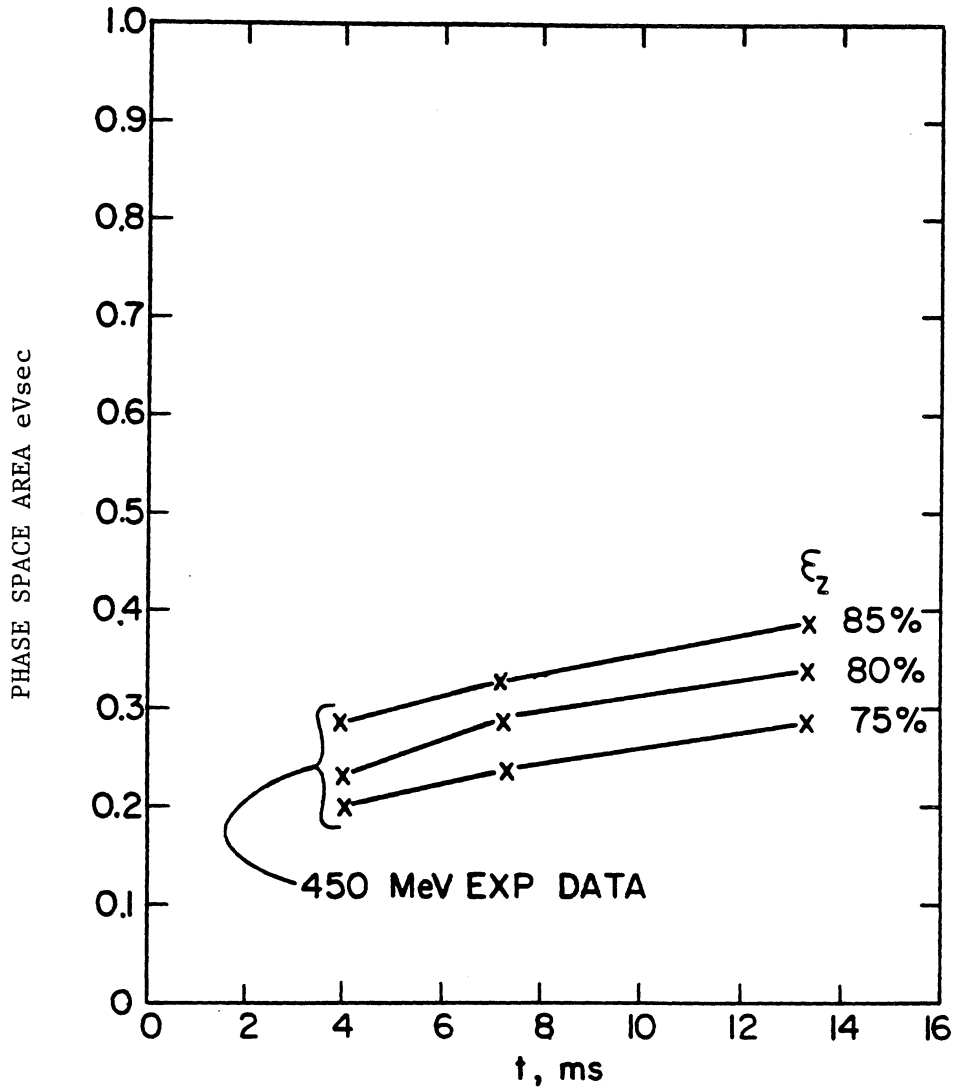
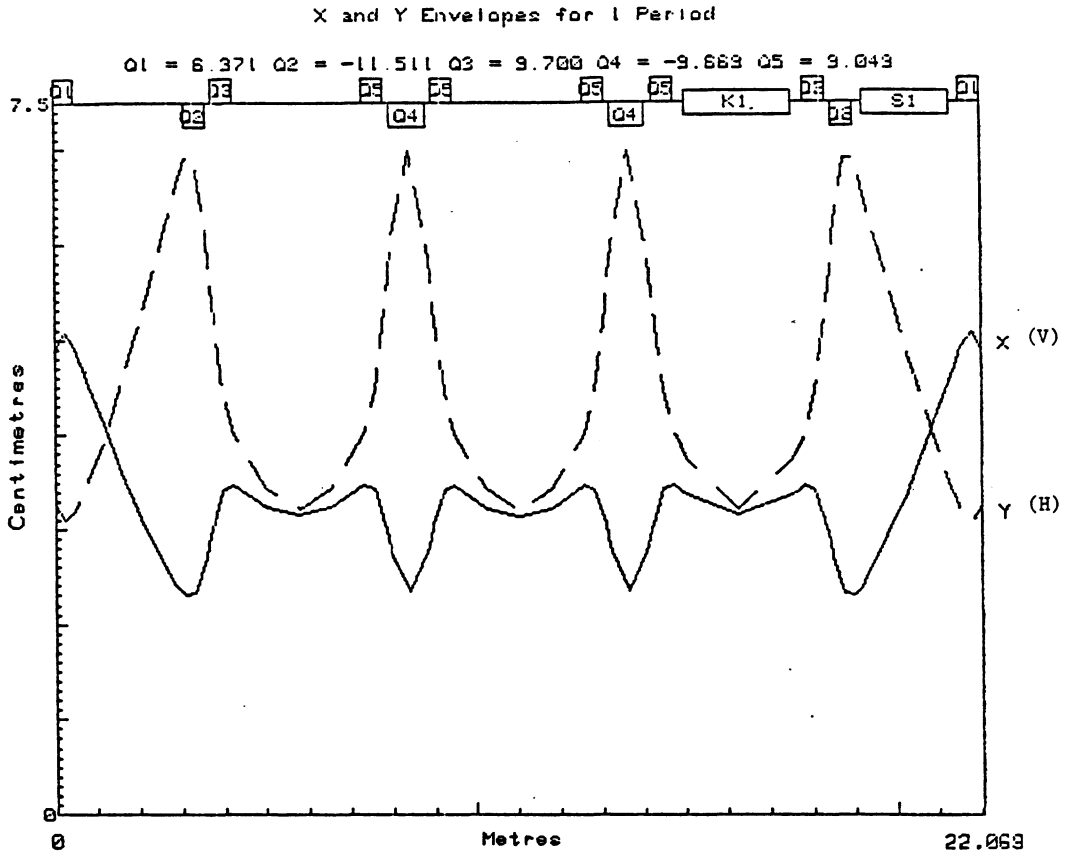


Fig. II.7-1 ANL IPNS-RCS Bunch Area Measurements



BEAM RIGIDITY=6.03800 X,Y EMITT=30.0000,50.0000 PI CM-MR,DPP=.01000													COMMANDS				
ELEMENTS: 15 ELEMENT DEFINITIONS													BEAM				
NAM	TYPE	VAR	LEN, ANG	B, B'	N, GAP	S1	KICK	0.0	2.5000	.07000	28.98		ELEMENTS				
D1	DRFT	0.0	.64700	0.0000	0.000	DK	DRFT	0.0	.30000	0.0000	0.000		LATTICE				
DM	DRFT	0.0	.90000	0.0000	0.000	DS	DRFT	0.0	.24228	0.0000	0.000		PERIODS				
Q1	QUAD	0.0	.50000	6.3709	0.000								FIT				
Q2	QUAD	0.0	.50000	-11.51	0.000								*TRANSPOR				
Q3	QUAD	0.0	.50000	9.7000	0.000								*INSERT				
D2	DRFT	0.0	1.5500	0.0000	0.000								MATRIX				
D3	DRFT	0.0	.15000	0.0000	0.000								GO				
D4	DRFT	0.0	.39056	0.0000	0.000								CYCLE				
DX	DRFT	0.0	.87200	0.0000	0.000								GRAPH				
Q4	QUAD	0.0	.85000	-9.663	0.000								ITERATE				
Q5	QUAD	0.0	.50000	9.0490	0.000								HELP				
LATTICE: 32 ELEMENTS: Q1 D1 DM D1 D4 Q2 D3 Q3 D2 D2 Q5 D3													SAVE				
Q4	D3	Q5	D2	D2	Q5	D3	Q4	D3	Q5	DK	K1	DK	Q3	D3	Q2	DS	RECALL
S1	DS	Q1											QUIT				
PERIODS	FIT: NU X =2.300, NU Y =3.300,											NEW CASE					
1												PRINT					

Fig. II.8-1 Beam Envelopes through Extraction Kicker and Septum

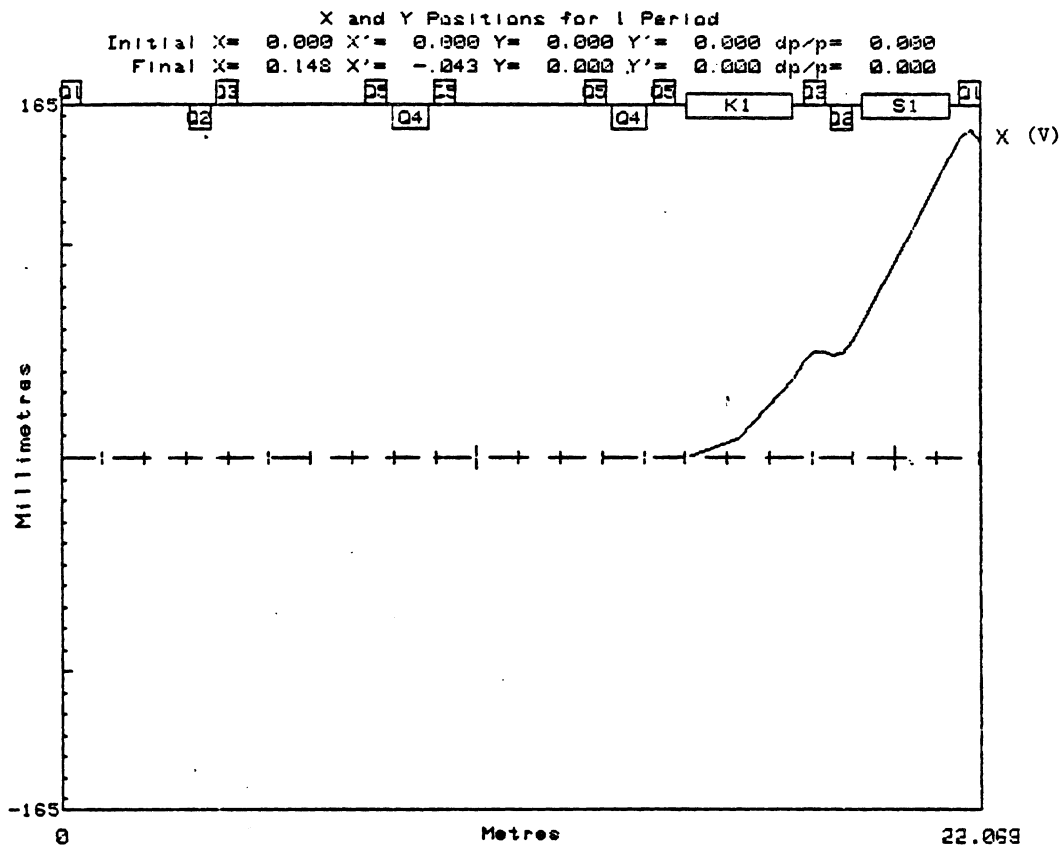


Fig. II.8-2 Extraction Orbit with Septum off

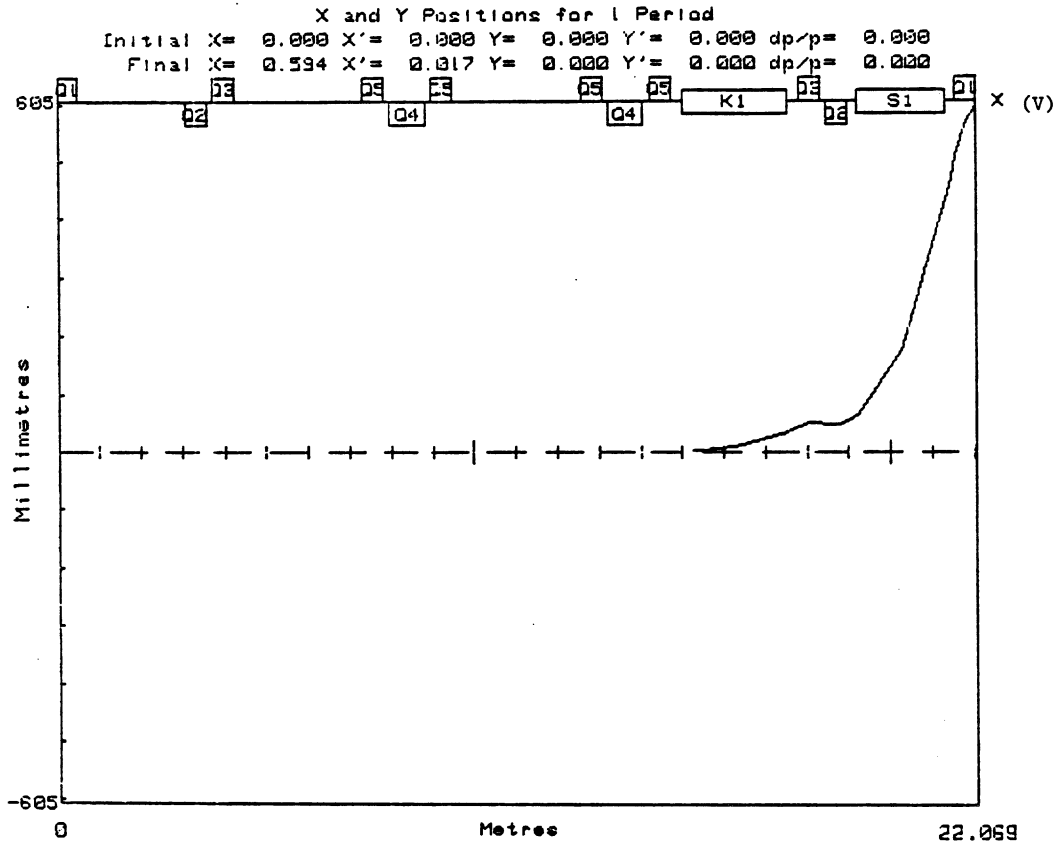


Fig. II.8-3 Extraction Orbit with Kicker and Septum on

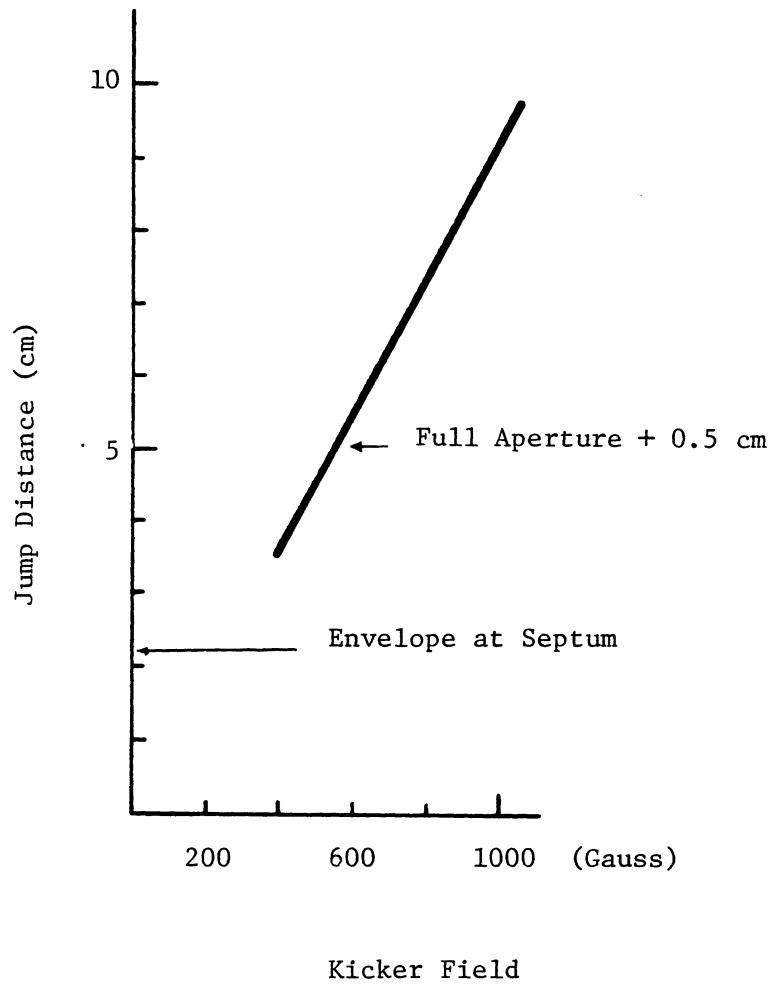


Fig. II.8-5 Jump Distance versus Kicker Field.

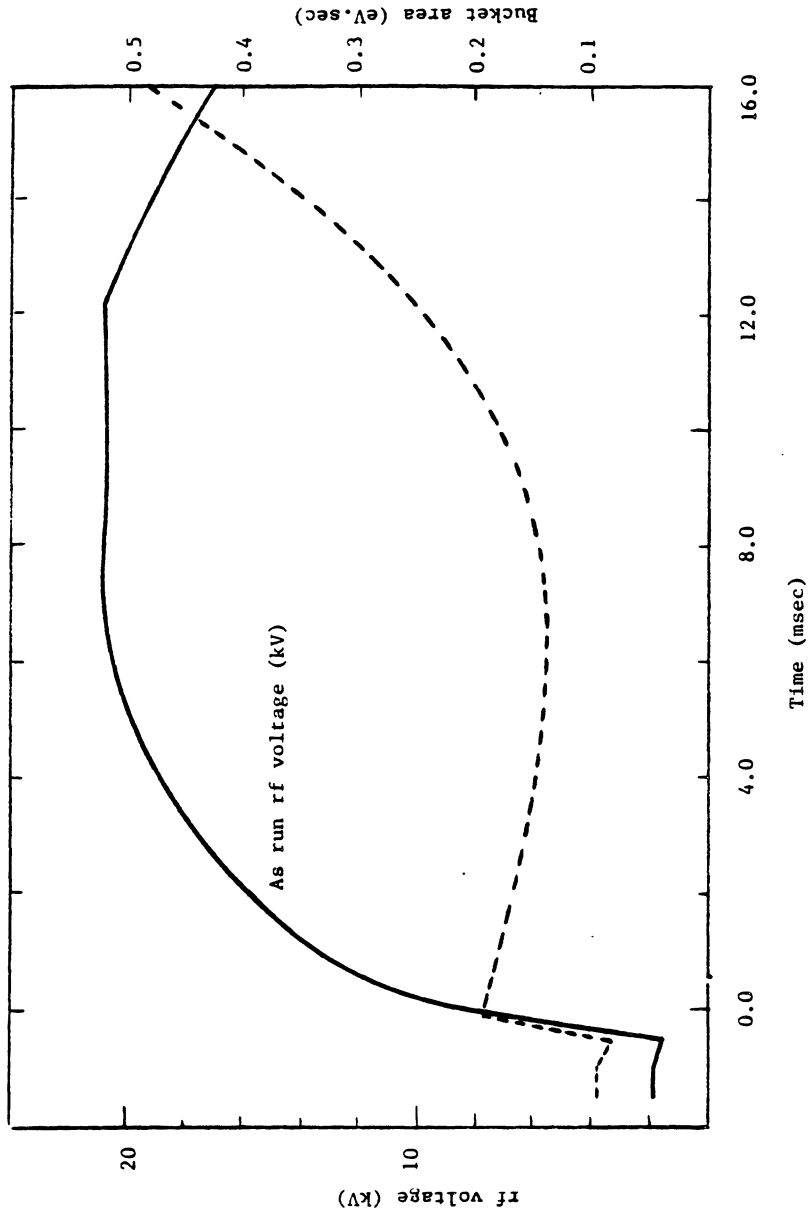


Fig. II.10-1 ANL IPNS-RCS rf voltage program and bucket area ($\Delta E/2, \Delta t/2$)

**CONCEPTUAL DESIGN OF A RAPID-CYCLING SYNCHROTRON FOR
KFA-JULICH SPALLATION NEUTRON SOURCE**

SECTION III

SYNCHROTRON COMPONENTS

III.1 RING MAGNETS

The ring magnet parameters are given in the table in Section I.3, where the usable half-apertures for all magnets are defined by the dimensions of the circulating beam envelopes. One cm was added to the usable half apertures for a ceramic vacuum chamber wall and rf shield similar to the SNS design and an additional 0.5 cm for beam errors. Since accessible space is allowed in later calculations for the dipole field edges, this extra space was NOT added to the horizontal apertures of the bending magnets. The full apertures, pole to pole, are then twice the above results. The Q_2 and Q_3 quadrupoles are positioned in the extraction and injection areas of the ring and the required apertures are defined in the injection and extraction sections of this report. To maintain the fourfold symmetry of the SRA, all Q_2 and Q_3 magnets in the lattice are identical.

The equivalent quadrupole bore diameters used here are related to the full apertures required (H and V) by the following relation:

$$D = [2 * (.9H) * (.9V)]^{1/2} .$$

This in effect has cut the corners of the usable aperture by a few percent. It also assumes that the vacuum chamber has an elliptical rather than circular cross section. A summary of the final total apertures for all the magnets in the ring lattice is located in Table III.1-1 along with the other basic parameters.

The two bending magnets differ in gap width only. If the M1 width is made as large as the M width, the total inductance in 1/8 of the ring is increased by only about 3%. Only one bending magnet lamination geometry, B_m , therefore, is used here. Also, QD and Q1 were assumed to be identical magnets due to the near equality in the aperture and gradient requirements.

TABLE III.1-1
Required Basic Parameters and Bore Dimensions

<u>Magnet</u>	# <u>Req'd</u>	<u>L_{eff}</u> <u>(cm)</u>	<u>B or B'</u> <u>(T or T/m)</u>	<u>Total Aperture</u>		<u>Full Bore Diameter</u> <u>(cm)</u>
				<u>H</u> <u>(cm)</u>	<u>V</u> <u>(cm)</u>	
M]	24	90	1.054	14.6*	11.0	
M1]	32	45	1.054	12.4*	10.6	
QF	28	50	6.03	20.8	7.6	16.00
QD(Q1)	32	50	6.63	11.8	13.2	15.88
Q2	8	50	11.5	17.4	17.4	22.15
Q3	8	50	9.7	14.2	18.0	20.35
Q4	8	85	9.7	17.4	8.6	15.57
Q5	16	50	9.1	14.0	10.0	15.06

* - usable dimension

The generic forms chosen for the dipole and quadrupole magnets are shown in Figs. III.1-1 and III.1-2. Both have the coils out of the midplanes which protects the coils from being directly struck by lost beam. The dimensions of the cores for each magnet were designed to give an average flux density in each yoke of about 1.3 T. All magnets will be fabricated from .036 cm thick laminations and hollow copper conductor, .734 cm sq x .409 cm dia hole. The cores are assumed to be dry stacked with a 3 cm thick stainless steel end plate at each end to which tie bars are welded in such a manner as to hold the core under compression. The magnet coils are assumed to be insulated with mica, fiberglass and vacuum impregnated epoxy.

The effective number of turns used for the large bending magnet, M, was made as small as possible but was limited by a maximum desirable RMS supply current of about 3000 A. Once the supply current was defined for the M magnet, the same current was used to determine the effective number of turns for all the quadrupole magnets in the lattice. The diameter of the QF quadrupole was enlarged by about 5% so that the supply currents for the QD and QF quadrupoles are the same. This current and that for all the other magnets

were allowed to differ since each type is driven by an independent power supply. The final dipole and quadrupole magnet parameters are listed in Appendix A.2.

The final coil designs are capable of handling the necessary dc currents at 1100 MeV while having maximum temperature rises around 17° C (30° F) for a cooling water pressure gradient equal to 689 kPa (100 psi).

A representative 1/4 section of the dipole and the quadrupole magnets are shown in Figs. III.1-1 and 2. Calculations for all the magnets were performed during the design and cost estimating procedures.¹ The results for only a representative dipole, M, and quadrupole, QD, are included in Appendix A.2 to show the types of details that are involved in the design of each magnet. All of the magnets have several conductors electrically connected in parallel. Calculations were done for one of the water cooling circuits in each of the magnet types run continuously at the dc current needed for 1100 MeV operation, the worst case condition. The results of the representative coil calculations² for a dipole and a quadrupole magnet also are included in Appendix A.2, along with some of the details of the design calculations for these magnets. The supply currents and voltages for the ac operation with a simple sinusoidal excitation from 200 MeV to 1100 MeV at 50 Hz are also included in addition to a table of the major assumptions entering into the magnet designs. The results of the calculations for the designs of all the magnets are listed elsewhere.¹ A summary of the individual parameters for each magnet type plus the associated totals for an entire ring are shown in Table III.1-2.

Cost breakdowns for the representative magnet designs are included in Appendix A.2. The costs listed assume that 10% more magnets are built for each type to serve as spares. The major unit-costs on which the cost

estimates were based are given and a summary of the total estimated costs of the ring magnets included. This total cost estimate is \$9.8M.

The Q2 quadrupole design produces a field at the edge of the pole (max. field at pole tip) that is higher than desired. This can be reduced to an acceptable value by lengthening the Q2 magnet by about 10 cm. This, however, will require another iteration on the lattice.

III.2 RING MAGNET POWER SUPPLIES

Introduction

Rapid cycling synchrotrons are usually excited by a dc-biased sinewave current as shown in Fig. III.2-1. More efficient beam capture during injection (lower beam losses) and a significant reduction of rf peak voltage requirements during acceleration can be achieved with a magnet current as shown in Fig. III.2-2.

For the SNQ a repetition rate of 50 pps, a flat injection field of 1.5 msec duration, an accelerating field of 33.3 Hz and a falling field of 142.9 Hz will be used.

Choice of Power Source

Capacitors are used to resonate with the magnets in order to save energy. The energy losses during each cycle will be supplied by continuous excitation from a modulated multi-phase dc power supply.³ This method is proposed for the SNQ-SRA because of its ability to operate over a wide frequency range, to provide continuous excitation for a dual-frequency system, to phase-lock to the line or to a stable oscillator,⁴ and to provide both dc and ac excitation from one power source.

Figure III.2-3 illustrates an ac-dc power source which generates the desired wave shape by modulating a 48-phase rectifier power supply. A 48-phase system is obtained by connecting in series four identical 12-phase dc power supplies, which have their 50 Hz, 3-phase ac-inputs phase shifted by 7.5 electrical degrees with respect to each other. The phase shifting is done by an autotransformer. A slightly under-damped filter⁵ attenuates ripple above the operating frequency ω_0 .

Neglecting saturation effects, the time-variation of the magnet current during acceleration is

$$i_M = I_{dc} - I_{ac} \cos \omega t \quad . \quad (1)$$

The choke and capacitor currents are given by

$$i_{CH} = I_{dc} + \frac{L_M}{L_{CH}} I_{ac} \cos \omega t \quad , \quad (2)$$

$$i_C = i_M - i_{CH} = - \frac{L_{CH} + L_M}{L_{CH}} I_{ac} \cos \omega t, \quad (3)$$

where

I_{dc} = dc bias current,

I_{ac} = ac current,

L_M = magnet inductance,

L_{CH} = choke inductance,

$$\omega = \frac{L_{CH} + L_M}{C L_{CH} L_M}^{1/2} \quad , \quad (4)$$

C = circuit capacitance.

Except for losses the total network-stored energy is constant and the choke-stored energy is transferred to the magnet and back again, once per cycle, through the resonant capacitor.

In order to achieve complete transfer of the inductively stored energies, the inductance of the choke is made equal to the inductance of the magnets. For $L_M = L_{CH} = L$ the circuit currents become:

$$i_M = I_{dc} - I_{ac} \cos \omega t \quad (1)$$

$$i_{CH} = I_{dc} + I_{ac} \cos \omega t \quad (2')$$

$$i_C = i_M - i_{CH} = -2 I_{ac} \cos \omega t \quad (3')$$

$$\omega = \frac{2}{LC}^{1/2} \quad (4')$$

and

$$e_C = -\frac{2 I_{ac}}{\omega C} \sin \omega t \quad (5)$$

A flat-bottom field of 3.74 kG will be maintained for 1.5 msec with a crowbar circuit. A 50 Hz pulse repetition rate and a lower frequency magnetic guide field during acceleration is obtained by accelerating at 33-1/3 Hz and resetting the magnets at 142.9 Hz. This reduces the peak value of \dot{B} by 33.3% and the rf peak power by 55.6% as compared to simple sinusoidal 50 Hz acceleration. During the 142.9 Hz reset period the magnet and choke voltages will be 286% higher as compared to 50 Hz sinusoidal operation. Figure III.2-2 illustrates the desired magnet current shape which can be produced by the circuit shown in Fig. III.2-3. The horizontal and vertical tunes of the synchrotron are 10.3 and 11.3; in order to minimize harmonic perturbations, the ring magnets are powered from four feed points (see Figs. III.2-3, -10 and -11). For the circuit of Fig. III.2-3 the current waveforms of the magnets, capacitors and choke are shown in Fig. III.2-4 together with voltage and stored-energy curves.

Figure III.2-5a is a simplified diagram of the circuit of Fig. III.2-3. This idealized circuit is initially energized from the ac-dc power supply with switches S_I and S_{II} open. In this mode the circuit oscillates at 142.9 Hz between 1.44 kA (3.74 kG injection field) and 4.04 kA (10.52 kG ejection field). A flat-bottom magnet current for beam injection is initiated at times

t_0 , t_5 etc. in Fig. III.2-4 when switch S_I is closed; as illustrated in this figure the power supply voltage maintains the magnet current until time t_1 . It is not essential to also maintain the choke current constant between times t_0 and t_1 , which can be accomplished with a power source, E_S , in the crowbar as will be explained later. Depending on the values of these dc voltages \dot{B} values of zero, positive or negative are possible. At time t_1 switch S_{II} is closed and switch S_I opens. With capacitors C_1 and C_2 connected in parallel the circuit oscillates at 33-1/3 Hz until time t_3 . At that time, with all the circuit energy in the inductances, switch S_{II} is opened. Between times t_3 and t_5 the circuit oscillates at 142.9 Hz; the decaying current resets the magnets to the injection field value. The above cycle repeats after time t_5 .

A Solid State Switching Circuit

A solid state switching circuit that performs the functions of the ideal switches, S_I and S_{II} , is shown in Fig. III.2-5b. As mentioned before to start-up the circuit it is run at 142.9 Hz while the magnitudes of the dc and ac currents are being adjusted to the desired operating values. Just before normal circuit operation commences turn-off capacitor C_x must be charged. This is done by turning on thyristor S_3 once when the choke current begins to rise as will be described later. The circuit operation is described with reference to Figs. III.2-4 and III.2-6. In Fig. III.2-6 heavy lines indicate current flow, a capacitor symbol drawn heavy indicates a charge on the capacitor. The following is the time sequence of events:

For $t_0 \leq t < t_1$ — All the energy is stored in the circuit inductances. As shown in Fig. III.2-6a silicon controlled rectifiers (thyristors) S_5 are turned on, crowbaring the ring magnets and the choke. The difference between these currents $i = i_{CH} - i_M = (I_{dc} + I_{ac}) - (I_{dc} - I_{ac}) = 2 I_{ac}$ flows

through the crowbar. As will be described later, the crowbar may or may not contain a power source in addition to the 48-phase power supply, to allow the beam to be injected into:

- a) a falling field ($\dot{B} < 0$, passive crowbar),
- b) a rising field ($\dot{B} > 0$, active crowbar),
- c) a constant field ($\dot{B} = 0$, active crowbar),
- d) a combination of the above.

At $t = t_1$ (Fig. III.2-6b) -- Thyristors S_1 and S_4 are turned on. Thyristor S_4 provides discharge paths for turn-off capacitor C_x via the crowbar S_5 (current i'_x) and via C_1 and L_x (current i''_x). Inductance L_x limits current i''_x . Thyristor S_1 is back-biased until the charge on C_x reverses.

At $(t + 25 \mu s) < t < t_2$ (Fig. III.2-6c) -- The reverse current i'_x has turned off crowbar thyristors S_5 . The charge on C_x is reversing, and thyristor S_1 connects capacitor C_2 in parallel with C_1 . The choke energy discharges at 33-1/3 Hz into the magnets and the parallel connection of C_1 , C_2 and C_x .

At $t = t_2$ (Fig. III.2-6d) -- The capacitor current is zero, $i_M = i_{CH}$, and thyristors S_1 and S_4 turn off. All capacitors are at their 33-1/3 Hz peak voltage.

At $t_2 < t < t_3$ (Fig. III.2-6e) -- With thyristor S_2 turned on, the capacitor current of C_1 and C_2 reverses. The charge on C_x remains at its value obtained at time t_2 .

At $t = t_3$ (Fig. III.2-6f) -- The capacitor current is at its peak; capacitors C_1 and C_2 are discharged. The circuit energy is stored in the inductances. At this time S_3 is turned on. This provides discharge paths for turn-off capacitor C_x via S_2 and C_2 (current i'_x) and via L_x and C_1 (current i''_x).

At $(t_3 + 25 \mu s) < t < t_4$ (Fig. III.2-6g) -- Reverse current i'_x has turned off S_2 , disconnecting C_2 from the circuit. The magnet discharges at 142.9 Hz into the choke and the parallel connected capacitors C_1 and C_x .

At $t = t_4$ (Fig. III.2-6h) -- The capacitor current is zero, $i_M = i_{CH}$, and thyristor S_3 turns off. Capacitors C_1 and C_x are charged to the 142.9 Hz peak voltage.

At $t_4 < t < t_5$ (Fig. III.2-6i) -- The capacitor current reverses. At time t_5 capacitor C_1 is discharged. With all the circuit energy stored in the inductors and with the charge on C_x as shown, the circuit is ready to repeat the above cycle.

Flat-Bottom Crowbar Circuits

For magnets with a large L/R time constant, a passive crowbar will be sufficient to keep the current flat to within 0.1% for 1.5 msec. Magnets with small time constants require a dc driving voltage in the power supply and/or in the crowbar. Figure III.2-7 shows equivalent circuits for passive and for active crowbars. In these circuits the crowbar thyristors are represented by an ideal switch, S, in series with a diode, D, (unidirectional current flow) and a resistor, R_S . The crowbar resistance R_S will, for practical purposes, be constant during the 1.5 msec injection time. Its value depends on the number of thyristors connected in series. The nominal crowbar current has the same value as the capacitor current at $t = t_o$,

$$I = I_{CH} - I_M = 2 I_{ac} = 2.6 \text{ kA} \quad .$$

At 2.6 kA the voltage drop per thyristor will be approximately 2.36 V. Therefore, with n thyristors connected in series, the crowbar voltage drop will be $e_S = 2.36 n$ volts and the crowbar resistance

$$R_S = \frac{2.36 n}{2.6 \text{ kA}} = 0.91 n \text{ (milliohms)} \quad .$$

The transient response of the circuit of Fig. III.2-7b to closure of switch S at time $t = t_0$ is shown in Fig. III.2-9b for 6 type M and 8 type M_1 bending magnets energized from one power supply. The circuit component values are as shown on Fig. III.2-9 and the initial conditions at $t = t_0$ are:

$$I_M = \text{magnet current} = 1.44 \text{ kA}$$

$$I_C = \text{capacitor current} = 2.60 \text{ kA}$$

$$I_{CH} = \text{choke current} = 4.04 \text{ kA}$$

Without a driving voltage in the crowbar and with zero voltage on the capacitor the magnet and choke currents change at time $t = t_0$ at the following rates:

$$\frac{di_M}{dt} = -\frac{I_M R_M}{L_M} = -\frac{1.44 \text{ kA} \times 31.8 \text{ m}\Omega}{23.4 \text{ mH}} = -1.96 \text{ kA s}^{-1} \quad (6)$$

$$\frac{di_{CH}}{dt} = -\frac{I_{CH} R_{CH}}{L_{CH}} = -\frac{4.04 \text{ kA} \times 31.8 \text{ m}\Omega}{23.4 \text{ mH}} = -5.49 \text{ kA s}^{-1} \quad (7)$$

With $L' = 0$ the current transfers from the capacitor to the crowbar in about 6 μs . With $L' > 0$ this transfer takes longer and is oscillatory with a frequency of

$$f = \frac{1}{2\pi\sqrt{L'C}} .$$

For $L' = 0.2 \mu\text{H}$ the capacitor current, i_C , oscillates at 32.7 kHz above and below its steady state value of zero for about 200 μs ; the crowbar current i_S , oscillates at the same frequency and for the same time around its steady state value of 2.6 kA.

For $L' = 1 \mu\text{H}$ the oscillations are at 14.6 kHz and last for about 1 msec. These oscillations have a negligible effect on the magnet and on the choke current. After the capacitor current has been transferred to the crowbar, the rate of change in the magnet current is,

$$\frac{di_M}{dt} = - \frac{I_M R_M - 2.36 \text{ n}}{L_M} , \quad (8)$$

while the choke current changes as

$$\frac{di_{CH}}{dt} = - \frac{I_{CH} R_{CH} + 2.36 \text{ n}}{L_{CH}} . \quad (9)$$

Note, the crowbar voltage drop, $e_S = 2 I_{ac} \times R_S = 2.36 \text{ n}$, reduces the current decay in the magnets but increases the current decay in the choke. For the bending magnets, with $2.36 \text{ n} = 33 \text{ V}$, we have

$$\frac{di_M}{dt} = - \frac{1.44 \text{ kA} \times 31.8 \text{ m}\Omega - 33 \text{ V}}{23.4 \text{ mH}} = - 0.402 \text{ kA s}^{-1} ,$$

$$\frac{\Delta i_M}{I_M} = \frac{0.402 \text{ kA s}^{-1} \times 1.5 \text{ ms}}{1440} = 4.2 \times 10^{-4} = 0.042\% ,$$

and

$$\frac{di_{CH}}{dt} = - \frac{4.04 \text{ kA} \times 31.8 \text{ m}\Omega + 33 \text{ V}}{31.8 \text{ mH}} = - 5.08 \text{ kA s}^{-1} ,$$

$$\frac{\Delta i_{CH}}{I_{CH}} = \frac{5.08 \text{ kA s}^{-1} \times 1.5 \text{ ms}}{4040} = 0.0019 = 0.19\% .$$

A passive crowbar is sufficient for the bending magnets.

For magnets with small L/R time constants or if the magnet current must be held within tolerances $\ll 0.1\%$ during the crowbar-time, an active power

source is required. The power source may either be in the crowbar, E_S , or in the magnet circuit, E_M , or in both as shown in Fig. III.2-7a.

The inductance of the crowbar power source must be small in order not to delay transfer of the current from the capacitor to the crowbar. This requires a low voltage capacitor bank in parallel with the crowbar power supply as shown in Fig. III.2-8. In this figure an extended foil capacitor provides an ultra-low impedance path for fast transients; the relatively inexpensive electrolytic capacitor bank, C_S , supplies the crowbar current.⁶

The transient response of the circuit of Fig. III.2-7a is shown in Fig. III.2-9a for the bending magnets and for $L' = 0$; it illustrates the effects of the power sources E_M and E_S . A circuit inductance $L' > 0$ would cause an oscillatory delay of the transfer of the current from the capacitor to the crowbar as was illustrated for the passive crowbar. Of the three circuit conditions illustrated by Fig. III.2-9a, the most practical one has only one power source, $E_M = 12.8$ V, in the magnet circuit.⁷

For any crowbar circuit (active or passive), the circuit inductance L' in conjunction with the available forcing voltage will determine the switching time (current transfer time). In order to reduce the commutation reactance to its smallest practicable value, the thyristors will be located close to the capacitor banks. In addition, the inductance of the capacitor banks will be kept small by using transmission lines (strip lines, coaxial cables, coaxial fuse mountings, etc.) for the internal and external connections. Values for the switching reactances can be calculated after a more detailed design has determined the geometry of the capacitor banks. Although this is beyond the scope of the present preliminary design study, a value of $\leq 2 \mu\text{H}$, can be assumed for these inductances.

Cost Estimates

The magnet characteristics for the ring are given in Table III.2-1. In order that all magnets can be adjusted independently seven power supplies are required per quadrant, for a total of 28. Figures III.2-10 and III.2-11 illustrate the resonant circuit arrangements. To reduce cost, power supply P2, in conjunction with trimming chokes, is used to control both the QF and the QD magnets. Six trimming chokes are connected in parallel with each set of quadrupoles as shown in Fig. III.2-12. These six chokes have relative admittances of 1, 2, 2, 5, 10, 10. In this way 10% of the magnet current can be changed in 30 steps of 1/3% per step. In order to keep the overall inductance constant, the switches of the two groups are interlocked; reducing the inductance by 1/3% on one side will increase the inductance on the other side by the same amount. Table III.2-2 summarizes component costs for the circuits of Fig. III.2-10.

The cost estimates are based on the following assumptions:

- a) Magnet power requirements and electrical parameters are as shown in Section III.1.
- b) 200 kVA, 60 Hz capacitors with two bushings are used throughout. They cost \$946 each as of May 1982. An additional 93% is added to this cost for support structures, fuses and interconnections within the capacitor bank.
- c) Chokes have the same inductance as the magnets and cost 15% of the magnet cost. Large tape-wound C-cores weighing 220 kg each, and simple coil geometries will be used for coil construction.⁶ (The same adjustable coil winding- and impregnation-fixtures can be used for all chokes because all cores are made up from the same C-core module.)

- d) Interconnections. With a total of 158 magnets and 28 resonant circuits the total cost is estimated to be 30% of the magnet cost.
- e) At this time large 12-phase dc power supplies cost \$120/kW. This figure is being doubled to include the phase-shifting auto transformers to obtain 48-phase systems and to cover additional power supply modifications such as feedback and feedforward loops and filters, etc. For smaller power supplies the cost per kVA is increased as shown in Table III.2-2.

f) Circuit losses are estimated to have the following distribution:

Ring Magnets	Chokes	Capacitors	Inter-Connections	Filters	Power Supplies
35%	35%	5%	5%	4%	16%

- g) At ANL we have a solid-state switch, rated at PFV=PRV=13 kV and 13 kA. Prices for switches S_1 and S_2 as shown in Fig. III.2-10, are scaled from this switch.
- h) The cost of trimming chokes is 15% of the cost of the magnets to be trimmed.

III.3 OTHER MAGNETS AND POWER SUPPLIES

In addition to the ring magnets discussed in Section III.1, there are a number of other magnets required. These include a transport system from the linac to the synchrotron, injection system magnets, correction magnets in the ring, extraction system magnets, and a transport system from the ring to the spallation targets. With the possible exception of the extraction kicker and septum magnets none of these magnets or power supplies are other than routine, and since they do not represent a very large cost item, detailed design of these magnets and power supplies have not been carried out in this study, although an estimate of their cost is included. The list and characteristics of the auxiliary magnets for injection, extraction, and ring orbit and tune compensation is given in Table III.3-1. These were calculated in earlier sections of the report.

Table III.3-1

<u>Type/Number</u>	<u>Auxiliary Magnets</u>		<u>Aperture</u>
	<u>B(T)</u>	<u>Length (m)</u>	
Injection System			
Bump Magnets B ₁	0.080	0.5	
B ₂	0.037	0.5	
B ₃	0.091	0.5	
B ₄	0.11	0.5	
Septum Magnet	0.40	0.8	
Horizontal Sweeping Magnet (or fast Horizontal Bump Magnets)	0.07	0.5	
Extraction System			
Fast Kicker Magnet (2 sections)	.070	1.25	9 x 9 cm
	.070	1.25	9 x 11 cm
Septum Magnet (3 sections)	0.80	0.7	15 x 6 cm
	0.80	0.7	10 x 8 cm
	0.80	0.7	8 x 10 cm

Correction Magnets

Orbit correction dipole, horizontal - 44 - $B\ell = 6 \times 10^{-3} \text{ T-m}$

Orbit correction dipole, vertical - 44 - $B\ell = 6 \times 10^{-3} \text{ T-m}$

Sextupole magnets for chromaticity - 16 - $B_{\text{pole}} = 2\text{T}$, $\ell = 35 \text{ cm}$

Octupole magnets for Landau damping - 16 - $B_{\text{pole}} = 0.27\text{T}$, $\ell = 20 \text{ cm}$

The required integrated field strengths of the orbit correction dipoles to give 1 cm correction is very small. The requirements on the multipoles were derived in Section II.4 as a conservative estimate. The maximum pole tip fields and magnet lengths specified above can be adjusted as desired to give the same product. A knowledge of the multipole fields of the bending magnets and quadrupole magnets is required before the actual required strengths of the sextupoles and octupoles can be rigorously specified. Detailed computer calculations of the magnetic fields would be needed, and this is presently beyond the scope of this study. In addition, comparison with field measurements on model magnets is important.

The kicker magnet for the extraction system requires a very fast rise time ($\leq 400 \text{ nsec}$) and is a critical element. By way of comparison the extraction system of the ANL-RCS has undergone a great deal of modification to make it reliable. The kicker magnet and drive system have been reported in the literature, ^{8,9} and the requirements are quite similar to those of the SNQ-SRA synchrotron. In fact, scaling the RCS extraction kicker design to the SNQ-SRA synchrotron indicates that the required pulse-forming network voltage is only 35 kV compared to 43 kV for the system in operation on the RCS. The feasibility of the extraction kicker magnets is therefore considered assured. A scaling to the requirements of the SNQ-SRA extraction system is included¹⁰ as Table III.3-2.

III.4 RF SYSTEM DESIGN

Introduction

In this section we will describe the design of a typical rf accelerating cavity and driving amplifier. As discussed in Section II.7, we have selected a cathode-follower amplifier as the system which seems to cope with the large beam loading currents in the most straightforward way. The alternatives, a feed-forward system similar to the ISR, or SNS, or an improved conventional system, might also perform acceptably but are not treated in detail.

Both the proposed amplifier and the cavities they drive are conservatively designed with respect to power and voltage limitations, and the accelerating voltage can be produced without using all the available space in the ring. This conservatism means that additional accelerating voltage (above 200 kV) or the addition of cavities operating at the second harmonic (to manipulate the bunch length) could be added without major modifications to the lattice.

Cavity Design

The proposed cavities are standard coaxial structures with a reentrant beam pipe forming the inner conductor, shorted to the tank at one end and providing a gap at the other. The important dimensions of the cavity are determined by the ferrite dimensions, and these can be found from the required ferrite area given by

$$A = V_{\text{peak}} / \omega B_{\text{rf}} = 2.94\text{m}^2 ,$$

where the peak voltage and frequency are taken at 5.5 msec. The total length of ferrite is a function of the inner and outer radii of the ferrite rings,

$$L = \frac{A}{R_o - R_i} = 14.5m \quad ,$$

where

A = ferrite cross section area

$\omega = 2\pi f = 2\pi(0.9 \times 10^6 \text{ Hz})$

$R_{rf} = 120 \text{ gauss}$

$V_{peak} = 200 \text{ kV}$

$R_o = \text{ferrite toroid outer radius} = 0.44$

$R_i = \text{ferrite toroid inner radius} = 0.24$

In this case, the total ferrite volume is roughly

$$V = \pi(R_o^2 - R_i^2)L = 6.14m^3$$

which would involve a total cost of about \$1.8M, assuming $\rho = 4600 \text{ kg/m}^3$ and a cost of \$75/kg.

The proposed ring has four long straight sections with each having three spaces between quadrupoles with $\eta = 0$ and length adequate for cavities. Ten of these are available for rf cavities. Each of these drift spaces has a length of 3.1 m. Thus, the total length available for cavities is 31.0 m. An additional 6 straight sections of 2.59 m each could also be available if needed, but this use is not presently planned. The proposed cavities are more easily operated at voltages $\pm 10 \text{ kV}$, and at least 200 kV is required. Thus it is necessary to operate ~ 20 cavities, 2 between each quadrupole pair (or possibly 10 symmetric cavities using a common central gap with 20 kV across the gap).

Power is coupled into the cavity with the least dissipation in the tubes when the cavity inductance is high, and beam loading is minimized when the gap capacitance is high. Tuning range and efficiency are also conflicting

requirements since the cavity couples most efficiently in the tube at the bottom of the tuning range, whereas most power is required at higher frequencies. The allowable range of these parameters is determined by the relations¹¹

$$L_c = [\mu_{\text{eff}} \mu_0 L_1 \ln(R_o/R_i)]/2\pi = 10 \sim 35 \mu\text{H}$$

and

$$C_g = \frac{1}{(2\pi f_\ell)^2 L_c} = 2.6 \sim 1.3 \text{ nf}$$

where the parameters can span the ranges

$$\mu_{\text{eff}} = 1 + x (\mu - 1) = 130 - 300 \text{ (ferroxcube 4H ferrite)}$$

$$f_\ell = \text{lowest tuned frequency} = 0.7 - 0.8 \text{ MHz}$$

$$L_1 = \text{ferrite length} = 0.72 \text{ m}$$

$$x = \text{radial ferrite filling factor} \sim 0.7 - 0.9$$

$$\mu_0 = 4 \pi \times 10^{-7} \text{ h/m.}$$

Using $f_\ell = 0.8 \text{ MHz}$ (which is stable against the Robinson instability for $\gamma < \gamma_T$) loses some efficiency at lower frequencies but gives the values

$$L_c = 20 \mu\text{H}, C_g = 2.0 \text{ nf.}$$

The comparatively high value of C_g enables the gap capacitance to dominate the amplifier output capacitance, cavity distributed and stray capacitances. In addition, the large value of C_g tends to insure that there will be less beam excitation of the higher harmonics of the system.

The maximum cavity voltage is required only for a part of the acceleration cycle (near B maximum), and the tuning range is narrow enough so that it may be possible to produce the extra current required to drive the cavity off resonance. In the interests of reducing the overall power consumption, however, it seems desirable to absorb the added complexity of a tuned cavity.

Amplifier Design

There are two primary problems with cathode-follower operation. These are the high power consumption and the possibilities of oscillations. Figure III.4-1 shows a possible amplifier circuit capable of driving ± 11 kV in the cavity in Class A operation using an Amperex 8918 super power triode.¹² The possibilities of resonant oscillation have been minimized by resistors in the grid circuit and the possible addition of capacitance between the grid and anode. The output power comes from the cathode of the Amperex 8918 triode coupled directly to the accelerating gap. The tube is described in Fig. III.4-2. High voltage is supplied to the anode and power for the heaters by low capacitance filament transformers, thus the cavity is at dc ground, eliminating coupling capacitors. The Amperex 8918 exhibits a plate transconductance of $0.23 \Omega^{-1}$ (at $I_b = 15A$, $V_b = 16$ kV where I_b and V_b are the plate current and voltage), thus the output impedance would be about $4-10 \Omega$, significantly reducing waveform distortion due to beam loading.

The current required to drive this cavity in the absence of beam loading is roughly

$$I_{\max} = \frac{V}{Q\omega L_c} = 10 \text{ A}$$

for a cavity voltage of 10 kV and a Q of 10. Assuming a plate supply voltage of 14 kV and a maximum beam current of ~ 40 A, the maximum power approaches the power rating of the Amperex 8918 tube.

For a single bunch passing through a single cavity, the maximum total energy/turn required for acceleration is

$$U_{\text{acc}} = ne V \sin \phi_s$$

$$= (6.25 \times 10^{13}) \times (1.6 \times 10^{-19}) \times (5 \text{ kV}) = 0.05 \text{ J}$$

The cavity stores a maximum energy of

$$U_s = \frac{1}{2} C_g V^2 = 0.1 \text{ J}$$

The total loading on the gap voltage, however, is determined by the cathode-follower circuit. The maximum beam loading voltage is given by the relation

$$V^{\max} = I_{\text{beam}}^{\max} r_o \sim 230 \text{ V}$$

where

$$I_{\text{beam}}^{\max} = \text{maximum beam current} \sim 30 \text{ A}$$

$$r_o = \text{output impedance of cathode follower}$$

$$= \frac{1}{g_m} \left(1 + \frac{C_k \text{ ground}}{C_{gk}} \right) \sim 7.6 \Omega$$

where g_m , C_k , and C_{gk} are the transconductance and cathode capacitances to ground and grid. The effect of this beam loading is to alter the stable synchronous phase angle of the beam by a small amount ($< 2^\circ$).

The average power over the whole acceleration time, τ , are given by the relations below

$$P_{\text{beam}} = nq V_{\text{max}} \sin \phi / \tau = 500 \text{ kW}$$

$$P_{\text{tube}} = \frac{1}{\tau} \int_0^{\tau} V_b i_b dt = 160 \text{ kW}$$

where we have assumed

$$V_b^{\text{max}} \sim 14 \text{ kV}$$

$$I_b^{\text{max}} \approx I_{\text{beam}}^{\text{max}}$$

The total average power is $20 \times 0.16 = 3.2 \text{ MW}$.

The total power required from the line is roughly

$$\begin{aligned} P &= (P_{\text{tube}} + P_{\text{ferrite}} + P_{\text{beam}})/\epsilon \\ &= (3.2 \text{ MW} + 0.6 \text{ MW} + 0.5 \text{ MW})/0.5 \\ &= 8.6 \text{ MW} \end{aligned}$$

with an efficiency $\epsilon = 0.5$ for converting input to rf power.

Total costs can be estimated by assuming \$1.25/W and adding ferrite costs and cavity construction costs. The result is

$$\begin{aligned} \text{Cost} &= (8.6 \text{ MW} \times \$1.25/\text{MW}) + \$1.8 \text{ M} + \$1 \text{ M} \\ &= \$13.5 \text{ M.} \end{aligned}$$

The final stage amplifiers would have to be carefully protected against failure which would cause high voltages to be developed between the cathode and grid. This protection can be done with spark gaps. Current overload and temperature interlocks are of the usual type.

If the Q of the cavity is reasonably high (>5-10) and the beam loading only appears at part of the cycle, it is only required that the tube conduct around the time when the beam is going through the cavity, thus Class AB or B operation is, in theory, possible³. This could significantly reduce the overall power consumption. Even in Class A operation, the tube would be shut off with a -1000 V grid bias between acceleration periods.

Mechanical Structure

It is desirable to have the final amplifier tubes as close as possible to the gap. One possible configuration would be to have the final amplifiers, heater circuit inductance, etc., in a cabinet mounted so that they can be moved perpendicular to the cavity axis with the bus making contact with the outer and inner parts of the cavity by means of spring fingers. When service or repair of the amplifier is required, the whole unit can be withdrawn out of the cavity on the perpendicular rails, then transferred to rails parallel to the beam and rolled out of the accelerator tunnel quickly. This is a design similar to that proposed for the SNS.

The final amplifiers for one gap would occupy about 1.3m^3 and weigh ~ 1000 kg (most of this weight in the coupling inductance). Power and water connections and diagnostic signals should be the quick disconnect type.

SNQ-SRA RF SYSTEM PARAMETERS

RF Stations	10
Accelerating Cavities	20
Gaps per Cavity	1
Power Amplifiers	20
Amplifier Type	Cathode-follower
Frequency Range	0.71 to 1.13 MHz
Accelerating Voltage	200 kV peak
Voltage per Gap	10 kV peak
Average Power Delivered to Beam (at \dot{B} max)	1.16 MW

Conclusion

The simple models presented here show that the requirements of acceleration can be met using conservative limits on ferrite and power amplifiers. Since the short drift spaces are not efficiently filled, it seems desirable to add more ferrite and build cavities capable of operating at higher than 200 kV. A more detailed design should explore the limits in using all the available space and power to provide the highest possible accelerating voltage.

Serious theoretical questions requiring further study include optimization of the cathode-follower system to provide: 1) protection against oscillation, 2) optimum handling of higher beam loading harmonics, and 3) minimum power consumption. In addition, it is necessary to provide detailed studies of beam losses to insure that these can be kept below roughly 0.1% of the extracted beam intensity. These losses depend primarily on the shape and growth of the bunch in longitudinal phase space, which depend on many other systems in the accelerator.

III.5 VACUUM SYSTEM, CONTROL SYSTEM, DIAGNOSTICS

A detailed design of the vacuum system was not carried out in this study. Since the Rutherford-Appleton Laboratory has constructed ceramic vacuum chambers containing rf shield wires, which will be quite adequate for 50 Hz operation at 10^{-7} Torr and with comparable magnet apertures, it was decided initially to utilize this design for the SNQ-SRA system and to scale the costs appropriately. In some ways the construction of the chamber might be simpler here than for the SNS machine since the magnets are much shorter and two-step assembly and baking of the individual chambers would not be required. For the same reason, many more joints to connect two chambers together will be required. Following the SNS design, the magnet apertures were sized to allow 1 cm on top, bottom, and sides for the vacuum chamber and rf shields.

A preliminary analysis of the vacuum pumping requirements was made in Section II.9 in order to determine that 10^{-7} Torr was achievable with realistic pumps in the available lattice straight sections. This seemed necessary in order to evaluate concerns of beam loss and instabilities arising from ionization of the residual gas. The analysis indicated that 4 roughing pumps and 44 high vacuum pumps with pumping speeds of 500 l/sec were adequate to achieve the desired vacuum of $< 10^{-7}$ Torr.

The allowable desorption coefficient in order to prevent pressure runaway from desorption is 4-5. While the desorption coefficient of stainless steel is well below this limit, little is known about the desorption coefficient of ceramic. In addition, little experience exists to date on the reliability of ceramic chambers, particularly with high circulating proton currents.

Therefore, it might be prudent to search for alternative solutions to the vacuum chamber question.

One such alternative might be to enclose the magnet laminations within a stainless steel vacuum skin. Two existing rapid cycling proton machines, the ANL-RCS and the FNAL booster, employ this type of vacuum system. If feasible, it also has the advantage of reduced magnet aperture requirements with the consequent cost savings, although rf shields may still be required to minimize the coupling impedance of the system for stability reasons. The ANL-RCS has such a shield, the FNAL booster does not.

The vacuum in the ANL-RCS is about 10^{-6} Torr, not adequate for the high current machine being studied. The operating pressure in the FNAL booster, however, is a few $\times 10^{-7}$ Torr average. It is felt by some that with good techniques and careful design, a vacuum of 10^{-8} Torr might be possible with the magnet laminations within the vacuum chamber, well within the requirements of this study. There is not total agreement on this subject, however, and problems pointed out are epoxy on the laminations, and ultimately the coil insulation. Cryopumping in selected places might help so that the feasibility of this approach remains an open question.

It seems somewhat premature in this study to do a detailed design of the control system. An adequate cost for such a system can be estimated by taking a percentage of the accelerator cost.

Likewise the diagnostic system, which is very important for achieving the high design current with sufficiently low beam loss, can nevertheless be roughly estimated without a detailed design of the many individual elements required.

References for Section III

1. K. Thompson, "SNQ-SRA Ring Magnets - Designs and Costs," AAD-N-25 (December 1982).
2. K. Thompson, "An Interactive Code for Optimization of Water-Cooled Conductors," Proc. 4th Int. Conf. on Magnet Technology, Report CONF-720908, p. 725 (1972).
3. W. Praeg, D. McGhee, "Ring Magnet Power Supply for a 500 MeV Synchrotron," Conference Record Industry Application Society, IEEE- IAS-1978, 13th Annual Meeting, Toronto, Oct. 1978.
4. W. Praeg, D. McGhee, G. Volk, "Phase Lock of Rapid Cycling Synchrotron and Neutron Choppers," IEEE Transactions on Nuclear Science, Vol. NS-28, No. 3, June 1981.
5. W. Praeg, "A High Current Low-Pass Filter for Magnet Power Supplies," IEEE Transactions on Industrial Electronics and Control Instrumentation," Vol. IECI-17, No. 1, Feb. 1970.
6. W. Praeg, "Pulsed Magnet Systems for High Energy Physics Beam Lines," Proceedings of 5th International Conference on Magnet Technology, Rome, Italy, April 1975.
7. W. Praeg, "A Ring Magnet Power Supply for Shaped Excitation of the 1.1 GeV Spallation Neutron Quelle," AAD-N-24, December 1982.
8. D. E. Suddeth and G. J. Volk, "Rapid Cycling Synchrotron (RCS) Single Stage Kicker Magnet," IEEE Conference Records of 1980 Fourteenth Pulse Power Modulator Symposium, pp. 289-291.
9. D. E. Suddeth and G. J. Volk, "The Rapid Cycling Synchrotron Extraction Kicker Magnet Drive System," IEEE Trans. Nuc. Sci., Vol. NS-28, No. 3 (June 1981).
10. These calculations were performed by G. J. Volk, ANL.
11. C. Bovet, et al., "A Selection of Formulae and Data Useful for the Design of the A. G. Synchrotron," CERN/MPS-S1/INT, DL/70/4.
12. IPNS, A National Facility for Condensed Matter Research, Argonne National Laboratory Report, ANL-78-88 (1978).
13. A. Luccio, M. Puglisi, IEEE Transactions on Nuclear Science, NS-28, 2893 (1981).

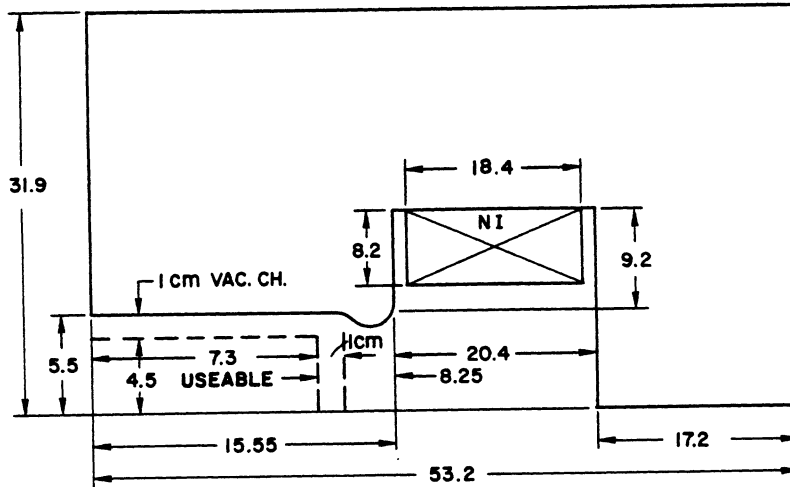


Fig. III.1-1 SNQ-SRA Dipole Magnet
(1/4 Section Not Shown to Scale)

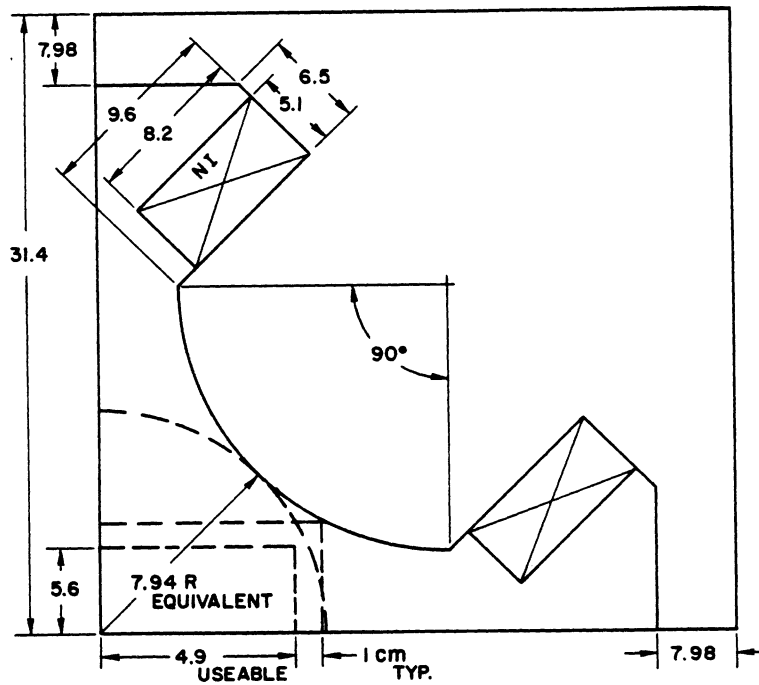
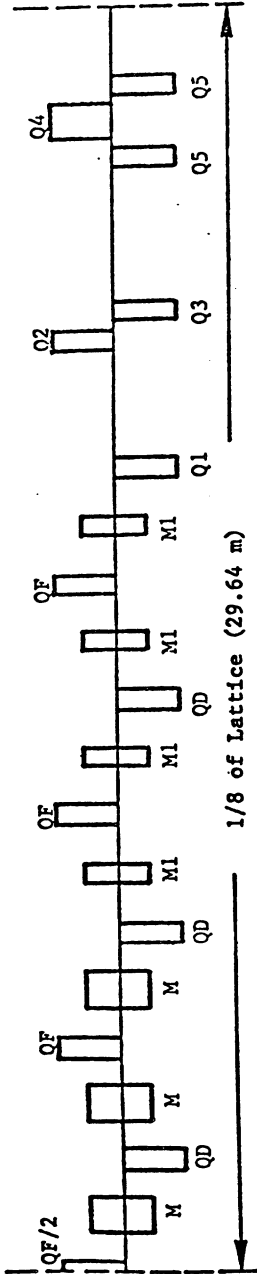


Fig. III.1-2 SNQ-SRA QD (Q1) Quadrupole Magnet
(1/4 Section Not Shown to Scale)



	M	M1	QF	QD	Q1	Q2	Q3	Q4	Q5	Totals
Bore or Aperture (cm)	14.6x11.0	14.6x11.0	16.65	15.88	22.15	20.35	15.57	15.06		
Effective Length (cm)	90	45	50	50	50	50	85	50		
L (mH)	2.34	1.17	0.45	0.47	11.6	4.55	2.62	0.87		
T (s)	0.85	0.61	0.44	0.46	7.25	3.11	1.72	0.68		
E (V)	965	484	202	212	4945	1938	1091	383		
Iac (A)	1301	1301	1409	1409	1358	1354	1321	1391		
Idc (A)	2741	2741	2967	2967	2861	2851	2782	2930		
Irms (A)	2891	2891	3130	3130	3018	3008	2935	3091		
P (kW)	36.5	22.8	13.8	13.8	50.5	31.0	26.4	17.1		
W (kJ)	19.1	9.6	4.3	4.5	103.0	40.2	22.0	8.1		
Qty	24 + 1	32	28	24 + 1	8	8	8	16		158
ΣP (kW)	912	731	388	345	404	248	211	273		3,620
ΣW (kJ)	478	306	121	114	824	322	176	130		2,500
ΣK\$	1545	1575	1225	1028	1601	949	673	817		9,760

Table III.1-2 Summary of Magnet Characteristics for SNQ-SRA Lattice

Power System	Rating kVA	Cost/kVA (Power Supply)	Power Supply	C1	C2	S1	S2	Chokes	Inter Connections	Totals
P1	4 x 1543	0.240	1,480	700	655	160	100	411	1083	4,589
P2	4 x 688	0.250	688	83	77	22	15	297	1007	2,249
P3	4 x 103	0.300	124	25	24	7	5	66	150	401
P4	4 x 380	0.260	395	580	540	164	100	210	150	2,139
P5	4 x 234	0.280	262	230	214	65	40	132	150	1,097
P6	4 x 200	0.280	224	125	120	36	25	92	150	772
P7	4 x 257	0.280	288	95	90	26	17	112	305	933
Totals			3,461	1,838	1,720	480	302	1,380	2,995	12,176

Table III.2-2 Cost Estimate for Power Systems in K\$

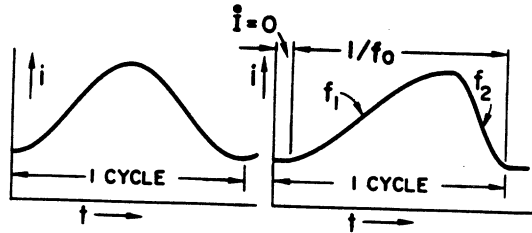


Fig. III.2-1
DC-Biased Sinewave
Excitation

Fig. III.2-2
DC-Biased Dual
Frequency
Excitation
with Flat-Bottom

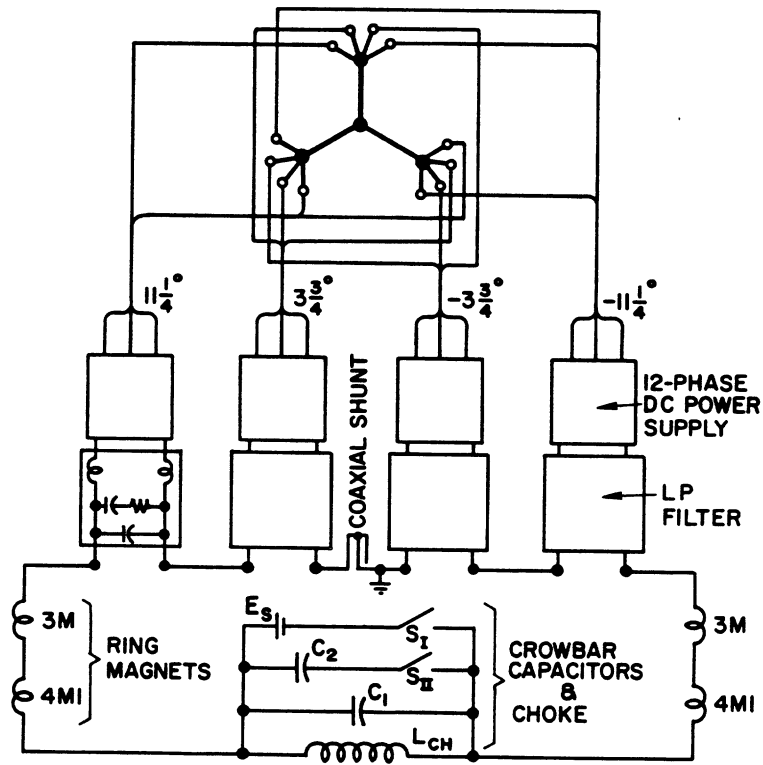


Fig. III.2-3
48-Phase Power Supply for Bending Magnets

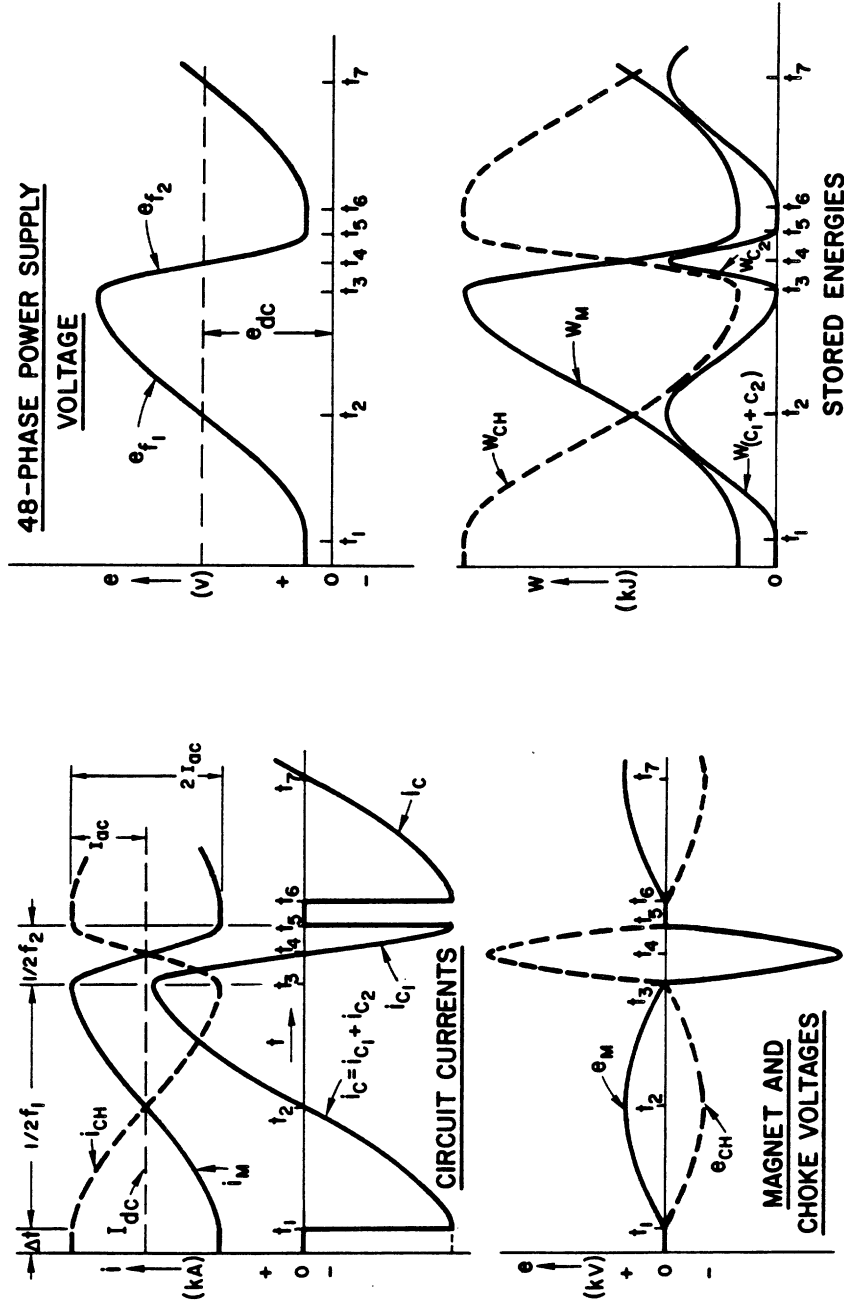
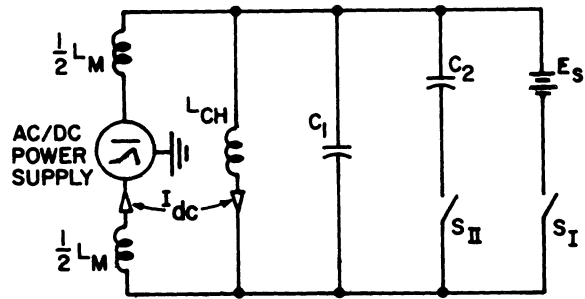
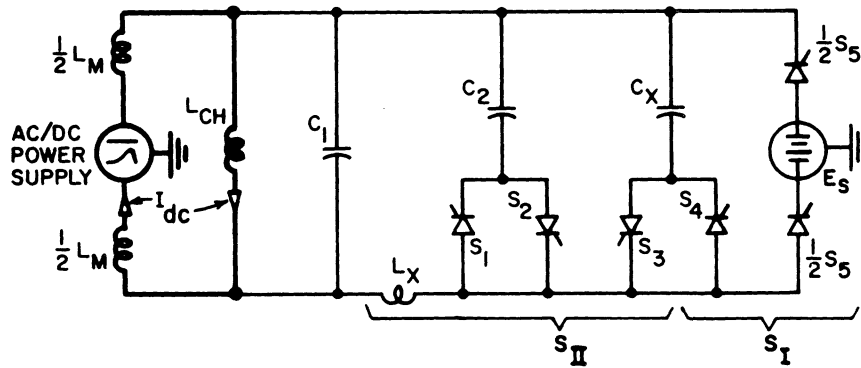


Fig. III-2-4
Waveforms of Currents, Voltages and Energies for the Circuit of Fig. III.2-3



a) Ideal Circuit



b) Solid State Circuit

Fig. III.2-5
Switching Circuits

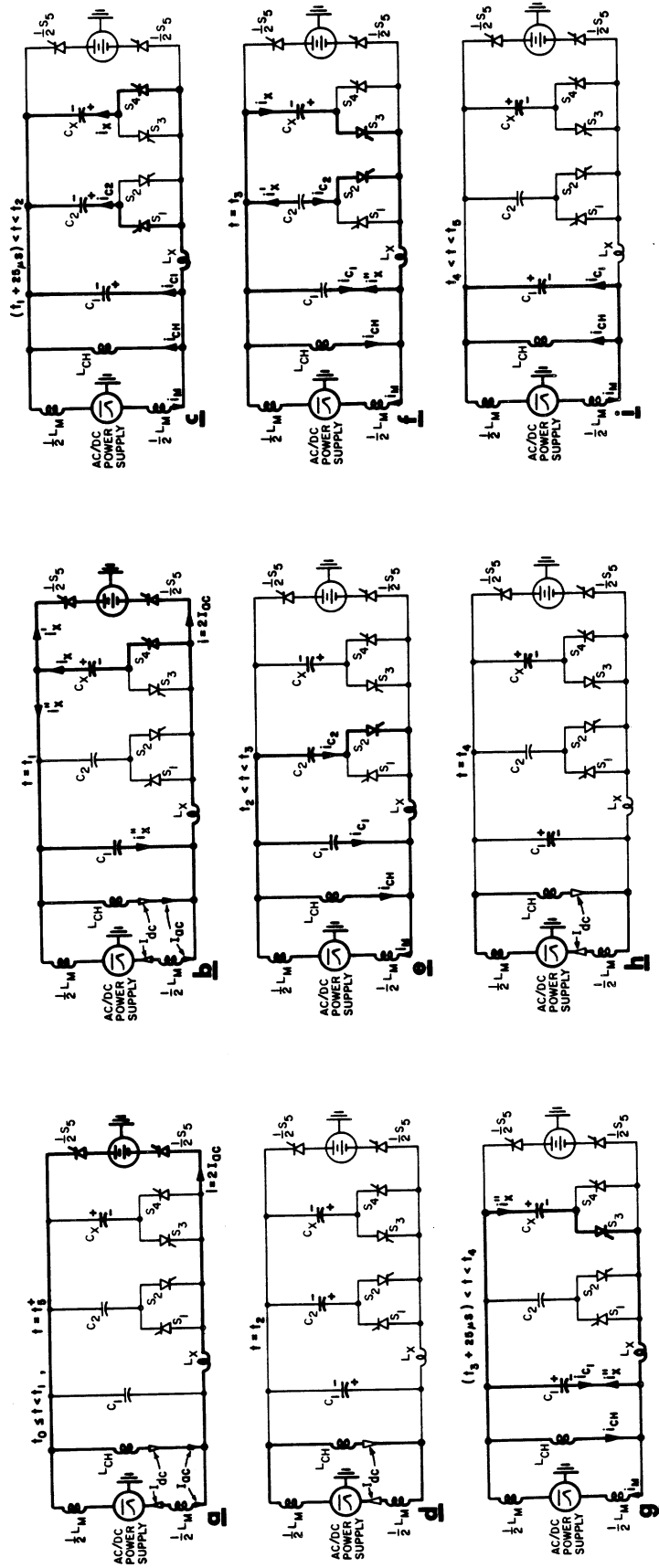
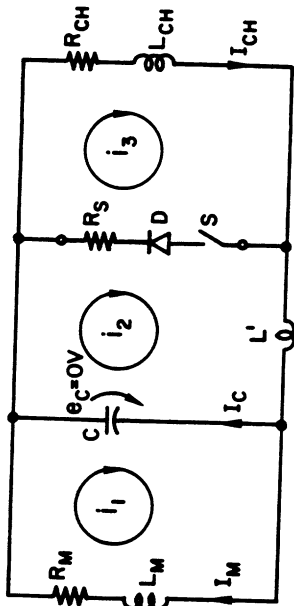
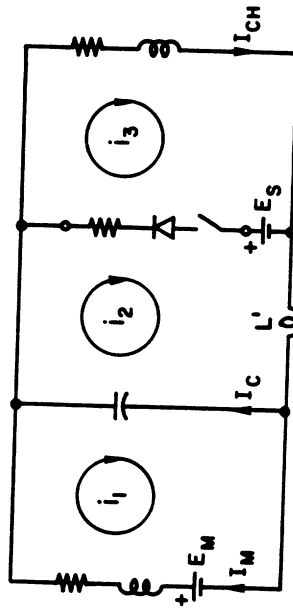


Fig. III.2-6
Diagrams of Circuit Response at Various Times During a Cycle



b) Passive Crowbar



a) Active Crowbar

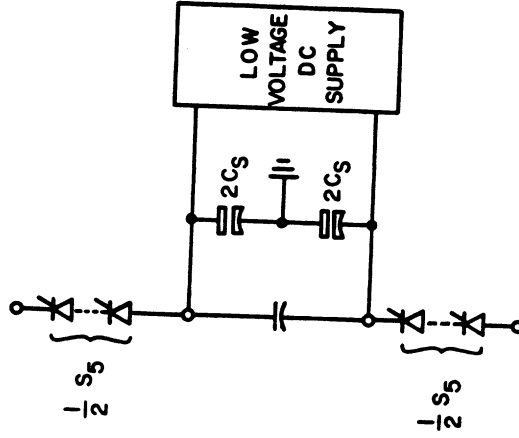


Fig. III.2-8
Crowbar Power Source

Fig. III.2-7
Crowbar Circuits

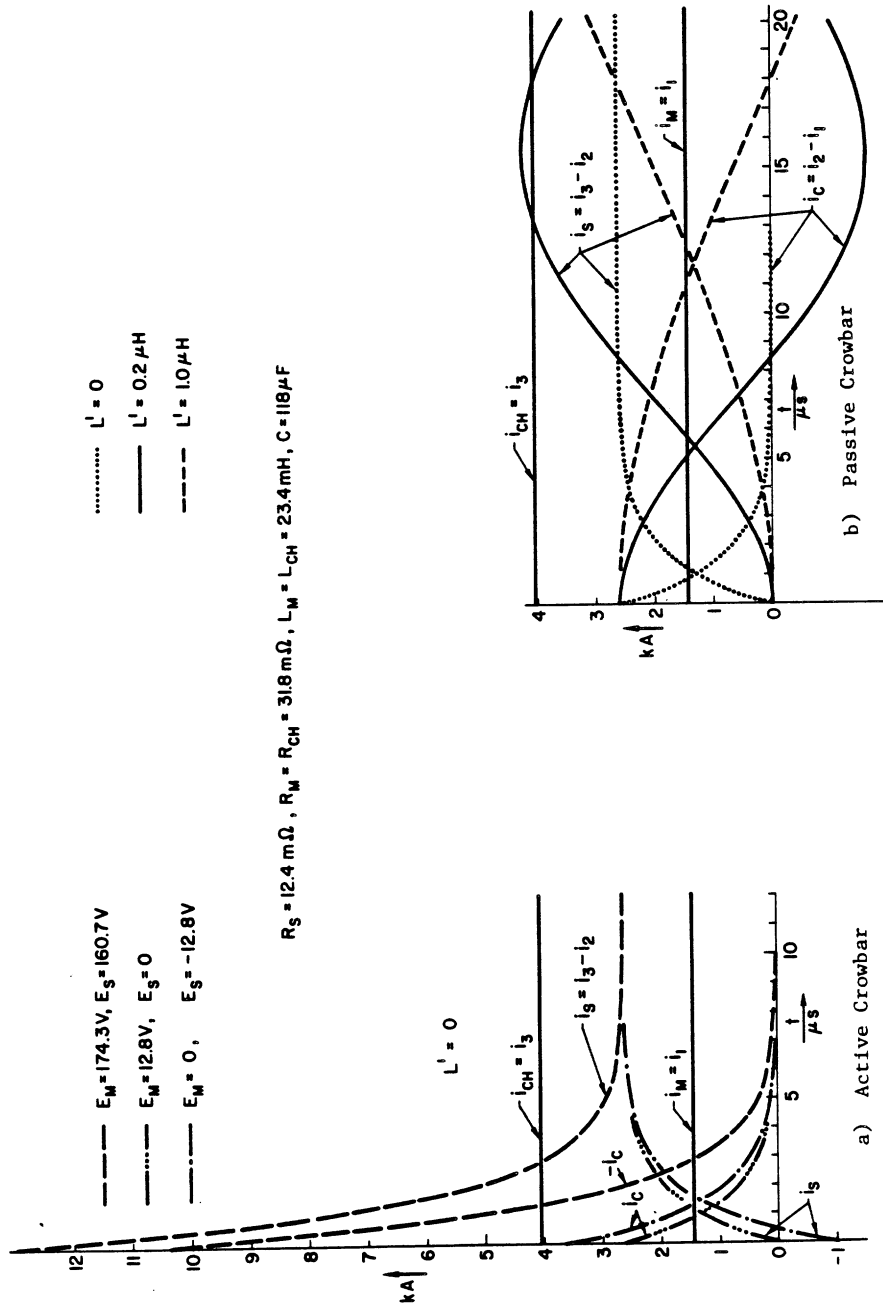


Fig. III.2-9
Transient Response of Crowbar Circuits

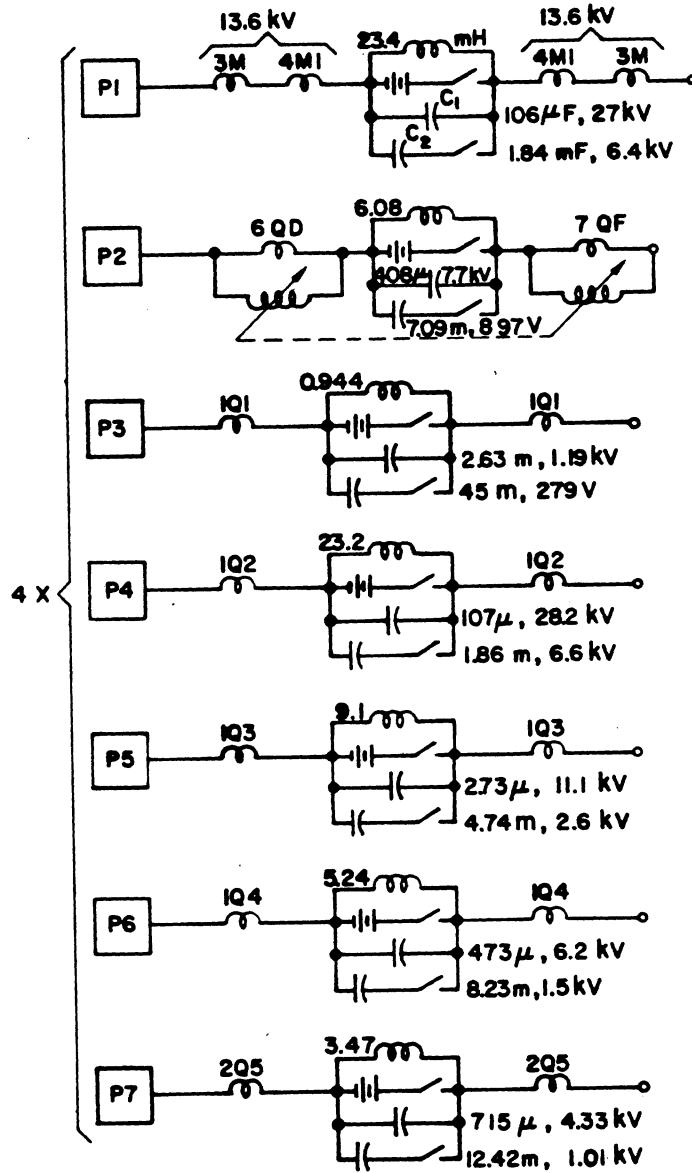


Fig. III.2-10
Ring Magnet Power Supply Circuits

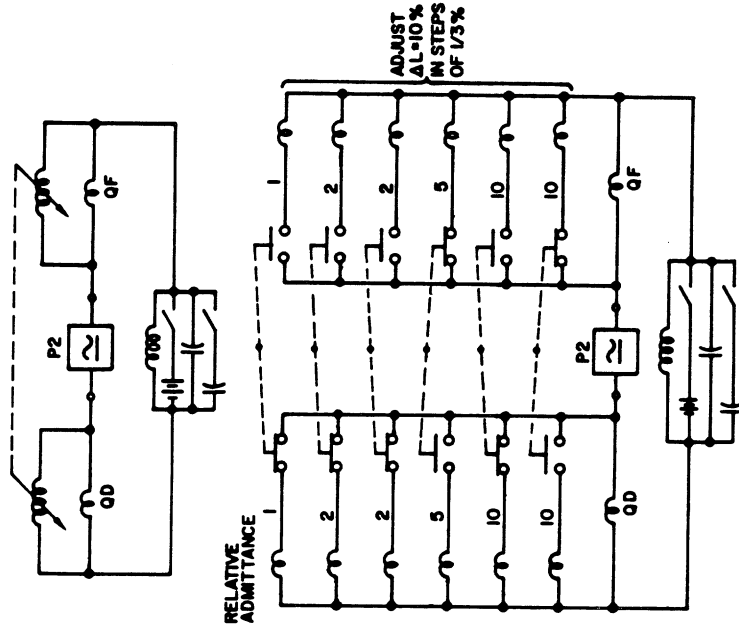


Fig. III.2-12

Detail of Trimming Choke Circuit.

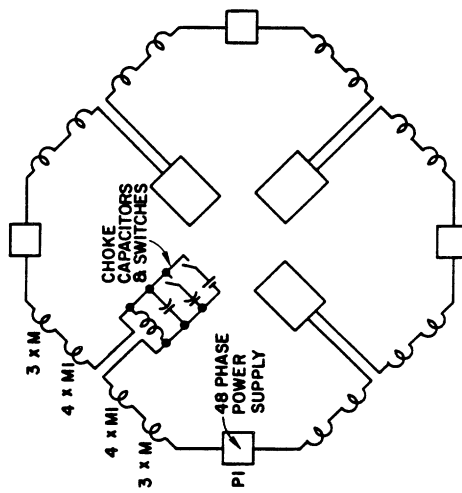
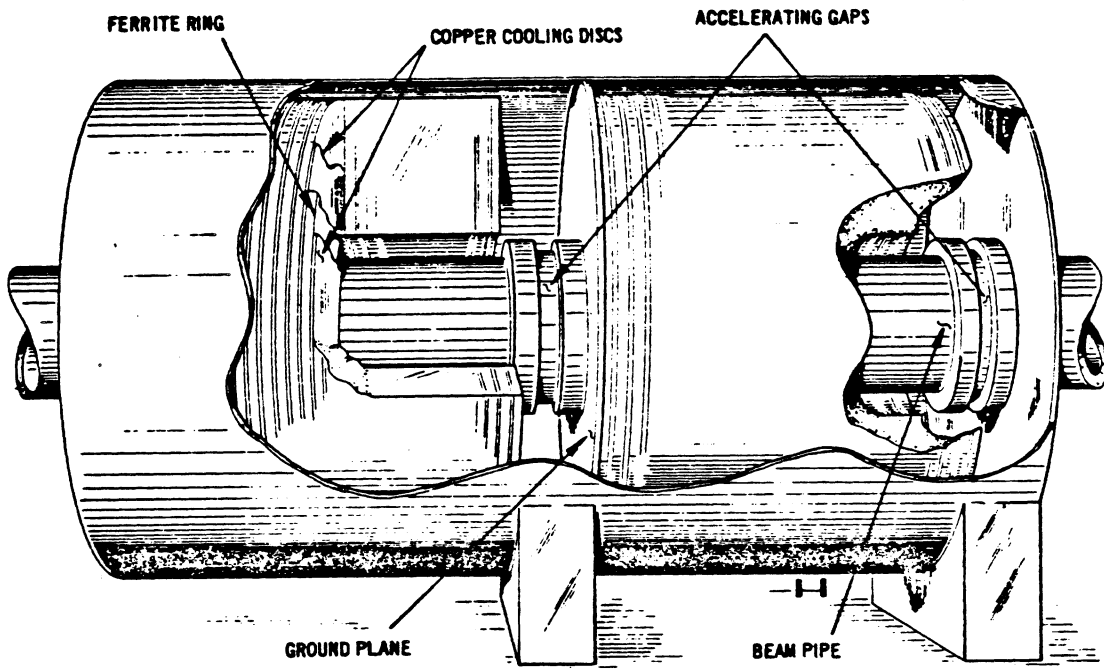


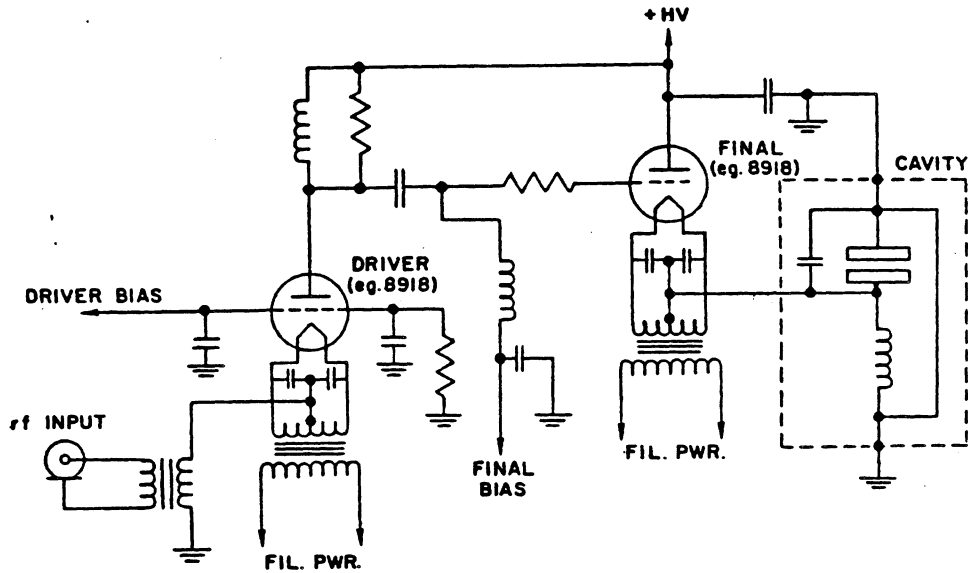
Fig. III.2-11
Ring Magnet Power Supply
for Bending Magnets

ARGONNE NATIONAL LABORATORY		DIVISION	PROJECT	FILE NO.	PAGE	
ENGINEERING NOTE						
SUBJECT SNQ Extraction Kicker Magnet Vertical Extraction		NAME G. Volk				
		DATE 12/9/82		REV. DATE		
		Cell 1	Cell 2			
		l	1.25 m	1.25 m		
		W _g	9 cm	9 cm		
		h _g	9 cm	11 cm		
				$B_{max} = 700 \text{ Gauss } (.07T)$ $\tau_{R max} = 400 \text{ nsec}$		
Ferrite-Ceramic Magnet Type C2050 ($\mu_o = 4\pi \times 10^{-7}$)						
$\frac{\partial L}{\partial l} = \frac{\mu_o h_g}{W_g} = \frac{(4\pi \times 10^{-7})(9)}{9} = 1.26 \times 10^{-6} \text{ H/m} \quad \text{Cell 1}$						
$= \frac{4\pi \times 10^{-7}(11)}{9} = 1.54 \times 10^{-6} \text{ H/m} \quad \text{Cell 2}$						
$L_m = \left(\frac{\partial L}{\partial l}\right) l = 1.58 \times 10^{-6} \text{ H} \quad \text{Cell 1}$						
$= 1.92 \times 10^{-6} \text{ H} \quad \text{Cell 2}$						
$I_m = \frac{B W_g}{\mu_o} = \frac{(.07)(.09)}{4\pi \times 10^{-7}} = 5000 \text{ amps} \quad \text{Both cells}$						
Limiting the maximum voltage to $< 40 \text{ kV} - Z_o = 8 \Omega$						
Two Belden YR 10914 cables in parallel sets $Z_o = 7 \Omega$						
Magnetic field fill time = $L/Z = 225.7 \times 10^{-9} \text{ sec} \quad \text{Cell 1}$						
$= 274.3 \times 10^{-9} \text{ sec} \quad \text{Cell 2}$						
Required PFN voltage for matched system = $I_m Z_o = 35 \text{ kV}$						
For lumped LC magnet the trim capacitors are						
$C_m = L/Z^2 = .032 \mu\text{f} \quad \text{Cell 1}$						
$= .039 \mu\text{f} \quad \text{Cell 2}$						

Table III.3-2



Schematic of Cavity



Schematic Design

Fig. III.4-1 Cavity and schematic of acceleration system.

**CONCEPTUAL DESIGN OF A RAPID-CYCLING SYNCHROTRON FOR
KFA-JULICH SPALLATION NEUTRON SOURCE**

SECTION IV

CONVERSION TO FULL ENERGY ACCUMULATOR RING

Amperex Electronic Corporation
A NORTH AMERICAN PHILIPS COMPANY

HICKSVILLE DIVISION

230 Duffy Avenue
Telephone: 516/931-6200

Hicksville, L.I., N.Y. 11802
TWX: 510/221-1839

**TUBE TYPE
8918**

TYPE	TRIODE
COOLING	WATER
ENVELOPE	CERAMIC
MAX. PWR. INPUT	750 kW
MAX. PLATE DISS.	300 kW
MAX. FREQ.	30 MHz

The Amperex 8918 is a super power triode capable of delivering over 500 kW at anode voltages up to 19.2 kV. It is a new industrial tube available as part of the coaxial ceramic triode line.

The tube is constructed with a mesh cathode and mesh grid for extreme ruggedness and small size. The exclusive, special process "K" grid makes possible the ability of this tube to retain its characteristics in spite of potentially dangerous overloads.

Excellent thermal efficiency is obtained because of the specially designed heavy walled anode. The tube requires only 0.14 gallons of water per minute per kilowatt of plate dissipation.

GENERAL CHARACTERISTICS

MECHANICAL

Mounting Position	vertical with anode up or down
Net Weight	66 lbs.
Accessories	
Center Filament Connector	S-331980
Outer Filament Connector	S-331981
L.F. Grid Connector \leq 4MHz	S-331979
H.F. Grid Connector $>$ 4MHz	S-332751
Maximum Operating Temperatures	
Envelope Temperature	240°C
Recommended Max. Envelope Temperature under continuously loaded conditions	200°C
Water Inlet Temperature	50°C max.
Water Pressure	6 atmospheres max.

Cooling Characteristics ¹

Plate and Grid Dissipation (kW)	Inlet Temperature (°C)	Water Flow (GPM)	Inlet Pressure (psi)	Output Temperature (°C)
300	20	42.5	23.5	48
	50	63.5	45.5	69
240	20	31.7	14.7	50
	50	47.6	26.5	70
200	20	25.1	9.6	52
	50	38.0	17.6	71
160	20	19.0	6.2	54
	50	29.0	11.0	72

¹At low frequencies the seals are sufficiently cooled if the filament connectors are water-cooled by a flow of about 1 quart per min. At high frequencies, however, an additional airflow of about 210 C.F.M. must be led along the seals from a 2½ inch diameter nozzle positioned at a distance of 12 inches from the tube header.



Amperex®

Information furnished by Amperex is believed to be accurate and reliable. However, no license for its use is hereby conveyed under any patent and no responsibility is assumed by Amperex for its use; nor for any infringements of patents or other rights of third parties which may result from its use.

Revised July 1975

Amperex® . . . Tomorrow's Thinking in Today's Products®

Fig. III.4-2

IV. CONVERSION TO FULL ENERGY ACCUMULATOR RING

Introduction

The ultimate goal of the SNQ program is to operate an accelerator system with an average current of 5 mA of 1.1 GeV protons and a pulse length suitable for use as a pulsed spallation neutron source and as a particle physics facility. The pulse length goal is taken as a beam duration of 200 nsec. It is assumed that the accelerator system will consist of a 1.1 GeV linac and an accumulator/compressor ring to produce the very short pulse duration at very high pulse current. The purpose of this section is to investigate the feasibility of utilizing the SRA synchrotron as this full energy accumulator/compressor ring.

The goal of achieving a 200 nsec pulse duration is quite different than that of the IKOR study. This difference raises questions as to whether or not the accumulator/compressor ring is an isochronous ring such as IKOR or the SNQ-SRA modified to be isochronous, the SNQ-SRA with its designed non-isochronous characteristics, or any other ring of a new design. These questions involve the very high average charge desired which result in extremely high currents when the pulse duration is limited to 200 nsec. Any ring designed for this purpose will have a circumference not very different for 1.1 GeV protons than the SNQ-SRA at ~ 240 m so that the projected currents for the SNQ-SRA will be nearly the same for other rings. If we assume a repetition frequency of 100 Hz, then we want to accumulate 3.1×10^{14} protons per pulse at 1.1 GeV. In the SNQ-SRA this would result in an average current of 56 A with a revolution period of 890 nsec. If this beam is bunched to 600 nsec, the average current during the bunch would be 83 A, at 400 nsec it would be 124 A, and at 200 nsec 248 A. If we now fold in a factor of 1.5 as the

peak current for a parabolic distribution of a bunched beam, the latter current is 372 A.

These results are not very sensitive to the ring chosen for the accumulator/compressor ring and significantly exceed any existing experience. The current at a bunch length of 200 nsec will be shown to be very close to the transverse space charge limit of the SNQ-SRA with a betatron tune of about 11 and would exceed the limit if the betatron tune were reduced to about 4 to make it isochronous like the IKOR machine (by about a factor of 3). In addition, accumulating a chopped beam such that the beam occupies only 200 nsec of the 890 nsec period of the ring places unrealistic, and possibly unrealizable, restrictions on the linac. For instance, the accumulation of 3.1×10^{14} protons per pulse would require 200 mA of H^- for 250 μ sec for an unchopped linac beam (assuming 100% injection efficiency), if chopped to 400 nsec each 890 nsec, the same current would require 556 μ sec, and chopped to 200 nsec each 890 nsec, would require 1.1 μ sec. A shorter linac pulse would require higher currents.

For an isochronous machine it is not possible to do bunch length manipulation so that chopped 200 nsec injection would be required. In addition to possibly exceeding the transverse space charge limit, the longitudinal space charge forces would require an rf capability which is a significant part of the SNQ-SRA rf system to contain the beam. Thus for such short pulse durations, there seems to be few advantages for an isochronous accumulator/compressor ring, particularly if the SNQ-SRA synchrotron can be converted to serve this purpose. It would avoid the problems discussed above by accumulating longer pulses and performing bunch length manipulation with an rf system (possibly the existing one) prior to extraction.

In order to investigate this possibility we would propose to inject into the machine chopped beam with pulses of 600 nsec each 890 nsec (revolution period) synchronously with the rf frequency. This would require, for instance, 148 mA of H^- for 500 μ sec from the linac. Assumed linac beam parameters of transverse emittance (both planes) of 4.4π mm-mr and $\Delta p/p$ of 5×10^{-3} appear easily achievable and are quite adequate for the present purpose. The longitudinal emittance of such a beam $\epsilon = \Delta E \cdot \Delta t = 2.4$ eV-sec, accidentally very similar to the longitudinal emittances used in the synchrotron study of this report. The main results of this report are therefore applicable except that here we must take into account longitudinal space charge forces. With these assumptions we will examine transverse space charge effects, longitudinal and transverse instabilities, bunch length manipulation, and longitudinal space charge effects.

Transverse Space Charge Effect

We can compare the transverse space charge limits of the ring at 1100 MeV and that of the SNQ-SRA at 200 MeV. Since the number of protons per pulse being compared is a factor of five, the space charge limit of the accumulator ring has to be greater than that of the SNQ-SRA by a factor of five or more. The $\beta^2 \gamma^3$ term for 200 MeV and 1100 MeV protons are 0.572 and 8.08, respectively, and the ratio of these two numbers is about 1 to 14. Now we must take into account the bunching factors in the comparison. To do this we note that in the case of the SNQ-SRA the circulating protons occupy about 70% of the circumference when the transverse space charge effect is maximal. If we were to choose to inject into a 200 nsec bunch, then the bunching factor term would reduce this ratio to 1 to 4.5. In calculating the space charge limit for the synchrotron case we have used a parabolic distribution of

charges in the bunch, and a factor of 1.5 is used to relate the peak density to the average value. Thus the ratio can be either 1:4.5 for a parabolic distribution or 1:6.7 for a uniform distribution in the accumulator ring. As an 1100 MeV accumulator ring the SNQ-SRA would be about at its space charge limit with a bunch length of 200 nsec and using the full aperture of the machine. If the tune were reduced to about 4 to make it isochronous, the 200 nsec bunch length would clearly be beyond the space charge limit of the machine. For injection into a 600 nsec bunch length in the SNQ-SRA the circulating current would be about a factor of 3 below the space charge limit so that the beam need not use all of the available aperture. This condition would certainly enhance the possibility of loss free extraction.

Longitudinal Stability of Fully Stacked Beam in the SNQ-SRA

A beam occupying the full aperture of the machine minus clearance, calculated by the methods of Section II.4, would have a longitudinal coupling impedance, χ_{\parallel}/η , of about 70 Ω . With this Z_{\parallel} we calculate the longitudinal instability threshold momentum spread, $(\Delta p/p)_{FWHM}$ for various accumulated peak currents. The threshold momentum spread and the instability risetime for the $\Delta p/p = 0$ beam are shown in Fig. IV-1. It shows that the $\Delta p/p$ is in a reasonably attainable range for various peak currents, and at the same time the risetime of the instability, under the assumption of $\Delta p/p = 0$, is about 1/2 millisecc. With the beam uniform over 600 nsec the current during the bunch would be 84 A. For a parabolic charge distribution the peak current would be 126 A.

Transverse Stability of Fully Stacked Beam in the SRA

A beam occupying the full aperture minus clearance would have a transverse coupling impedance of about 660 kΩ/m. This value of Z_{\perp} should be compared with 4.6 MΩ/m of Z_{\perp} for a fully damped beam of the synchrotron at 1.1 GeV. The factor of seven comes from the differences in the beam sizes of the fully damped beam and the injected beam. As in Section II.4 the coasting beam transverse stability criterion can be written

$$|Z_{\perp}| < 2\pi \frac{E_o}{e} \frac{v\beta\gamma}{RI} \left[\frac{\Delta p}{p} |\eta (n-v) - v\xi| + \Delta v^{\text{oct}} \right] \Omega/\text{m} .$$

As we have done previously, we divide the above equation into three parts and consider each separately with the current, I, as a variable

$$\begin{aligned} \eta \text{ term: } & 2\pi \frac{E_o}{e} \frac{v\beta\gamma}{RI} \left[\frac{\Delta p}{p} (n - v)|\eta| \right] \\ & = 2.1 \times 10^6 / I \text{ } [\Omega/\text{m}] \end{aligned}$$

$$\begin{aligned} \xi \text{ term: } & 2\pi \frac{E_o}{e} \frac{v\beta\gamma}{RI} \left[\frac{\Delta p}{p} |v\xi| \right] \\ & = 2.5 \times 10^7 / I \text{ } [\Omega/\text{m}] \end{aligned}$$

$$\begin{aligned} \Delta v^{\text{oct}} \text{ term: } & 2\pi \frac{E_o}{e} \frac{v\beta\gamma}{RI} [\Delta v^{\text{oct}}] \\ & = 4.7 \times 10^8 / I \text{ } [\Omega/\text{m}] \end{aligned}$$

where we have made the following assumptions:

$$\frac{\Delta p}{p} = 5 \times 10^{-3} \qquad \eta = 0.195$$

$$\nu = 11.3$$

$$\xi = -0.15$$

$$n = 12$$

$$\Delta\nu^{\text{oct}} = 0.15 \text{ across the stack}$$

Having derived each contributing term to the stability criterion, it would be instructive to calculate the threshold current by each term independently. To do so we compare the above three terms to $Z_{\perp} = 660 \text{ k}\Omega/\text{m}$. The calculated threshold current should be viewed as the peak current of the stack. Then from each term we obtain:

$$\begin{array}{ll} \eta \text{ term:} & \hat{I} = 3\text{A} \\ \xi \text{ term:} & \hat{I} = 37\text{A} \\ \Delta\nu^{\text{oct}} \text{ term:} & \hat{I} = 700\text{A} \end{array}$$

These results show that the octupole term is essential, and this term can contain a substantial current as far as this consideration goes. It is interesting to note that amongst the above three terms, the η and ξ terms depend on the $\Delta p/p$ of the stack, and the octupole term does not. Thus the $\Delta p/p$ consideration in the design is strictly for the longitudinal stability.

Risetime of the Longitudinal Instability During Accumulation:

With a 600 nsec bunch the average current within the bunch is 82 A and assuming a parabolic bunch, the peak current is 123 A to be accumulated in 560 turns or 0.5 msec. During this period, the filling of the acceptance is assumed to be proportional to the number of turns being accumulated. With these conditions, we can calculate the risetime of the longitudinal instability at a given instant of accumulation. The result shown in Fig. IV-2 is for $\Delta p/p = 0$ beam. From this figure, we can calculate an average

integrated risetime from the start of injection by integrating the growth rate.

The result of this integrated average is 0.93 msec. This means that after injection, there will be approximately 0.4 msec to manipulate the bunch length before the e-folding time takes over.

Bunch Length Compression with the SNQ-SRA Optics
and the Longitudinal Space Charge Effect

The longitudinal phase space estimated for the accumulator ring is similar to that of the synchrotron case, and therefore the compression of bunch length discussed in Section II.5 can be applied here. However, the number of protons per pulse involved in this discussion is a factor of five larger than that of the synchrotron, and thus the longitudinal space charge force should be considered. To estimate this effect, we consider the required rf voltage to contain N protons in a τ sec long bunch with a parabolic distribution. Then we can write the required voltage to be:

$$\frac{V}{h} > \frac{\frac{\Delta\phi}{2}}{\sin \frac{\Delta\phi}{2}} \frac{6gNe}{\epsilon_o \gamma^2 |\Delta\phi|^3 R} = \frac{3gNe}{\sin \frac{\Delta\phi}{2} |\Delta\phi|^2 \epsilon_o \gamma^2 R}$$

where

$$\Delta\phi = \omega\tau h = 1.41 \text{ radians for } h = 1, = 2.82 \text{ for } h = 2$$

$$\omega = \text{angular rotation frequency}$$

$$g = 1 + 2 \ln \frac{b}{a} = 1.36$$

$$b = \text{vacuum chamber gap half-height} = 5.4 \text{ cm}$$

$$a = \text{radius of beam} = 4.5 \text{ cm}$$

$$N = \text{number of protons in ring } 3.1 \times 10^{14}$$

$$\epsilon_o = \text{dielectric constant} = 8.85 \times 10^{-12} \text{ A} \cdot \text{sec/v} \cdot \text{m}$$

- γ = relativistic variable
- h = harmonic number of rf system = 1 or 2
- e = electric charge = 1.6×10^{-19} A · sec
- R = mean radius of machine.

Substituting the above numerical values, we find that the rf voltage should be: $V > 97$ kV for $h = 1$ and $V > 37$ kV for $h = 2$. It is worthwhile to note that when the bunch length is short $\Delta\phi \ll 2\pi$, the required voltage to overcome the space charge forces is inversely proportional to the cube of the bunch length. Therefore, a short bunch length before necessary should be avoided, if possible. Having noted the need to consider the longitudinal space charge effect, we now summarize the bunch length compression.

In Section II.5 it was shown that one bunch of $\epsilon = 2.4$ eV-sec can be compressed adiabatically to a bunch length of 300 nsec with a peak rf voltage of about 200 kV. In this case, the space charge effect needs some 30 kV to contain the beam into a 300 nsec long bunch. The adiabatic compression is a slow process by definition, and the time needed to accomplish this is several synchrotron periods and it may turn out to be of the order of 1 msec which is too long. On the other hand, the use of a fast bunch rotation technique can be used to compress a 600 nsec bunch to a 200 nsec bunch within ~ 100 μ sec after the accumulation.

Two 300 nsec bunch accumulation by the converted SNQ-SRA with an $h = 2$ rf system seems to have many advantages over single bunch mode as far as the bunch length compression is concerned. The trade-off is to have a complicated extraction system, and this alternative, although it has not been studied in detail is attractive.

Direct Conversion of SNQ-SRA to Accumulator Ring:

The most economical and also flexible conversion seems to use the SNQ-SRA as proposed to accumulate the full current. Because of the higher tune value of the machine, the space charge limit is high, and the system would have the capability of manipulating the bunch length after the accumulation. To ease the linac requirements, we can either accumulate in a 600 nsec bunch or two 300 nsec bunches. For the case of a 600 nsec initial bunch, we can rotate the bunch by a fast method as described earlier, or in the case of two 300 nsec bunch accumulation, little or no rf programming seems necessary. Especially for the later case, the hole-keeper rf system proposed for IKOR can be used to maintain the bunch formations. Although this discussion is the first pass of the conversion issue, there seems no major extrapolations from the previous study, such as the IKOR study. Further study, however, is warranted.

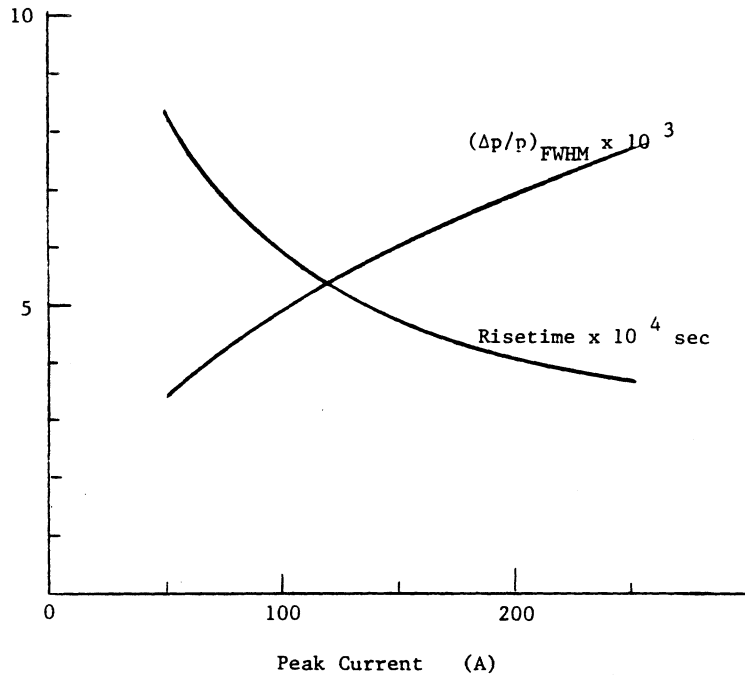


Fig. IV.-1 Longitudinal Stability Threshold Momentum Spread and the Risetime of Instability for $\Delta p/p=0$ Beam as a Function of Peak Current in the Stack

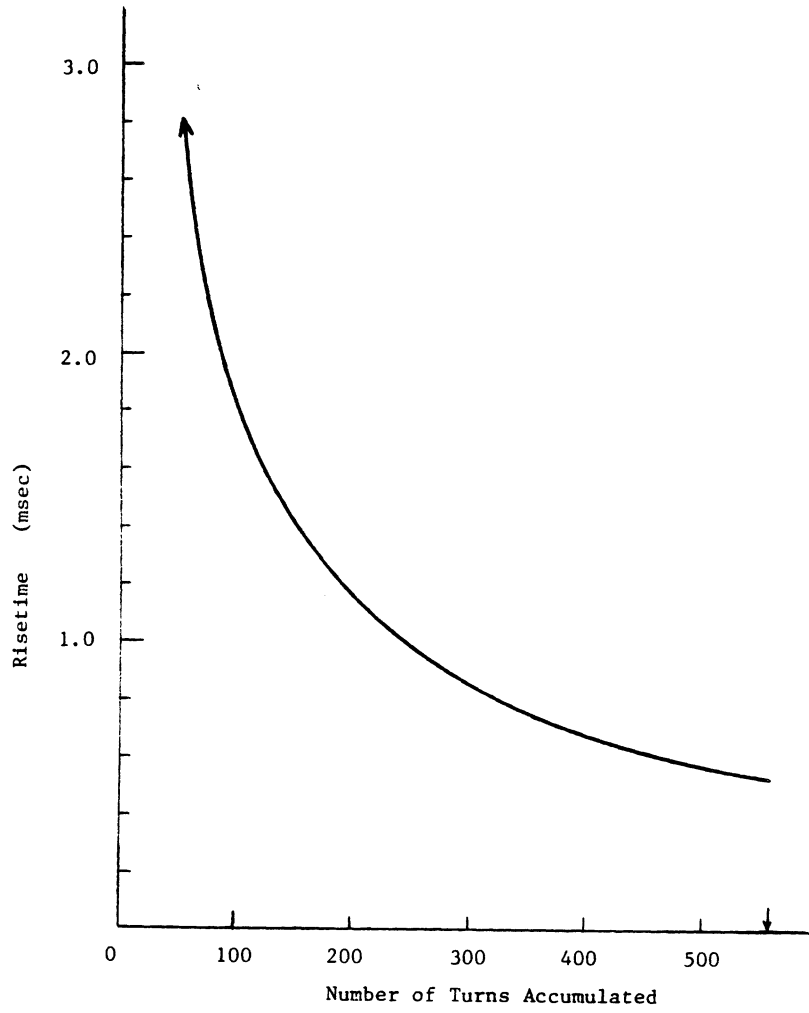


Fig. IV-2 Longitudinal Instability Risetime During Accumulation

CONCEPTUAL DESIGN OF A RAPID-CYCLING SYNCHROTRON FOR
KFA-JULICH SPALLATION NEUTRON SOURCE

SECTION V

RECOMMENDATIONS FOR FURTHER STUDY AND R & D

V. RECOMMENDATIONS FOR FURTHER STUDY AND R & D

We believe that the present study has confirmed the feasibility of achieving a proton synchrotron system with the characteristics desired. Further effort would be beneficial, however, to continue to study the major issues and uncertainties, to optimize the design of components for possibly reducing cost, to detail the design of some of the technical systems and components, and to carry out R&D and modeling studies to resolve engineering and technical issues.

The major uncertainties and limitations on beam intensity are expected to be beam loss and instabilities not anticipated (due to construction and alignment errors, and unplanned discontinuities inside the chamber). The latter is always a possibility when entering a new region of operating parameters. Further study of beam loss is warranted although quantitative projections are somewhat difficult, especially to the level of certainty required here. Any beam experiments on the ANL-RCS or the SNS that could demonstrate the advantages of any of the suggested techniques to reduce beam loss would be highly beneficial. Further study of the beam coupling impedances of the ring structures, particularly the rf cavities, ferrite kicker magnets, and other vacuum chamber discontinuities might be quite important.

Cost optimization studies might reveal some significant cost savings. In particular, the cost of magnets and power supplies vs. magnet aperture should be studied as well as the possibility of reducing the number of magnets by utilizing combined function magnets in addition to quadrupoles, or the possibility of reducing the number of different quadrupoles in the lattice while retaining the low dispersion design. The flat field for 1.5 msec for

injection and beam capture and manipulation is a significant cost factor for the power supply and might be considerably reduced if the time duration of the flat field could be relaxed, even by as much as 1/4 msec. Finally, continued study and modeling of the rf and vacuum systems could provide lower cost solutions to these components. In particular, the rf system might benefit from a much more intensive study including cleverly designed experiments to better understand the fundamental questions dealing with heavy beam loading of rf cavities. The experience to date with this question is not very great, and it remains a critical issue in the feasibility of such intense synchrotrons as proposed here.

The present study was primarily concerned with producing a credible design which could meet the goals set out with realistic and buildable components. Many systems were not designed in enough detail to proceed with an engineering design, and some component optimization might produce a less demanding design. In the latter category is reducing the pole face field (on the inner edge) of the Q_2 magnet from 19.8 kG to about 16 kG with a 10 cm increase in its length. A detailed computer calculation of the field distribution of the ring magnets is required to determine their multipole field content in order to specify the required sextupole and octupole field strengths. A detailed study of the complete injection system including the techniques of matching simultaneously in 6-dimensional phase space, transport from the linac with elimination of non- H^- beam and beam halo, and collection of non-stripped beam in the ring will be required. The stripping foil construction, insertion, lifetime, and replacement requires study. The control system needs to be detailed and diagnostic devices specified. In particular the tuneup procedure, which could require quite special diagnostics, should be outlined. A study of the advantages and implications

of superimposing a second harmonic rf could be expanded. Finally, the beam transport system for the extracted beam from the ring to the neutron target could be specified.

In addition to the R&D and model work mentioned above (rf system, vacuum system, minimizing beam loss techniques), one should build model magnets and power supplies, extraction kicker magnet and power supply, and stripping foils. Finally, assignment of personnel, particularly accelerator physicists and engineers, to major operating facilities to gain practical experience is very important to learn about and avoid some of the startup problems encountered in most such facilities.

**CONCEPTUAL DESIGN OF A RAPID-CYCLING SYNCHROTRON FOR
KFA-JULICH SPALLATION NEUTRON SOURCE**

APPENDIX A.1

LATTICE PROPERTIES

A.1 LATTICE PROPERTIES

Lattice detail referred to in Section II.1 is included here. For the lattice with $\nu_x = 11.30$ and $\nu_y = 11.25$, Figs. A.1-1-2, and -3 are the β and γ of: 1) the normal cell, 2) the dispersion and matching and straight section cells, and 3) the entire section consisting of 1/4 of the machine. Tables A.1-1, -2, and -3 list the lattice properties corresponding to the figures.

For the lattice with $\nu_x = 10.38$ and $\nu_y = 11.25$, similar information is included in Figs. A.1-4, -5, and -6 and Tables A.1-4, -5, -6. The beam envelopes are shown in Fig. A.1-7 and listed in Table A.1-7 for assumed emittance values of $500 \pi \text{ mm-mr}$ and $300 \pi \text{ mm-mr}$ for horizontal and vertical planes, respectively, and a momentum spread $\Delta p/p = \pm 1.5\%$.

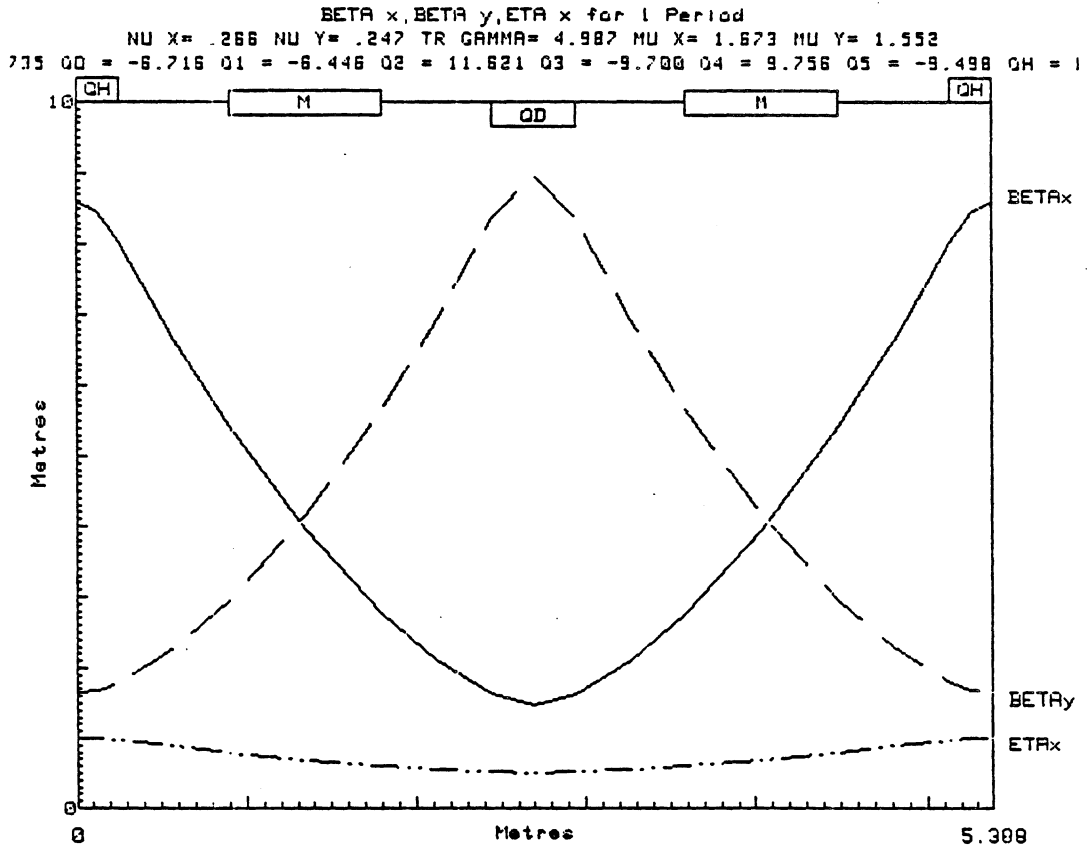


Fig. A.1-1

BEAM RIGIDITY=6.03800 X,Y EMITT=50.0000,30.0000 PI CM-MR,DPP=.01000										COMMANDS		
ELEMENTS: 18 ELEMENT DEFINITIONS										BEAM		
NAM	TYPE	VAR	LEN,ANG	B,B'	N,GAP	DX	DRFT	0.0	.25150	0.0000	0.000	ELEMENTS
QF	QUAD	1.2	.50000	6.7353	0.000	M1	BEND	0.0	.45000	1.0538	0.000	LATTICE
D1	DRFT	0.0	.64700	0.0000	0.000	Q4	QUAD	0.0	.85000	9.7558	0.000	PERIODS
E	EDGE	0.0	2.0000	1.0538	0.000	Q5	QUAD	0.0	.50000	-9.493	0.000	FIT
M	BEND	0.0	.90000	1.0538	0.000	D5	DRFT	0.0	1.5000	0.0000	0.000	TRANSPOR
QD	QUAD	2.2	.50000	-6.716	0.000	QH	QUAD	1.2	.25000	6.7353	0.000	INSERT
DM	DRFT	0.0	.90000	0.0000	0.000							MATRIX
Q1	QUAD	0.0	.50000	-6.446	0.000							GO
Q2	QUAD	0.0	.50000	11.620	0.000							CYCLE
Q3	QUAD	0.0	.50000	-9.700	0.000							GRAPH
D2	DRFT	0.0	1.5200	0.0000	0.000							ITERATE
D3	DRFT	0.0	.15000	0.0000	0.000							HELP
LATTICE: 9 ELEMENTS: QH D1 M D1 QD D1 M D1 QH										SAVE		
PERIODS FIT: NU X =3.300,NU Y =3.250,										RECALL		
1												QUIT
												NEW CASE
												PRINT

MATCHED FUNCTIONS FOR 1 PERIOD(S)

TOTAL LENGTH= 5.3880 METERS, TOTAL BEND= 17.9995 DEGREES

BETAX= 8.5957 METERS ALPHAX= 0.0000 HUX= 0.2662

BETAY= 1.6456 METERS ALPHAY= -0.0000 NUY= 0.2471

ETAX = 1.0092 METERS ETA'X = -0.0000 TRGAMMA= 4.9372

ELEM	LTH	SUM L	BETAX	ALPHAX	ETAX	ETA'X	PSIX	X	BETAY	ALPHAY	PSIY	Y
	(M)	(M)	(M)		(M)	(RAD)	(DEG)	(CM)	(M)		(DEG)	(CM)
	0.00	0.00	8.60	0.00	1.01	-0.00	0.0	7.6	1.65	-0.00	0.0	2.2
QH	0.13	0.13	8.45	1.17	1.00	-0.14	0.8	7.5	1.68	-0.31	4.3	2.2
QH	0.13	0.25	8.02	2.26	0.97	-0.28	1.7	7.3	1.80	-0.64	8.4	2.3
D1	0.32	0.57	6.64	2.01	0.88	-0.28	4.2	6.6	2.30	-0.89	17.6	2.6
D1	0.32	0.90	5.41	1.77	0.79	-0.28	7.3	6.0	2.96	-1.15	24.7	3.0
M	0.45	1.35	3.95	1.48	0.68	-0.21	12.9	5.1	4.15	-1.50	32.1	3.5
M	0.45	1.80	2.76	1.15	0.61	-0.14	20.7	4.3	5.65	-1.85	37.4	4.1
D1	0.32	2.12	2.11	0.88	0.56	-0.14	28.4	3.8	6.93	-2.10	40.4	4.6
D1	0.32	2.44	1.63	0.61	0.52	-0.14	38.5	3.4	8.37	-2.36	42.8	5.0
QD	0.25	2.69	1.48	0.00	0.50	-0.00	47.9	3.2	8.98	0.00	44.5	5.2
QD	0.25	2.94	1.63	-0.61	0.52	0.14	57.3	3.4	8.37	2.36	46.1	5.0
D1	0.32	3.27	2.11	-0.88	0.56	0.14	67.4	3.8	6.93	2.10	48.5	4.6
D1	0.32	3.59	2.76	-1.15	0.61	0.14	75.1	4.3	5.65	1.85	51.5	4.1
M	0.45	4.04	3.95	-1.48	0.68	0.21	82.9	5.1	4.15	1.50	56.8	3.5
M	0.45	4.49	5.41	-1.77	0.79	0.28	88.5	6.0	2.96	1.15	64.2	3.0
D1	0.32	4.81	6.64	-2.01	0.88	0.28	91.6	6.6	2.30	0.89	71.3	2.6
D1	0.32	5.14	8.02	-2.26	0.97	0.28	94.1	7.3	1.80	0.64	80.5	2.3
QH	0.13	5.26	8.45	-1.17	1.00	0.14	95.0	7.5	1.68	0.31	84.6	2.2
QH	0.13	5.39	8.60	-0.00	1.01	0.00	95.8	7.6	1.65	0.00	88.9	2.2

ELEM	LTH	SUM L	BETAX	ALPHAX	ETAX	ETA'X	PSIX	X	BETAY	ALPHAY	PSIY	Y
	(M)	(M)	(M)		(M)	(RAD)	(DEG)	(CM)	(M)		(DEG)	(CM)
	0.00	0.00	8.60	0.00	1.01	-0.00	0.0	7.6	1.65	-0.00	0.0	2.2

Table A.1-1

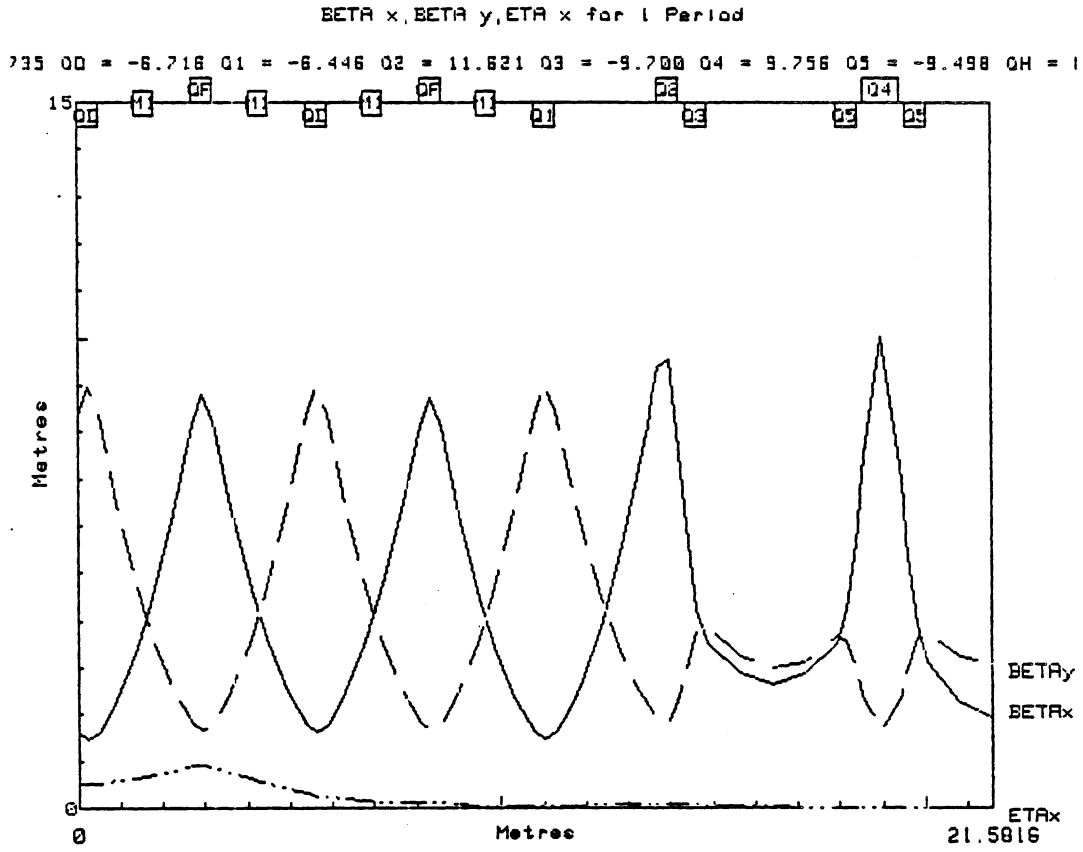


Fig. A.1-2

ELEM	LTH (M)	SUM L (M)	BETAX (M)	ALPHAX	ETAX (M)	ETA'X (RAD)	PSIX (DEG)	X (CM)	BETAY (M)	ALPHAY	PSIY (DEG)	Y (CM)
QD	0.00	0.00	1.63	0.61	0.52	-0.14	0.0	2.9	8.37	-2.36	0.0	5.0
QD	0.25	0.25	1.48	-0.00	0.50	0.00	9.4	3.2	8.98	0.00	1.6	5.2
QD	0.25	0.50	1.63	-0.61	0.52	0.14	18.8	3.4	8.37	2.36	3.3	5.0
DX	0.44	0.94	2.31	-0.97	0.58	0.14	31.8	4.0	6.47	2.01	6.7	4.4
DX	0.44	1.37	3.32	-1.34	0.64	0.14	40.8	4.7	4.86	1.67	11.1	3.8
M1	0.23	1.60	3.97	-1.50	0.67	0.17	44.4	5.1	4.15	1.50	14.0	3.5
M1	0.23	1.82	4.68	-1.66	0.72	0.21	47.4	5.6	3.51	1.32	17.4	3.2
DX	0.44	2.26	5.27	-2.01	0.81	0.21	52.0	6.4	2.51	0.98	25.8	2.7
DX	0.44	2.69	8.18	-2.36	0.90	0.21	55.5	7.3	1.80	0.64	37.7	2.3
QF	0.25	2.94	8.79	-0.05	0.92	-0.05	57.1	7.5	1.65	0.00	46.1	2.2
QF	0.25	3.19	8.22	2.27	0.88	-0.30	58.8	7.3	1.80	-0.64	54.6	2.3
DX	0.44	3.63	6.39	1.94	0.75	-0.30	62.3	6.4	2.51	-0.98	66.4	2.7
DX	0.44	4.07	4.84	1.62	0.62	-0.30	66.8	5.5	3.51	-1.32	74.8	3.2
M1	0.23	4.29	4.14	1.48	0.55	-0.26	69.6	5.1	4.15	-1.50	78.2	3.5
M1	0.23	4.52	3.51	1.33	0.50	-0.23	73.0	4.7	4.86	-1.67	81.1	3.8
DX	0.44	4.95	2.50	0.98	0.40	-0.23	81.5	3.9	6.47	-2.01	85.5	4.4
DX	0.44	5.39	1.79	0.64	0.30	-0.23	93.4	3.3	8.37	-2.36	88.9	5.0
QD	0.25	5.64	1.63	0.00	0.25	-0.15	101.9	3.1	8.98	-0.00	90.6	5.2
QD	0.25	5.89	1.79	-0.63	0.23	-0.08	110.4	3.2	8.37	2.36	92.2	5.0
DX	0.44	6.32	2.48	-0.97	0.19	-0.08	122.4	3.7	6.47	2.01	95.6	4.4
DX	0.44	6.76	3.48	-1.31	0.15	-0.08	130.9	4.3	4.86	1.67	100.1	3.8
M1	0.23	6.99	4.10	-1.46	0.14	-0.04	134.3	4.7	4.15	1.50	102.9	3.5
M1	0.23	7.21	4.79	-1.60	0.13	-0.01	137.2	5.0	3.51	1.32	106.3	3.2
DX	0.44	7.65	6.33	-1.92	0.13	-0.01	141.8	5.8	2.51	0.98	114.8	2.7
DX	0.44	8.08	8.15	-2.25	0.13	-0.01	145.2	6.5	1.80	0.64	126.6	2.3
QF	0.25	8.33	8.71	0.05	0.12	-0.04	146.9	6.7	1.65	-0.00	135.1	2.2
QF	0.25	8.58	8.10	2.33	0.11	-0.07	148.6	6.5	1.80	-0.64	143.5	2.3
DX	0.44	9.02	6.22	1.99	0.07	-0.07	152.1	5.7	2.51	-0.98	155.3	2.7
DX	0.44	9.45	4.64	1.64	0.04	-0.07	156.8	4.9	3.51	-1.32	163.8	3.2
M1	0.23	9.68	3.93	1.49	0.03	-0.03	159.8	4.5	4.15	-1.50	167.2	3.5
M1	0.23	9.90	3.30	1.33	0.03	0.00	163.4	4.1	4.86	-1.67	170.0	3.8
DX	0.44	10.34	2.30	0.96	0.03	0.00	172.5	3.4	6.47	-2.01	174.5	4.4
DX	0.44	10.78	1.62	0.60	0.03	0.00	185.5	2.9	8.37	-2.36	177.9	5.0
Q1	0.25	11.03	1.47	0.01	0.03	0.01	194.9	2.7	9.00	-0.10	179.5	5.2
Q1	0.25	11.28	1.61	-0.58	0.04	0.02	204.4	2.9	8.47	2.18	181.1	5.0
D1	0.32	11.60	2.08	-0.85	0.05	0.02	214.6	3.3	7.12	1.96	183.5	4.6
D1	0.32	11.92	2.71	-1.12	0.05	0.02	222.4	3.7	5.93	1.74	186.4	4.2
DM	0.45	12.37	3.88	-1.49	0.06	0.02	230.4	4.5	4.49	1.44	191.4	3.7
DM	0.45	12.82	5.39	-1.86	0.07	0.02	236.0	5.3	3.34	1.13	198.1	3.2
D1	0.32	13.15	6.68	-2.13	0.08	0.02	239.1	5.9	2.68	0.91	204.3	2.8
D1	0.32	13.47	8.14	-2.40	0.09	0.02	241.6	6.5	2.16	0.69	212.0	2.5
D4	0.13	13.60	8.76	-2.50	0.09	0.02	242.5	6.7	2.00	0.60	215.5	2.4
D4	0.13	13.72	9.40	-2.60	0.09	0.02	243.3	7.0	1.86	0.52	219.2	2.4
Q2	0.25	13.97	9.57	1.98	0.09	-0.02	244.7	7.0	1.86	-0.51	227.0	2.4
Q2	0.25	14.22	7.58	5.64	0.08	-0.07	246.4	6.2	2.41	-1.78	234.0	2.7
D3	0.08	14.30	6.76	5.32	0.08	-0.07	247.0	5.9	2.68	-1.91	235.7	2.8
D3	0.08	14.37	5.98	4.99	0.07	-0.07	247.7	5.5	2.98	-2.04	237.2	3.0
Q3	0.25	14.62	4.22	2.38	0.06	-0.04	250.6	4.7	3.75	-0.93	241.4	3.4
Q3	0.25	14.87	3.52	0.57	0.05	-0.02	254.4	4.2	3.85	0.54	245.1	3.4
D2	0.76	15.63	2.87	0.29	0.04	-0.02	268.2	3.8	3.23	0.28	257.6	3.1
D2	0.76	16.39	2.65	0.00	0.03	-0.02	284.2	3.7	2.99	0.03	271.7	3.0
D2	0.76	17.15	2.87	-0.29	0.01	-0.02	300.2	3.8	3.13	-0.22	286.1	3.1
D2	0.76	17.91	3.52	-0.57	0.00	-0.02	314.0	4.2	3.67	-0.48	299.1	3.3
Q5	0.25	18.16	4.21	-2.27	-0.00	-0.02	317.8	4.6	3.57	0.88	303.0	3.3
Q5	0.25	18.41	5.94	-4.88	-0.01	-0.02	320.7	5.5	2.84	1.91	307.4	2.9
D3	0.08	18.49	6.70	-5.20	-0.01	-0.02	321.4	5.8	2.57	1.79	309.0	2.8
D3	0.08	18.56	7.50	-5.51	-0.01	-0.02	322.0	6.1	2.31	1.67	310.7	2.6
Q4	0.43	18.99	10.03	0.16	-0.02	-0.01	324.7	7.1	1.67	-0.01	323.9	2.2
Q4	0.43	19.41	7.28	5.66	-0.02	0.00	327.4	6.1	2.33	-1.71	337.0	2.6
D3	0.08	19.49	6.46	5.32	-0.02	0.00	328.0	5.7	2.60	-1.84	338.7	2.8
D3	0.08	19.56	5.69	4.98	-0.02	0.00	328.7	5.3	2.88	-1.96	340.3	2.9
Q5	0.25	19.81	3.90	2.40	-0.02	-0.00	331.8	4.4	3.63	-0.92	344.6	3.3
Q5	0.25	20.06	3.13	0.79	-0.02	-0.01	336.0	4.0	3.75	0.47	348.5	3.4
D2	0.76	20.32	2.23	0.39	-0.03	-0.01	352.7	3.4	3.22	0.22	361.1	3.1
D2	0.76	21.58	1.93	0.00	-0.04	-0.01	374.2	3.1	3.07	-0.02	375.1	3.0
ELEM	LTH	SUM L	BETAX	ALPHAX	ETAX	ETA'X	PSIX	X	BETAY	ALPHAY	PSIY	Y

Table A.1-2

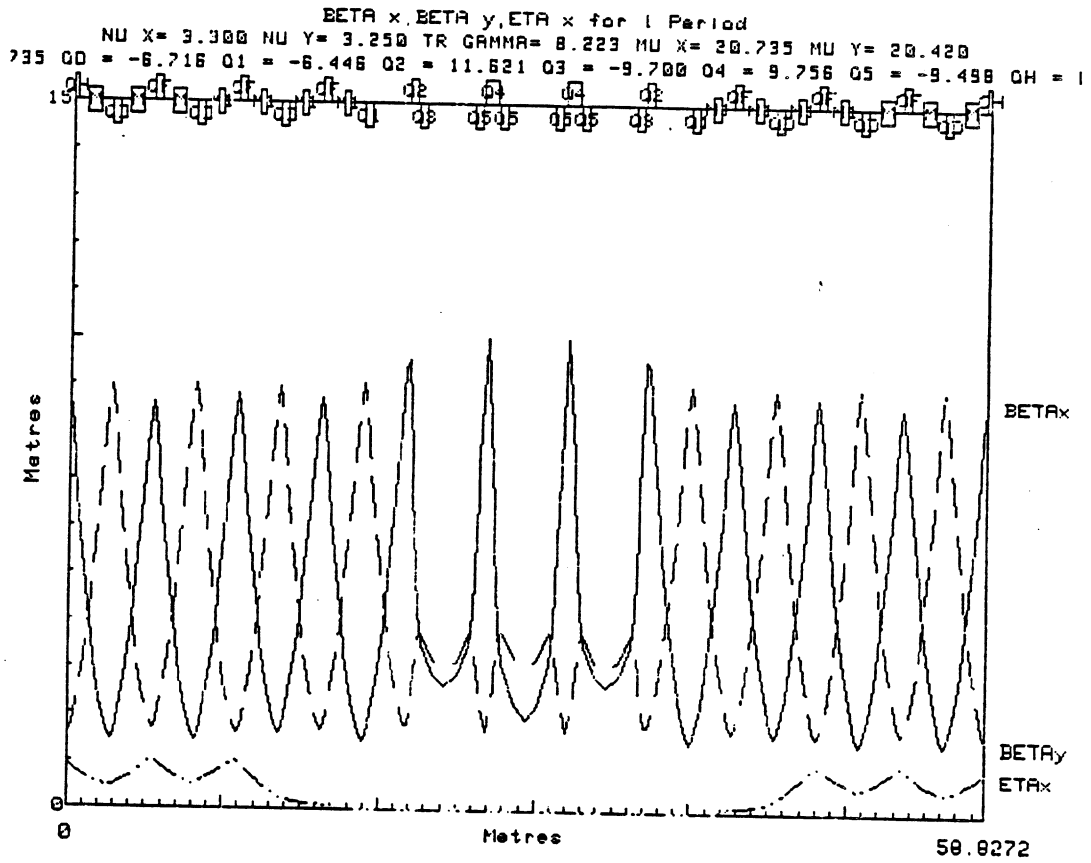


Fig. A.1-3

BEAM RIGIDITY=6.03800 X,Y EMITT=50.0000,30.0000 PI CM-MR,DPP=.01000													COMMANDS				
ELEMENTS: 13 ELEMENT DEFINITIONS													BEAM				
NAM	TYPE	VAR	LEN,ANG	B,B'	N,GAP	D4	DRFT	0.0	.25150	0.0000	0.000		ELEMENTS				
QF	QUAD	1.2	.50000	6.7353	0.000	M1	BEND	0.0	.45000	1.0538	0.000		LATTICE				
D1	DRFT	0.0	.64700	0.0000	0.000	Q4	QUAD	0.0	.85000	9.7558	0.000		PERIODS				
E	EDGE	0.0	2.0000	1.0538	0.000	Q5	QUAD	0.0	.50000	-9.498	0.000		FIT				
M	BEND	0.0	.90000	1.0538	0.000	D5	DRFT	0.0	1.5000	0.0000	0.000		TRANSPOR				
QD	QUAD	2.2	.50000	-6.716	0.000	QH	QUAD	1.2	.25000	6.7353	0.000		INSERT				
DM	DRFT	0.0	.90000	0.0000	0.000								MATRIX				
Q1	QUAD	0.0	.50000	-6.446	0.000								GO				
Q2	QUAD	0.0	.50000	11.620	0.000								CYCLE				
Q3	QUAD	0.0	.50000	-9.700	0.000								GRAPH				
D2	DRFT	0.0	1.5200	0.0000	0.000								ITERATE				
D3	DRFT	0.0	.15000	0.0000	0.000								HELP				
LATTICE: 45 ELEMENTS: QH D1 M D1 QD D1 M D1 QF D1 M D1													SAVE				
QD	DX	M1	DX	QF	DX	M1	DX	QD	DX	M1	DX	QF	DX	M1	DX	Q1	RECALL
D1	DM	D1	D4	Q2	D3	Q3	D2	D2	Q5	D3	Q4	D3	Q5	D2	RFL		QUIT
PERIODS	FIT: NU X =3.300,NU Y =3.250,															NEW CASE	
4																PRINT	

MATCHED FUNCTIONS FOR 4 PERIOD(S)

TOTAL LENGTH= 235.3000 METERS, TOTAL BEND= 359.9900 DEGREES

BETAX= 0.5964 METERS ALPHAX= -0.0000 NUX= 3.3000

BETAY= 1.6027 METERS ALPHAY= -0.0000 NUY= 3.2500

ETAX = 0.9149 METERS ETAX = 0.0000 TRGAMMA= 3.2228

Table A.1-3(a)

ELEM	LTH (M)	SUM L (M)	BETAX (M)	ALPHAX	ETA'X (M)	ETA'X (RAD)	PSIX (DEG)	X (CM)	BETAY (M)	ALPHAY	PSIY (DEG)	Y (CM)
	0.00	0.00	8.60	-0.00	0.91	0.00	0.0	7.5	1.60	-0.00	0.0	2.2
QH	0.13	0.13	8.45	1.17	0.91	-0.13	0.8	7.4	1.64	-0.31	4.4	2.2
QH	0.13	0.25	8.02	2.26	0.88	-0.25	1.7	7.2	1.76	-0.63	8.7	2.3
D1	0.32	0.57	6.64	2.01	0.80	-0.25	4.2	6.6	2.25	-0.89	18.0	2.6
D1	0.32	0.90	5.41	1.77	0.72	-0.25	7.3	5.9	2.91	-1.15	25.3	3.0
M	0.45	1.35	3.95	1.48	0.62	-0.18	12.9	5.1	4.10	-1.50	32.8	3.5
M	0.45	1.80	2.76	1.15	0.56	-0.11	20.7	4.3	5.62	-1.86	38.2	4.1
D1	0.32	2.12	2.11	0.88	0.52	-0.11	28.4	3.8	6.90	-2.12	41.2	4.6
D1	0.32	2.44	1.63	0.61	0.48	-0.11	38.5	3.3	8.36	-2.38	43.6	5.0
QD	0.25	2.69	1.48	0.00	0.47	0.02	47.9	3.2	8.97	-0.03	45.2	5.2
QD	0.25	2.94	1.63	-0.61	0.49	0.15	57.3	3.3	8.38	2.33	46.9	5.0
D1	0.32	3.27	2.11	-0.88	0.54	0.15	67.4	3.8	6.96	2.08	49.3	4.6
D1	0.32	3.59	2.76	-1.15	0.59	0.15	75.1	4.3	5.69	1.84	52.2	4.1
M	0.45	4.04	3.95	-1.48	0.68	0.22	82.9	5.1	4.19	1.49	57.5	3.5
M	0.45	4.49	5.41	-1.77	0.79	0.29	88.5	6.0	3.01	1.14	64.8	3.0
D1	0.32	4.81	6.63	-2.01	0.89	0.29	91.6	6.6	2.35	0.90	71.8	2.7
D1	0.32	5.14	8.02	-2.26	0.98	0.29	94.1	7.3	1.85	0.65	80.7	2.4
QF	0.25	5.39	8.60	-0.00	1.02	0.01	95.8	7.6	1.69	-0.00	89.0	2.3
QF	0.25	5.64	8.02	2.26	0.99	-0.27	97.5	7.3	1.85	-0.65	97.2	2.4
D1	0.32	5.96	6.63	2.01	0.90	-0.27	100.1	6.7	2.35	-0.90	106.1	2.7
D1	0.32	6.29	5.41	1.77	0.81	-0.27	103.2	6.0	3.01	-1.15	113.1	3.0
M	0.45	6.74	3.95	1.48	0.70	-0.20	108.8	5.1	4.20	-1.49	120.4	3.5
M	0.45	7.19	2.76	1.15	0.63	-0.13	116.6	4.3	5.70	-1.84	125.7	4.1
D1	0.32	7.51	2.11	0.88	0.59	-0.13	124.3	3.8	6.97	-2.09	128.6	4.6
D1	0.32	7.83	1.63	0.61	0.54	-0.13	134.4	3.4	8.40	-2.34	131.0	5.0
QD	0.25	8.08	1.48	-0.00	0.53	0.02	143.7	3.2	8.99	0.03	132.7	5.2
QD	0.25	8.33	1.63	-0.61	0.55	0.17	153.1	3.4	8.38	2.38	134.3	5.0
DX	0.44	8.77	2.31	-0.97	0.62	0.17	166.1	4.0	6.45	2.03	137.7	4.4
DX	0.44	9.20	3.32	-1.34	0.70	0.17	175.2	4.8	4.83	1.69	142.2	3.8
M1	0.23	9.43	3.97	-1.50	0.74	0.20	178.7	5.2	4.11	1.51	145.1	3.5
M1	0.23	9.65	4.68	-1.66	0.79	0.23	181.7	5.6	3.47	1.33	148.5	3.2
DX	0.44	10.09	6.27	-2.01	0.89	0.23	186.3	6.5	2.46	0.98	157.1	2.7
DX	0.44	10.53	8.18	-2.36	0.99	0.23	189.8	7.4	1.76	0.63	169.2	2.3
QF	0.25	10.78	8.79	-0.05	1.01	-0.05	191.5	7.6	1.60	0.00	177.8	2.2
QF	0.25	11.03	8.22	2.27	0.97	-0.32	193.2	7.4	1.76	-0.63	186.5	2.3
DX	0.44	11.46	6.39	1.94	0.82	-0.32	196.6	6.5	2.46	-0.98	198.6	2.7
DX	0.44	11.90	4.84	1.62	0.68	-0.32	201.1	5.6	3.46	-1.32	207.2	3.2
M1	0.23	12.12	4.14	1.48	0.61	-0.29	204.0	5.2	4.09	-1.50	210.7	3.5
M1	0.23	12.35	3.51	1.33	0.55	-0.25	207.4	4.7	4.81	-1.68	213.6	3.8
DX	0.44	12.78	2.50	0.98	0.44	-0.25	215.8	4.0	6.42	-2.03	218.1	4.4
DX	0.44	13.22	1.79	0.64	0.33	-0.25	227.7	3.3	8.34	-2.37	221.5	5.0
QD	0.25	13.47	1.63	0.00	0.28	-0.17	236.2	3.1	8.96	-0.03	223.1	5.2
QD	0.25	13.72	1.79	-0.63	0.24	-0.10	244.8	3.2	8.37	2.33	224.7	5.0
DX	0.44	14.16	2.48	-0.97	0.20	-0.10	256.7	3.7	6.48	1.99	228.1	4.4
DX	0.44	14.59	3.48	-1.31	0.16	-0.10	265.2	4.3	4.89	1.66	232.6	3.8
M1	0.23	14.82	4.10	-1.46	0.14	-0.06	268.7	4.7	4.18	1.49	235.4	3.5
M1	0.23	15.04	4.79	-1.60	0.13	-0.02	271.6	5.0	3.55	1.31	238.8	3.3
DX	0.44	15.48	6.33	-1.92	0.12	-0.02	276.1	5.7	2.55	0.98	247.1	2.8
DX	0.44	15.91	8.15	-2.25	0.11	-0.02	279.6	6.5	1.85	0.64	258.7	2.4
QF	0.25	16.16	8.71	0.05	0.10	-0.05	281.3	6.7	1.69	-0.00	266.9	2.3
QF	0.25	16.41	8.10	2.33	0.09	-0.08	282.9	6.5	1.85	-0.65	275.1	2.4
DX	0.44	16.85	6.22	1.99	0.05	-0.08	286.5	5.6	2.56	-0.99	286.7	2.8
DX	0.44	17.29	4.64	1.64	0.02	-0.08	291.1	4.8	3.57	-1.32	295.0	3.3
M1	0.23	17.51	3.93	1.49	0.00	-0.04	294.1	4.4	4.21	-1.50	298.3	3.6
M1	0.23	17.74	3.30	1.33	0.00	-0.00	297.7	4.1	4.92	-1.67	301.1	3.8
DX	0.44	18.17	2.30	0.96	0.00	-0.00	305.8	3.4	6.52	-2.01	305.6	4.4
DX	0.44	18.61	1.62	0.60	0.00	-0.00	319.9	2.8	8.42	-2.34	308.9	5.0

Table A.1-3(b)

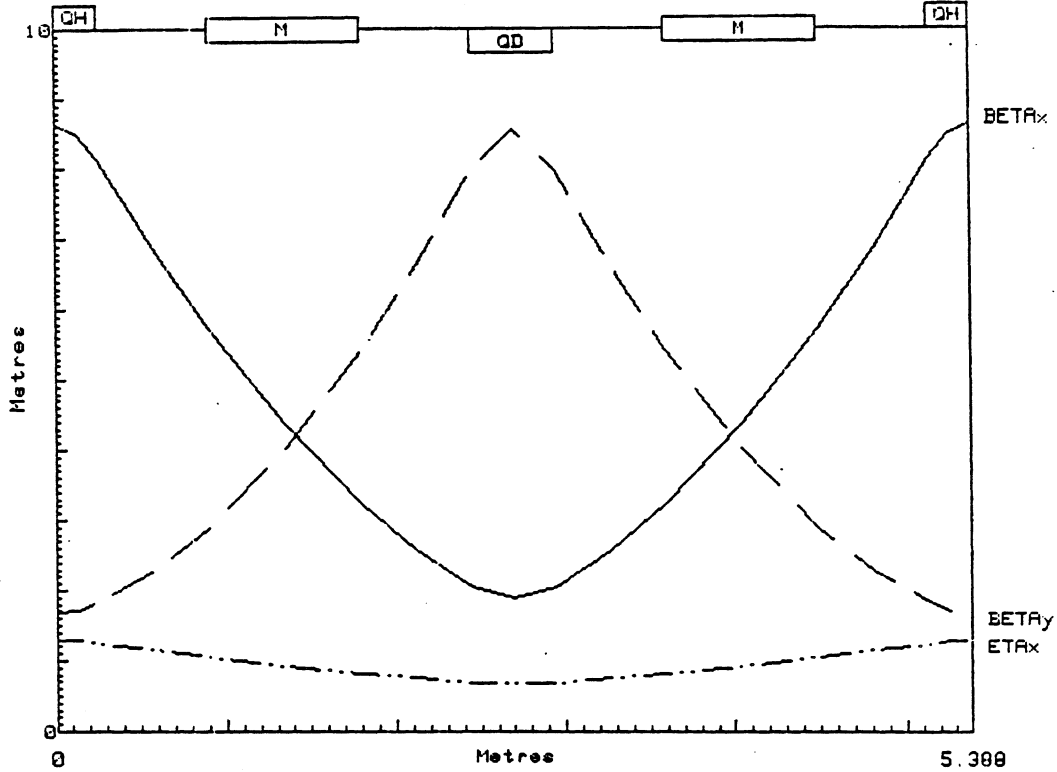
Q1	0.25	18.86	1.47	0.01	0.00	0.00	329.3	2.7	9.03	-0.07	310.6	5.2
Q1	0.25	19.11	1.61	-0.58	0.00	0.00	338.7	2.8	8.49	2.22	312.2	5.0
D1	0.32	19.43	2.03	-0.85	0.00	0.00	348.9	3.2	7.13	1.99	314.6	4.6
D1	0.32	19.76	2.71	-1.12	0.00	0.00	356.7	3.7	5.91	1.77	317.4	4.2
DM	0.45	20.21	3.88	-1.49	0.00	0.00	364.7	4.4	4.46	1.45	322.4	3.7
DM	0.45	20.66	5.39	-1.86	0.00	0.00	370.4	5.2	3.30	1.14	329.2	3.1
D1	0.32	20.98	6.68	-2.13	0.00	0.00	373.4	5.8	2.63	0.91	335.5	2.8
D1	0.32	21.30	8.14	-2.40	0.00	0.00	376.0	6.4	2.12	0.69	343.4	2.5
D4	0.13	21.43	8.76	-2.50	0.00	0.00	376.8	6.6	1.95	0.60	346.9	2.4
D4	0.13	21.55	9.40	-2.60	0.00	0.00	377.6	6.9	1.81	0.51	350.7	2.3
Q2	0.25	21.80	9.57	1.98	0.00	-0.00	379.1	6.9	1.81	-0.49	358.8	2.3
Q2	0.25	22.05	7.58	5.64	0.00	-0.00	380.7	6.2	2.35	-1.74	365.9	2.7
D3	0.08	22.13	6.76	5.32	0.00	-0.00	381.3	5.8	2.62	-1.87	367.7	2.8
D3	0.08	22.20	5.99	4.99	0.00	-0.00	382.0	5.5	2.91	-2.00	369.2	3.0
Q3	0.25	22.45	4.22	2.30	0.00	-0.00	384.9	4.6	3.66	-0.92	373.5	3.3
Q3	0.25	22.70	3.52	0.57	0.00	-0.00	388.7	4.2	3.77	0.51	377.3	3.4
D2	0.76	23.46	2.87	0.29	0.00	-0.00	402.5	3.8	3.18	0.26	390.0	3.1
D2	0.76	24.22	2.65	0.00	0.00	-0.00	418.5	3.6	2.98	0.00	404.3	3.0
D2	0.76	24.98	2.87	-0.29	-0.00	-0.00	434.5	3.8	3.17	-0.25	418.6	3.1
D2	0.76	25.74	3.52	-0.57	-0.00	-0.00	448.4	4.2	3.75	-0.51	431.3	3.4
Q5	0.25	25.99	4.21	-2.27	-0.00	-0.00	452.2	4.6	3.65	0.89	435.1	3.3
Q5	0.25	26.24	5.94	-4.88	-0.00	-0.00	455.1	5.5	2.91	1.95	439.5	3.0
D3	0.08	26.32	6.70	-5.20	-0.00	-0.00	455.8	5.8	2.63	1.83	441.0	2.8
D3	0.08	26.39	7.50	-5.51	-0.00	-0.00	456.4	6.1	2.37	1.70	442.7	2.7
Q4	0.43	26.82	10.03	0.16	-0.00	-0.00	459.0	7.1	1.71	-0.01	455.6	2.3
Q4	0.43	27.24	7.28	5.66	-0.00	0.00	461.8	6.0	2.38	-1.73	468.3	2.7
D3	0.08	27.32	6.46	5.32	-0.00	0.00	462.4	5.7	2.65	-1.86	470.0	2.8
D3	0.08	27.39	5.68	4.98	-0.00	0.00	463.1	5.3	2.94	-1.98	471.6	3.0
Q5	0.25	27.64	3.90	2.40	-0.00	0.00	466.2	4.4	3.69	-0.91	475.8	3.3
Q5	0.25	27.89	3.13	0.79	-0.00	-0.00	470.4	4.0	3.80	0.50	479.6	3.4
D2	0.76	28.65	2.23	0.39	-0.00	-0.00	487.1	3.3	3.22	0.25	492.2	3.1
D2	0.76	29.41	1.93	-0.00	-0.00	-0.00	508.5	3.1	3.03	-0.00	506.2	3.0
D2	0.76	30.17	2.23	-0.39	-0.00	-0.00	530.0	3.3	3.22	-0.25	520.3	3.1
D2	0.76	30.93	3.13	-0.79	-0.00	-0.00	546.7	4.0	3.80	-0.50	532.8	3.4
Q5	0.25	31.18	3.90	-2.40	-0.00	-0.00	550.9	4.4	3.69	0.91	536.6	3.3
Q5	0.25	31.43	5.68	-4.98	-0.00	-0.00	553.9	5.3	2.94	1.98	540.9	3.0
D3	0.08	31.51	6.46	-5.32	-0.00	-0.00	554.7	5.7	2.65	1.86	542.4	2.8
D3	0.08	31.58	7.28	-5.66	-0.00	-0.00	555.3	6.0	2.38	1.73	544.1	2.7
Q4	0.43	32.01	10.03	-0.16	-0.00	0.00	558.0	7.1	1.71	0.01	556.9	2.3
Q4	0.43	32.43	7.50	5.51	-0.00	0.00	560.7	6.1	2.37	-1.70	569.7	2.7
D3	0.08	32.51	6.70	5.20	-0.00	0.00	561.3	5.8	2.63	-1.83	571.4	2.8
D3	0.08	32.58	5.94	4.88	-0.00	0.00	562.0	5.5	2.91	-1.95	573.0	3.0
Q5	0.25	32.83	4.21	2.27	-0.00	0.00	564.9	4.6	3.65	-0.89	577.3	3.3
Q5	0.25	33.08	3.52	0.57	-0.00	0.00	568.7	4.2	3.75	0.51	581.1	3.4
D2	0.76	33.84	2.87	0.29	-0.00	0.00	582.5	3.8	3.17	0.25	593.9	3.1
D2	0.76	34.60	2.65	-0.00	-0.00	0.00	598.5	3.6	2.98	-0.00	608.2	3.0
D2	0.76	35.36	2.87	-0.29	0.00	0.00	614.5	3.8	3.18	-0.26	622.4	3.1
D2	0.76	36.12	3.52	-0.57	0.00	0.00	628.3	4.2	3.77	-0.51	635.1	3.4
Q3	0.25	36.37	4.22	-2.30	0.00	0.00	632.1	4.6	3.66	0.92	638.9	3.3
Q3	0.25	36.62	5.98	-4.99	0.00	0.00	635.0	5.5	2.91	2.00	643.2	3.0
D3	0.08	36.70	6.76	-5.32	0.00	0.00	635.7	5.8	2.62	1.87	644.8	2.8
D3	0.08	36.77	7.58	-5.64	0.00	0.00	636.3	6.2	2.35	1.74	646.5	2.7
Q2	0.25	37.02	9.57	-1.98	0.00	0.00	637.9	6.9	1.81	0.49	653.6	2.3
Q2	0.25	37.27	9.40	2.60	0.00	-0.00	639.4	6.9	1.81	-0.51	661.8	2.3
D4	0.13	37.40	9.76	2.50	0.00	-0.00	640.2	6.6	1.95	-0.60	665.6	2.4
D4	0.13	37.53	3.14	2.40	0.00	-0.00	641.1	6.4	2.12	-0.69	669.1	2.5
D1	0.32	37.85	6.68	2.13	0.00	-0.00	643.6	5.8	2.63	-0.91	677.0	2.8
D1	0.32	38.17	5.39	1.86	0.00	-0.00	646.7	5.2	3.30	-1.14	683.3	3.1
DM	0.45	38.62	3.88	1.49	0.00	-0.00	652.3	4.4	4.46	-1.45	690.1	3.7
DM	0.45	39.07	2.71	1.12	0.00	-0.00	660.3	3.7	5.91	-1.77	695.1	4.2
D1	0.32	39.40	2.08	0.85	0.00	-0.00	669.1	3.2	7.13	-1.99	697.9	4.6
D1	0.32	39.72	1.61	0.58	0.00	-0.00	678.3	2.8	8.49	-2.22	700.3	5.0
Q1	0.25	39.97	1.47	-0.01	0.00	0.00	687.7	2.7	9.03	0.07	701.9	5.2
Q1	0.25	40.22	1.62	-0.60	0.00	0.00	697.2	2.8	8.42	2.34	703.6	5.0
DX	0.44	40.66	2.30	-0.96	0.00	0.00	710.2	3.4	6.52	2.01	706.9	4.4
DX	0.44	41.09	3.30	-1.33	0.00	0.00	719.3	4.1	4.92	1.67	711.4	3.8

Table A.1-3(c)

M1	0.23	41.32	3.93	-1.49	0.00	0.04	722.9	4.4	4.21	1.50	714.2	3.6
M1	0.23	41.54	4.64	-1.64	0.02	0.08	725.9	4.8	3.57	1.32	717.5	3.3
DX	0.44	41.98	6.22	-1.99	0.05	0.08	730.6	5.6	2.56	0.99	725.8	2.8
DX	0.44	42.41	8.10	-2.33	0.09	0.08	734.1	6.5	1.85	0.65	737.4	2.4
QF	0.25	42.66	8.71	-0.05	0.10	0.05	735.8	6.7	1.69	0.00	745.6	2.3
QF	0.25	42.91	8.15	2.25	0.11	0.02	737.4	6.5	1.85	-0.64	753.8	2.4
DX	0.44	43.35	6.33	1.92	0.12	0.02	740.9	5.7	2.55	-0.98	765.4	2.8
DX	0.44	43.79	4.79	1.60	0.13	0.02	745.5	5.0	3.55	-1.31	773.7	3.3
M1	0.23	44.01	4.10	1.46	0.14	0.06	748.4	4.7	4.18	-1.49	777.1	3.5
M1	0.23	44.24	3.48	1.31	0.16	0.10	751.8	4.3	4.89	-1.66	779.9	3.8
DX	0.44	44.67	2.48	0.97	0.20	0.10	760.3	3.7	6.48	-1.99	784.3	4.4
DX	0.44	45.11	1.79	0.63	0.24	0.10	772.3	3.2	8.37	-2.33	787.7	5.0
QD	0.25	45.36	1.63	-0.00	0.28	0.17	780.8	3.1	8.96	0.03	789.4	5.2
QD	0.25	45.61	1.79	-0.64	0.33	0.25	789.3	3.3	8.34	2.37	791.0	5.0
DX	0.44	46.04	2.50	-0.98	0.44	0.25	801.2	4.0	6.42	2.03	794.4	4.4
DX	0.44	46.48	3.51	-1.33	0.55	0.25	809.7	4.7	4.81	1.68	798.9	3.8
M1	0.23	46.70	4.14	-1.48	0.61	0.29	813.0	5.2	4.09	1.50	801.8	3.5
M1	0.23	46.93	4.84	-1.62	0.68	0.32	815.9	5.6	3.46	1.32	805.3	3.2
DX	0.44	47.37	6.39	-1.94	0.82	0.32	820.4	6.5	2.46	0.98	813.9	2.7
DX	0.44	47.80	8.22	-2.27	0.97	0.32	823.9	7.4	1.76	0.63	826.0	2.3
QF	0.25	48.05	8.79	0.05	1.01	0.05	825.5	7.6	1.60	-0.00	834.7	2.2
QF	0.25	48.30	8.18	2.36	0.99	-0.23	827.2	7.4	1.76	-0.63	843.3	2.3
DX	0.44	48.74	6.27	2.01	0.89	-0.23	830.7	6.5	2.46	-0.98	855.4	2.7
DX	0.44	49.17	4.68	1.66	0.79	-0.23	835.3	5.6	3.47	-1.33	864.0	3.2
M1	0.23	49.40	3.97	1.58	0.74	-0.20	838.3	5.2	4.11	-1.51	867.4	3.5
M1	0.23	49.62	3.32	1.34	0.70	-0.17	841.9	4.8	4.83	-1.69	870.3	3.8
DX	0.44	50.06	2.31	0.97	0.62	-0.17	850.9	4.0	6.45	-2.04	874.8	4.4
DX	0.44	50.50	1.63	0.61	0.55	-0.17	863.9	3.4	8.38	-2.38	878.2	5.0
QD	0.25	50.75	1.48	0.00	0.53	-0.02	873.3	3.2	8.99	-0.03	879.8	5.2
QD	0.25	51.00	1.63	-0.61	0.54	0.13	882.7	3.4	8.40	2.34	881.5	5.0
D1	0.32	51.32	2.11	-0.88	0.59	0.13	892.8	3.8	6.97	2.09	883.9	4.6
D1	0.32	51.64	2.76	-1.15	0.63	0.13	900.5	4.3	5.70	1.84	886.8	4.1
M	0.45	52.09	3.95	-1.48	0.70	0.20	908.3	5.1	4.20	1.49	892.1	3.5
M	0.45	52.54	5.41	-1.77	0.81	0.27	913.9	6.0	3.01	1.15	899.4	3.0
D1	0.32	52.87	6.63	-2.01	0.90	0.27	917.0	6.7	2.35	0.90	906.4	2.7
D1	0.32	53.19	8.02	-2.26	0.99	0.27	919.5	7.3	1.85	0.65	915.3	2.4
QF	0.25	53.44	8.60	0.00	1.02	-0.01	921.2	7.6	1.69	0.00	923.5	2.3
QF	0.25	53.69	8.02	2.26	0.98	-0.29	922.9	7.3	1.85	-0.65	931.8	2.4
D1	0.32	54.01	6.63	2.01	0.89	-0.29	925.4	6.6	2.35	-0.90	940.7	2.7
D1	0.32	54.34	5.41	1.77	0.79	-0.29	928.5	6.0	3.01	-1.14	947.7	3.0
M	0.45	54.79	3.95	1.48	0.68	-0.22	934.1	5.1	4.19	-1.49	955.0	3.5
M	0.45	55.24	2.76	1.15	0.59	-0.15	941.9	4.3	5.69	-1.84	960.3	4.1
D1	0.32	55.56	2.11	0.88	0.54	-0.15	949.7	3.8	6.96	-2.08	963.2	4.6
D1	0.32	55.88	1.63	0.61	0.49	-0.15	959.7	3.3	8.38	-2.33	965.6	5.0
QD	0.25	56.13	1.48	-0.00	0.47	-0.02	969.1	3.2	8.97	0.03	967.3	5.2
QD	0.25	56.38	1.63	-0.61	0.48	0.11	978.5	3.3	8.36	2.38	968.9	5.0
D1	0.32	56.71	2.11	-0.88	0.52	0.11	988.6	3.8	6.90	2.12	971.3	4.6
D1	0.32	57.03	2.76	-1.15	0.56	0.11	996.3	4.3	5.62	1.86	974.3	4.1
M	0.45	57.48	3.95	-1.48	0.62	0.181004.1	5.1	4.10	1.50	979.7	3.5	
M	0.45	57.93	5.41	-1.77	0.72	0.251009.7	5.9	2.91	1.15	987.2	3.0	
D1	0.32	58.25	6.64	-2.01	0.80	0.251012.8	6.6	2.25	0.89	994.5	2.6	
D1	0.32	58.58	8.02	-2.26	0.88	0.251015.3	7.2	1.76	0.631003.8	2.3		
QH	0.13	58.70	8.45	-1.17	0.91	0.131016.2	7.4	1.64	0.301008.1	2.2		
QH	0.13	58.83	8.60	-0.00	0.91	0.001017.0	7.5	1.60	-0.001012.5	2.2		
ELEM	LTH	SUM L	BETAX	ALPHAX	ETAX	ETA'X	PSIX	X	BETAY	ALPHAY	PSIY	ψ
	(M)	(M)	(M)		(M)	(RAD)	(DEG)	(CM)	(N)		(DEG)	(CM)

Table A.1-3(d)

BETA x, BETA y, ETA x for 1 Period
 NU X = .228 NU Y = .250 TR GAMMA = 4.319 MU X = 1.433 MU Y = 1.571
 327 QD = -6.628 Q1 = -6.371 Q2 = 11.511 Q3 = -9.700 Q4 = 9.669 QH = 6.027 C5 = -!



BEAM RIGIDITY=6.03800 X,Y EMITT=50.0000,30.0000 PI CM-MR,DPP=.01000										COMMANDS	
ELEMENTS: 17 ELEMENT DEFINITIONS										BEAM	
NAM	TYPE	VAR	LEN,ANG	B,B',N,GAP	D4	DRFT	0.0	.39056	0.0000	0.000	ELEMENTS
QF	QUAD	1.2	.50000	6.0268 0.000	DX	DRFT	0.0	.87200	0.0000	0.000	LATTICE
D1	DRFT	0.0	.64700	0.0000 0.000	M1	BEND	0.0	.45000	1.0538	0.000	PERIODS
E	EDGE	0.0	2.0000	1.0538 0.000	Q4	QUAD	0.0	.85000	9.6691	0.000	FIT
M	BEND	0.0	.90000	1.0538 0.000	QH	QUAD	1.2	.25000	6.0268	0.000	TRANSPOR
QD	QUAD	2.2	.50000	-6.628 0.000	Q5	QUAD	0.0	.50000	-9.049	0.000	INSERT
DM	DRFT	0.0	.90000	0.0000 0.000							MATRIX
Q1	QUAD	0.0	.50000	-6.370 0.000							GO
Q2	QUAD	0.0	.50000	11.511 0.000							CYCLE
Q3	QUAD	0.0	.50000	-9.700 0.000							GRAPH
D2	DRFT	0.0	1.5500	0.0000 0.000							ITERATE
D3	DRFT	0.0	.15000	0.0000 0.000							HELP
LATTICE: 9 ELEMENTS: QH D1 M D1 QD D1 M D1 QH										SAVE	
PERIODS FIT: NU X =2.300,NU Y =3.300,										RECALL	
1										QUIT	
										NEW CASE	
										PRINT	

Fig. A.1-4

ELEM	LTH (M)	SUM L (M)	BETAX (M)	ALPHAX	ETAX (M)	ETA'X (RAD)	PSIX (DEG)	X (CM)	BETAY (M)	ALPHAY	PSIY (DEG)	Y (CM)
	0.00	0.00	8.64	0.00	1.29	-0.00	0.0	7.9	1.68	0.00	0.0	2.2
QH	0.13	0.13	8.51	1.05	1.28	-0.16	0.8	7.8	1.72	-0.29	4.2	2.3
QH	0.13	0.25	8.12	2.04	1.25	-0.32	1.7	7.6	1.83	-0.59	8.3	2.3
D1	0.32	0.57	6.87	1.83	1.15	-0.32	4.2	7.0	2.29	-0.83	17.4	2.6
D1	0.32	0.90	5.75	1.63	1.04	-0.32	7.1	6.4	2.91	-1.07	24.6	3.0
M	0.45	1.35	4.38	1.40	0.91	-0.25	12.3	5.6	4.02	-1.40	32.1	3.5
M	0.45	1.80	3.23	1.14	0.82	-0.19	19.1	4.8	5.43	-1.74	37.7	4.0
D1	0.32	2.12	2.57	0.91	0.76	-0.19	25.6	4.3	6.63	-1.97	40.8	4.5
D1	0.32	2.44	2.05	0.68	0.69	-0.19	33.7	3.9	7.99	-2.21	43.3	4.9
QD	0.25	2.69	1.89	0.00	0.67	-0.00	41.0	3.7	8.55	-0.00	45.0	5.1
QD	0.25	2.94	2.05	-0.68	0.69	0.19	48.4	3.9	7.99	2.21	46.7	4.9
D1	0.32	3.27	2.57	-0.91	0.76	0.19	56.5	4.3	6.63	1.97	49.3	4.5
D1	0.32	3.59	3.23	-1.14	0.82	0.19	63.0	4.8	5.43	1.74	52.4	4.0
M	0.45	4.04	4.38	-1.40	0.91	-0.25	69.8	5.6	4.02	1.40	57.9	3.5
M	0.45	4.49	5.75	-1.63	1.04	0.32	75.0	6.4	2.91	1.07	65.5	3.0
D1	0.32	4.81	6.87	-1.83	1.15	0.32	77.9	7.0	2.29	0.83	72.7	2.6
D1	0.32	5.14	8.12	-2.04	1.25	0.32	80.4	7.6	1.83	0.59	81.8	2.3
QH	0.13	5.26	8.51	-1.05	1.28	0.16	81.2	7.8	1.72	0.29	85.8	2.3
QH	0.13	5.39	8.64	0.00	1.29	-0.00	82.1	7.9	1.68	-0.00	90.0	2.2

ELEM	LTH (M)	SUM L (M)	BETAX (M)	ALPHAX	ETAX (M)	ETA'X (RAD)	PSIX (DEG)	X (CM)	BETAY (M)	ALPHAY	PSIY (DEG)	Y (CM)
------	------------	--------------	--------------	--------	-------------	----------------	---------------	-----------	--------------	--------	---------------	-----------

MATCHED FUNCTIONS FOR 1 PERIOD(S)

TOTAL LENGTH= 5.3980 METERS, TOTAL BEND= 17.9995 DEGREES

BETAX= 8.6429 METERS ALPHAX= 0.0000 NUX= 0.2280

BETAY= 1.6345 METERS ALPHAY= 0.0000 NUY= 0.2501

ETAX = 1.2389 METERS ETA'X = -0.0000 TRGAMMA= 4.3194

Table A.1-4

INJECTION MODE

BETA0X=	2.0544	ALPHA0X=	0.6807
BETA0Y=	7.9853	ALPHA0Y=	-2.2130
ETA0=	0.6948	ETA0'=	-0.1864

BETA x, BETA y, ETA x for 1 Period

327 00 = -8.628 01 = -8.371 02 = 11.511 03 = -9.700 04 = 9.669 0H = 6.027 05 = -!

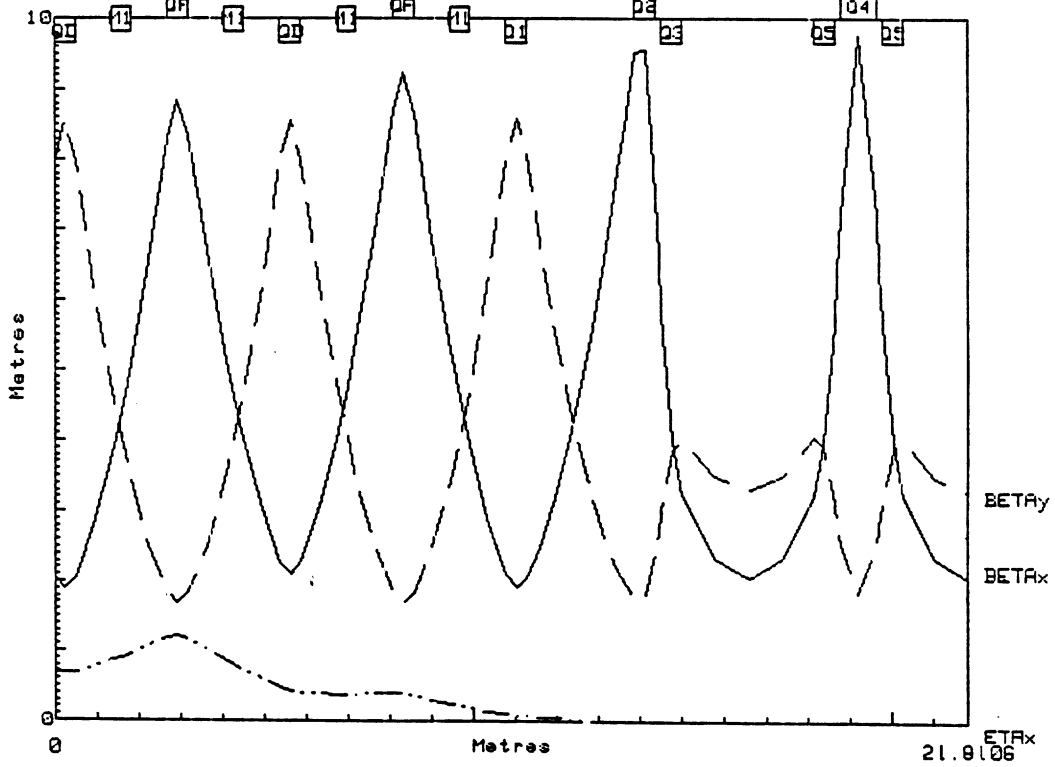


Fig. A.1-5

BEAM RIGIDITY=6.03800 X,Y EMITT=50.0000,30.0000 PI CM-MR,DPP=.01000													COMMANDS				
ELEMENTS: 17 ELEMENT DEFINITIONS													D4 DRFT 0.0 .39056 0.0000 0.000				
NAM	TYPE	VAR	LEN,ANG	B,B'	N,GAP	DX	DRFT	0.0	.87200	0.0000	0.000		BEAM				
QF	QUAD	1.2	.50000	6.0268	0.000	M1	BEND	0.0	.45000	1.0538	0.000		ELEMENTS				
D1	DRFT	0.0	.64700	0.0000	0.000	Q4	QUAD	0.0	.85000	9.6691	0.000		LATTICE				
E	EDGE	0.0	2.0000	1.0538	0.000	QH	QUAD	1.2	.25000	6.0268	0.000		PERIODS				
M	BEND	0.0	.90000	1.0538	0.000	Q5	QUAD	0.0	.50000	-9.049	0.000		FIT				
QD	QUAD	2.2	.50000	-6.628	0.000								*TRANSPOR				
DM	DRFT	0.0	.90000	0.0000	0.000								*INSERT				
Q1	QUAD	0.0	.50000	-6.370	0.000								MATRIX				
Q2	QUAD	0.0	.50000	11.511	0.000								GO				
Q3	QUAD	0.0	.50000	-9.700	0.000								CYCLE				
D2	DRFT	0.0	1.5500	0.0000	0.000								GRAPH				
D3	DRFT	0.0	.15000	0.0000	0.000								ITERATE				
LATTICE: 32 ELEMENTS: QD DX M1 DX QF DX M1 DX QD DX M1 DX													HELP				
QF	DX	M1	DX	Q1	D1	DM	D1	D4	Q2	D3	Q3	D2	D2	Q5	D3	Q4	SAVE
D3	Q5	D2															RECALL
PERIODS													QUIT				
FIT:													NEW CASE				
1																	PRINT

TOTAL LENGTH= 21.8106 METERS, TOTAL BEND= 17.9995 DEGREES

BETAX= 2.0562 METERS ALPHAX= -0.0003 NUX= 0.0000

BETAY= 3.2390 METERS ALPHAY= 0.0000 NUY= 0.0000

ETA X= -0.0700 METERS ETA X = 0.0614

X(CM)= 3.2064 X'(MR)= 15.5940 R12= 0.0003

Y(CM)= 3.1407 Y'(MR)= 9.5521 R34= -0.0000

M(1,6)= -0.7436 M(2,6)= -0.0329 M(5,6)= -0.1295

Table A.1-5(a)

ELEM	LTH (M)	SUM L (M)	BETAX (M)	ALPHAX	ETAX (M)	ETA'X (RAD)	PSIX (DEG)	X (CM)	BETAY (M)	ALPHAY	PSIY (DEG)	Y (CM)
	0.00	0.00	2.05	0.68	0.69	-0.19	0.0	3.2	7.99	-2.21	0.0	4.9
QD	0.25	0.25	1.89	-0.00	0.67	0.00	7.4	3.7	8.55	-0.00	1.7	5.1
QD	0.25	0.50	2.05	-0.68	0.69	0.19	14.8	3.9	7.99	2.21	3.4	4.9
DX	0.44	0.94	2.78	-0.99	0.78	0.19	25.3	4.5	6.20	1.89	7.0	4.3
DX	0.44	1.37	3.78	-1.30	0.86	0.19	33.0	5.2	4.69	1.57	11.6	3.7
M1	0.23	1.60	4.40	-1.43	0.90	0.22	36.1	5.6	4.02	1.40	14.6	3.5
M1	0.23	1.82	5.07	-1.55	0.96	0.25	38.9	6.0	3.42	1.24	18.1	3.2
DX	0.44	2.26	6.55	-1.85	1.07	0.25	43.2	6.8	2.49	0.91	26.7	2.7
DX	0.44	2.69	8.29	-2.14	1.18	0.25	46.6	7.6	1.83	0.59	38.5	2.3
QF	0.25	2.94	8.85	-0.06	1.20	-0.05	48.3	7.9	1.68	-0.00	46.7	2.2
QF	0.25	3.19	8.35	2.04	1.15	-0.34	49.9	7.6	1.83	-0.59	55.0	2.3
DX	0.44	3.63	6.68	1.77	1.01	-0.34	53.3	6.8	2.49	-0.91	66.8	2.7
DX	0.44	4.07	5.26	1.50	0.86	-0.34	57.5	6.0	3.43	-1.24	75.4	3.2
M1	0.23	4.29	4.60	1.39	0.78	-0.31	60.1	5.6	4.02	-1.40	78.9	3.5
M1	0.23	4.52	4.00	1.28	0.72	-0.27	63.1	5.2	4.69	-1.57	81.8	3.8
DX	0.44	4.95	3.01	0.99	0.60	-0.27	70.3	4.5	6.20	-1.89	86.5	4.3
DX	0.44	5.39	2.27	0.70	0.48	-0.27	79.9	3.9	7.99	-2.21	90.0	4.9
QD	0.25	5.64	2.11	-0.02	0.43	-0.15	86.5	3.7	8.55	-0.00	91.7	5.1
QD	0.25	5.89	2.30	-0.75	0.40	-0.04	93.1	3.8	7.99	2.21	93.5	4.9
DX	0.44	6.32	3.09	-1.05	0.39	-0.04	102.5	4.3	6.20	1.89	97.0	4.3
DX	0.44	6.76	4.13	-1.35	0.37	-0.04	109.6	4.9	4.69	1.57	101.7	3.8
M1	0.23	6.99	4.77	-1.47	0.37	0.00	112.5	5.3	4.02	1.40	104.6	3.5
M1	0.23	7.21	5.46	-1.58	0.37	0.04	115.0	5.6	3.43	1.24	108.1	3.2
DX	0.44	7.65	6.96	-1.86	0.39	0.04	119.1	6.3	2.49	0.91	116.7	2.7
DX	0.44	8.08	8.71	-2.14	0.40	0.04	122.3	7.0	1.83	0.59	128.5	2.3
QF	0.25	8.33	9.24	0.05	0.40	-0.06	123.8	7.2	1.68	0.00	136.8	2.2
QF	0.25	8.58	8.66	2.23	0.37	-0.16	125.4	7.0	1.83	-0.59	145.0	2.3
DX	0.44	9.02	6.85	1.93	0.30	-0.16	128.7	6.2	2.49	-0.91	156.8	2.7
DX	0.44	9.45	5.30	1.63	0.23	-0.16	132.8	5.4	3.42	-1.24	165.4	3.2
M1	0.23	9.68	4.60	1.50	0.20	-0.12	135.4	5.0	4.02	-1.40	168.9	3.5
M1	0.23	9.90	3.95	1.37	0.18	-0.09	138.5	4.6	4.69	-1.57	171.9	3.7
DX	0.44	10.34	2.89	1.05	0.14	-0.09	145.9	3.9	6.20	-1.89	176.5	4.3
DX	0.44	10.78	2.11	0.74	0.10	-0.09	156.0	3.4	7.99	-2.21	180.1	4.9
Q1	0.25	11.03	1.92	0.06	0.08	-0.06	163.2	3.2	8.57	-0.09	181.8	5.1
Q1	0.25	11.28	2.05	-0.59	0.07	-0.04	170.6	3.3	8.07	2.06	183.5	4.9
D1	0.32	11.60	2.50	-0.81	0.06	-0.04	178.3	3.6	6.81	1.85	186.0	4.5
D1	0.32	11.92	3.09	-1.02	0.05	-0.04	185.5	4.0	5.68	1.64	189.0	4.1
DM	0.45	12.37	4.15	-1.32	0.03	-0.04	192.7	4.6	4.34	1.35	194.2	3.6
DM	0.45	12.82	5.47	-1.62	0.01	-0.04	198.1	5.2	3.26	1.05	201.1	3.1
D1	0.32	13.15	6.59	-1.83	-0.00	-0.04	201.2	5.7	2.64	0.84	207.4	2.8
D1	0.32	13.47	7.84	-2.05	-0.02	-0.04	203.8	6.3	2.16	0.63	215.2	2.5
D4	0.20	13.67	8.66	-2.17	-0.02	-0.04	205.1	6.6	1.94	0.51	220.6	2.4
D4	0.20	13.86	9.54	-2.30	-0.03	-0.04	206.4	6.9	1.77	0.38	226.7	2.3
Q2	0.25	14.11	9.55	2.27	-0.04	-0.02	207.9	7.0	1.82	-0.61	234.9	2.3
Q2	0.25	14.36	7.45	5.80	-0.04	-0.00	209.6	6.1	2.43	-1.90	241.8	2.7
D3	0.08	14.44	6.61	5.45	-0.04	-0.00	210.2	5.8	2.72	-2.05	243.5	2.9
D3	0.08	14.51	5.81	5.10	-0.04	-0.00	210.9	5.4	3.04	-2.19	245.0	3.0
Q3	0.25	14.76	3.99	2.42	-0.05	-0.02	213.9	4.5	3.88	-1.07	249.1	3.4
Q3	0.25	15.01	3.23	0.75	-0.05	-0.04	218.0	4.1	4.04	0.47	252.7	3.5
D2	0.78	15.79	2.35	0.38	-0.09	-0.04	234.3	3.5	3.49	0.23	264.6	3.2
D2	0.78	16.56	2.06	0.00	-0.12	-0.04	255.0	3.3	3.31	-0.00	277.7	3.2
D2	0.78	17.34	2.35	-0.38	-0.15	-0.04	275.6	3.6	3.50	-0.23	290.9	3.2
D2	0.78	18.11	3.23	-0.75	-0.18	-0.04	291.9	4.2	4.04	-0.47	302.8	3.5
Q5	0.25	18.36	3.97	-2.31	-0.20	-0.11	296.0	4.7	3.91	0.97	306.3	3.4
Q5	0.25	18.61	5.69	-4.77	-0.24	-0.19	299.1	5.6	3.13	2.05	310.4	3.1
D3	0.08	18.69	6.42	-5.08	-0.25	-0.19	299.8	5.9	2.83	1.93	311.8	2.9
D3	0.08	18.76	7.21	-5.39	-0.27	-0.19	300.4	6.3	2.56	1.80	313.4	2.8
Q4	0.43	19.19	9.75	0.00	-0.31	0.01	303.2	7.3	1.85	0.00	325.2	2.4
Q4	0.43	19.61	7.21	5.39	-0.26	0.20	305.9	6.3	2.55	-1.79	337.1	2.8
D3	0.08	19.69	6.42	5.08	-0.24	0.20	306.6	5.9	2.82	-1.91	338.7	2.9
D3	0.08	19.76	5.68	4.77	-0.23	0.20	307.3	5.6	3.12	-2.04	340.1	3.1
Q5	0.25	20.01	3.97	2.31	-0.19	0.13	310.4	4.6	3.89	-0.96	344.2	3.4
Q5	0.25	20.26	3.22	0.75	-0.17	0.06	314.4	4.2	4.02	0.47	347.7	3.5
D2	0.78	21.04	2.35	0.38	-0.12	0.06	330.8	3.5	3.47	0.24	359.7	3.2
D2	0.78	21.81	2.06	-0.00	-0.07	0.06	351.4	3.3	3.29	-0.00	373.0	3.1
ELEM	LTH	SUM L	BETAX	ALPHAX	ETAX	ETA'X	PSIX	X	BETAY	ALPHAY	PSIY	Y

Table A.1-5(b)

BEAM RIGIDITY=6.03800 X,Y EMITT=50.0000,30.0000 PI CM-MR,DPP=.01500												COMMANDS					
ELEMENTS:	17	ELEMENT	DEFINITIONS	D4	DRFT	0.0	.39056	0.0000	0.000			BEAM					
NAM	TYPE	VAR	LEN,ANG	B,B'	M,GAP	DX	DRFT	0.0	.87200	0.0000	0.000	ELEMENTS					
QF	QUAD	1.2	.50000	6.0268	0.000	M1	BEND	0.0	.45000	1.0538	0.000	LATTICE					
D1	DRFT	0.0	.64700	0.0000	0.000	Q4	QUAD	0.0	.85000	9.6691	0.000	PERIODS					
E	EDGE	0.0	2.0000	1.0538	0.000	QH	QUAD	1.2	.25000	6.0268	0.000	FIT					
M	BEND	0.0	.90000	1.0538	0.000	Q5	QUAD	0.0	.50000	-9.049	0.000	TRANSPOR					
QD	QUAD	2.2	.50000	-6.628	0.000							INSERT					
DM	DRFT	0.0	.90000	0.0000	0.000							MATRIX					
Q1	QUAD	0.0	.50000	-6.370	0.000							GO					
Q2	QUAD	0.0	.50000	11.511	0.000							CYCLE					
Q3	QUAD	0.0	.50000	-9.700	0.000							GRAPH					
D2	DRFT	0.0	1.5500	0.0000	0.000							ITERATE					
D3	DRFT	0.0	.15000	0.0000	0.000							HELP					
LATTICE: 45 ELEMENTS: QH D1 M D1 QD D1 M D1 QF D1 M D1												SAVE					
QD	DX	M1	DX	QF	DX	M1	DX	QD	DX	M1	DX	QF	DX	M1	DX	Q1	RECALL
D1	DM	D1	D4	Q2	D3	Q3	D2	D2	Q5	D3	Q4	D3	Q5	D2	RFL		QUIT
PERIODS	FIT: NU X =2.300, NU Y =3.300,											NEW CASE					
4												PRINT					

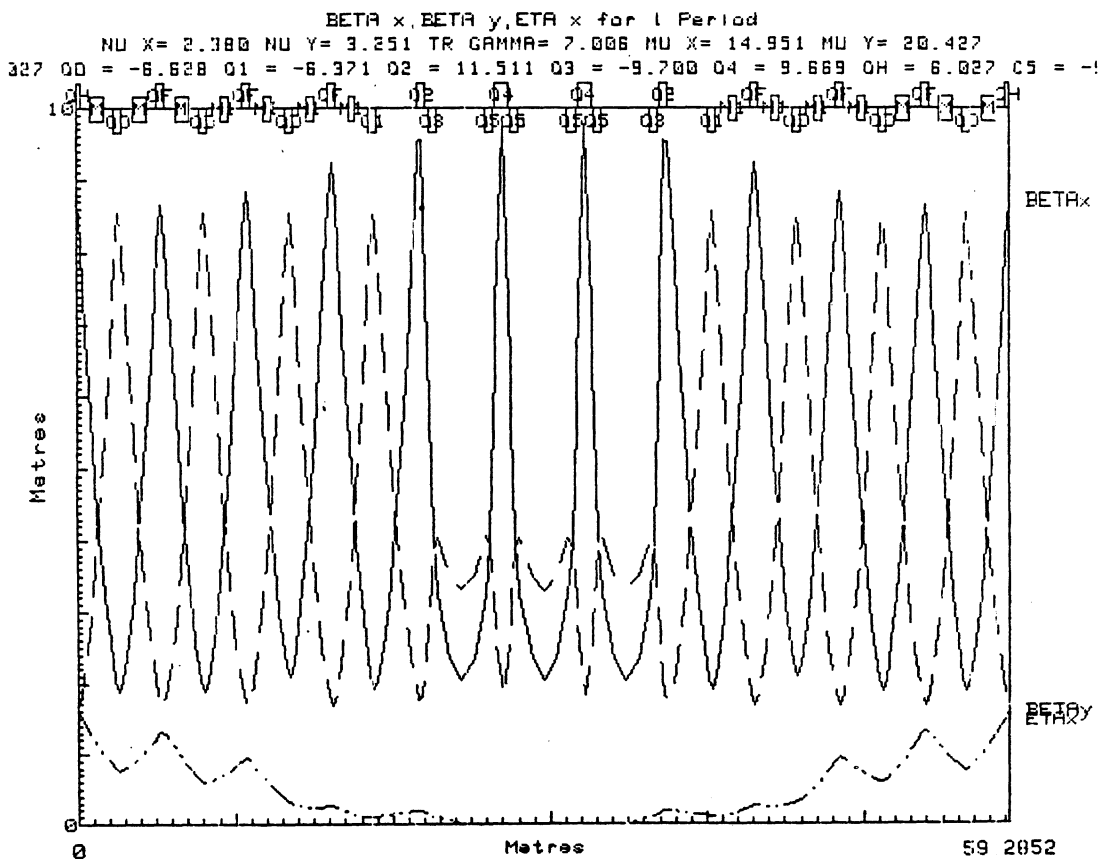


Fig. A.1-6

ELEM	LTH (M)	SUM L (M)	BETA _X (M)	ALPHA _X	ETA _X (M)	ETA' _X (RAD)	PSIX (DEG)	X (CM)	BETA _Y (M)	ALPHA _Y	PSI _Y (DEG)	Y (CM)
	0.00	0.00	3.64	0.00	1.56	-0.00	0.0	8.1	1.68	0.00	0.0	2.2
QH	0.13	0.13	3.51	1.05	1.55	-0.19	0.8	8.1	1.72	-0.29	4.2	2.3
QH	0.13	0.25	3.12	2.04	1.51	-0.39	1.7	7.9	1.83	-0.59	8.3	2.3
D1	0.32	0.57	6.86	1.83	1.39	-0.39	4.2	7.2	2.29	-0.83	17.4	2.6
D1	0.32	0.90	5.74	1.63	1.26	-0.39	7.1	6.6	2.91	-1.07	24.6	3.0
M	0.45	1.35	4.38	1.40	1.10	-0.32	12.3	5.8	4.02	-1.40	32.1	3.5
M	0.45	1.80	3.23	1.14	0.97	-0.26	19.1	5.0	5.43	-1.74	37.7	4.0
D1	0.32	2.12	2.57	0.91	0.89	-0.26	25.6	4.5	6.63	-1.97	40.8	4.5
D1	0.32	2.44	2.05	0.68	0.80	-0.26	33.7	4.0	7.99	-2.21	43.3	4.9
QD	0.25	2.69	1.89	-0.00	0.77	-0.04	41.1	3.8	8.55	-0.00	45.0	5.1
QD	0.25	2.94	2.05	-0.68	0.78	0.17	48.4	4.0	7.99	2.21	46.7	4.9
D1	0.32	3.27	2.57	-0.91	0.84	0.17	56.5	4.4	6.63	1.97	49.3	4.5
D1	0.32	3.59	3.23	-1.14	0.89	0.17	63.8	4.9	5.43	1.74	52.4	4.0
M	0.45	4.04	4.38	-1.40	0.98	0.23	69.8	5.7	4.02	1.40	57.9	3.5
M	0.45	4.49	5.75	-1.63	1.10	0.30	75.0	6.5	2.91	1.07	65.5	3.0
D1	0.32	4.81	6.87	-1.84	1.20	0.30	77.9	7.1	2.29	0.83	72.7	2.6
D1	0.32	5.14	8.13	-2.04	1.29	0.30	80.4	7.7	1.83	0.59	81.8	2.3
QF	0.25	5.39	3.65	-0.00	1.33	-0.03	82.1	7.9	1.68	-0.00	90.0	2.2
QF	0.25	5.64	3.13	2.04	1.28	-0.36	83.8	7.7	1.83	-0.59	98.3	2.3
D1	0.32	5.96	6.37	1.84	1.16	-0.36	86.3	7.0	2.29	-0.83	107.4	2.6
D1	0.32	6.29	5.75	1.63	1.05	-0.36	89.2	6.4	2.91	-1.07	114.6	3.0
M	0.45	6.74	4.38	1.40	0.90	-0.29	94.3	5.6	4.02	-1.40	122.2	3.5
M	0.45	7.19	3.24	1.14	0.78	-0.23	101.2	4.8	5.43	-1.74	127.7	4.0
D1	0.32	7.51	2.57	0.91	0.71	-0.23	107.6	4.3	6.63	-1.97	130.8	4.5
D1	0.32	7.83	2.06	0.68	0.64	-0.23	115.7	3.8	7.99	-2.21	133.3	4.9
QD	0.25	8.08	1.89	0.00	0.60	-0.06	123.1	3.7	8.55	0.00	135.0	5.1
QD	0.25	8.33	2.05	-0.68	0.61	0.11	130.5	3.8	7.99	2.21	136.6	4.9
DX	0.44	8.77	2.78	-0.99	0.66	0.11	141.0	4.4	6.20	1.89	140.3	4.3
DX	0.44	9.20	3.78	-1.30	0.70	0.11	148.7	5.1	4.69	1.57	145.0	3.8
M1	0.23	9.43	4.40	-1.43	0.73	0.14	151.9	5.4	4.02	1.40	147.9	3.5
M1	0.23	9.65	5.07	-1.55	0.77	0.18	154.6	5.8	3.42	1.24	151.4	3.2
DX	0.44	10.09	6.55	-1.85	0.85	0.18	158.9	6.6	2.49	0.91	160.0	2.7
DX	0.44	10.53	8.29	-2.14	0.92	0.18	162.3	7.4	1.83	0.59	171.8	2.3
QF	0.25	10.78	8.85	-0.06	0.94	-0.06	164.0	7.6	1.68	0.00	180.1	2.2
QF	0.25	11.03	8.34	2.04	0.90	-0.29	165.6	7.4	1.83	-0.59	188.3	2.3
DX	0.44	11.46	6.63	1.77	0.77	-0.29	167.0	6.6	2.49	-0.91	200.1	2.7
DX	0.44	11.90	5.25	1.50	0.65	-0.29	173.2	5.8	3.42	-1.24	208.7	3.2
M1	0.23	12.12	4.60	1.39	0.59	-0.25	175.8	5.4	4.02	-1.40	212.2	3.5
M1	0.23	12.35	4.00	1.28	0.53	-0.22	178.8	5.0	4.69	-1.57	215.2	3.7
DX	0.44	12.78	3.01	0.99	0.44	-0.22	186.1	4.3	6.20	-1.89	219.8	4.3
DX	0.44	13.22	2.27	0.70	0.35	-0.22	195.6	3.7	7.99	-2.21	223.4	4.9
QD	0.25	13.47	2.11	-0.02	0.30	-0.13	202.3	3.5	8.55	-0.00	225.1	5.1
QD	0.25	13.72	2.30	-0.76	0.28	-0.05	208.9	3.7	7.99	2.21	226.8	4.9
DX	0.44	14.16	3.09	-1.05	0.26	-0.05	218.3	4.2	6.20	1.89	230.4	4.3
DX	0.44	14.59	4.13	-1.35	0.24	-0.05	225.3	4.8	4.69	1.57	235.0	3.8
M1	0.23	14.82	4.77	-1.47	0.23	-0.01	228.2	5.1	4.02	1.40	238.0	3.5
M1	0.23	15.04	5.46	-1.58	0.24	0.03	230.8	5.5	3.43	1.24	241.4	3.2
DX	0.44	15.48	6.96	-1.86	0.25	0.03	234.8	6.1	2.49	0.91	250.0	2.7
DX	0.44	15.91	8.71	-2.15	0.26	0.03	238.0	6.9	1.83	0.59	261.8	2.3
QF	0.25	16.16	9.25	0.05	0.26	-0.04	239.6	7.1	1.68	-0.00	270.1	2.2
QF	0.25	16.41	8.66	2.23	0.24	-0.10	241.2	6.8	1.83	-0.59	278.4	2.3
DX	0.44	16.85	6.85	1.93	0.20	-0.10	244.4	6.1	2.49	-0.91	290.2	2.7
DX	0.44	17.29	5.30	1.63	0.15	-0.10	248.6	5.3	3.43	-1.24	298.3	3.2
M1	0.23	17.51	4.60	1.50	0.14	-0.06	251.2	4.9	4.02	-1.40	302.2	3.5
M1	0.23	17.74	3.95	1.37	0.13	-0.02	254.2	4.6	4.69	-1.57	305.2	3.8
DX	0.44	18.17	2.89	1.05	0.12	-0.02	261.6	3.9	6.20	-1.89	309.8	4.3
DX	0.44	18.61	2.11	0.74	0.11	-0.02	271.8	3.4	7.99	-2.21	313.4	4.9
Q1	0.25	18.86	1.92	0.06	0.10	0.00	279.0	3.2	8.57	-0.09	315.1	5.1
Q1	0.25	19.11	2.05	-0.59	0.11	0.03	286.3	3.3	8.07	2.06	316.8	4.9
D1	0.32	19.43	2.50	-0.81	0.12	0.03	294.5	3.7	6.81	1.85	319.3	4.5
D1	0.32	19.76	3.10	-1.02	0.13	0.03	301.2	4.1	5.68	1.64	322.3	4.1
DM	0.45	20.21	4.15	-1.32	0.14	0.03	308.4	4.7	4.34	1.35	327.5	3.6
DM	0.45	20.66	5.47	-1.62	0.16	0.03	313.8	5.4	3.26	1.05	334.4	3.1
D1	0.32	20.98	6.59	-1.83	0.17	0.03	316.9	5.9	2.64	0.84	340.7	2.8
D1	0.32	21.30	7.84	-2.04	0.18	0.03	319.5	6.4	2.16	0.63	348.5	2.5
D4	0.20	21.50	8.66	-2.17	0.19	0.03	320.9	6.8	1.84	0.51	354.0	2.4

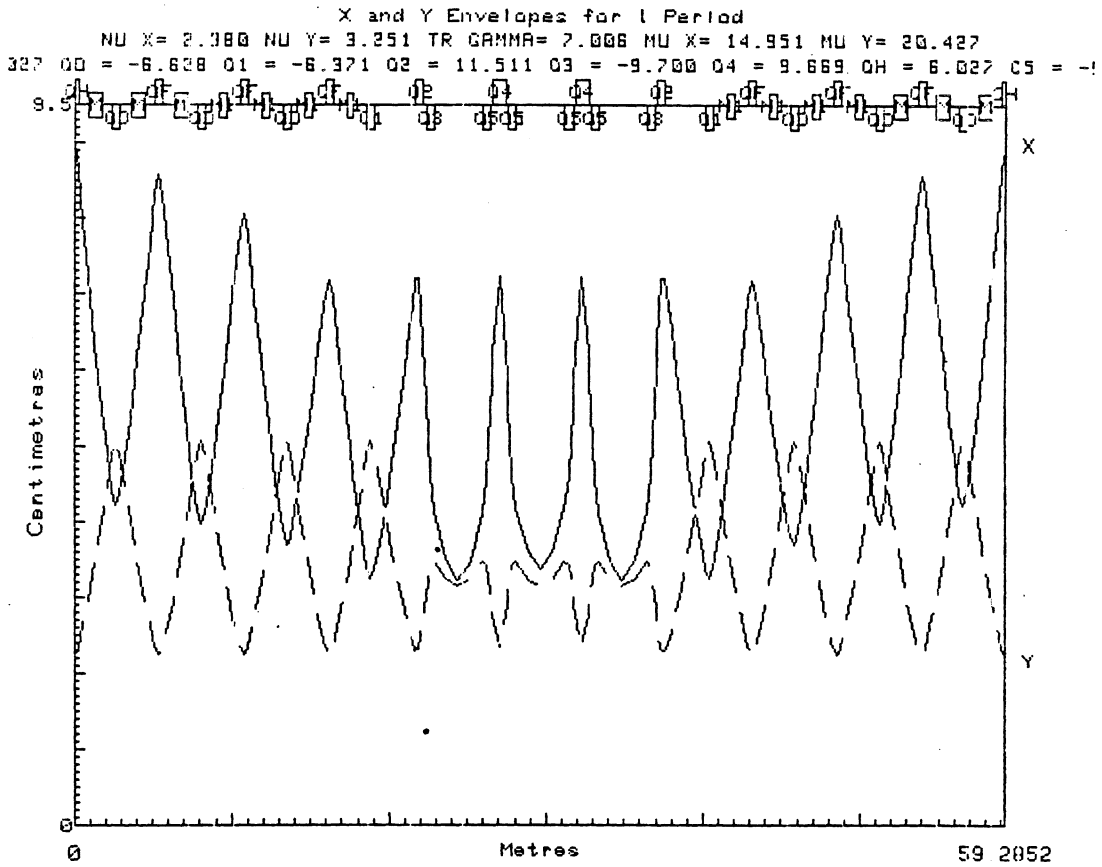
Table A.1-6(a)

D4	0.20	21.69	9.54	-2.38	0.19	0.03	322.1	7.1	1.77	0.38	360.0	2.3
Q2	0.25	21.94	9.55	2.27	0.19	-0.06	323.6	7.1	1.92	-0.61	368.2	2.3
Q2	0.25	22.19	7.45	5.88	0.16	-0.14	325.3	6.3	2.42	-1.90	375.2	2.7
D3	0.08	22.27	6.60	5.45	0.15	-0.14	325.9	5.9	2.72	-2.05	376.9	2.9
D3	0.08	22.34	5.81	5.10	0.14	-0.14	326.6	5.5	3.04	-2.19	378.3	3.0
Q3	0.25	22.59	3.99	2.42	0.11	-0.09	329.7	4.6	3.88	-1.07	382.4	3.4
Q3	0.25	22.84	3.23	0.75	0.09	-0.05	333.7	4.1	4.04	0.47	386.0	3.5
D2	0.78	23.62	2.35	0.38	0.05	-0.05	350.1	3.5	3.49	0.23	397.9	3.2
D2	0.78	24.39	2.06	-0.00	0.01	-0.05	370.7	3.2	3.31	-0.00	411.1	3.2
D2	0.78	25.17	2.35	-0.38	-0.03	-0.05	391.3	3.5	3.50	-0.23	424.2	3.2
D2	0.78	25.94	3.23	-0.75	-0.07	-0.05	407.7	4.1	4.04	-0.47	436.1	3.5
Q5	0.25	26.19	3.97	-2.31	-0.09	-0.08	411.8	4.5	3.91	0.97	439.7	3.4
Q5	0.25	26.44	5.69	-4.77	-0.11	-0.12	414.8	5.4	3.13	2.05	443.7	3.1
D3	0.08	26.52	6.42	-5.08	-0.12	-0.12	415.5	5.8	2.84	1.93	445.2	2.9
D3	0.08	26.59	7.21	-5.39	-0.13	-0.12	416.2	6.1	2.56	1.80	446.7	2.8
Q4	0.43	27.02	9.75	0.00	-0.16	-0.02	418.9	7.1	1.85	0.00	458.6	2.4
Q4	0.43	27.44	7.21	5.39	-0.14	0.09	421.7	6.1	2.55	-1.79	470.4	2.8
D3	0.08	27.52	6.42	5.08	-0.14	0.09	422.3	5.8	2.82	-1.91	472.0	2.9
D3	0.08	27.59	5.69	4.77	-0.13	0.09	423.0	5.5	3.12	-2.04	473.5	3.1
Q5	0.25	27.84	3.97	2.31	-0.11	0.04	426.1	4.6	3.89	-0.96	477.5	3.4
Q5	0.25	28.09	3.22	0.75	-0.11	0.00	430.2	4.1	4.02	0.47	481.1	3.5
D2	0.78	28.87	2.35	0.38	-0.11	0.00	446.5	3.5	3.47	0.24	493.0	3.2
D2	0.78	29.64	2.06	0.00	-0.11	0.00	467.2	3.3	3.29	0.00	506.3	3.1
D2	0.78	30.42	2.35	-0.38	-0.11	0.00	487.8	3.5	3.47	-0.24	519.6	3.2
D2	0.78	31.19	3.22	-0.75	-0.11	0.00	504.2	4.1	4.02	-0.47	531.5	3.5
Q5	0.25	31.44	3.97	-2.31	-0.11	-0.04	508.3	4.6	3.89	0.96	535.1	3.4
Q5	0.25	31.69	5.69	-4.77	-0.13	-0.09	511.3	5.3	3.12	2.04	539.2	3.1
D3	0.08	31.77	6.42	-5.08	-0.14	-0.09	512.0	5.8	2.82	1.91	540.6	2.9
D3	0.08	31.84	7.21	-5.39	-0.14	-0.09	512.7	6.1	2.55	1.79	542.2	2.8
Q4	0.43	32.27	9.75	-0.00	-0.16	0.02	515.4	7.1	1.85	-0.00	554.1	2.4
Q4	0.43	32.69	7.21	5.39	-0.13	0.12	518.2	6.1	2.56	-1.80	565.9	2.8
D3	0.08	32.77	6.42	5.08	-0.12	0.12	518.8	5.8	2.83	-1.93	567.5	2.9
D3	0.08	32.84	5.69	4.77	-0.11	0.12	519.5	5.4	3.13	-2.05	568.9	3.1
Q5	0.25	33.09	3.97	2.31	-0.09	0.08	522.6	4.5	3.91	-0.97	572.9	3.4
Q5	0.25	33.34	3.23	0.75	-0.07	0.05	526.7	4.1	4.04	0.47	576.5	3.5
D2	0.78	34.12	2.35	0.38	-0.03	0.05	543.0	3.5	3.50	0.23	588.4	3.2
D2	0.78	34.89	2.06	0.00	0.01	0.05	563.7	3.2	3.31	0.00	601.5	3.2
D2	0.78	35.67	2.35	-0.38	0.05	0.05	584.3	3.5	3.49	-0.23	614.7	3.2
D2	0.78	36.44	3.23	-0.75	0.09	0.05	600.6	4.1	4.04	-0.47	626.6	3.5
Q3	0.25	36.69	3.99	-2.42	0.11	0.09	604.7	4.6	3.88	1.07	630.2	3.4
Q3	0.25	36.94	5.81	-5.10	0.14	0.14	607.7	5.5	3.04	2.19	634.3	3.0
D3	0.08	37.02	6.60	-5.45	0.15	0.14	608.4	5.9	2.72	2.05	635.8	2.9
D3	0.08	37.09	7.45	-5.80	0.16	0.14	609.0	6.3	2.43	1.90	637.5	2.7
Q2	0.25	37.34	9.55	-2.27	0.19	0.06	610.7	7.1	1.82	0.61	644.4	2.3
Q2	0.25	37.59	9.54	2.30	0.19	-0.03	612.1	7.1	1.77	-0.38	652.6	2.3
D4	0.20	37.79	8.66	2.17	0.19	-0.03	613.3	6.8	1.94	-0.51	658.7	2.4
D4	0.20	37.98	7.84	2.04	0.18	-0.03	614.7	6.4	2.16	-0.63	664.1	2.5
D1	0.32	38.31	6.59	1.83	0.17	-0.03	617.3	5.9	2.64	-0.84	671.9	2.8
D1	0.32	38.63	5.47	1.62	0.16	-0.03	620.4	5.4	3.26	-1.05	678.2	3.1
DM	0.45	39.08	4.15	1.32	0.14	-0.03	625.8	4.7	4.34	-1.35	685.1	3.6
DM	0.45	39.53	3.10	1.02	0.13	-0.03	633.0	4.1	5.68	-1.64	690.3	4.1
D1	0.32	39.85	2.50	0.81	0.12	-0.03	639.7	3.7	6.81	-1.85	693.3	4.5
D1	0.32	40.18	2.05	0.59	0.11	-0.03	647.9	3.3	8.07	-2.06	695.8	4.9
Q1	0.25	40.43	1.92	-0.06	0.10	-0.00	655.2	3.2	8.57	0.09	697.5	5.1
Q1	0.25	40.68	2.11	-0.74	0.11	0.02	662.4	3.4	7.99	2.21	699.2	4.9
DX	0.44	41.11	2.89	-1.05	0.12	0.02	672.6	3.9	6.20	1.89	702.8	4.3
DX	0.44	41.55	3.95	-1.37	0.13	0.02	680.0	4.6	4.69	1.57	707.4	3.7
M1	0.23	41.77	4.60	-1.50	0.14	0.06	683.0	4.9	4.02	1.40	710.4	3.5
M1	0.23	42.00	5.30	-1.63	0.15	0.10	685.6	5.3	3.42	1.24	713.9	3.2
DX	0.44	42.44	6.85	-1.93	0.20	0.10	689.8	6.1	2.49	0.91	722.5	2.7
DX	0.44	42.87	8.66	-2.23	0.24	0.10	693.0	6.8	1.83	0.59	734.2	2.3
QF	0.25	43.12	9.25	-0.05	0.26	0.04	694.6	7.1	1.68	-0.00	742.5	2.2
QF	0.25	43.37	3.71	2.15	0.26	-0.03	696.2	6.9	1.83	-0.59	750.8	2.3
DX	0.44	43.91	6.96	1.86	0.25	-0.03	699.4	6.1	2.49	-0.91	762.6	2.7
DX	0.44	44.24	5.46	1.58	0.24	-0.03	703.4	5.5	3.42	-1.24	771.2	3.2

Table A.1-6(b)

M1	0.23	44.47	4.77	1.47	0.23	0.01	706.0	5.1	4.02	-1.40	774.7	3.5
M1	0.23	44.69	4.13	1.35	0.24	0.05	708.9	4.8	4.69	-1.57	777.6	3.8
DX	0.44	45.13	3.09	1.05	0.26	0.05	715.9	4.2	6.20	-1.89	782.3	4.3
DX	0.44	45.57	2.30	0.76	0.28	0.05	725.3	3.7	7.99	-2.21	785.8	4.9
QD	0.25	45.82	2.11	0.02	0.30	0.13	731.9	3.5	8.55	-0.00	787.5	5.1
QD	0.25	46.07	2.27	-0.70	0.35	0.22	738.5	3.7	7.99	2.21	789.3	4.9
DX	0.44	46.50	3.01	-0.99	0.44	0.22	748.1	4.3	6.20	1.89	792.8	4.3
DX	0.44	46.94	4.00	-1.28	0.53	0.22	755.3	5.0	4.69	1.57	797.4	3.8
M1	0.23	47.16	4.60	-1.39	0.59	0.25	758.4	5.4	4.02	1.40	800.4	3.5
M1	0.23	47.39	5.25	-1.50	0.65	0.29	761.0	5.8	3.43	1.24	803.9	3.2
DX	0.44	47.82	6.68	-1.77	0.77	0.29	765.2	6.6	2.49	0.91	812.5	2.7
DX	0.44	49.26	8.34	-2.04	0.90	0.29	768.5	7.4	1.83	0.59	824.3	2.3
QF	0.25	48.51	8.85	0.06	0.94	0.06	770.2	7.6	1.68	0.00	832.6	2.2
QF	0.25	48.76	8.29	2.14	0.92	-0.18	771.8	7.4	1.83	-0.59	840.8	2.3
DX	0.44	49.20	6.55	1.85	0.85	-0.18	775.2	6.6	2.49	-0.91	852.6	2.7
DX	0.44	49.63	5.07	1.55	0.77	-0.18	779.6	5.8	3.42	-1.24	861.2	3.2
M1	0.23	49.86	4.40	1.43	0.73	-0.14	782.3	5.4	4.02	-1.40	864.7	3.5
M1	0.23	50.08	3.78	1.30	0.70	-0.11	785.5	5.1	4.69	-1.57	867.7	3.8
DX	0.44	50.52	2.78	0.99	0.66	-0.11	793.2	4.4	6.20	-1.89	872.3	4.3
DX	0.44	50.95	2.05	0.68	0.61	-0.11	803.7	3.8	7.99	-2.21	875.9	4.9
QD	0.25	51.20	1.89	-0.00	0.60	0.06	811.1	3.7	8.55	0.00	877.6	5.1
QD	0.25	51.45	2.06	-0.68	0.64	0.23	818.5	3.8	7.99	2.21	879.3	4.9
D1	0.32	51.78	2.57	-0.91	0.71	0.23	826.5	4.3	6.63	1.97	881.8	4.5
D1	0.32	52.10	3.23	-1.14	0.78	0.23	833.0	4.8	5.43	1.74	884.9	4.0
M	0.45	52.55	4.38	-1.40	0.90	0.29	839.8	5.6	4.02	1.40	890.5	3.5
M	0.45	53.00	5.75	-1.63	1.05	0.36	845.0	6.4	2.91	1.07	898.0	3.0
D1	0.32	53.32	6.87	-1.84	1.16	0.36	847.9	7.0	2.29	0.83	905.2	2.6
D1	0.32	53.65	8.13	-2.04	1.28	0.36	850.4	7.7	1.83	0.59	914.3	2.3
QF	0.25	53.90	8.65	0.00	1.33	0.03	852.1	7.9	1.68	-0.00	922.6	2.2
QF	0.25	54.15	8.13	2.04	1.29	-0.30	853.8	7.7	1.83	-0.59	930.9	2.3
D1	0.32	54.47	6.87	1.84	1.20	-0.30	856.3	7.1	2.29	-0.83	940.0	2.6
D1	0.32	54.79	5.75	1.63	1.10	-0.30	859.2	6.5	2.91	-1.07	947.2	3.0
M	0.45	55.24	4.38	1.40	0.98	-0.23	864.4	5.7	4.02	-1.40	954.7	3.5
M	0.45	55.69	3.23	1.14	0.89	-0.17	871.2	4.9	5.43	-1.74	960.3	4.0
D1	0.32	55.02	2.57	0.91	0.84	-0.17	877.7	4.4	6.63	-1.97	963.3	4.5
D1	0.32	56.34	2.05	0.68	0.78	-0.17	885.8	4.0	7.99	-2.21	965.9	4.9
QD	0.25	56.59	1.89	0.00	0.77	0.04	893.1	3.8	8.55	-0.00	967.6	5.1
QD	0.25	56.84	2.05	-0.68	0.80	0.26	900.5	4.0	7.99	2.21	969.3	4.9
D1	0.32	57.16	2.57	-0.91	0.89	0.26	908.6	4.5	6.63	1.97	971.9	4.5
D1	0.32	57.49	3.23	-1.14	0.97	0.26	915.0	5.0	5.43	1.74	975.0	4.0
M	0.45	57.94	4.38	-1.40	1.10	0.32	921.9	5.8	4.02	1.40	980.5	3.5
M	0.45	58.39	5.74	-1.63	1.26	0.39	927.1	6.6	2.91	1.07	988.1	3.0
D1	0.32	58.71	6.86	-1.83	1.39	0.39	930.0	7.2	2.29	0.83	995.3	2.6
D1	0.32	59.04	8.12	-2.04	1.51	0.39	932.5	7.9	1.83	0.59	1004.3	2.3
QH	0.13	59.16	8.51	-1.05	1.55	0.19	933.4	8.1	1.72	0.29	1008.4	2.3
QH	0.13	59.29	8.64	0.00	1.56	-0.00	934.2	8.1	1.68	0.00	1012.6	2.2
ELEM	LTH	SUM L	BETAX	ALPHAX	ETAX	ETA'X	PSIX	X	BETAY	ALPHAY	PSIY	Y
	(M)	(M)	(M)		(M)	(RAD)	(DEG)	(CM)	(M)		(DEG)	(CM)

Table A.1-6(c)



MATCHED FUNCTIONS FOR 4 PERIOD(S)

TOTAL LENGTH= 237.1408 METERS, TOTAL BEND= 359.9900 DEGREES
BETAX= 8.6382 METERS ALPHAX= 0.0000 NUX= 2.3796
BETAY= 1.6844 METERS ALPHAY= 0.0000 NUY= 3.2510
ETAX = 1.5593 METERS ETA'X = -0.0000 TRGAMMA= 7.0061

Fig. A.1-7

ELEM	LTH (M)	SUM L (M)	BETAX (M)	ALPHAX	ETAX (M)	ETA'X (RAD)	PSIX (DEG)	X (CM)	BETAY (M)	ALPHAY	PSIY (DEG)	Y (CM)
QH	0.00	0.00	8.64	0.00	1.56	-0.00	0.0	8.9	1.68	0.00	0.0	2.2
QH	0.13	0.13	8.51	1.05	1.55	-0.19	0.8	8.8	1.72	-0.29	4.2	2.3
D1	0.32	0.57	6.86	1.83	1.39	-0.39	4.2	7.9	2.29	-0.83	17.4	2.6
D1	0.32	0.90	5.74	1.63	1.26	-0.39	7.1	7.3	2.91	-1.07	24.6	3.0
M	0.45	1.35	4.38	1.40	1.10	-0.32	12.3	6.3	4.02	-1.40	32.1	3.5
M	0.45	1.80	3.23	1.14	0.97	-0.26	19.1	5.5	5.43	-1.74	37.7	4.0
D1	0.32	2.12	2.57	0.91	0.89	-0.26	25.6	4.9	6.63	-1.97	40.8	4.5
D1	0.32	2.44	2.05	0.68	0.80	-0.26	33.7	4.4	7.99	-2.21	43.3	4.9
QD	0.25	2.69	1.89	-0.00	0.77	-0.04	41.1	4.2	8.55	-0.00	45.0	5.1
QD	0.25	2.94	2.05	-0.68	0.78	0.17	48.4	4.4	7.99	2.21	46.7	4.9
D1	0.32	3.27	2.57	-0.91	0.84	0.17	56.5	4.8	6.63	1.97	49.3	4.5
D1	0.32	3.59	3.23	-1.14	0.89	0.17	63.0	5.4	5.43	1.74	52.4	4.0
M	0.45	4.04	4.38	-1.40	0.98	0.23	69.8	6.2	4.02	1.40	57.9	3.5
M	0.45	4.49	5.75	-1.63	1.10	0.30	75.0	7.0	2.91	1.07	65.5	3.0
D1	0.32	4.81	6.87	-1.84	1.20	0.30	77.9	7.7	2.29	0.83	72.7	2.6
D1	0.32	5.14	8.13	-2.04	1.29	0.30	80.4	8.3	1.83	0.59	81.8	2.3
QF	0.25	5.39	8.65	-0.00	1.33	-0.03	82.1	8.6	1.68	-0.00	90.0	2.2
QF	0.25	5.64	8.13	2.04	1.28	-0.36	83.8	8.3	1.83	-0.59	98.3	2.3
D1	0.32	5.96	6.87	1.84	1.16	-0.36	86.3	7.6	2.29	-0.83	107.4	2.6
D1	0.32	6.29	5.75	1.63	1.05	-0.36	89.2	6.9	2.91	-1.07	114.6	3.0
M	0.45	6.74	4.38	1.40	0.90	-0.29	94.3	6.0	4.02	-1.40	122.2	3.5
M	0.45	7.19	3.24	1.14	0.78	-0.23	101.2	5.2	5.43	-1.74	127.7	4.0
D1	0.32	7.51	2.57	0.91	0.71	-0.23	107.6	4.7	6.63	-1.97	130.8	4.5
D1	0.32	7.83	2.06	0.68	0.64	-0.23	115.7	4.2	7.99	-2.21	133.3	4.9
QD	0.25	8.08	1.89	0.00	0.60	-0.06	123.1	4.0	8.55	0.00	135.0	5.1
QD	0.25	8.33	2.05	-0.68	0.61	0.11	130.5	4.1	7.99	2.21	136.8	4.9
DX	0.44	8.77	2.78	-0.99	0.66	0.11	141.0	4.7	6.20	1.89	140.3	4.3
DX	0.44	9.20	3.78	-1.30	0.70	0.11	148.7	5.4	4.69	1.57	145.0	3.8
M1	0.23	9.43	4.40	-1.43	0.73	0.14	151.9	5.8	4.02	1.40	147.9	3.5
M1	0.23	9.65	5.07	-1.55	0.77	0.18	154.6	6.2	3.42	1.24	151.4	3.2
DX	0.44	10.09	6.55	-1.85	0.85	0.18	158.9	7.0	2.49	0.91	160.0	2.7
DX	0.44	10.53	8.29	-2.14	0.92	0.18	162.3	7.8	1.83	0.59	171.8	2.3
QF	0.25	10.78	8.85	-0.06	0.94	-0.06	164.0	8.1	1.68	0.00	180.1	2.2
QF	0.25	11.03	8.34	2.04	0.90	-0.29	165.6	7.8	1.83	-0.59	188.3	2.3
DX	0.44	11.46	6.68	1.77	0.77	-0.29	169.0	6.9	2.49	-0.91	200.1	2.7
DX	0.44	11.90	5.25	1.50	0.65	-0.29	173.2	6.1	3.42	-1.24	208.7	3.2
M1	0.23	12.12	4.60	1.39	0.59	-0.25	175.8	5.7	4.02	-1.40	212.2	3.5
M1	0.23	12.35	4.00	1.28	0.53	-0.22	178.8	5.3	4.69	-1.57	215.2	3.2
DX	0.44	12.78	3.01	0.99	0.44	-0.22	186.1	4.5	6.20	-1.89	219.8	4.3
DX	0.44	13.22	2.27	0.70	0.35	-0.22	195.6	3.9	7.99	-2.21	223.4	4.9
QD	0.25	13.47	2.11	-0.02	0.30	-0.13	202.3	3.7	8.55	-0.00	225.1	5.1
QD	0.25	13.72	2.30	-0.76	0.28	-0.05	208.9	3.8	7.99	2.21	226.8	4.9
DX	0.44	14.16	3.09	-1.05	0.26	-0.05	218.3	4.3	6.20	1.89	230.4	4.3
DX	0.44	14.59	4.13	-1.35	0.24	-0.05	225.3	4.9	4.69	1.57	235.0	3.8
M1	0.23	14.82	4.77	-1.47	0.23	-0.01	228.2	5.2	4.02	1.40	238.0	3.5
M1	0.23	15.04	5.46	-1.58	0.24	0.03	230.8	5.6	3.43	1.24	241.4	3.2
DX	0.44	15.48	6.96	-1.86	0.25	0.03	234.8	6.3	2.49	0.91	250.0	2.7
DX	0.44	15.91	8.71	-2.15	0.26	0.03	238.0	7.0	1.83	0.59	261.8	2.3
QF	0.25	16.16	9.25	0.05	0.26	-0.04	239.6	7.2	1.68	-0.00	270.1	2.2
QF	0.25	16.41	8.66	2.23	0.24	-0.10	241.2	6.9	1.83	-0.59	278.4	2.3
DX	0.44	16.85	6.85	1.93	0.20	-0.10	244.4	6.2	2.49	-0.91	290.2	2.7
DX	0.44	17.29	5.30	1.63	0.15	-0.10	248.6	5.4	3.43	-1.24	298.8	3.2
M1	0.23	17.51	4.60	1.50	0.14	-0.06	251.2	5.0	4.02	-1.40	302.2	3.5
M1	0.23	17.74	3.95	1.37	0.13	-0.02	254.2	4.6	4.69	-1.57	305.2	3.8
DX	0.44	18.17	2.89	1.05	0.12	-0.02	261.6	4.0	6.20	-1.89	309.8	4.3
DX	0.44	18.61	2.11	0.74	0.11	-0.02	271.8	3.4	7.99	-2.21	313.4	4.9
Q1	0.25	18.86	1.92	0.06	0.10	0.00	279.0	3.3	8.57	-0.09	315.1	5.1
Q1	0.25	19.11	2.05	-0.59	0.11	0.03	286.3	3.4	8.07	2.06	316.8	4.9
D1	0.32	19.43	2.50	-0.81	0.12	0.03	294.5	3.7	6.81	1.85	319.3	4.5
D1	0.32	19.76	3.10	-1.02	0.13	0.03	301.2	4.1	5.68	1.64	322.3	4.1
DM	0.45	20.21	4.15	-1.32	0.14	0.03	308.4	4.8	4.34	1.35	327.5	3.6

Table A.1-7(a)

DM	0.45	20.66	5.47	-1.62	0.16	0.03	313.8	5.5	3.26	1.05	334.4	3.1
D1	0.32	20.98	6.59	-1.83	0.17	0.03	316.9	6.0	2.64	0.84	340.7	2.8
D1	0.32	21.30	7.84	-2.04	0.18	0.03	319.5	6.5	2.16	0.63	348.5	2.5
D4	0.20	21.50	8.66	-2.17	0.19	0.03	320.9	6.9	1.94	0.51	354.0	2.4
D4	0.20	21.69	9.54	-2.30	0.19	0.03	322.1	7.2	1.77	0.38	360.0	2.3
Q2	0.25	21.94	9.55	2.27	0.19	-0.06	323.6	<u>7.2</u>	1.82	-0.61	368.2	2.3
Q2	0.25	22.19	7.45	5.80	0.16	-0.14	325.3	6.3	2.42	-1.90	375.2	2.7
D3	0.08	22.27	6.60	5.45	0.15	-0.14	325.9	6.0	2.72	-2.05	376.8	2.9
D3	0.08	22.34	5.81	5.10	0.14	-0.14	326.6	5.6	3.04	-2.19	378.3	3.0
Q3	0.25	22.59	3.99	2.42	0.11	-0.09	329.7	<u>4.6</u>	3.88	-1.07	382.4	3.4
Q3	0.25	22.84	3.23	0.75	0.09	-0.05	333.7	4.2	4.04	0.47	386.0	3.5
D2	0.78	23.62	2.35	0.38	0.05	-0.05	350.1	3.5	3.49	0.23	397.9	3.2
D2	0.78	24.39	2.06	-0.00	0.01	-0.05	370.7	3.2	3.31	-0.00	411.1	3.2
D2	0.78	25.17	2.35	-0.38	-0.03	-0.05	391.3	3.5	3.50	-0.23	424.2	3.2
D2	0.78	25.94	3.23	-0.75	-0.07	-0.05	407.7	4.1	4.04	-0.47	436.1	3.5
Q5	0.25	26.19	3.97	-2.31	-0.09	-0.08	411.8	4.6	3.91	0.97	439.7	3.4
Q5	0.25	26.44	5.69	-4.77	-0.11	-0.12	414.8	<u>5.5</u>	3.13	2.05	443.7	3.1
D3	0.08	26.52	6.42	-5.08	-0.12	-0.12	415.5	5.8	2.84	1.93	445.2	2.9
D3	0.08	26.59	7.21	-5.39	-0.13	-0.12	416.2	6.2	2.56	1.80	446.7	2.8
Q4	0.43	27.02	9.75	0.00	-0.16	-0.02	418.9	<u>7.2</u>	1.85	0.00	458.6	2.4
Q4	0.43	27.44	7.21	5.39	-0.14	0.09	421.7	6.2	2.55	-1.79	470.4	2.8
D3	0.08	27.52	6.42	5.08	-0.14	0.09	422.3	5.9	2.82	-1.91	472.0	2.9
D3	0.08	27.59	5.69	4.77	-0.13	0.09	423.0	<u>5.5</u>	3.12	-2.04	473.5	3.1
Q5	0.25	27.84	3.97	2.31	-0.11	0.04	426.1	4.6	3.89	-0.96	477.5	3.4
Q5	0.25	28.09	3.22	0.75	-0.11	0.00	430.2	4.2	4.02	0.47	481.1	3.5
D2	0.78	28.87	2.35	0.38	-0.11	0.00	446.5	3.6	3.47	0.24	493.0	3.2
D2	0.78	29.64	2.06	0.00	-0.11	0.00	467.2	3.4	3.29	0.00	506.3	3.1
D2	0.78	30.42	2.35	-0.38	-0.11	0.00	487.8	3.6	3.47	-0.24	519.6	3.2
D2	0.78	31.19	3.22	-0.75	-0.11	0.00	504.2	4.2	4.02	-0.47	531.5	3.5
Q5	0.25	31.44	3.97	-2.31	-0.11	-0.04	508.3	4.6	3.89	0.96	535.1	3.4
Q5	0.25	31.69	5.69	-4.77	-0.13	-0.09	511.3	<u>5.5</u>	3.12	2.04	539.2	3.1
D3	0.08	31.77	6.42	-5.08	-0.14	-0.09	512.0	<u>5.9</u>	2.82	1.91	540.6	2.9
D3	0.08	31.84	7.21	-5.39	-0.14	-0.09	512.7	6.2	2.55	1.79	542.2	2.8
Q4	0.43	32.27	9.75	-0.00	-0.16	0.02	515.4	<u>7.2</u>	1.85	-0.00	554.1	2.4
Q4	0.43	32.69	7.21	5.39	-0.13	0.12	518.2	6.2	2.56	-1.80	565.9	2.8
D3	0.08	32.77	6.42	5.08	-0.12	0.12	518.8	5.8	2.83	-1.93	567.5	2.9
D3	0.08	32.84	5.69	4.77	-0.11	0.12	519.5	<u>5.5</u>	3.13	-2.05	568.9	3.1
Q5	0.25	33.09	3.97	2.31	-0.09	0.08	522.6	4.6	3.91	-0.97	572.9	3.4
Q5	0.25	33.34	3.23	0.75	-0.07	0.05	526.7	4.1	4.04	0.47	576.5	3.5
D2	0.78	34.12	2.35	0.38	-0.03	0.05	543.0	3.5	3.50	0.23	588.4	3.2
D2	0.78	34.89	2.06	0.00	0.01	0.05	563.7	3.2	3.31	0.00	601.5	3.2
D2	0.78	35.67	2.35	-0.38	0.05	0.05	584.3	3.5	3.49	-0.23	614.7	3.2
D2	0.78	36.44	3.23	-0.75	0.09	0.05	600.6	4.2	4.04	-0.47	626.6	3.5
Q3	0.25	36.69	3.99	-2.42	0.11	0.09	604.7	4.6	3.88	1.07	630.2	3.4
Q3	0.25	36.94	5.81	-5.10	0.14	0.14	607.7	<u>5.6</u>	3.04	2.19	634.3	3.0
D3	0.08	37.02	6.60	-5.45	0.15	0.14	608.4	6.0	2.72	2.05	635.8	2.9
D3	0.08	37.09	7.45	-5.80	0.16	0.14	609.0	6.3	2.43	1.90	637.5	2.7
Q2	0.25	37.34	9.55	-2.27	0.19	0.06	610.7	7.2	1.82	0.61	644.4	2.7
Q2	0.25	37.59	9.54	2.30	0.19	-0.03	612.1	<u>7.2</u>	1.77	-0.38	652.6	2.3
D4	0.20	37.79	8.66	2.17	0.19	-0.03	613.3	6.9	1.94	-0.51	658.7	2.4
D4	0.20	37.98	7.84	2.04	0.18	-0.03	614.7	6.5	2.16	-0.63	664.1	2.5
D1	0.32	38.31	6.59	1.83	0.17	-0.03	617.3	6.0	2.64	-0.84	671.9	2.8
D1	0.32	38.63	5.47	1.62	0.16	-0.03	620.4	5.5	3.26	-1.05	678.2	3.1
DM	0.45	39.08	4.15	1.32	0.14	-0.03	625.8	4.8	4.34	-1.35	685.1	3.6
DM	0.45	39.53	3.10	1.02	0.13	-0.03	633.0	4.1	5.68	-1.64	690.3	4.1
D1	0.32	39.85	2.50	0.81	0.12	-0.03	639.7	3.7	6.81	-1.85	693.3	4.5
D1	0.32	40.18	2.05	0.59	0.11	-0.03	647.9	3.4	8.07	-2.06	695.8	4.9
Q1	0.25	40.43	1.92	-0.06	0.10	-0.00	655.2	3.3	8.57	0.09	697.5	5.1
Q1	0.25	40.68	2.11	-0.74	0.11	0.02	662.4	<u>3.4</u>	7.99	2.21	699.2	4.9
DX	0.44	41.11	2.89	-1.05	0.12	0.02	672.6	4.0	6.20	1.89	702.8	4.3
DX	0.44	41.55	3.95	-1.37	0.13	0.02	680.0	4.6	4.69	1.57	707.4	3.7
M1	0.23	41.77	4.60	-1.50	0.14	0.06	683.0	5.0	4.02	1.40	710.4	3.5
M1	0.23	42.00	5.30	-1.63	0.15	0.10	685.6	<u>5.4</u>	3.42	1.24	713.9	3.2
DX	0.44	42.44	6.85	-1.93	0.20	0.10	689.8	6.2	2.49	0.91	722.5	2.7
DX	0.44	42.87	8.66	-2.23	0.24	0.10	693.0	6.9	1.83	0.59	734.2	2.3
QF	0.25	43.12	9.25	-0.05	0.26	0.04	694.6	7.2	1.68	-0.00	742.5	2.2

Table A.1-7(b)

QF	0.25	43.37	8.71	2.15	0.26	-0.03	696.2	7.0	1.83	-0.59	750.8	2.3
DX	0.44	43.91	6.96	1.86	0.25	-0.03	699.4	6.3	2.49	-0.91	762.6	2.7
DX	0.44	44.24	5.46	1.58	0.24	-0.03	703.4	5.6	3.42	-1.24	771.2	3.2
M1	0.23	44.47	4.77	1.47	0.23	0.01	706.0	5.2	4.02	-1.40	774.7	3.5
M1	0.23	44.69	4.13	1.35	0.24	0.05	708.9	4.9	4.69	-1.57	777.6	3.8
DX	0.44	45.13	3.09	1.05	0.26	0.05	715.9	4.3	6.20	-1.89	782.3	4.3
DX	0.44	45.57	2.30	0.76	0.28	0.05	725.3	3.8	7.99	-2.21	785.8	4.9
QD	0.25	45.82	2.11	0.02	0.30	0.13	731.9	3.7	8.55	-0.00	787.5	5.1
QD	0.25	46.07	2.27	-0.70	0.35	0.22	738.5	3.9	7.99	2.21	789.3	4.9
DX	0.44	46.50	3.01	-0.99	0.44	0.22	748.1	4.5	6.20	1.89	792.8	4.3
DX	0.44	46.94	4.00	-1.28	0.53	0.22	755.3	5.3	4.69	1.57	797.4	3.8
M1	0.23	47.16	4.60	-1.39	0.59	0.25	758.4	5.7	4.02	1.40	800.4	3.5
M1	0.23	47.39	5.25	-1.50	0.65	0.29	761.0	6.1	3.43	1.24	803.9	3.2
DX	0.44	47.82	6.68	-1.77	0.77	0.29	765.2	6.9	2.49	0.91	812.5	2.7
DX	0.44	48.26	8.34	-2.04	0.90	0.29	768.5	7.8	1.83	0.59	824.3	2.3
QF	0.25	48.51	8.85	0.06	0.94	0.06	770.2	8.1	1.68	0.00	832.6	2.2
QF	0.25	48.76	8.29	2.14	0.92	-0.18	771.8	7.8	1.83	-0.59	840.8	2.3
DX	0.44	49.20	6.55	1.85	0.85	-0.18	775.2	7.0	2.49	-0.91	852.6	2.7
DX	0.44	49.63	5.07	1.55	0.77	-0.18	779.6	6.2	3.42	-1.24	861.2	3.2
M1	0.23	49.86	4.40	1.43	0.73	-0.14	782.3	5.8	4.02	-1.40	864.7	3.5
M1	0.23	50.08	3.78	1.30	0.70	-0.11	785.5	5.4	4.69	-1.57	867.7	3.8
DX	0.44	50.52	2.78	0.99	0.66	-0.11	793.2	4.7	6.20	-1.89	872.3	4.3
DX	0.44	50.95	2.05	0.68	0.61	-0.11	803.7	4.1	7.99	-2.21	875.9	4.9
QD	0.25	51.20	1.89	-0.00	0.60	0.06	811.1	4.0	8.55	0.00	877.6	5.1
QD	0.25	51.45	2.06	-0.68	0.64	0.23	818.5	4.2	7.99	2.21	879.3	4.9
D1	0.32	51.78	2.57	-0.91	0.71	0.23	826.5	4.7	6.63	1.97	881.8	4.5
D1	0.32	52.10	3.23	-1.14	0.78	0.23	833.0	5.2	5.43	1.74	884.9	4.0
M	0.45	52.55	4.38	-1.40	0.90	0.29	839.8	6.0	4.02	1.40	890.5	3.5
M	0.45	53.00	5.75	-1.63	1.05	0.36	845.0	6.9	2.91	1.07	898.0	3.0
D1	0.32	53.32	6.87	-1.84	1.16	0.36	847.9	7.6	2.29	0.83	905.2	2.6
D1	0.32	53.65	8.13	-2.04	1.28	0.36	850.4	8.3	1.83	0.59	914.3	2.3
QF	0.25	53.90	8.65	0.00	1.33	0.03	852.1	8.6	1.68	-0.00	922.6	2.2
QF	0.25	54.15	8.13	2.04	1.29	-0.30	853.8	8.3	1.83	-0.59	930.9	2.3
D1	0.32	54.47	6.87	1.84	1.20	-0.30	856.3	7.7	2.29	-0.83	940.0	2.6
D1	0.32	54.79	5.75	1.63	1.10	-0.30	859.2	7.0	2.91	-1.07	947.2	3.0
M	0.45	55.24	4.38	1.40	0.98	-0.23	864.4	6.2	4.02	-1.40	954.7	3.5
M	0.45	55.69	3.23	1.14	0.89	-0.17	871.2	5.4	5.43	-1.74	960.3	4.0
D1	0.32	56.02	2.57	0.91	0.84	-0.17	877.7	4.8	6.63	-1.97	963.3	4.5
D1	0.32	56.34	2.05	0.68	0.78	-0.17	885.8	4.4	7.99	-2.21	965.9	4.9
QD	0.25	56.59	1.89	0.00	0.77	0.04	893.1	4.2	8.55	-0.00	967.6	5.1
QD	0.25	56.84	2.05	-0.68	0.80	0.26	900.5	4.4	7.99	2.21	969.3	4.9
D1	0.32	57.16	2.57	-0.91	0.89	0.26	908.6	4.9	6.63	1.97	971.9	4.5
D1	0.32	57.49	3.23	-1.14	0.97	0.26	915.0	5.5	5.43	1.74	975.0	4.0
M	0.45	57.94	4.38	-1.40	1.10	0.32	921.9	6.3	4.02	1.40	980.5	3.5
M	0.45	58.39	5.74	-1.63	1.26	0.39	927.1	7.3	2.91	1.07	988.1	3.0
D1	0.32	58.71	6.86	-1.83	1.39	0.39	930.0	7.9	2.29	0.83	995.3	2.6
D1	0.32	59.04	8.12	-2.04	1.51	0.39	932.5	8.6	1.83	0.59	1004.3	2.3
QH	0.13	59.16	8.51	-1.05	1.55	0.19	933.4	8.8	1.72	0.29	1008.4	2.3
QH	0.13	59.29	8.64	0.00	1.56	-0.00	934.2	8.9	1.68	0.00	1012.6	2.2
ELEM	LTH	SUM L	BETAX	ALPHAX	ETAX	ETA'X	PSIX	X	BETAY	ALPHAY	PSIY	ψ
	(M)	(M)	(M)		(M)	(RAD)	(DEG)	(CM)	(M)		(DEG)	(CM)

Table A.1-7(c)

**CONCEPTUAL DESIGN OF A RAPID-CYCLING SYNCHROTRON FOR
KFA-JULICH SPALLATION NEUTRON SOURCE**

APPENDIX A.2

RING MAGNETS

A.2 RING MAGNETS

This appendix contains details on some representative calculations on ring magnet designs and cost estimates referred to in Section III.1 of the report.

The required basic parameters and bare dimensions of the eight different types of magnets are given in Table III.1-1 of the text. The diameter of the QF quadrupole was enlarged by about 5% so that the supply currents for the QD and QF quadrupoles will be the same, and the width of the shorter bending magnet was increased so that only one bending magnet lamination geometry is required. The final dipole and quadrupole magnet parameters, on which the designs and cost estimates are based, are listed in Table A.2-1.

TABLE A.2-1

Final Magnet Parameters

<u>Magnet</u>	<u># Req'd.</u>	<u>L_{eff.} (cm)</u>	<u>B or B' (T or T/m)</u>	<u>Full Aperture (cm)</u>
M	24	90	1.054	14.6H* 11.0V
M1	32	45	1.054	
QF	28	50	6.03	16.65 dia.
QD (Q1)	32	50	6.63	15.85 dia.
Q2	8	50	11.5	22.15 dia.
Q3	8	50	9.7	20.35 dia.
Q4	8	85	9.7	15.57 dia.
Q5	16	50	9.1	15.06 dia.

* - usable dimension

A list of the magnet design assumptions is given in Table A.2-2 and the major unit costs in Table A.2-3.

TABLE A.2-2

Magnet Design Assumptions

1.	Lamination thickness	0.36 cm
2.	Conductor	.734 cm x .734 cm x .409 cm
3.	Cooling water pressure gradient	689 kPa (100 psi)
4.	Bending magnet core length	$L_{\text{core}} = L_{\text{eff.}} - H_{\text{gap}}$
5.	Quad core length	$L_{\text{core}} = L_{\text{eff.}} - .87 R_{\text{bore}}$
6.	Quad lengths and gradients are as specified.	Bore radius increased to match resulting ampere turns.
7.	Yoke thickness chosen to give	$\bar{B} \approx 1.3 \text{ T}$
8.	Bending magnet pole is $1.5 \times H_{\text{gap}}$	wider than the usable gap width
9.	Quadrupole pole radius is $1.14 \times R_{\text{bore}}$	
10.	Quadrupole pole is circular arc, 90°	long
11.	Quadrupole coils are out of the midplane	

TABLE A.2-3

Major Unit Costs

Steel sheet	\$ 1.80/kg (\$0.80/lb.)
Conductor and insulation	\$ 8.80/kg (\$4/lb.)
Stainless steel	\$ 3.84/kg (\$1.70/lb.)
End plate fabrication	\$6000/magnet
Bending magnet lamination stamping	\$1.05/piece
Quadrupole magnet lamination stamping	\$ 1.20/2 pieces
Lamination die(s)	Bending Magnet \$50K/magnet type
	Quadrupole Magnet \$30K/magnet type
Electrical power	\$0.04/kW-hr
Labor costs	\$3924/man month

Tables A.2-4 and 5 show for a representative dipole, magnet M, and quadrupole magnet, QD, the details involved in the designs and cost estimates of the magnets. Such detail for all of the magnets exists in the initial report.

Calculations were done for one of the water cooling circuits in each of the magnet types under the condition that the magnet operate continuously at the dc current required for 1100 MeV operation. Operation in this mode would be necessary if the SNQ-SRA was modified for use as a full energy compressor ring in a later stage of the neutron source program. The results of representative calculations for dipole and quadrupole coils are given in Tables A.2-6 and -7.

Finally, Table A.2-8 shows a summary of estimated costs for the lattice magnets of the complete SNQ-SRA ring.

ARGONNE NATIONAL LABORATORY		DIVISION	PROJECT	FILE NO.	PAGE																																																			
ENGINEERING NOTE		FPPET	SNQ		21																																																			
SUBJECT		NAME																																																						
SNQ-SPA Ring Magnets		K Thompson																																																						
- M - Magnet Design and Costs		DATE	REV. DATE																																																					
		12/8/82																																																						
<p>Number of poles = 2 Number of magnets = 24 Injection energy (MeV) = 200 Extraction energy (MeV) = 1100 Field length (cm) = 90 Radius of bend (cm) = 572.960 Peak gap magnetic field (Gauss) = 10523.399 Usable gap height (cm) = 9 Usable gap width (cm) = 14.600 Distance between poles (cm) = 11 Sagitta of beam (cm) = 1.770 Pole width (cm) = 32.870</p> <p>Coil Parameters: Width per pole (cm) = 18.360 Height per pole (cm) = 8.160 Number of layers = 8 Number of rows = 18 Amp-turns (RMS) per pole (Amp) = 34691.771 Average turn length (cm) = 293.987 Effective turns per magnet = 24 Turns per water circuit = 12 Inductance per magnet (mH) = 2.343 Resistance per magnet (mOhm) = 2.763 Eddy current losses (Watts) = 4404.439</p> <p>Core Parameters: Width of core (cm) = 109.103 Height of core (cm) = 64.833 Mass of laminated iron (kg) = 3400.171 Area of bore surface (sqcm) = 19154.399 Core losses (Watts) = 8976.452 Maximum stored energy (J) = 19137.216 Supply current-AC (Peak) (Amp) = 1361.205 -DC (Amp) = 2740.657 -RMS (Amp) = 2890.981 Supply voltage-Peak (Volt) = 965.604</p> <p>Ring water requirements: Pressure gradient (kPa) = 688.735 Temperature gradient (°C) = 7.646 Water flow (1/sec) = 27.560</p> <p>Cost estimates for the entire ring:</p> <table border="0"> <thead> <tr> <th></th> <th>Quant</th> <th>\$1000</th> </tr> </thead> <tbody> <tr> <td>Silicon steel sheet</td> <td>137201kg</td> <td>247</td> </tr> <tr> <td>Stamping die(s):</td> <td>2</td> <td>52</td> </tr> <tr> <td>Laminations</td> <td>59908</td> <td>63</td> </tr> <tr> <td>Stainless steel parts fabrication</td> <td>9468kg</td> <td>191</td> </tr> <tr> <td>Conductor and insulation</td> <td>24435m</td> <td>73</td> </tr> <tr> <td>Coil fabrication plus tooling</td> <td>15309mhr</td> <td>444</td> </tr> <tr> <td>Misc hardware and tooling items</td> <td></td> <td>92</td> </tr> <tr> <td>Shipping</td> <td>159277kg</td> <td>10</td> </tr> <tr> <td>Partial total:</td> <td></td> <td>1171 - 75.8%</td> </tr> <tr> <td colspan="3">Labor costs:</td> </tr> <tr> <td>Core assembly</td> <td>11mmo</td> <td>42</td> </tr> <tr> <td>Coil installation</td> <td>14mmo</td> <td>56</td> </tr> <tr> <td>Final acceptance tests</td> <td>5mmo</td> <td>19</td> </tr> <tr> <td>Partial total:</td> <td></td> <td>117 - 7.6%</td> </tr> <tr> <td>Contingency</td> <td>20%</td> <td>258 - 16.7%</td> </tr> <tr> <td>TOTAL:</td> <td></td> <td>1545 - 100.0%</td> </tr> </tbody> </table> <p>Mass of an assembled magnet 3999kg Electrical power losses in ring 875kW Water pump supply power 27kW</p> <p>307/100%-year 10/100%-year</p>							Quant	\$1000	Silicon steel sheet	137201kg	247	Stamping die(s):	2	52	Laminations	59908	63	Stainless steel parts fabrication	9468kg	191	Conductor and insulation	24435m	73	Coil fabrication plus tooling	15309mhr	444	Misc hardware and tooling items		92	Shipping	159277kg	10	Partial total:		1171 - 75.8%	Labor costs:			Core assembly	11mmo	42	Coil installation	14mmo	56	Final acceptance tests	5mmo	19	Partial total:		117 - 7.6%	Contingency	20%	258 - 16.7%	TOTAL:		1545 - 100.0%
	Quant	\$1000																																																						
Silicon steel sheet	137201kg	247																																																						
Stamping die(s):	2	52																																																						
Laminations	59908	63																																																						
Stainless steel parts fabrication	9468kg	191																																																						
Conductor and insulation	24435m	73																																																						
Coil fabrication plus tooling	15309mhr	444																																																						
Misc hardware and tooling items		92																																																						
Shipping	159277kg	10																																																						
Partial total:		1171 - 75.8%																																																						
Labor costs:																																																								
Core assembly	11mmo	42																																																						
Coil installation	14mmo	56																																																						
Final acceptance tests	5mmo	19																																																						
Partial total:		117 - 7.6%																																																						
Contingency	20%	258 - 16.7%																																																						
TOTAL:		1545 - 100.0%																																																						

Table A.2-4

ARGONNE NATIONAL LABORATORY		DIVISION	PROJECT	FILE NO.	PAGE																																																																								
ENGINEERING NOTE		FPPET	SNO		25																																																																								
SUBJECT		NAME																																																																											
SNC-SPA Ring Magnets		K Thompson																																																																											
- QD(C1) - Quad Design and Costs		DATE	REV. DATE																																																																										
		12/17/82																																																																											
<p>Number of poles = 4</p> <p>Number of magnets = 32</p> <p>Injection energy (MeV) = 200</p> <p>Extraction energy (MeV) = 1100</p> <p>Field length (cm) = 50</p> <p>Peak field gradient (Gauss/cm) = 663</p> <p>Usable bore diameter (cm) = 13.880</p> <p>Distance between poles (cm) = 15.880</p> <p>Pole width (cm) = 12.801</p> <p>Max field at pole tip (Gauss) = 8204.561</p> <p>Coil Parameters:</p> <p>Width per pole (cm) = 8.160</p> <p>Height per pole (cm) = 5.100</p> <p>Number of layers = 5</p> <p>Number of rows = 8</p> <p>Amp-turns(RMS) per pole(Amp) = 12519.411</p> <p>Average turn length (cm) = 136.533</p> <p>Effective turns per magnet = 16</p> <p>Turns per water circuit = 16</p> <p>Inductance per magnet (mH) = .472</p> <p>Resistance per magnet (mOhm) = 1.024</p> <p>Eddy current losses (Watts) = 1136.395</p> <p>Core Parameters:</p> <p>Radius to inside of yoke(cm) = 23.391</p> <p>Width of core (cm) = 62.738</p> <p>Height of core (cm) = 62.738</p> <p>Mass of laminated iron (kg) = 993.841</p> <p>Area of bore surface (sqcm) = 9800.385</p> <p>Core losses (Watts) = 2623.741</p> <p>Maximum stored energy (J) = 4520.274</p> <p>Supply current-AC(Peak) (Amp) = 1408.719</p> <p>-DC (Amp) = 2967.109</p> <p>-RMS (Amp) = 3129.853</p> <p>Supply voltage-Peak (Volt) = 212.101</p> <p>Ring water requirements:</p> <p>Pressure gradient (kPa) = 688.708</p> <p>Temperature gradient (°C) = 6.117</p> <p>Water flow (1/sec) = 17.392</p>																																																																													
<p>Cost estimates for the entire ring:</p> <table border="1"> <thead> <tr> <th></th> <th>Quant</th> <th>\$1000</th> <th></th> </tr> </thead> <tbody> <tr> <td>Silicon steel sheet</td> <td>57743kg</td> <td>104</td> <td></td> </tr> <tr> <td>Stamping die(s)</td> <td>1</td> <td>30</td> <td></td> </tr> <tr> <td>Laminations</td> <td>44071</td> <td>53</td> <td></td> </tr> <tr> <td>Stainless steel parts fabrication</td> <td>7092kg</td> <td>236</td> <td></td> </tr> <tr> <td>Conductor and insulation</td> <td>8487m</td> <td>25</td> <td></td> </tr> <tr> <td>Coil fabrication plus tooling</td> <td>11550mhr</td> <td>340</td> <td></td> </tr> <tr> <td>Misc hardware and tooling items</td> <td></td> <td>114</td> <td></td> </tr> <tr> <td>Shipping</td> <td>72470kg</td> <td>4</td> <td></td> </tr> <tr> <td></td> <td>Partial total:</td> <td>907</td> <td>- 66.1%</td> </tr> <tr> <td colspan="4">Labor costs:</td> </tr> <tr> <td>Core assembly</td> <td>15mmo</td> <td>58</td> <td></td> </tr> <tr> <td>Coil installation</td> <td>39mmo</td> <td>152</td> <td></td> </tr> <tr> <td>Final acceptance tests</td> <td>6mmo</td> <td>25</td> <td></td> </tr> <tr> <td></td> <td>Partial total:</td> <td>236</td> <td>- 17.2%</td> </tr> <tr> <td colspan="4">Contingency</td> </tr> <tr> <td></td> <td>20%</td> <td>228</td> <td>- 16.7%</td> </tr> <tr> <td></td> <td>TOTAL:</td> <td>1371</td> <td>- 100.0%</td> </tr> </tbody> </table>							Quant	\$1000		Silicon steel sheet	57743kg	104		Stamping die(s)	1	30		Laminations	44071	53		Stainless steel parts fabrication	7092kg	236		Conductor and insulation	8487m	25		Coil fabrication plus tooling	11550mhr	340		Misc hardware and tooling items		114		Shipping	72470kg	4			Partial total:	907	- 66.1%	Labor costs:				Core assembly	15mmo	58		Coil installation	39mmo	152		Final acceptance tests	6mmo	25			Partial total:	236	- 17.2%	Contingency					20%	228	- 16.7%		TOTAL:	1371	- 100.0%
	Quant	\$1000																																																																											
Silicon steel sheet	57743kg	104																																																																											
Stamping die(s)	1	30																																																																											
Laminations	44071	53																																																																											
Stainless steel parts fabrication	7092kg	236																																																																											
Conductor and insulation	8487m	25																																																																											
Coil fabrication plus tooling	11550mhr	340																																																																											
Misc hardware and tooling items		114																																																																											
Shipping	72470kg	4																																																																											
	Partial total:	907	- 66.1%																																																																										
Labor costs:																																																																													
Core assembly	15mmo	58																																																																											
Coil installation	39mmo	152																																																																											
Final acceptance tests	6mmo	25																																																																											
	Partial total:	236	- 17.2%																																																																										
Contingency																																																																													
	20%	228	- 16.7%																																																																										
	TOTAL:	1371	- 100.0%																																																																										
<p>Mass of an assembled magnet 1257kg</p> <p>Electrical power losses in ring 441kW</p> <p>Water pump supply power 17kW</p> <p>155/100%-year</p> <p>6/100%-year</p>																																																																													

Table A.2-5

ARGONNE NATIONAL LABORATORY ENGINEERING NOTE		DIVISION FPPET	PROJECT SNQ	FILE NO.	PAGE 15
SUBJECT SNQ-SRA Ring Magnet - Worst Case Cooling Circuit in - Bm - Magnet			NAME K Thompson		
			DATE 12/8/82	REV. DATE	
This is an <u>h-frame</u> magnet.			[Try #1]		
<u>MAGNET HALF-GAP PARAMETERS:</u>					
5	Field strength	(kG) =			
6	Gap half-height	(cm) =			
7	Magnetic efficiency	(%) =			95.000
<u>HALF-COIL PARAMETERS:</u>					
11	Ampere turns	(kAmperes) =			2.022
12	Maximum coil voltage	(Volts) =			
13	Maximum coil current	(Amperes) =			
14	Operating coil current	(Amperes) =			337.000
15	Number of electrical turns	=			6.000
16	Number of layers	=			1.000
17	Number of rows	=			6.000
18	Number of cooling circuits	=			.500
19	Maximum coil height	(cm) =			1.222
20	Maximum coil width	(cm) =			5.730
21	Minimum turn insulation	(cm) =			.080
22	Minimum ground insulation	(cm) =			.160
23	Minimum coil-to-core clearance	(cm) =			
<u>COOLING CIRCUIT PARAMETERS:</u>					
27	Coolant supply temperature	(C) =			30.000
28	Coolant temperature gradient	(C) =			15.300
29	Maximum pressure gradient	(psi) =			100.000
30	Hydraulic bend factor	=			1.100
31	Reynold's number	(thousands) =			12.9/14.0
<u>CONDUCTOR PARAMETERS:</u>					
35	Conductor maximum temperature	(C) =			45.6/45.6
36	Average electrical turn length	(cm) =			293.987
37	Average coolant circuit length	(cm) =			3527.844
38	Conductor ACS conductivity	(%) =			100.000
39	Conductor height	(cm) =			.734;.008
40	Conductor width	(cm) =			.734;.008
41	Conductor hole diameter	(cm) =			.409;.008
42	Conductor corner radius	(cm) =			.150;.025
43	Conductor section area	(sq cm) =			.410/.365
<u>MAGNET OPERATING PARAMETERS:</u>					
47	Operating resistance	(milliOhms) =	T		15.9/17.9
48	Operating voltage	(Volts) =	T		5.35/6.02
49	Operating current	(Amperes) =	T		337.000
50	Power dissipation	(kW) =	T		1.80/2.03
51	Operating pressure gradient	(psi) =	T		96.8/99.9
52	Required coolant flow	(gpm) =	T		.450/.505
53	Orifice diameter to give $dP=dP(MAX)$	(cm) =	T		.298/.750
54	Transverse force on coil	(psi) =			

Table A.2-6

ARGONNE NATIONAL LABORATORY		DIVISION	PROJECT	FILE NO.	PAGE
ENGINEERING NOTE		FPPET	SNQ		16
SUBJECT SNQ-SPA Ping Magnet - Worst Case Cooling Circuit in - QD(Q1)- Magnet		NAME K Thompson			
		DATE 12/17/82	REV. DATE		
This is a <u>quadrupole</u> magnet.		[Try #1]			
<u>MAGNET BORE PARAMETERS:</u>					
5	Field gradient	(kG/cm) =			
6	Bore radius	(cm) =			
7	Magnetic efficiency	(%) =	90.000		
<u>POLE-COIL PARAMETERS:</u>					
11	Ampere turns	(kAmperes) =	1.750		
12	Maximum coil voltage	(Volts) =			
13	Maximum coil current	(Amperes) =			
14	Operating coil current	(Amperes) =	437.583		
15	Number of electrical turns	=	4.000		
16	Number of layers	=	1.000		
17	Number of rows	=	4.000		
18	Number of cooling circuits	=	.250		
19	Maximum coil height	(cm) =	1.222		
20	Maximum coil width	(cm) =	3.926		
21	Minimum turn insulation	(cm) =	.080		
22	Minimum ground insulation	(cm) =	.160		
23	Minimum coil-to-core clearance	(cm) =			
<u>COOLING CIRCUIT PARAMETERS:</u>					
27	Coolant supply temperature	(C) =	30.000		
28	Coolant temperature gradient	(C) =	12.208		
29	Maximum pressure gradient	(psi) =	100.000		
30	Hydraulic bend factor	=	1.100		
31	Reynold's number	(thousands) =	16.4/17.7		
<u>CONDUCTOR PARAMETERS:</u>					
35	Conductor maximum temperature	(C) =	42.6/42.7		
36	Average electrical turn length	(cm) =	136.533		
37	Average coolant circuit length	(cm) =	2184.528		
38	Conductor ACS conductivity	(%) =	100.000		
39	Conductor height	(cm) =	.734;.008		
40	Conductor width	(cm) =	.734;.008		
41	Conductor hole diameter	(cm) =	.409;.008		
42	Conductor corner radius	(cm) =	.150;.025		
43	Conductor section area	(sq cm) =	.410/.365		
<u>MAGNET OPERATING PARAMETERS:</u>					
47	Operating resistance	(milliOhms) = T	9.78/11.0		
48	Operating voltage	(Volts) = T	4.28/4.81		
49	Operating current	(Amperes) = T	437.583		
50	Power dissipation	(kW) = T	1.87/2.11		
51	Operating pressure gradient	(psi) = T	96.8/ 100		
52	Required coolant flow	(gpm) = T	.585/.658		
53	Orifice diameter to give dP=dP(MAX)	(cm) = T	.341/1.02		
54	Transverse force on coil	(psi) =			

ARGONNE NATIONAL LABORATORY		DIVISION	PROJECT	FILE NO.	PAGE
ENGINEERING NOTE		FPPET	SNQ		7
SUBJECT			NAME		
SNQ-SRA Ring Magnets Cost Summary			K Thompson		
			DATE	REV. DATE	
			12/21/82		
Summary of costs for a ring made up of two magnet types:					
	Magnet 1		Magnet 2		Sum(1+2)
Procurements:					
Steel	390 - 12.5%		631 - 9.5%		1021 - 10.5%
Die	52 - 1.7%		180 - 2.7%		232 - 2.4%
Laminations	99 - 3.2%		177 - 2.7%		276 - 2.8%
Stainless steel	448 - 14.4%		827 - 12.5%		1275 - 13.1%
Conductor+ins.	141 - 4.5%		206 - 3.1%		347 - 3.6%
Coil	1021 - 32.7%		2301 - 34.7%		3322 - 34.1%
Misc	188 - 6.0%		410 - 6.2%		598 - 6.1%
Shipping	16 - .5%		26 - .4%		42 - .4%
Partial total:	<u>2355 - 75.5%</u>		<u>4758 - 71.7%</u>		<u>7113 - 72.9%</u>
Labor:					
Core	69 - 2.2%		209 - 3.1%		278 - 2.8%
Coil	132 - 4.2%		482 - 7.3%		614 - 6.3%
Tests	44 - 1.4%		81 - 1.2%		125 - 1.3%
Partial total:	<u>245 - 7.9%</u>		<u>772 - 11.6%</u>		<u>1017 - 10.4%</u>
Contingency	520 - 16.7%		1106 - 16.7%		1626 - 16.7%
TOTAL:	<u>3120 - 100.0%</u>		<u>6636 - 100.0%</u>		<u>9756 - 100.0%</u>
Power/year	587		714		1301

Table A.2-8

CONCEPTUAL DESIGN OF A RAPID-CYCLING SYNCHROTRON FOR
KFA-JULICH SPALLATION NEUTRON SOURCE

APPENDIX A.3

COST ESTIMATE

A.3 COST ESTIMATE

The estimate of costs for the SNQ-SRA system designed is given in Table A.3-1. These costs are for the accelerator system only, exclusive of the injector linac and linac building, the transport system between the linac and synchrotron, and the transport system from the synchrotron to the experimental targets. It is clear that the major cost items of the accelerator system included are the ring magnets, power supplies, and the rf system. Design and costing of these components are thus most critical to the overall cost of the accelerator.

The cost of the ring magnets, 56 bending magnets and 100 quadrupole magnets, is detailed in Section III.1 and is based on a cost of 80¢/lb. for sheet steel and \$4/lb. for conductor and insulation. A significant cost item because of the large number of magnets utilized for the SNQ-SRA is that for end plate fabrication, \$6000/magnet. These costs are likely to be reasonably accurate, at least for U.S. fabrication. They are higher than proposed in the August review because the number of magnets costed in the latter estimate was inadvertently not the correct number.

Power supply cost estimates are detailed in Section III.2. These costs include capacitors, switches, chokes, and interconnections as well as the 28 power supplies. Again, these costs are probably reasonably accurate for costs in the United States. They are greater than estimated in August because the latter was for 21 dual frequency 33-100 Hz power supplies, whereas the present 28 supplies provide a 1.5 msec constant current, a rising current at a 33-1/3 Hz rate, and resetting the field at a 143 Hz rate. Significant cost savings might be realized if the time duration of the constant field could be reduced (and still be compatible with very low loss injection, beam manipulation, and

capture) because this determines the high rate of resetting the field and consequently the voltage rating required for the switches.

The estimated cost of the rf system is also greater than presented in August. The latter was an extrapolation of the costs of the rf system for the SNS machine. Initially, it was anticipated that 10 of the SNS cavities of 2 gaps each (instead of the 6 cavities of the SNS) would be adequate. Scaling the SNS costs in pounds (3.55 M # - 1981) by a factor of 1.6 to convert to \$, a factor of 1.165 to escalate to FY 1983, and a factor of 10/6 for the larger number of cavities one arrives at a cost of the rf system of \$6.9M. Subsequently, however, it was felt that these cavities might not be suitable because the average required power level of the SNQ-SRA rf system was 3.5 times that of the SNS (peak power level 2.5 times greater) rather than the 1.7 used in the extrapolation. If one scales the SNS costs by the average rf power requirements the result is \$14.5M, a very large increase in the estimate and likely closer to what actual costs might be. However, concern about the "Robinson Instability" has caused us to propose a high-power, low-impedance cavity/driver system. A preliminary design of this system, described in Section III.4, was costed at a rate of \$1.25/W average plus ferrite and cavity construction costs.

These rf system costs are significantly more uncertain than the estimates for the magnets and power supplies. We have adopted a high cost solution in order to feel confident that the rf system will operate as anticipated. However, the possibility of considerable cost savings is obvious from the discussion above if technical uncertainties of lower cost systems can be resolved.

The cost of the vacuum system was obtained by extrapolating the SNS costs (1981) by a factor of 1.6 for conversion to U.S. \$, 1.165 to escalate to FY

1983 costs, and by the ratio of the circumference factor of the two machines. The aperture of the SNQ-SRA machine is somewhat smaller but this factor might not lead to much of a cost factor. The magnets are much shorter so that the two-step process in the fabrication (curing) of the chambers is avoided, but the added number of chambers might offset this advantage.

By contrast the vacuum system for the Fermilab booster, scaled to FY 1983 dollars, would cost \$1.34M, less than half that estimated here. The booster vacuum system has the magnet laminations and coils inside the outer stainless steel vacuum skin. It has epoxy between the laminations and does not contain RF shields, which are required in the SNQ-SRA in order to shield the beam from coupling to the laminations. The Fermilab booster vacuum of few times 10^7 Torr is not adequate for the SNQ-SRA but could possibly be made so with improvements. If so considerable cost savings might be effected.

The estimate for correction element magnets and power supplies has been increased to \$2.5M because we now project the need for 16 sextupoles and 16 octupoles. The other elements of the system (diagnostics \$1.5M, injection system \$1.0M, and extraction system \$1.0M) are not large cost factors and hence the uncertainties due to lack of detailed designs do not have much impact on the overall cost of the accelerator system.

The beam transport system from the linac to the ring, beam transport system from the ring to the neutron sources, remote handling equipment, and laboratories and laboratory equipment are not included in this cost estimate. These items were estimated in the IKOR study and might be modified as necessary to be compatible with the requirements of the SNQ-SRA.

The estimate for utilities (power and water distribution) have been increased because of the increasing estimates for some components of the accelerator system. The cost of buildings may depend more strongly on local

construction costs so that we include here only a very rough estimate; refinements, depending on an evaluation of the building needs, should be done by KFA.

The inclusion of EDIA (Engineering, Design, Inspection, Administration) and contingency follows recent (October 1982) guidelines from DOE for a major accelerator construction proposal being submitted (the multi-GeV Electron Microtron Project). These guidelines are 15% EDIA and 20% contingency on the total (including EDIA), except where new and unproven technologies are to be used. In the latter case the contingency should be 25 - 30%. Since the RF system with low impedance drivers is the only major unproven technology, we include 25% contingency of this system even though we believe we have been quite conservative in estimating the cost and if anything erring on the high side.

The design of the injector linac was not considered in detail so that the cost estimate is not included in Table A.3-1. It is obviously a very substantial cost item and the cost estimate should bear some relationship to that of the rather detailed linac design being conducted by the group at Julich. In such a comparison account should be taken of the fact that the average current of the 200 MeV linac injector proposed here is 0.5 mA compared to the 5 mA of a full current linac as an alternative first stage of the spallation neutron source.

Perhaps an upper limit to the injector linac cost might be an extrapolation of the actual cost of the Fermilab 200 MeV linac. The construction cost was given in 1971 dollars. The extrapolation factor to relate these costs to FY 1983 dollars is 2.953. With this escalation, the linac costs become:

Tank	\$ 3.0 M
RF	12.0 (37 MW pk)
Driver	0.9
Modulators, Pulsers	1.3
Preaccelerator	0.5
Water System	0.8
Diagnostics	0.3
Controls	1.9
Installation	2.4
Vacuum	0.8
Beam Transport, Hardware	<u>0.2</u>
	\$24.1 M

Some savings might be realized by electroplating the linac tank and drift tubes, a less costly process than the copper cladding of the Fermilab tanks.

No advantage is taken here of projected savings which might be realized by adopting PIGMI type techniques (higher frequency linac employing klystron rf systems rather than conventional power types, RFQ preaccelerator, disc and washer structures and permanent rare earth cobalt quadrupoles in the drift tubes). None of these techniques have been demonstrated adequately to determine their reliability, which is critical to the use of the SNQ-SRA. In addition actual costs of these projected systems are considerable extrapolations from prototype costs and are not well established.

Table A.3-1

COST ESTIMATE

(Costs in \$M for FY 1983)

Ring Magnets	9.8
Ring Magnet Power Supply	12.1
Vacuum System	3.0
Correction Elements	2.5
RF System	13.5
Diagnostics	1.5
Control System	2.5
Injection System	1.0
Extraction System	<u>1.0</u>
Subtotal	46.9
Utilities	2.0
Buildings	20.0
EDIA	10.3
Contingency	<u>16.6</u>
Total	95.8

Utilities include water, cooling and power distribution. EDIA (engineering, design, inspection, and administration) is calculated at 15% and contingency at 20% except where new and unproven technologies are to be used. In the latter case (rf system), the contingency is 25%. Costs do not include R & D.